1989

Modeling the movement of a wetting front in the vadose zone beneath the drainage retention basin, Lawrence Livermore National Laboratory site

Richard Kurt Landgraf
San Jose State University

Order Number 1338705

Modeling the movement of a wetting front in the vadose zone beneath the drainage retention basin, Lawrence Livermore National Laboratory site

Landgraf, Richard Kurt, M.S.

San Jose State University, 1989

U·M·I
300 N. Zeeb Rd.
Ann Arbor, MI 48106

MODELING THE MOVEMENT OF A WETTING FRONT IN THE VADOSE ZONE BENEATH THE DRAINAGE RETENTION BASIN, LAWRENCE LIVERMORE NATIONAL LABORATORY SITE

A Thesis

Presented to

The Faculty of the Department of Geology

San Jose State University

In Partial Fulfillment

of the Requirements for the Degree

Master of Science

By

Richard Kurt Landgraf

August 1989

APPROVED FOR THE DEPARTMENT OF GEOLOGY

Dr. June A. Oberdorfer

Dr. John W. Williams

Mr. Fredric Hoffman

APPROVED FOR THE UNIVERSITY

ACKNOWLEDGEMENTS

I am deeply indebted to Lawrence Livermore National Laboratory's Environmental Restoration Division for providing the resources, opportunity, and funding for this research project. I would like to thank my thesis committee, Dr. June Oberdorfer and Dr. John Williams, of San Jose State University, and Mr. Fredric Hoffman, of Lawrence Livermore National Laboratory, for all their time and efforts in reviewing my thesis and providing valuable insight. I am also indebted to Kenneth Toney for supplying much of the geologic data and February 1986 storm data for this thesis study.

I would also like to thank June Cramer and Pat Boyd for their work in typing this thesis and typesetting the equations. Their work is greatly appreciated.

Last, I would like to thank my parents, Mr. and Mrs. William C. Landgraf, my family, and my wife, Sheri, for all their love and support throughout this project.

TABLE OF CONTENTS

LIST OF ILLUSTRATIONS

LIST OF TABLES

ABSTRACT

MODELING THE MOVEMENT OF A WETTING FRONT IN THE VADOSE ZONE BENEATH THE DRAINAGE RETENTION BASIN, LAWRENCE LIVERMORE NATIONAL LABORATORY SITE

by Richard K. Landgraf

A two-dimensional, variably saturated, finite element numerical model was used to model a 260 foot (79m) x 55.3 foot (16.9 m) NW-SE transect through the heterogeneous vadose zone beneath Lawrence Livermore National Laboratory's (LLNL) 28 acre foot (3.5 x 10^4 cubic meter) basin retention basin. The model was calibrated using the spatial and temporal wetting front patterns generated by an extensive network of basin vadose resistance cells during a severe mid-February 1986 storm.

The vadose zone model was used to study the wetting front movements produced during four simulations: the February 1986 storm, a deep ponding simulation, a lateral flow simulation, and a January 1988 storm. Wetting front migration was found to be dependent upon site geology, depth of ponded water, and surface moisture conditions.

The development of a moisture transmission zone at a silt/sand interface at 28 feet (8 m) below the basin surface was predicted by the model during each of the four simulations. In addition, the model helped to confirm the existence of a permeable zone in the southeast portion of the basin (not modeled).

INTRODUCTION

The purpose of this thesis project was to furnish Lawrence Livermore National Laboratory (LLNL) with a detailed simulation study of the movement of a wetting front in the heterogeneous vadose zone beneath the drainage retention basin at LLNL and to simulate the effect of ground water recharge beneath the basin. The two-dimensional numerical model UNSAT2 was used in this vadose zone study. The model was calibrated, spatially and temporally, using wetting front patterns generated by field vadose zone resistance cells during a severe mid-February 1986 storm. Four simulations are discussed in this paper. They are: the February 1986 storm simulation, a deep ponding simulation, a lateral flow simulation, and a January 1988 storm simulation.

Lawrence Livermore National Laboratory (LLNL) is located in the southeastern portion of the Livermore Valley, approximately 40 miles (65 km) east of San Francisco (figure 1). The Livermore Valley was created by the late Mesozoic–late Tertiary uplift of the Diablo Range. Valley sediments consist predominantly of detrital alluvial deposits of late Tertiary-Quaternary age which were deposited as a result of a "complex pattern of regional deformation, uplift, erosion, and deposition" (Carpenter et al., 1984). Sediment thicknesses may locally exceed 0.6 miles (1 km) in the valley. Age dating techniques performed on LLNL soils indicate that the upper 69 feet (21 meters) were deposited in the last 300,000 years.

Site geology consists of complexly interbedded and interlensed, Quaternary and Late Tertiary clays, silts, sands and gravels, deposited by a number of meandering streams and rivers which drained the Livermore Valley (Stone et al., 1982, and Carpenter et al., 1984). Ground water elevations fluctuate seasonally due to the influence of precipitation, local agricultural pumpage, and recharge from the drainage retention basin, the Arroyo

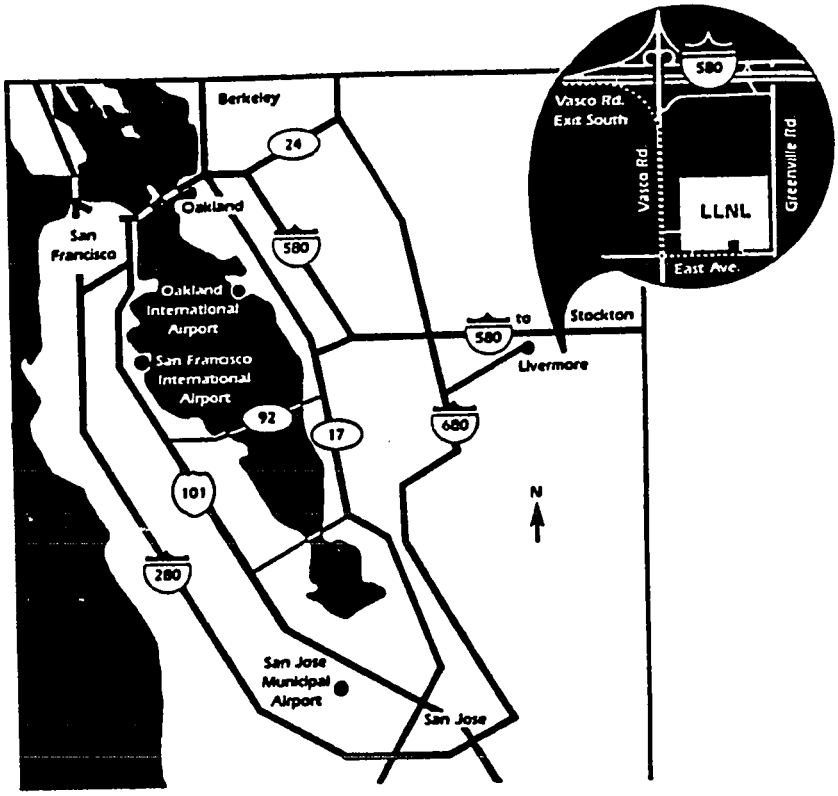

Figure 1. Location map of Lawrence Livermore National Laboratory (from Stone et al., 1982).

Seco, and the Arroyo Las Positas (figure 2). Ground water mounding beneath the drainage retention basin resulting from the percolation of ponded runoff water has been documented by authors Toney and Oberdorfer (1986) during their 1985-1986 hydrogeologic investigation of the drainage retention basin.

During their hydrogeologic investigation of the drainage retention basin, Oberdorfer and Toney (1986) installed three strings of paired resistance cells in a NW - SE transect across the drainage retention basin. Cells were installed at eight depths varying from 2 to 55 feet (61–1,680 cm) beneath the basin floor and were wired to a Campbell Scientific datalogger. Soil resistance readings are measured every 10 minutes, averaged each hour and magnetically recorded on a cassette tape. Through extensive monitoring of precipitation, basin water levels, basin soil resistance, and nearby ground water levels, the movement of a wetting front through the basin vadose zone was tracked, and ground water recharge was quantified.

In mid-February 1986, a severe storm hit the Livermore Valley, precipitating 4.89 inches (12.42 cm) of rain, most of which occurred over a six day period. The storm caused the 28 acre-foot (3.5×10^4 cubic meters) drainage retention basin to fill to its maximum level of 10 feet (3 m) and overflow for two days at its northern edge. As the ponded water percolated into the vadose zone, the resistance data generated a good record of the migration of the wetting front from the surface to the water table.

The wetting front generated by this storm was modeled using a two-dimensional, Galerkin finite element, numerical model, UNSAT2. The numerical model was calibrated using the wetting front field data to develop a useful model for future predictive wetting front analysis. Four percolation simulations were performed by the calibrated model: the February 1986 storm, a lateral flow simulation, a deep ponding simulation, and a January

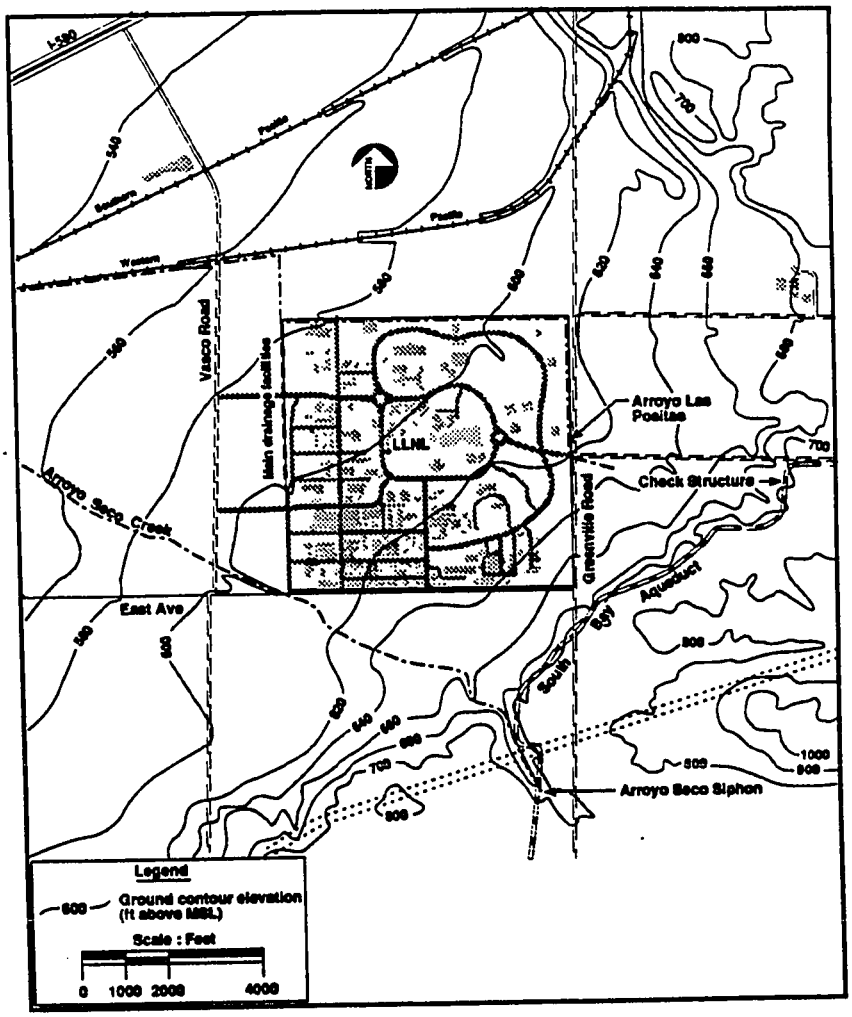

Figure 2. Location map of Lawrence Livermore National Laboratory, the drainage retention basin, the Arroyo Seco, and the Arroyo Las Positas (adapted from Carpenter et al., 1984).

1988 storm simulation. The results of these simulations are discussed in detail in this paper.

Objectives of Thesis Study

The purpose of this project was to furnish Lawrence Livermore National Laboratory with a detailed simulation study of infiltration into the vadose zone beneath the drainage retention basin at Lawrence Livermore National Laboratory. To complete this study, six objectives were established.

First, working soil parameters/properties were to be developed to calibrate the model and duplicate the known resistance data. Second, a sensitivity analysis of the model was to be performed to establish how the input parameters affect the model's performance. Third, the movement of the wetting front produced by the infiltration of ponded runoff water resulting from a severe mid-February, 1986, storm was to be simulated and used to calibrate the model. Fourth, once the computer model had been calibrated, it was to be studied at intermediate time steps to determine how, specifically, the wetting front migrates and how moisture patterns change in the vadose zone. Fifth, the simulation was to be used to study the effects heterogeneous alluvium have on the migration of the wetting front. Last, the calibrated soil characteristics/properties were to be used to determine the relative hydrogeologic conditions that prevail in the vadose zone under various scenarios.

Unsaturated Flow in the Vadose Zone

The purpose of this section is to familiarize the reader with some of the fundamental concepts of unsaturated flow in the vadose zone. For a more detailed discussion on the

physics of unsaturated flow, the author suggests Freeze and Cherry (1979), Bear (1979), Baver et al. (1972), Kirkham and Powers (1972), Hillel (1971), and Childs (1969).

Unsaturated flow in the vadose zone is a complex phenomenon, which may involve soil hystersis, variable hydraulic conductivity, variable moisture content, variable pressure head/suction, water uptake by plants, infiltration and/or evaporation, and a general dependence upon antecedent soil moisture content. Hydrogeologists typically define the vadose zone as the zone of soil/rock between the ground surface and the water table (saturated zone). For this reason, and the fact that saturated regions may occur in the vadose zone (i.e., a perched water table) the term "vadose zone" is preferred over the term "unsaturated zone."

In saturated soils, the water table represents the zero pressure head boundary ($\psi=0$), so that below the water table $\psi>0$ and above the water table $\psi<0$. The negative pressure head (ψ), or suction, is due to the physical affinity of the water to the soil-particle surfaces and capillary pores. Flow in the vadose zone is the result of gravitational forces and of pressure gradients, as in the saturated zone. However, in the vadose zone, the pressure gradients are due to contrasting matric suction (negative pressure heads) and, as a result of the suction gradients overcoming gravitational forces, water tends to flow from low suction zones to high suction zones (Hillel, 1971).

The affinity of the water to the soil particle (i.e., matric suction) is created by soil pore surface-tension forces. "A microscopic inspection would reveal a concave meniscus extending from grain to grain across each pore channel," (Freeze and Cherry, 1979) during unsaturated soil conditions (figure 3). The radius of curvature of the concave meniscus is a function of matric suction, grain size, and water content. The lower the water content, the higher the matric suction, and smaller the radius of curvature of each grain to grain

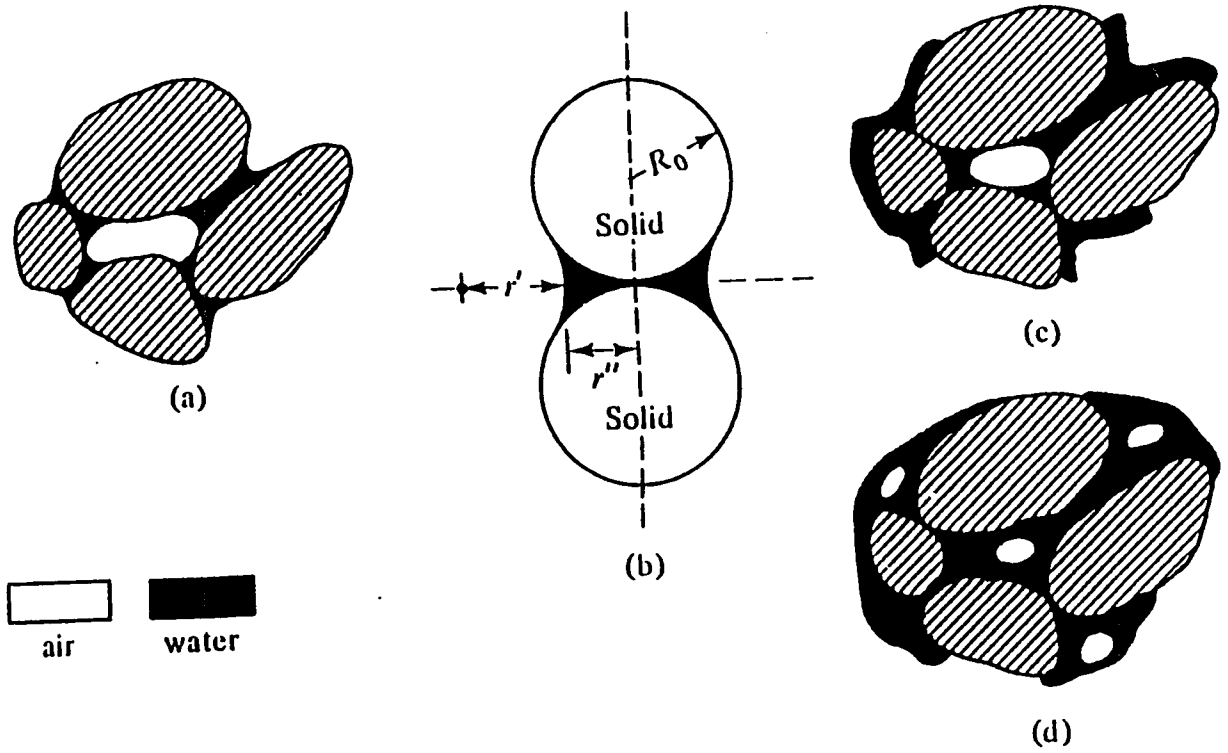

Figure 3. Menisci at various states of saturation. (a) Pendular saturation. (b) Radius of curvature and pendular rings between two spheres. (c) Funicular saturation. (d) Insular air saturation (from Bear, 1979).

meniscus. Smaller grained soils, such as clays and silts, can support smaller radii of curvature and therefore sustain much larger matric suction values than larger grained soils, such as coarse sands and gravels.

There are two primary driving forces which control unsaturated flow in the vadose zone. First, as mentioned above, the matric suction gradient acts as a moisture migrating force by pulling (or sucking) moisture from low suction zones to high suction zones. Second, in soils displaying uniform negative pressure heads (matric suction) throughout a vertical profile (i.e., no suction gradient exists), the moving force may be driven by gravitational forces, provided the gravitational forces can overcome the initial soil matric suction forces. This is what is otherwise known as drainage. Often, these two forces will act together during the passing of a wetting front through the vadose zone.

While the hydraulic conductivity of a homogeneous, isotropic saturated soil remains constant, the hydraulic conductivity of a homogeneous, isotropic unsaturated soil varies with respect to pressure head and moisture content. In saturated soils, all connecting pores are full and capable of transmitting water at a maximum conductivity. However, in unsaturated soils, some pores become filled with air, which blocks the flow of water, therefore a smaller number of pores can transmit water and the conductivity decreases. Typically, the larger the soil grain (and pore size) the faster the soil desaturates and the faster the unsaturated hydraulic conductivity decreases. Conversely, finer grained soils tend to retain moisture longer, under larger negative pressure heads, and do not desaturate as quickly. As a result, the unsaturated hydraulic conductivity of finer grained soils decreases more gradually than that of larger/coarser grained soils (figure 4). The hydraulic conductivity/moisture content and pressure head/moisture content relationships are known as soil characteristics.

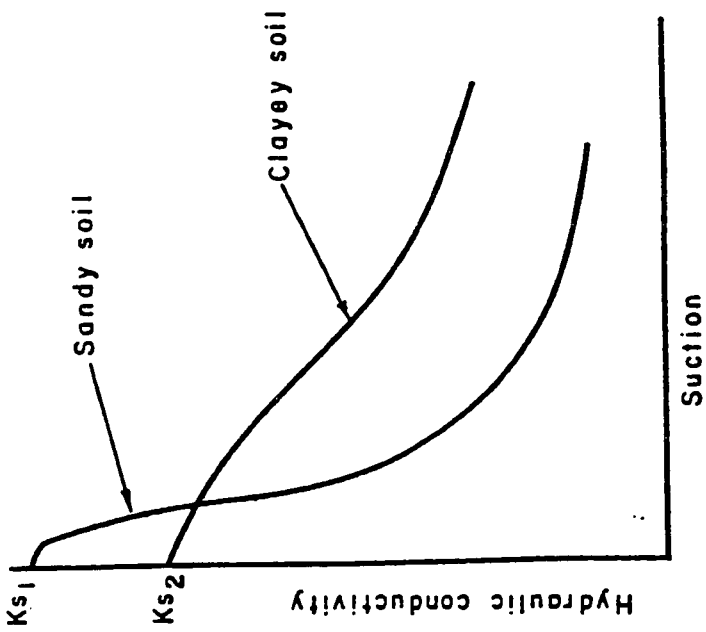

Figure 4. Dependence of conductivity on suction in soils of different texture (log-log scale) (from Hillel, 1971).

It is well known that in the saturated zone, soils with larger and more conductive pores (say, gravels) have higher hydraulic conductivity values than do soils with smaller and more restrictive pores (say, silts). However, in the vadose zone, as pressure heads decrease, gravels or other coarser grained soils will desaturate much more rapidly than soils with smaller pores (silts). Many of the silt pores will remain full and more conductive and, as the vadose zone desaturates, may become more conductive than the gravel. As a result, the gravel may actually impede flow of moisture, while greater moisture flux develops in the silt.

> Since in the field the soil is unsaturated most of the time, it often happens that flow is more appreciable and persists longer in clayey than in sandy soils. For this reason, the occurrence of a layer of sand in a fine-textured profile, far from enhancing flow, may actually impede unsaturated water movement until water accumulates above the sand and suction decreases sufficiently for water to enter the large pores of the sand (Hillel, 1971).

The unsaturated soil characteristics may have complex relationships with respect to antecedent moisture conditions and whether the soil is wetting or drying. In other words, soil characteristic curves may have different shapes depending if they are measured during the wetting or drying of the soil. This is known as soil hystersis (figure 5). An infinite number of scanning curves may exist between the wetting or drying curves. They describe the moisture content vs pressure head or hydraulic conductivity relationships during partial wetting or drying. Soil hysteresis is typically the result of trapped air in pore spaces during wetting, moisture contact angle ("the raindrop effect"), the increased suction required as water reenters smaller pores ("the ink-bottle effect") (Bear, 1979), and/or the shrink/swell potential of the soil. In some soils, the difference between the wetting and drying curves is minimal and often ignored. Since UNSAT2 assumes no soil hystersis, only single (non-hysteretic) characteristic curves were used.

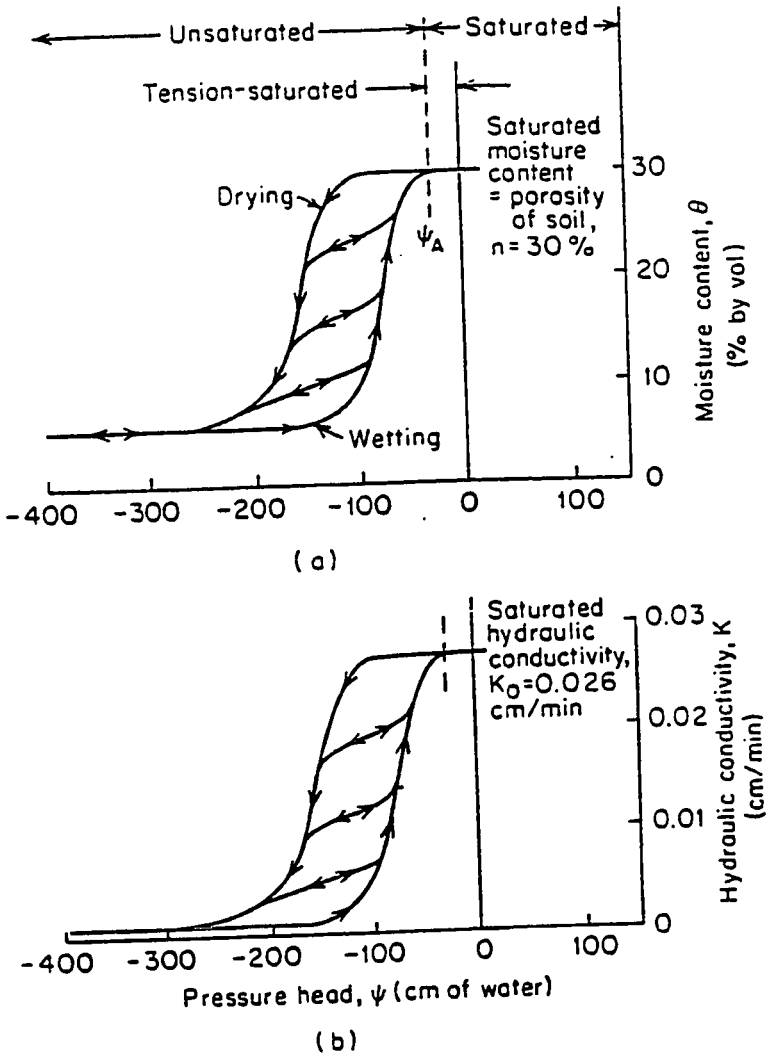

Figure 5. Characteristic curves relating hydraulic conductivity and moisture content to pressure head for a naturally occurring sand soil. Note soil hysteresis and scanning curves (from Freeze and Cherry, 1979).

BACKGROUND AND PREVIOUS STUDIES

A major portion of the background data used in this study was accumulated by San Jose State University graduate student Kenneth Toney as part of his drainage retention basin monitoring, from August 1985 to December 1986. Toney conducted a hydrogeologic investigation of ground water recharge near the drainage retention basin at LLNL (Toney, Thesis Draft 1988). His work included the drilling and logging of four bore holes (LR-1-R, LR-2-R, LR-3-R, and LR-4-P, (see figure 6 for location and Appendix A for logs) in the floor of the drainage retention basin; the construction of one piezometer (LR-4-P) and three paired resistance cell strings (LR-1-R, LR-2-R, and LR-3-R); the monitoring of vadose zone soil resistance, precipitation, basin water levels, and ground water levels in the vicinity of the basin; and performing infiltrometer and triaxial permeameter tests on some basin soils and core samples.

The three paired resistance cell strings were constructed by boring three approximately 50 foot (15 m) deep holes in the basin floor and installing eight pairs of Soiltest resistance cells at various depths in each hole. Each cell was embedded in 6 inches (15 cm) of electrically neutral, 200 mesh silica flour and sealed above and below with 1 foot (0.3 m) of bentonite pellets at approximately 2, 5, 10, 15, 20, 30, 40, and 50 foot (0.6, 1.5, 3, 4, 6, 9, 12, and 15 meters) depths in each boring (LR-1-R, LR-2-R, and LR-3-R) (Toney, Thesis draft, 1988). Depths of paired resistance cells are known specifically for each cell, but vary between each of the strings. Soil resistance at each cell is measured every 10 minutes, averaged each hour, and magnetically recorded on a cassette tape by a Campbell Scientific 21X datalogger. The soil resistance values yield, both spatially and temporally, a relative indication of the soil moisture and the pattern of the wetting front as it moves

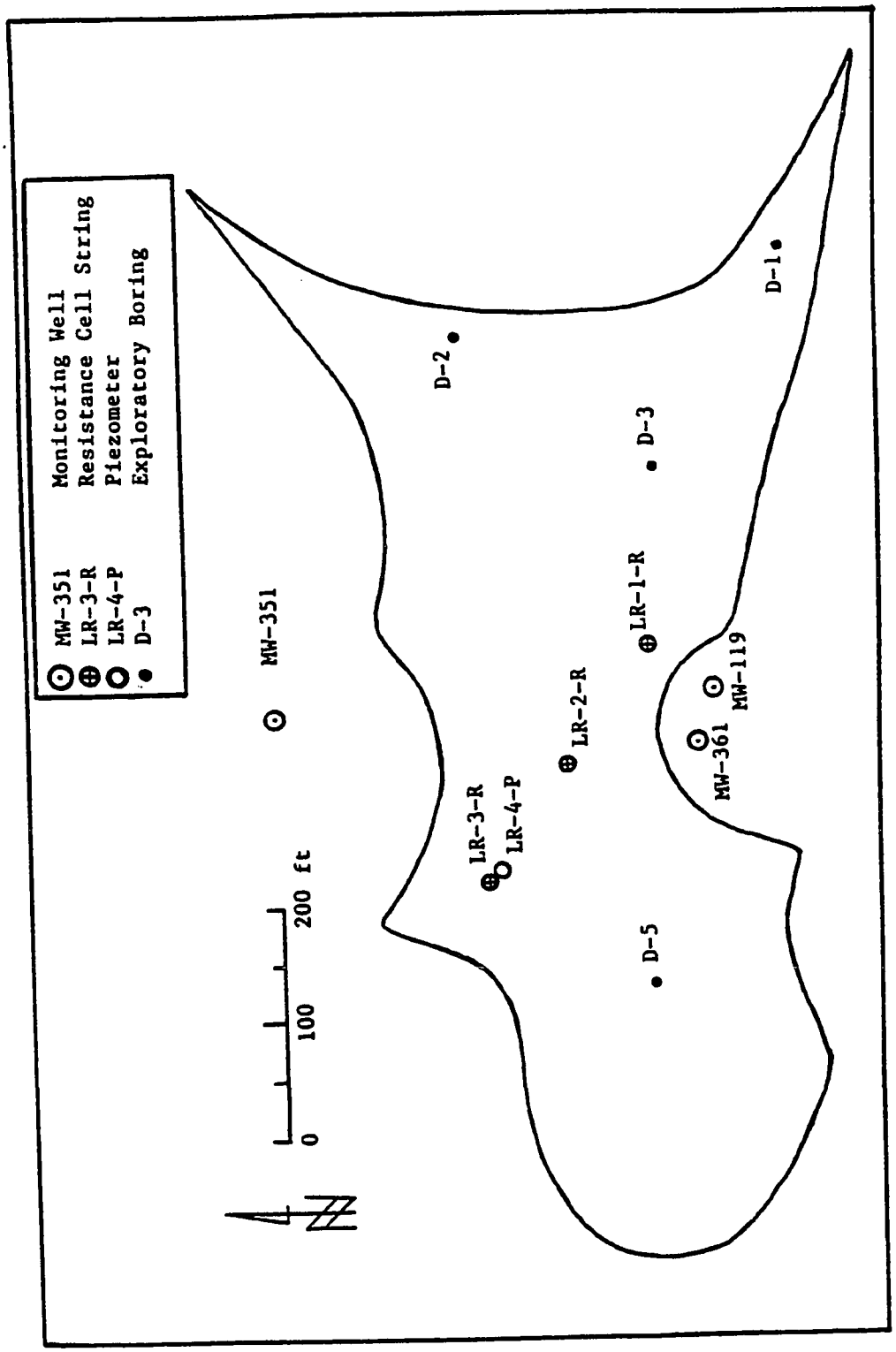

Figure 6. Map of drainage retention basin and locations of LR-series and D-series boreholes.

downward through the vadose zone during recharge events (an increase in soil moisture results in lower resistance values).

One particular recharge event occurred in 1986, between February 11 and February 19. During this storm, 4.89 inches (12.42 cm) of rain fell, causing the 28 acre-foot (3.5×10^4 cubic meters) drainage retention basin at LLNL to fill to its maximum depth of 10 feet (3.0 m) and eventually overflow at its northern edge. Vadose zone soil resistance, basin water level, precipitation, and nearby monitoring well water levels were monitored extensively during the storm. The modeling of the migration of the wetting front created by this storm is the focus of this thesis study.

Basin Lithology

The 4 acre (1.6×10^4 square meters) drainage retention basin is underlain by heterogeneous alluvial sediments consisting of interbedded and interlensed clays, silts, sands, and gravels. Several borehole logs (LR-1-R, LR-2-R, LR-3-R, LR-4-P, D-1, D-2, D-3, and D-5) (fig. 6) and three nearby monitoring well logs (MW-119, MW-361, and MW-351) (fig. 6) were used to determine subsurface basin lithology and geologic properties. Based upon the above geologic information, a generalized NW-SE trending geologic cross section (fig. 7) was drafted through the three logged borings (LR-1-R, LR-2-R, and LR-4-P). The cross section lithology was simplified for modeling purposes by combining adjacent geologic materials with similar hydrogeologic properties and characterizing them by their dominant constituents (as is commonly done when interpreting borehole data for alluvial sediments). The reason for creating a generalized cross section of the basin is that the individual heterogeneities characteristic of valley alluvium would be

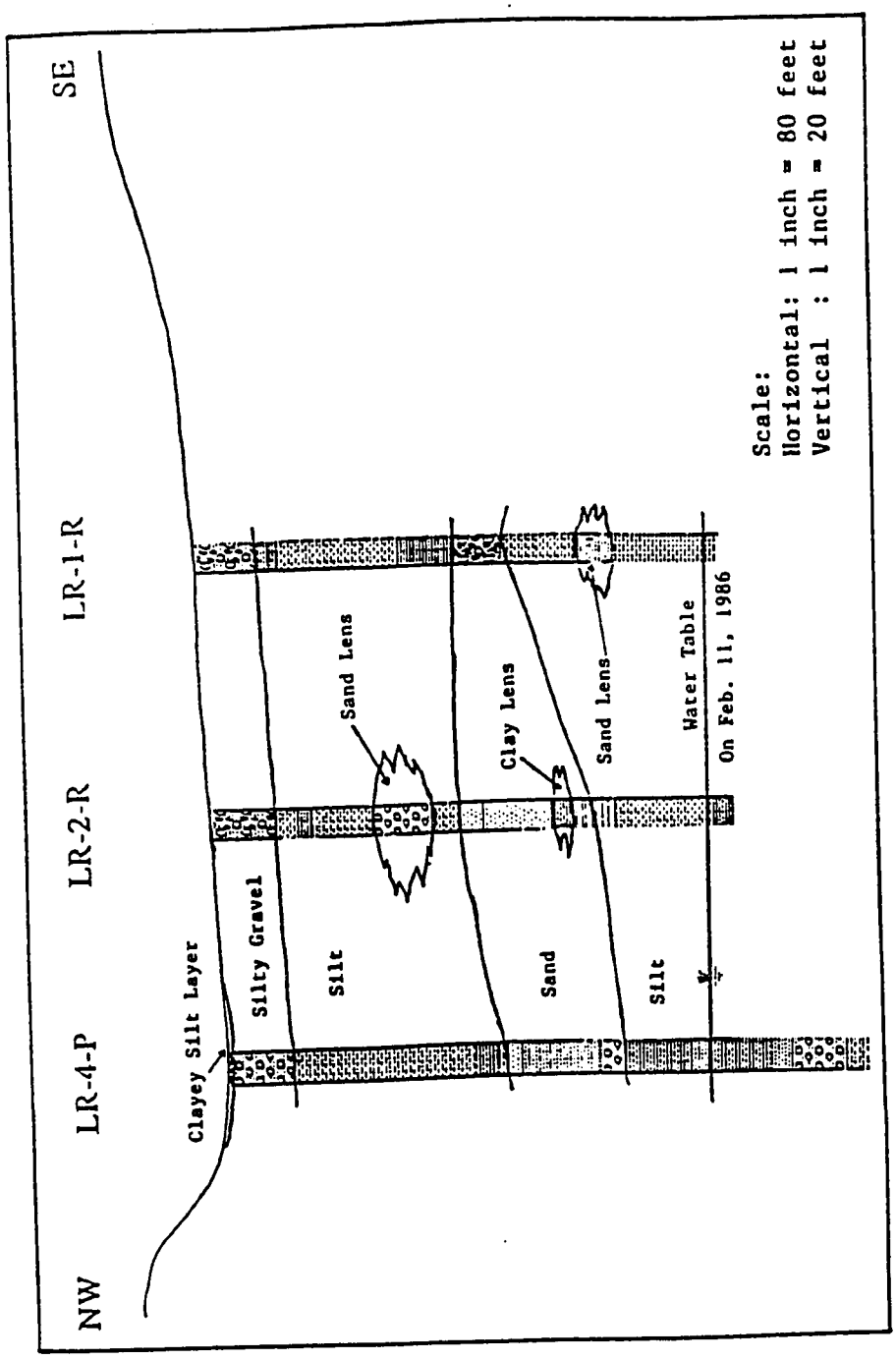

Figure 7. Generalized geologic cross-section of the portion modeled beneath the drainage retention basin through the three logged borings. Note, LR-4-P was chosen instead of LR-3-R because it is deeper.

extremely difficult (if not impossible) to model because they are typically small and unknown between boreholes.

The basin lithology between the LR-series boreholes at the center of the basin and the D-series boreholes (Carpenter, 1984) (primarily D-3, see Appendix A) does not correlate very well. The D-series boreholes (not used in the cross-section) indicate that a fairly thick , 20 to 30 foot (6–9 m) layer of moderate to high permeability silty-sandy, gravel exists under the southeast portion of the basin. In addition, high rates of infiltration are known to occur in the southeast corner of the drainage retention basin (Toney, Thesis Draft, 1988). The southeastern zone of moderate-high permeability is likely to affect local ground water recharge; it does not, however, seem to affect the migration of the wetting front between the resistance cell strings. In other words, the wetting front is not seen to migrate any faster at LR-1-R (closest to D-3) than at LR-3-R (furthest from D-3). For these reasons and because the resistance data modeled is known only for LR-3-R, LR-2-R, and LR-1-R, the basin cross section used in the simulation exists from LR-3-R to LR-1-R.

Infiltrometer and Permeameter Test Results

Double-ring infiltrometer tests were performed on the drainage retention basin floor between February and September, 1986. Infiltration rates were found to be dependent upon antecedent moisture conditions and lithology. In the deeper portions of the basin (near LR-3-R and LR-4-P), a 6-inch (15-cm) silt layer has been deposited over the 8-foot (2.4-m) thick silty gravel layer (basin floor) as a result of the deposition of silt sized particles transported into the basin by local runoff water. As a result, infiltration rates were found to be quite low, on the order of 0.01 ft/day (0.3 cm/day). Moving outward from the NW low spot, infiltration values began to increase, as a result of decreased silt deposition

on the basin floor. Infiltration rates reached a maximum value of nearly 1.9 ft/day (58 cm/day) along the outer edge of the drainage retention basin, where much of the silty gravel layer is exposed. Figure 8 is a contour map of the double-ring infiltrometer data from the drainage retention basin.

Triaxial permeameter tests were performed on three cores taken from the boreholes drilled in the basin floor. Table 1 summarizes the results from the permeameter tests. Steady-state hydraulic conductivity values obtained from the double-ring infiltrometer and the triaxial permeameter tests were found to be consistent (within an order of magnitude) with hydraulic conductivity values for similar soils listed in Freeze and Cherry (1979) (Toney, personal communication, 1987).

Table 1. Saturated hydraulic conductivity values from basin core samples. Conductivities determined by triaxial permeameter (Toney, Thesis Draft, 1988).

Sample Name	Soil Type	Saturated Conductivity (cm/day)
LR4P-55	Sandy Silt	5.5×10^{-4}
LR1R-40	Sandy Silt	1.8×10^{-3}
LR2R-30	Sand	680

Previous Vadose Zone Modeling Efforts

A number of one-dimensional, saturated-unsaturated flow programs have been written over the past 20 years (Freeze, 1969; Bhuiyan et al., 1971; Bond et al., 1982; Kunze and Nielson, 1982; Ragab et al., 1982; Kirby, 1985; and U.S. EPA, 1986). The one-dimensional models have been typically used to compare theoretical simulation results

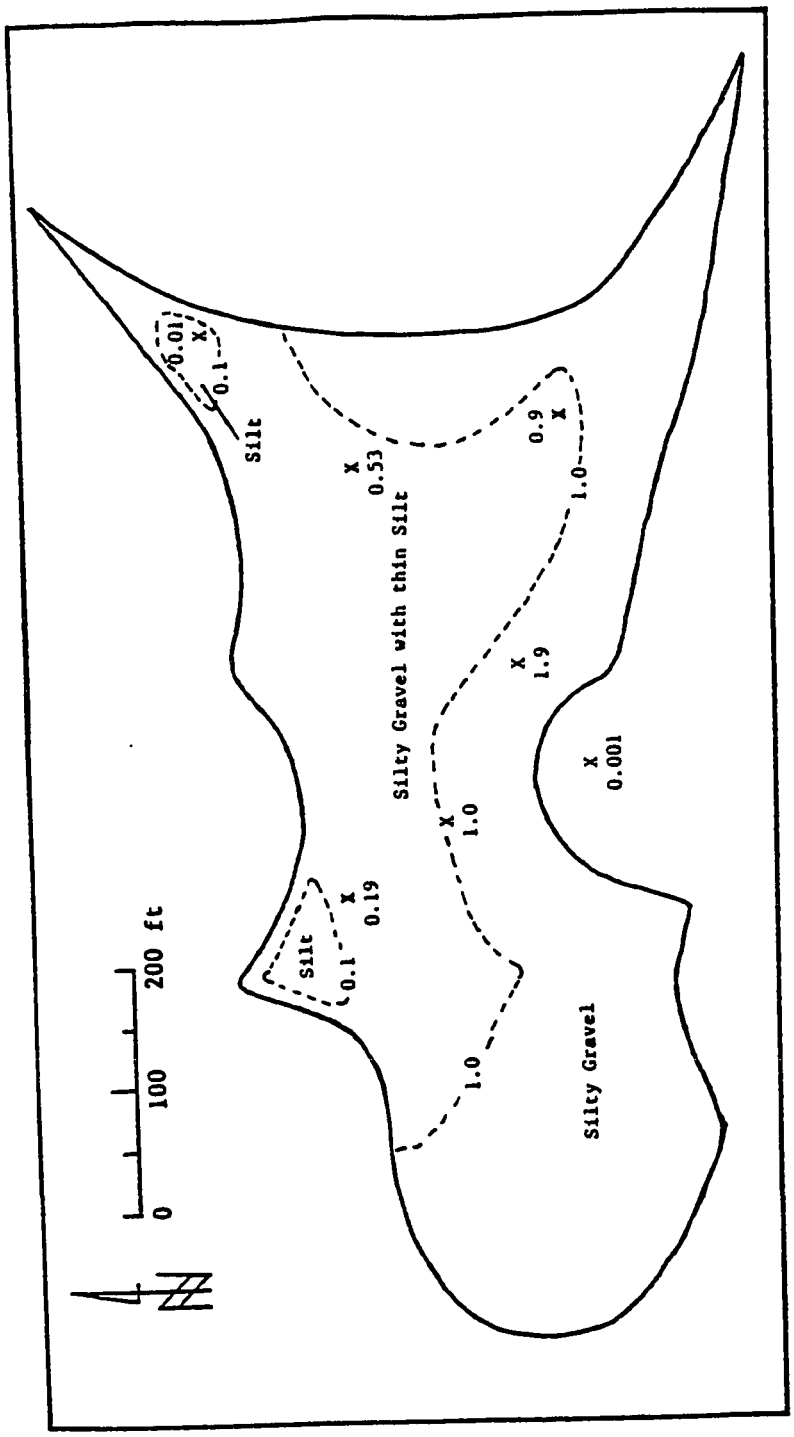

Figure 8. Contour map of the varying basin surface infiltration rates. Contours are based on the double-ring infiltrometer test results and surface soil type. Infiltration rates are in feet/day (adapted from Toney, Thesis Draft, 1988).

with laboratory column infiltration results to verify or validate the unsaturated flow programs, simulate vertical infiltration in homogeneous, istotropic materials, and simulate vertical infiltration at surface liquid impoundment facilities. Figure 9 is a typical moisture content vs depth plot of a homogeneous, isotropic material generated from a one-dimensional, variably saturated flow model. Unfortunately, the simplicity of the one-dimensional models prevents them from adequately describing the actual flow system in the field due to the anisotropies and heterogeneities inherent in a true field situation (Yeh et al., 1985).

One of the first multidimensional models was a three-dimensional, finite difference model, developed to describe saturated-unsaturated, transient flow in small nonhomogeneous, anisotropic geologic basins (maximum grid size: a few miles by 1000 feet deep). The model was useful in determining regional hydrologic responses of a ground water basin to pumping and infiltration (Freeze, 1971). The results of this model are commonly studied by undergraduate and graduate hydrogeology students in Freeze and Cherry's (1979) text, Groundwater.

At the same time Freeze's regional, three-dimensional, finite difference model was published, Neuman and Whitherspoon (1971) developed a two-dimensional, finite element model capable of describing the local, saturated-unsaturated vadose zone responses to infiltration, evaportranspiration, axisymmetric flow to a well, and the adjustment of the free surface within a dam due to the sudden lowering of the reservoir level in anisotropic, heterogeneous materials. The Neuman/Whitherspoon program, through a series of refinements, eventually became UNSAT2, which the writer has used for this study.

Two other multidimensional models have been used to simulate infiltration into the vadose zone. Authors Vauclin, Khanji, and Vachaud (1979) developed a three-dimensional saturated-unsaturated, finite difference model to simulate the response of a slab

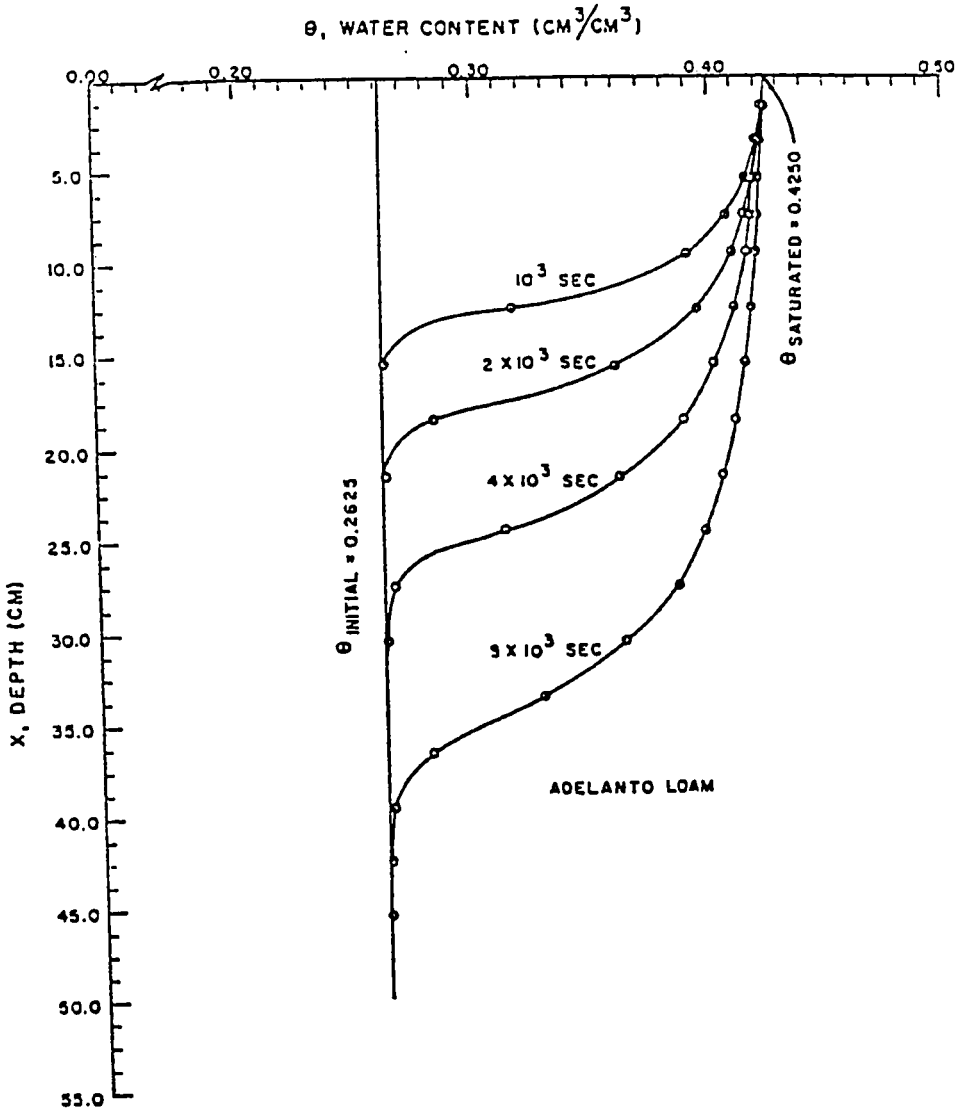

Figure 9. Typical moisture content vs. depth plot of a homogeneous material (Adelanto Loam), generated from a 1-D variably saturated flow model (from Bhuiyan et al., 1971).

of homogeneous soil to constant infiltration. The flow system was constructed in the laboratory and fitted with several pressure transducers and tensiometers to quantify the system's response to constant infiltration. The numerical model's simulation of the shape and advance of the wetting front, water content profiles, and water table mounding were all in excellent agreement with measured laboratory data. Unfortunately the model's program code and finite difference scheme prevented it from modeling heterogeneous materials with complex geometry/structure, such as the geology at the LLNL site.

Winter (1978) performed several numerical simulations of infiltration due to a variety of hypothetical, large-scale, lake configurations with a three-dimensional, finite difference code. The model only simulated general hydrogeologic changes in lake-ground water systems from surface infiltration and is not suitable for simulating infiltration in complex hydrogeologic settings.

A more recent modeling approach to unsaturated flow in heterogeneous soils is that of stochastic analysis. Stochastic analysis is based upon a statistical analysis of the three dimensionality of field heterogeneity and anisotropy. The overall goals are to determine the mean or effective large-scale behavior of the heterogeneous system and the degree of variation about the mean (Yeh et al., 1985). This approach is primarily for predicting large-scale flow characteristics of regional ground water systems and would not be suitable for the local vadose response to the infiltration of ponded runoff waters at LLNL, which is modeled in this study. For a more detailed discussion of stochastic modeling see Yeh et al. (1985), and Mantoglou and Gelhar (1987).

UNSAT2 has been used to successfully simulate one-dimensional and two-dimensional infiltration through a sand column and a sand flume system, respectively (Davis and Neuman, 1983). Both tests duplicated laboratory results, with a reasonable amount of agreement. In an earlier two-dimensional simulation of the nonsteady buildup of

a ground water mound due to infiltration, Neuman and Witherspoon (1971) found that their model's (i.e., UNSAT 2's) results compared favorably with both the analytical results of another modeler and laboratory experiments.

In 1983, the Illinois State Geological Survey used UNSAT2 to simulate infiltration into several hypothetical, layered covers for a low level radioactive trench to evaluate their effectiveness at isolating the buried waste. The model predicted pressure head and moisture content distributions that were in close agreement with laboratory soil column tests. The two-dimensional study enabled the Illinois State Geological Survey to study the vertical and lateral response to gravel and loess layers encountered in the trench cover, and to study the effects of moisture buildup and breakthrough in a layered system.

After several laboratory and computer simulations, it was concluded that "a layer of coarse textured, unsaturated material overlain by fine-grained material serves as a barrier to moisture movement. The effectiveness of the barrier is related to the contrast in saturated hydraulic conductivity and texture between the two layers" (Johnson et al., 1983). The barrier (or "wick effect") as predicted by UNSAT2 is consistent with the findings of other researchers studying the affects of moisture migration in layered soils with contrasting texture (Hillel, 1971; and Rojstaczer, 1981).

A fairly extensive field study and computer simulation (UNSAT2) of water flow through unsaturated soil beneath a 48 acre (1.9×10^5 square meters) liquid waste disposal pond was conducted by Trautwein et al. (1983). UNSAT2 was used to model a one-dimensional 400 foot (122 m) deep profile beneath the center of the pond to predict present and future wetting front migration, and the impact of contamination on an aquifer 390 feet (119 m) below the pond. The model accurately predicted the present wetting front location within 30 feet (9 m) (i.e., 8% error). Given the hydrogeologic simplifications required for simulation and the large number of uncertanties that exist in some of the input parameters

(i.e., limited permeability and soil characteristic data), the vadose simulation produced results that were realistic and very useful in determining the future propagation of the contaminated wetting front under a variety of corrective actions. The model was also useful in providing a background for a more complex multi-dimensional flow simulation of the site to be performed in the future.

Authors McMahon and Dennehy (1985) of the U.S. Geological Survey, South Carolina, successfully applied UNSAT2 to qualitatively simulate variably saturated flow in the vadose zone at two experimental waste-burial trenches. The model accurately predicted the hydraulic head distributions seen in field data and was useful in analyzing the complex flow patterns in and around the trenches due to the infiltration of runoff waters. It was found that UNSAT2 was very sensitive to the initial conditions of the three material, 10 x 12 meter (32.8 x 39.4 foot), finite element grid and by adjusting the initial conditions the model's accuracy could have been increased. The simulation was also useful in explaining the complex tracer distribution patterns found in field scale experiments.

UNSAT2 is presently available from Dr. Shlomo Neuman (at the University of Arizona) or the U.S. Nuclear Regulatory Commission in Cyber or CDC Fortran 77 forms. A few more variably saturated flow programs are also currently available. TRUST, a three-dimensional, finite difference model developed by Dr. Narasimhan at the University of California, Berkeley is available in a variety of altered forms, as the result of continued modification by his graduate students. VS2D is a two-dimensional, finite difference program which was recently made available by the USGS. The Geotrans company has produced two variably saturated flow models, Saturn and Flaminco. Both programs are capable of modeling variably saturated flow and contaminant transport with finite elements in two- and three-dimensions respectively.

Variably Saturated Flow Simulation

UNSAT 2 uses the following general equation to govern the flow of water in variably saturated porous media (Davis and Neuman, 1983). The first term on the right side is advection, the second drainage, the third storage, and the last term, S , represents a source or sink.

$$L(\psi) = \sum_{i=1}^{3}\sum_{j=1}^{3}\frac{\partial}{\partial x_i}\left[K^r(\psi)\,K^s_{ij}\frac{\partial \psi}{\partial x_j}\right] + \sum_{i=1}^{3}\frac{\partial}{\partial x_i}K^r(\psi)K^s_{i3} - \left[C(\psi) + \beta S_s\right]\frac{\partial h}{\partial t} - S = 0 \quad , \quad (1)$$

where
- L = quasilinear differential operator defined in the flow region (1/T),
- x_i = spatial coordinates (i=1,2,3 with x_3 the vertical) (L),
- K^r = relative hydraulic conductivity ($0 \le K^r \le 1$) (dimensionless),
- K^s_{ij} = hydraulic conductivity tensor at saturation (L/T),
- ψ = pressure head, positive in saturated zones, negative in unsaturated zones, and zero at a phreatic surface (L),
- C = specific moisture capacity = $d\theta/d\psi$ (1/L),
- θ = volumetric moisture content (dimensionless),
- β = 0 in unsaturated zone and 1 in saturated zone (dimensionless),
- S_S = specific storage (1/L),
- t = time (T),
- S = sink term (1/T),
- h = hydraulic head (L).

The specific storage, S_S, is allowed to drop out of Eq.(1) for unsaturated soils as the result of $\beta = 0$ (see above). The reasoning behind this is fairly simple. In unsaturated soils, "storage is controlled much more by moisture content than by compressibility

effects" (Davis and Neuman, 1983); as a result, the specific storage can be neglected and the specific moisture capacity, C, becomes the dominant storage term.

The general transient flow equation for saturated and unsaturated flow (Eq. 1) consists of equations describing advection, drainage, storage, and the influence of a source or sink. It is derived from Darcy's law in the following manner:

$$Q = -K\frac{dh}{dx}A \quad , \quad \text{(Darcy's law in 1-D)} \tag{2}$$

or

$$V = \frac{Q}{A} = -K\frac{dh}{dx} . \tag{3}$$

where Q = flow rate (L^3/T),

K = hydraulic conductivity (L/T),

A = cross-sectional area (L^2),

$\frac{dh}{dx}$ = hydraulic gradient (dimensionless),

V = specific discharge (L/T).

In 3-D, Darcy's law [Eq. (3)] may be written:

$$V_x = -K_{xx}\frac{\partial h}{\partial x} - K_{xy}\frac{\partial h}{\partial y} - K_{xz}\frac{\partial h}{\partial z} \quad ,$$

$$V_y = -K_{yx}\frac{\partial h}{\partial x} - K_{yy}\frac{\partial h}{\partial y} - K_{yz}\frac{\partial h}{\partial z} \quad ,$$

$$V_z = -K_{zx}\frac{\partial h}{\partial x} - K_{zy}\frac{\partial h}{\partial y} - K_{zz}\frac{\partial h}{\partial z} \quad ,$$

$$V(x,y,z) = V_x + V_y + V_z \tag{4}$$

or as

$$V(x,y,z) = -\sum_{i=1}^{3}\sum_{j=1}^{3} K_{ij}\frac{\partial h}{\partial x_i} \quad , \tag{5}$$

where x_i represents three orthogonal spacial coordinates (i = 1,2,3; with x_3 = vertical).

The law of conservation of mass and the equation of continuity describe flow through an elemental control volume (figure 10). They may be reduced to:

$$-\frac{\partial V_x}{\partial x} - \frac{\partial V_y}{\partial y} - \frac{\partial V_z}{\partial z} = 0 \quad , \qquad \text{(Steady-state)} \tag{6}$$

or

$$-\sum_{i=1}^{3} \frac{\partial}{\partial x_i} V_i = 0 \quad . \qquad \text{(Steady-state)} \tag{7}$$

Substituting in Darcy's law, the general steady-state flow equation may be obtained:

$$\frac{\partial}{\partial x}\left(K_{xx}\frac{\partial h}{\partial x} + K_{xy}\frac{\partial h}{\partial y} + K_{xz}\frac{\partial h}{\partial z}\right) + \frac{\partial}{\partial y}\left(K_{yx}\frac{\partial h}{\partial x} + K_{yy}\frac{\partial h}{\partial y} + K_{yz}\frac{\partial h}{\partial z}\right)$$

$$+\frac{\partial}{\partial z}\left(K_{zx}\frac{\partial h}{\partial h} + K_{zy}\frac{\partial h}{\partial y} + K_{zz}\frac{\partial h}{\partial z}\right) = 0 \quad . \tag{8}$$

or $$\sum_{i=1}^{3}\sum_{j=1}^{3} \frac{\partial}{\partial x_i}\left[\, K_{ij}\frac{\partial h}{\partial x_j}\right] = 0 \quad . \tag{9}$$

In the case of transient flow, the right-hand side of the steady-state flow equation does not equal zero; instead it equals the time rate of change of fluid storage:

$$\sum_{i=1}^{3}\sum_{j=1}^{3} \frac{\partial}{\partial x_i}\left[K_{ij}\frac{\partial h}{\partial x_j}\right] = S_s\frac{\partial h}{\partial t} \quad , \tag{10}$$

where $S_s\frac{\partial h}{\partial t}$ = time rate of change of fluid storage (1/T).

The above term is also seen in the storage equation in Eq. (1).

For steady-state, unsaturated flow, the hydraulic conductivity is a function of the pressure head (ψ) of the soil. The general steady-state flow equation (Eq. 9) may be rewritten to include unsaturated flow:

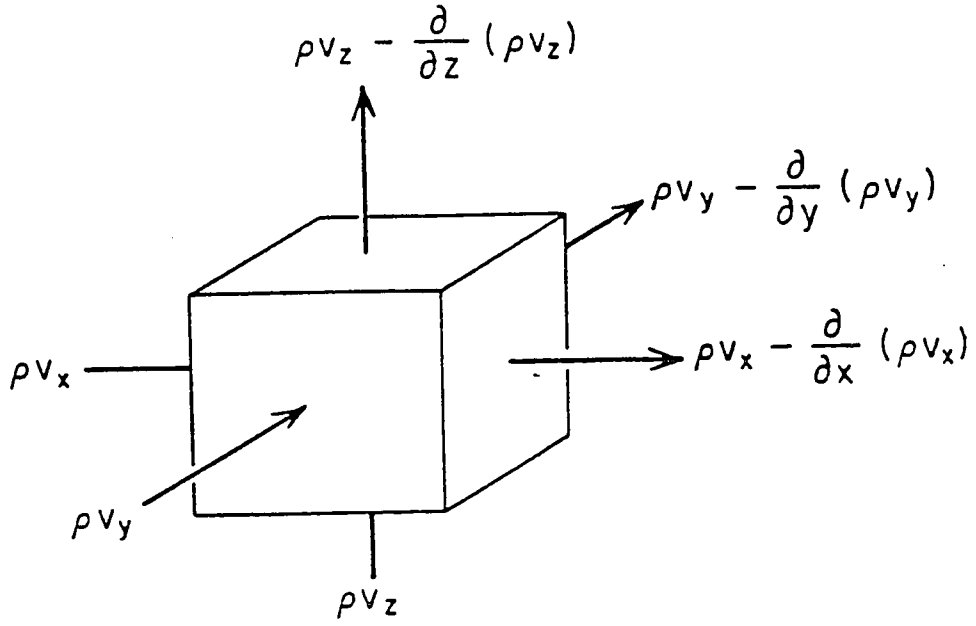

Figure 10. Elemental control volume for flow through porous media (from Freeze and Cherry, 1979).

$$\sum_{i=1}^{3}\sum_{j=1}^{3}\frac{\partial}{\partial x_i}\left[K^r(\psi)\,K^s_{ij}\frac{\partial h}{\partial x_j}\right]=0 \quad , \tag{11}$$

where

K^s_{ij} = hydraulic conductivity tensor at saturation (L/T),

$K^r(\psi)$ = relative hydraulic conductivity ($0 \le K^r \le 1$) where $K^r(\psi) = 1$ at saturation (dimensionless).

For transient, unsaturated flow, Eq. 11 is written:

$$\sum_{i=1}^{3}\sum_{j=1}^{3}\frac{\partial}{\partial x_i}\left[K^r(\psi)\,K^s_{ij}\frac{\partial h}{\partial x_j}\right]=\frac{\partial\theta}{\partial t} \quad , \tag{12}$$

where $\frac{\partial\theta}{\partial t}$ = the time rate of change in moisture (1/T).

Combining the transient saturated and unsaturated flow equations (Eqs. 10 and 12) yields a more general flow equation:

$$\sum_{i=1}^{3}\sum_{j=1}^{3}\frac{\partial}{\partial x_i}\left[K^r(\psi)\,K^s_{ij}\frac{\partial h}{\partial x_j}\right]=S_s\frac{\partial h}{\partial t}+\frac{\partial\theta}{\partial t} \quad , \tag{13}$$

Adding a vertical drainage term and a source/sink term completes the generalized, transient, variably saturated flow equation:

$$\sum_{i=1}^{3}\sum_{j=1}^{3}\frac{\partial}{\partial x_i}\left[K^r(\psi)\,K^s_{ij}\frac{\partial \psi}{\partial x_j}\right]+\sum_{i=1}^{3}\frac{\partial}{\partial x_i}K^r(\psi)\,K^s_{i3}-\frac{\partial\theta}{\partial t}-S_s\frac{\partial h}{\partial t}-S=0 \quad , \tag{14}$$

where $\sum_{i=1}^{3}\frac{\partial}{\partial x_i}K^r(\psi)\,K^s_{i3}$ = vertical drainage term and S = source/sink term.

The vertical drainage term is used to account for gravity drainage during a vertical plane simulation. For a more complete derivation of the transient variably saturated flow equation see Neuman (1973, 1975), Neuman et al. (1975), and Freeze and Cherry (1979).

UNSAT2 uses the Galerkin finite element method of weighted residuals to solve Equation 1. "A rather large number of articles on the applications of the finite element method, and especially of the Galerkin method, to the solution of two- and three-dimensional flow problems has been published in the literature of water resources and presented in special symposia, especially since the late 1960's" (Bear, 1979). As a result, the finite element method and the Galerkin method will not be further discussed. For a detailed discussion on the Galerkin method, the author suggests Pinder and Gray (1977), Bear (1979), and Wang and Anderson (1982).

Features of UNSAT2

UNSAT2 contains a variety of special features useful to the modeler. The special features include quadrilateral and triangular elements, variable flow direction, various boundaries (prescribed flux, seepage faces, evaporation or infiltration), the ability to handle water uptake by plant roots (various species), pumping wells (fully screened, partially screened, and/or variable pumping rates), steady-state or transient flow, non-linear soil properties, and the ability to model non-homogeneous anisotropic porous media. Three main assumptions are made by UNSAT2: no soil hysteresis, no soil deformation, and flow to a well (if used) is axisymmetric. If used with highly hysteretic or deformable soils, UNSAT2 may yield questionable results due to the model's assumptions.

Input parameters are divided into 19 "input groups" (which range from Group A - the Problem Title, to Group S - the Execution Terminator) to simplify the input process. Below is a complete list and explanation of the input parameters. The parameters marked with a "*" are required input for all problems. The parameters marked with a "+" are required for all unsaturated flow problems (Davis and Neuman, 1983).

Input Group:

* A: Problem Title - problem header or title, used to identify the problem's input and output.

* B: General Control Data - this group primarily consists of the cross-section data, such as number of nodal points, number of materials, type of flow system (horizontal, axisymmetric, or vertical), number of seepage faces, and maximum number of nodes along the seepage faces.

\+ C: Special Control Data - this group allows the user to access the various special functions of UNSAT2, such as well analysis, evaporation or infiltration, and plant transpiration.

* D: Material Control Data - the user must specify the number of paired entries of relative hydraulic conductivity vs moisture content, and pressure head vs moisture content for each discretized characteristic curve, corresponding to each unsaturated material.

E: Seepage Face Data - this group records the corresponding nodes for each seepage face.

F: Atmospheric Control Data - input required for this group is the maximum rate of infiltration or evaporation at the soil surface for each node that applies.

G: Soil Surface Geometric Data - the width of each evaporation or infiltration element at the surface must be specified in this input group to allow UNSAT2 to compute the flux through the evaporation or infiltration elements.

H: Root Zone Grid Data - data input for this input group is required only for the plant transpiration function. Input includes the number of vertical nodal columns and the number of nodes in each root zone column. Input must be repeated for each plant species.

I: Plant Species Data - data for this group are as required in Group H. Input consists of the wilting pressure head and maximum allowable rate of transpiration for each plant species.

J: Root Zone Data - data for this group are as required in group H. Input includes the width of each root zone, the sequential node numbers of each top and bottom node of each vertical root zone column, root-effectiveness coefficient for each plant species, and the soil material within each root zone.

K: Well Descriptive Date - input into this group requires that axisymmetric flow is specified in the General Control Data (Group B) and that the well lie along the left hand boundary of the finite element grid. Input consists of the nodal numbers of those nodes located at the bottom of the well, and of the seepage face nodes along the well casing (particularly if a well is partially screened or if it is partially penetrating the aquifer).

L: Well Control Data - this input group specifies the well parameters, such as the effective radius of the pumping well, radius of the well production tubing, discharge rate from the well, initial water level in the well, and an under-relaxation factor for iterative treatment of the well (default relaxation factor = 0.8).

* M: Time Step Data - for this input group, the user must specify the initial time step, maximum time step, initial time, multiplication factor for the time steps, maximum iteration time, and pressure head convergence criterion.

* N: Unit Conversion Factors - these parameters allow the user to input non-consistent unit data. UNSAT2 will convert the input data to consistent units, perform the calculations, and output in consistent or non-consistent units, depending upon the user's selection.

* O: Material Constant Properties - input data for this group are required for all problems. Input for this group supplies UNSAT2 with the constant hydraulic properties of each material. Input must include the first and second principal, saturated hydraulic conductivities (K^s_{11} and K^s_{22}, see figure 11), porosity, and specific storage of each material. For unsaturated flow, the specific storage is set equal to zero. Group O is repeated for each material.

\+ P: Unsaturated Material Properties - data required for this input group consist of the paired relative hydraulic conductivity vs moisture content values and the paired pressure head vs moisture content values that discretize each characteristic curve for each unsaturated material. Group P is repeated for each material.

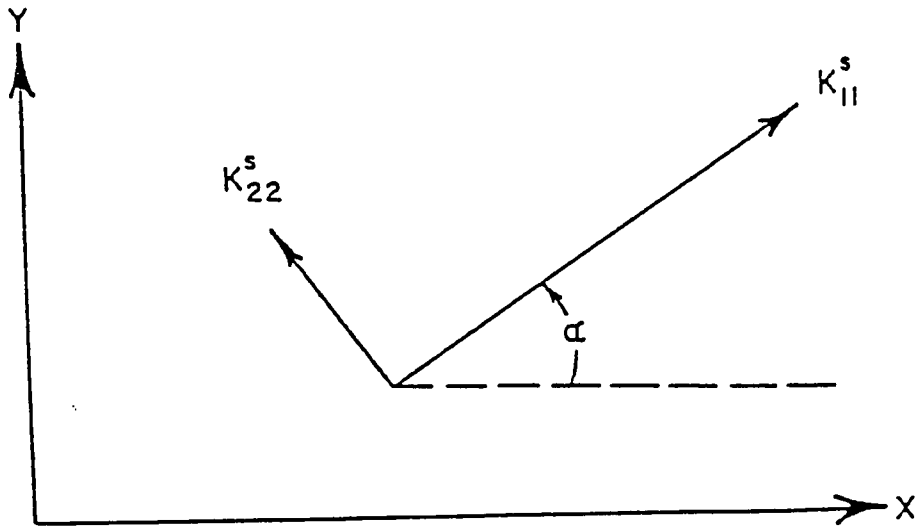

Figure 11. Angle α between the principal hydraulic conductivity and the X coordinate (from Davis and Neuman, 1983).

* Q: Nodal Point Data - data input of this group requires the user to specify the spacial coordinates (X and Y), boundary codes (no-flow, seepage face, etc.), initial pressure head values, boundary head values, boundary fluxes and/or source/sink terms for each nodal point.

* R: Element Data - input required for each element consists of the element number, the corner nodes of the element (i, j, k, l; for triangular elements k=l), the material assigned to the element, and the angle (in degrees) between the first principal hydraulic conductivity and the horizontal axis (fig. 11) used in the element.

RA-RG: Restart Feature - this input group enables the user to change a few input parameters/data and retain all the unchanged input data, thus only entering the changed parameters/data. This feature is useful in modeling transient situations, such as the changing pond level at LLNL's drainage retention basin.

* S: Execution Terminator - this function ends the program after the maximum program time (TMAX) has expired.

MODEL INPUT AND CALIBRATION

The following steps were used in configuring and calibrating UNSAT2 to simulate variably saturated flow in the vadose zone beneath the drainage retention basin of LLNL:

1. Define vadose zone lithology beneath the basin.
2. Construct the finite element grid.
3. Establish grid boundary conditions.
4. Estimate soil properties.
5. Estimate initial conditions.
6. Allow system to reach an equilibrium by simulating drainage to find relative steady-state initial condition values for nodes.
7. Perform computer simulation and compare results with field observations (i.e., resistance data).
8. Calibrate model - repeat steps 4-7 until strong correlation between computer simulation and field data develops.

UNSAT2 requires the input of a detailed finite element grid to simulate a specific flow region. The grid must be hydrogeologically accurate for proper simulation.

The development of the finite element grid for LLNL's drainage retention basin was a relatively detailed process. First, an accurate, scaled cross-section of the drainage retention basin, transecting LR-3-R, LR-4-P, LR-2-R, and LR-1-R, was drafted (figure 7). As previously mentioned, the basin lithology was simplified for modeling purposes by

combining adjacent geologic materials with similar hydrogeologic properties and characterizing them by their dominant constituents and by using simple lens shapes. A total of five different materials were grouped. They are: the upper clayey silt layer (material 1), the silty gravel unit (material 2), the upper silt unit (material 3), the upper sand lens (material 4), the lower sand unit (material 4), the lower silt unit (material 3), and the lower clay lens (material 5) (figure 12).

Second, a scaled finite element grid (55.3 feet x 260 feet; 1,680 cm x 7,920 cm) was created from the generalized geologic cross-section (figures 13 and 14). Element size was based on a number of contributing factors, such as lithology, anticipated pressure head changes and computer memory limitations. Smaller elements were used in areas where high hydraulic gradients were expected and in areas where lithology and resistance data were better known (i.e., in the vicinity of the borings). Larger elements were used in areas where lower hydraulic gradients were expected and where lithology and resistance data had to be interpolated (i.e., between boreholes). A strong effort was made to maintain fairly equidimensional element sizes, so as not to introduce additional numerical error into the flow problem.

The author chose boundary conditions according to node location and boundary function. The bottom nodes simulate the top of the water table and have been set as a no flow boundary to simulate the effect of a rising water table. The nodes along the right and left boundaries of the cross-section were set as no flow boundaries, permitting only vertical flow along those boundaries. Any other boundary (i.e., seepage face or constant head) would have been hydraulically incorrect and prevented vertical flow along the sides of the cross-section. Also, since the cross-section modeled does not extend to the basin margin, it is hydraulically "isolated" from the lateral flow effects that occur at the basin perimeter. As a result, these effects were not modeled. This type of boundary definition is consistent

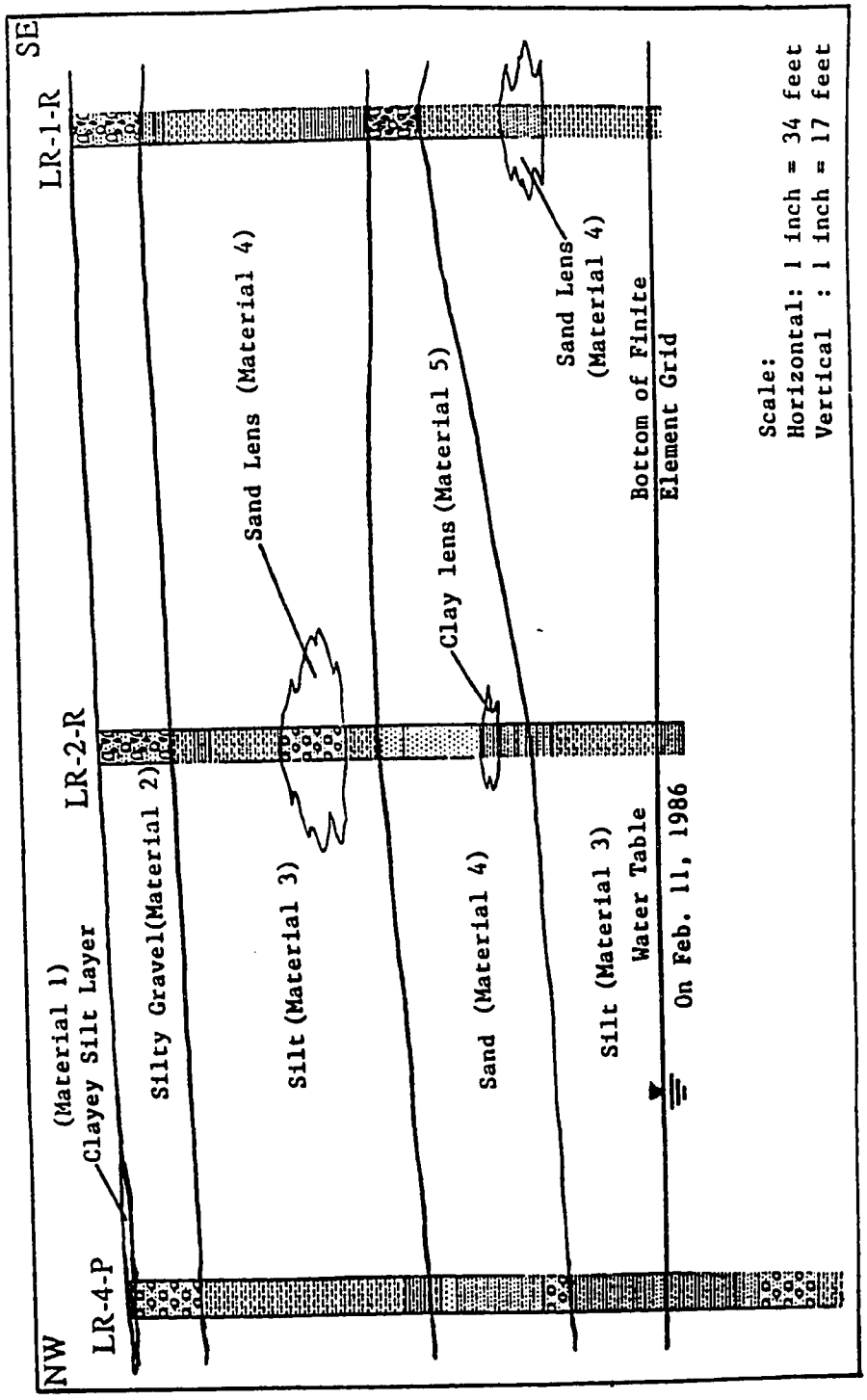

Figure 12. Generalized geologic cross-section through the drainage retention basin, showing the various materials used to model the basin lithology.

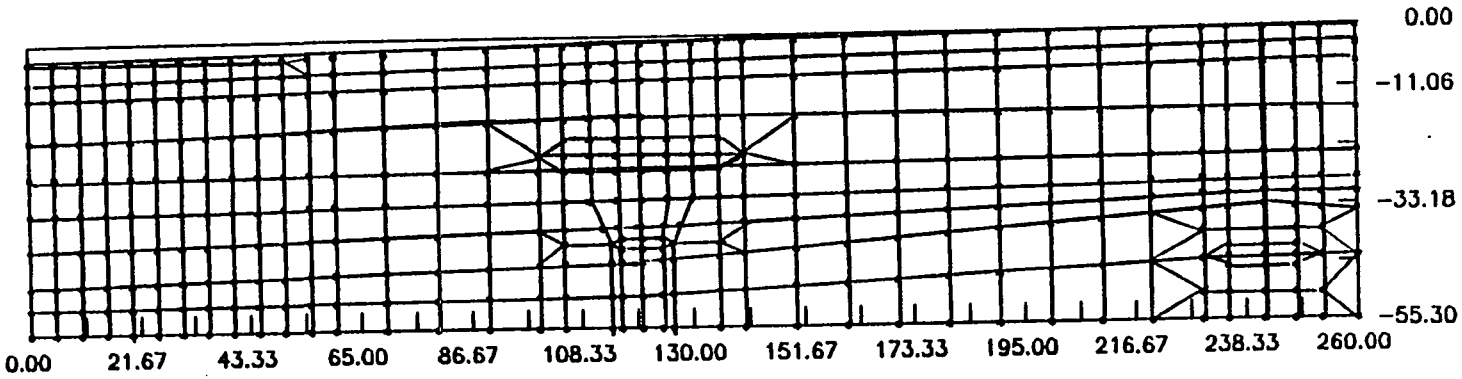

Figure 13. Finite element grid of drainage retention basin, displaying elements. X and Y axes are in feet. A total of 443 nodes and 414 elements were used in the construction of the finite element grid.

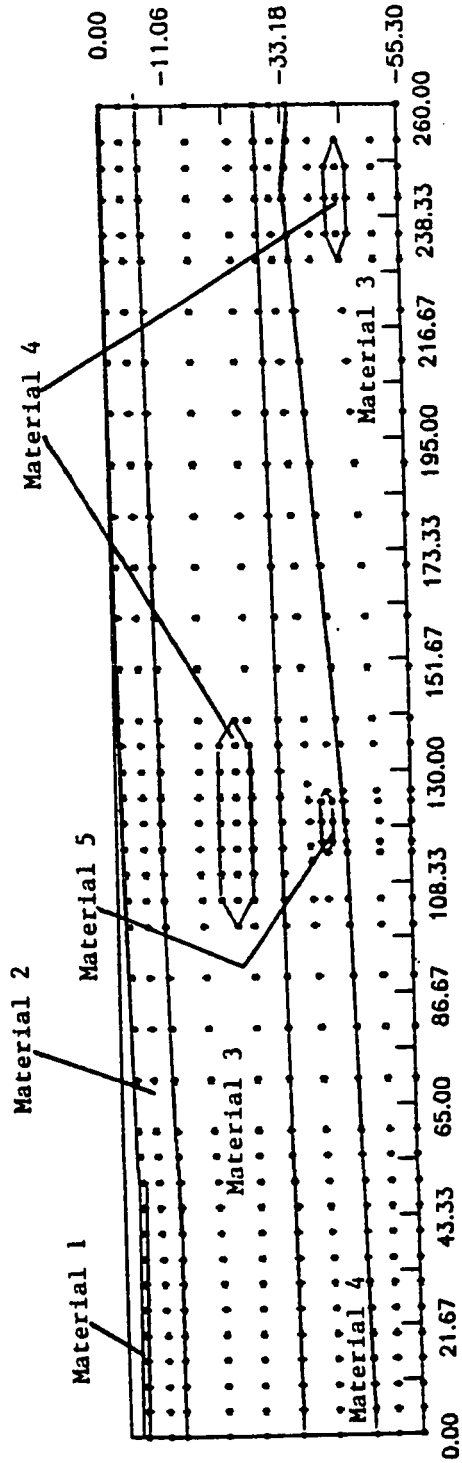

Figure 14. Cross-section of drainage retention basin displaying nodes and materials. X and Y axes are in feet.

with those of other researchers (Johnson et al., 1983; Trautwein et al., 1983; and McMahon and Dennehy, 1985) for simulating infiltration into the vadose zone. The primary purpose for this configuration is to isolate the modeled cross-section, to enable the model to simulate the ground water recharge contribution from only this section of the basin.

The surface nodes were set as constant head boundaries, signifying a constant pond level. For surface nodes where no ponded water was present, the nodes were treated as a boundary with no infiltration taking place.

Vadose zone resistance data were used to determine initial subsurface conditions. Figure 15 displays an initially saturated zone beneath the thin silt layer in the northwest portion of the basin. Past resistance data also indicates that this zone remains fairly moist throughout the fall, winter, and spring months. This is due to the fact that water is almost always ponded on the surface at this location. The permeability of the silt in the northwest corner is quite low and, as a result, runoff water will pond and slowly infiltrate into the vadose zone, keeping the soil beneath the silt layer in near saturated conditions throughout the rainy season.

To simulate the effects of intermittent precipitation, the non-ponded portion of the basin surface was initially assumed to be saturated for half a day, due to effects of the previous day's precipitation. This is consistent with the author's own recent observations and those of Toney (personal communication, 1988).

Unsaturated soil characteristic curves (pressure head vs moisture content and relative hydraulic conductivity vs moisture content) were chosen from Mualem (1976). Five soils were chosen, based upon their lithologic classification, constituent analysis, and measured hydraulic parameters to represent the site soil's hydrogeologic response to infiltration. All five soils chosen closely matched the descriptions and characteristics of the

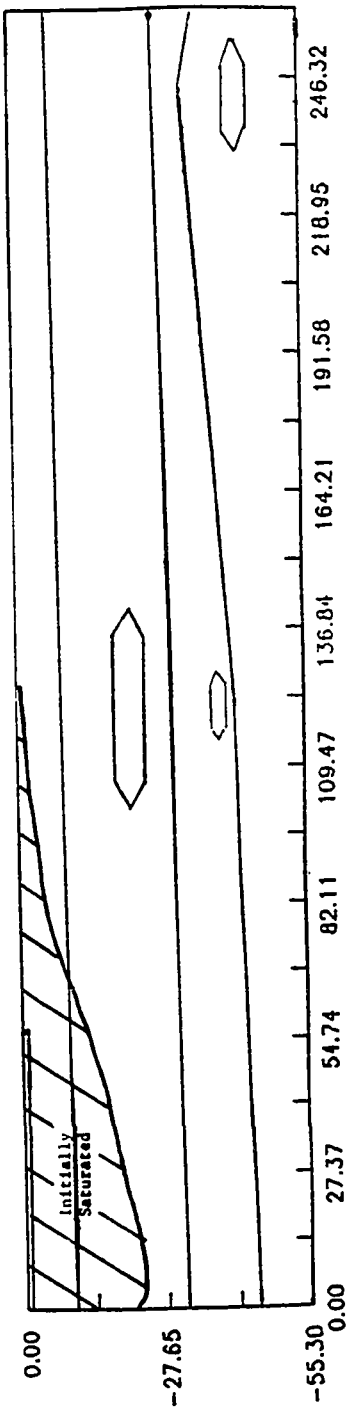

Figure 15. Initially saturated zone beneath LR-3-R. X and Y axes are in feet.

LLNL soils. When possible, drying curves were ignored and wetting curves were used, because the model does not incorporate hysteresis. If a wetting curve for the matching soil material had not been developed, then the drying curve was used for the soil. Appendix B contains the characteristic curves of the five soil materials used to simulate the LLNL site soils.

The reasoning behind choosing known soil characteristic curves to represent site soils instead of developing them for the site is three fold. First, it was not the focus of this study to develop soil characteristic curves for the site soils. Second, the process of measuring soil characteristics is a very long one, and would be extremely time consuming for this project. Last, soil characteristic curves from core samples at the site would not truly represent the site soils due to the heterogeneous nature of the site soils as indicated by the geologic well logs.

Qualitative initial soil moisture values were obtained by analyzing the soil resistance values on February 11, 1986, and the lowest resistance values obtained during the storm (for modeling purposes, these were assumed to indicate saturation). From this information, the author was able to calculate a relative change in moisture content, back calculate from the chosen characteristic curves, and obtain an initial moisture content value and therefore initial pressure head value for each material. These were only rough initial estimates and required several recalibrations to obtain proper initial conditions for a working simulation model, as discussed in the Simulation Results and Discussion section.

Modeling the February 1986 Storm

As previously mentioned, the significant storm used to calibrate the model occurred between February 11 and 19, 1986. Toney (personal communication, 1988) monitored the

hydrogeologic response to the storm by monitoring drainage retention basin water levels, local monitoring well water level responses, precipitation, and basin soil resistance. The basin water levels and finite element grid dimensions were converted into centimeters (for computer model unit consistency) and unknown water levels were extrapolated between known days, see Appendix C. The water levels (in centimeters) were used as surface node pressure heads, corresponding to the pond level at the particular time step. The surface nodes where no ponded water was initially present were set with an initial constant pressure head of zero for every other time step (time step = half day), signifying surface soil saturation from intermittent precipitation. This was repeated until the fourth day of simulation, when the entire modeled cross-section surface was submerged. Resistance data were used to develop the qualitative conceptual model of the downward propagation of the wetting front through the vadose zone. Figure 16 shows the spatial and temporal wetting front pattern (developed from the resistance data) to which the computer simulation was compared for calibration purposes for the February 1986 storm. By calibrating the computer model to simulate the propagation of the wetting front for this known set of data (i.e., February 1986 storm data), it was hoped to gain valuable knowledge as to how the wetting front migrates, to determine what effects the lithology might have on the migration pattern and the type of hydrogeologic conditions that prevail in the vadose zone beneath LLNL's drainage retention basin under severe storm conditions, and to develop a predictive tool to simulate other situations. Appendix D contains a complete copy of the February 1986 storm input data required by UNSAT2.

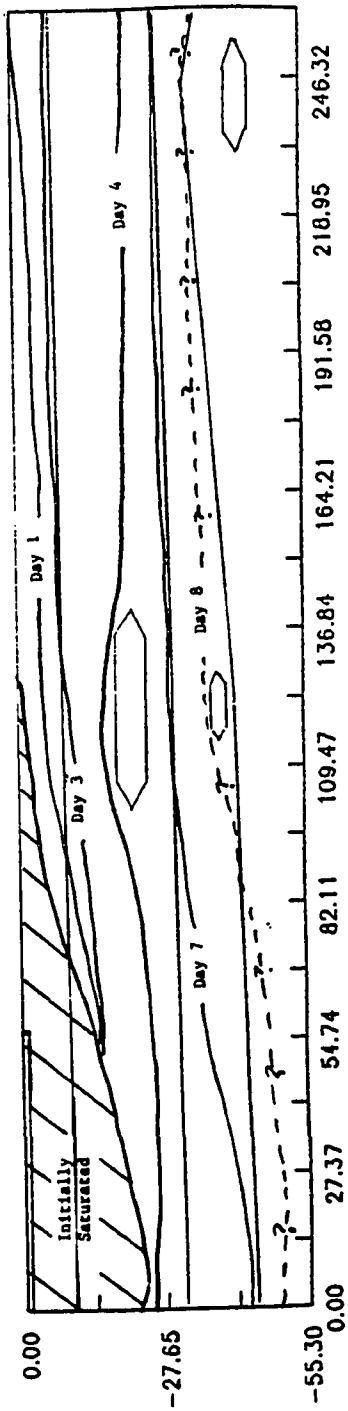

Figure 16. Wetting front movement in the vadose zone produced by the February 1986 storm (from resistance data). Note initially saturated zone corresponding to February 11, 1986. X and Y axes are in feet.

SIMULATION RESULTS AND DISCUSSION

Sensitivity Analysis

During the iterative model calibration process, a sensitivity analysis was performed on UNSAT2 to determine the model's sensitivity to the numerical and hydrogeologic parameters required for input into the model. The sensitivity of the model to a particular input variable was obtained by consecutively running the model, slightly changing the input variable after each iteration, while holding all other variables constant, and noting the change in model output created by the change in input. The following is a description of the results of the sensitivity analysis.

First, the model was found to be the most sensitive to the saturated hydraulic conductivity of each soil material. Major changes in the movement of the wetting front could be obtained by relatively small changes in the saturated hydraulic conductivity of a material. This was concluded after varying the saturated hydraulic conductivity of soil materials 2, 3, and 4, over several orders of magnitude, and observing the effects of the three separate analyses. This finding was consistent with that of Trautwein et al. (1983).

Second, by changing the unsaturated soil characteristic curves of one soil for those of a similar description, it was revealed that the characteristic curves are of significant importance. For example, a moisture content vs pressure head characteristic curve displaying a high air entry pressure caused the material to become effectively saturated at relatively high suction (i.e., negative pressure head). Due to the high suction and corresponding low relative hydraulic conductivity, a noticeable pressure head build up in

the soil occurred. It was important that the correct unsaturated characteristic curves were chosen to properly simulate the hydrogeologic effects of the LLNL soils.

Third, the model was found to be only moderately sensitive to the initial soil suction values, unless they were chosen to be excessively dry or excessively moist. This was concluded after varying the initial soil suction values from -400 cm to 0 cm, during the calibration process. If the initial soil suction values were chosen to be excessively moist relative to equilibrium or steady-state values, the model would allow the corresponding nodes to "drain" until relative steady-state values were obtained. The excess moisture drained from the moist nodes would eventually migrate to the bottom no-flow boundary and simulate a significant premature rise in the ground water table.

Last, element size was found to be an important factor in the model's accuracy. Large, less dense, elements tended to produce slightly less reasonable results. This is most likely the result of the model having to average soil material's hydrogeologic properties and pressure heads over a larger element area, therefore creating a less accurate average over the area. Generally, the averaging effect of the larger elements is small. However, in the event of significant changes in pressure heads (i.e., large moisture or pressure gradients) over one time step, the effect can be noticeable. This effect can be seen on the fourteenth day of simulation of the February 1986 storm near the bottom no-flow boundary at LR-1-R, when the water table "bows" a slight amount in the larger elements. Conversely, smaller elements and more densely spaced elements tended to produce more reasonable responses.

Results and Discussion

The following section contains a comprehensive discussion of the vadose zone computer simulation results. Four simulations were run with the calibrated model: the

February 1986 storm, a lateral flow simulation, a deep ponding simulation, and a January 1988 storm simulation. A list of figures is given at the beginning of each simulation discussion. The figures are to be followed during the discussion to enhance the reader's conception of the movement of the wetting front in the vadose zone created by these four modeled situations.

February 1986 Storm Simulation

On February 11, 1986, a severe storm hit the Livermore Valley, precipitating 4.89 inches (12.42 cm) of rain over a 9 day period, most of which was precipitated between February 15 - 20, 1986. As a result of the severe storm, LLNL's drainage retention basin filled to its 10 foot (304.8 cm) maximum level and overflowed for 2 days. Figures 17 through 31 contain scaled contour plots of the simulated wetting front propagation through the vadose zone during the severe February 11-20, 1986, storm at LLNL. The discussion below refers to these figures. For more detailed nodal point moisture content plots for the February 1986 storm, see Appendix E.

As previously mentioned, the spatial and temporal characteristics of the wetting front produced by the February 1986 storm were determined by soil resistance data. The resistance data was used to calibrate the model initially, and at 1, 3, 4, and 7 days after the onset of the storm (February 11, 1986). The resistance data for the intermediate time steps is fairly inconclusive; hence the need for computer simulation.

The initial subsurface pressure head values were determined through an iterative process consisting of approximating node pressure head values and allowing the model to drain for about 30 days (simulated), until a relative equilibrium had been reached. This procedure is consistent with modeling efforts of Trautwein et al. (1983). The "equilibrium" or steady-state pressure head values were used as approximate initial

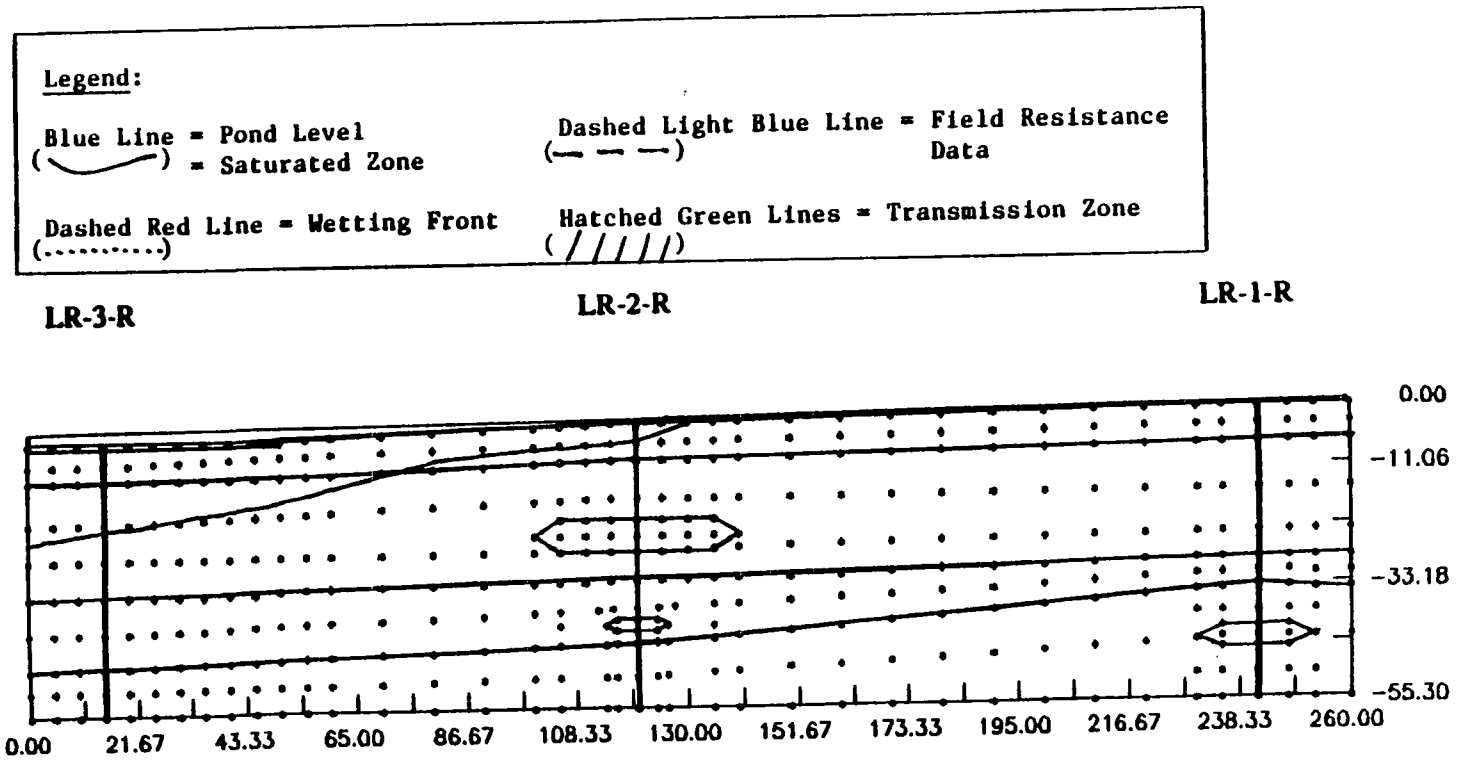

Figure 17. The initially saturated zone and saturated surface (blue line) used to simulate the February 1986 storm initial conditions (Feb. 11, 1986). The surface between LR-2-R and LR-1-R was saturated for one-half day to simulate the effects of precipitation. Initial pond level at LR-3-R is 1.73 feet (52.58 cm). Both the X and the Y coordinates are in feet.

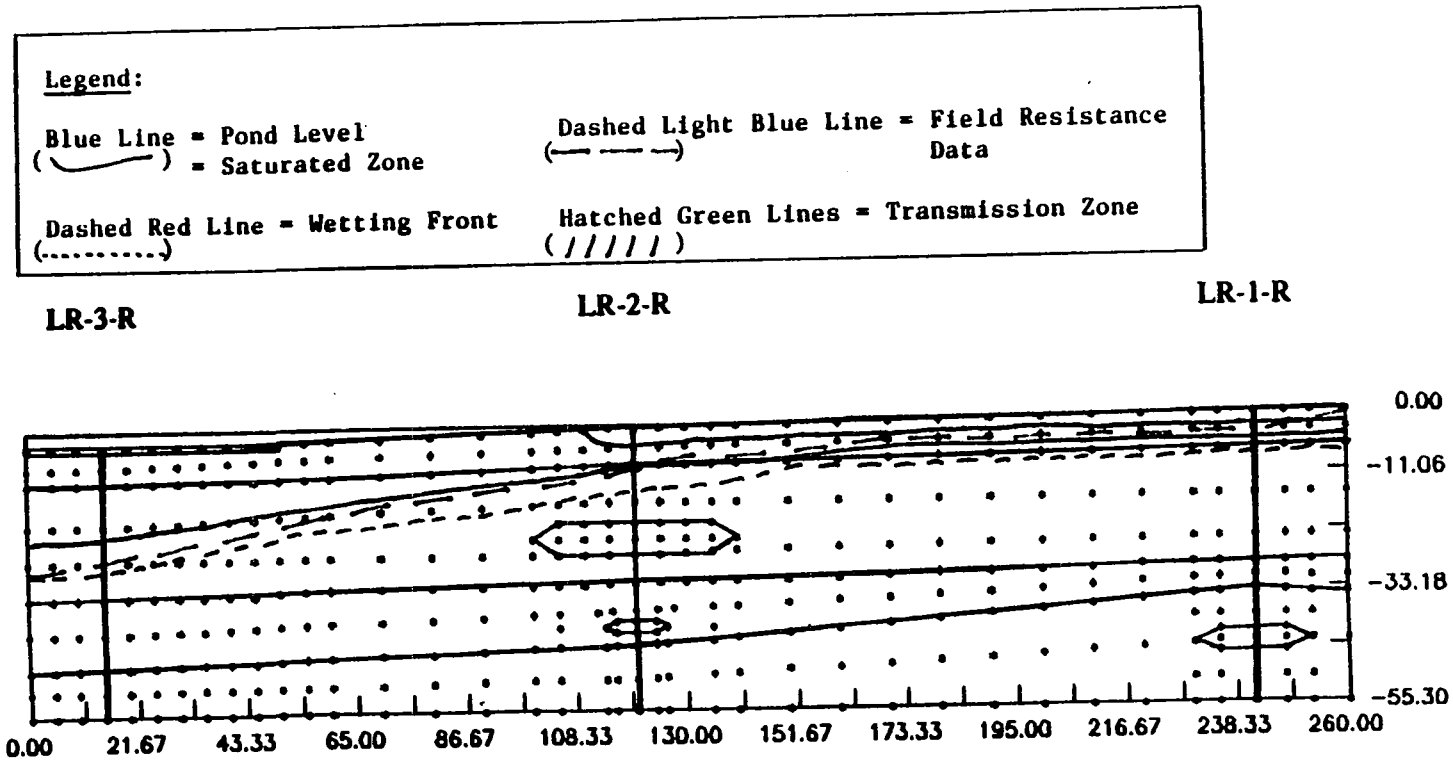

Figure 18. Saturated zone (blue contour) and wetting front (dashed red line) after 1 day of simulation. Dashed light blue line indicates position of wetting front determined by field soil resistance data, used to calibrate the model. Pond level at LR-3-R is 1.77 feet (54.03 cm).

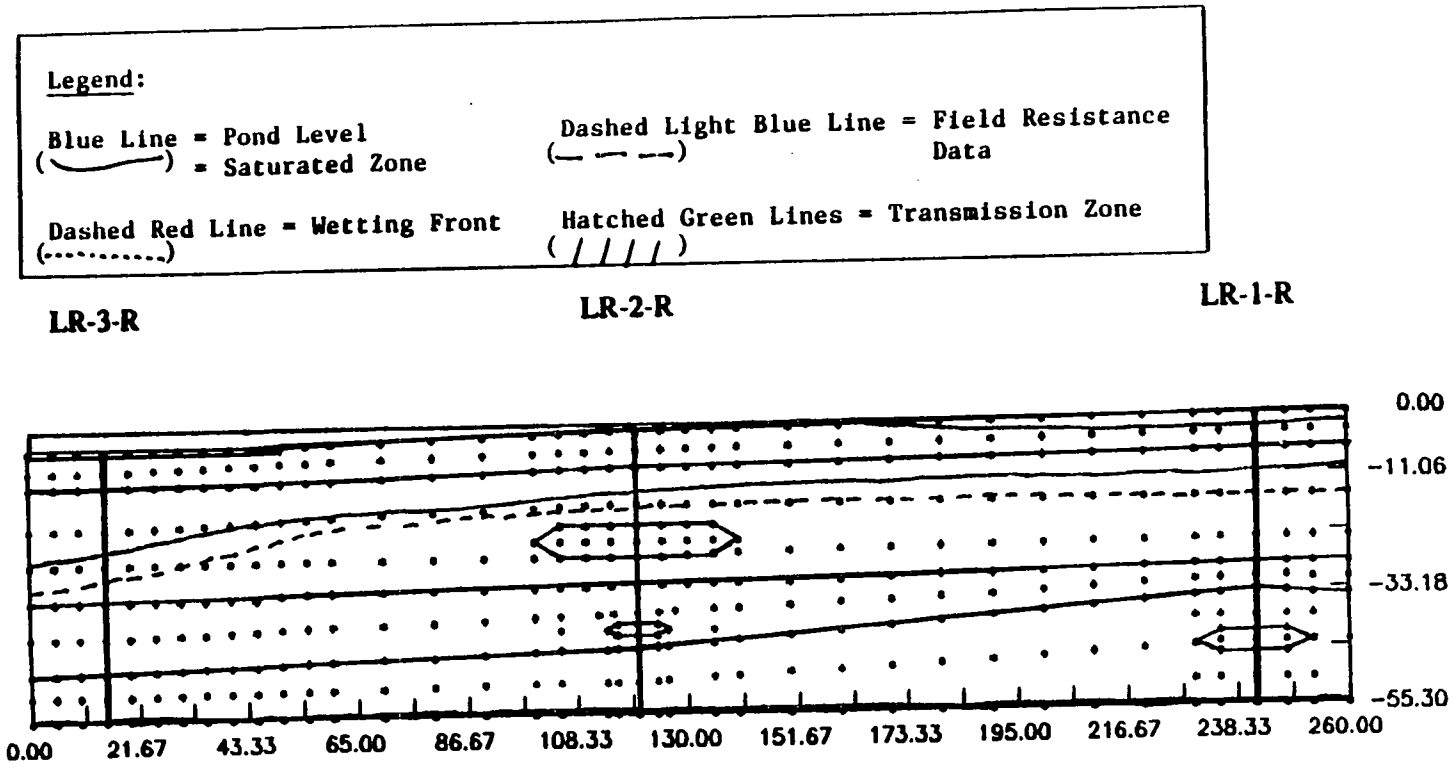

Figure 19. Saturated zone and wetting front after 2 days of simulation. Note insignificant rise in water table (bottom no-flow boundary) due to slight desaturation of lower nodes. Pond level at LR-3-R is 2.49 feet (75.9 cm). LR-2-R has become submerged at this time step.

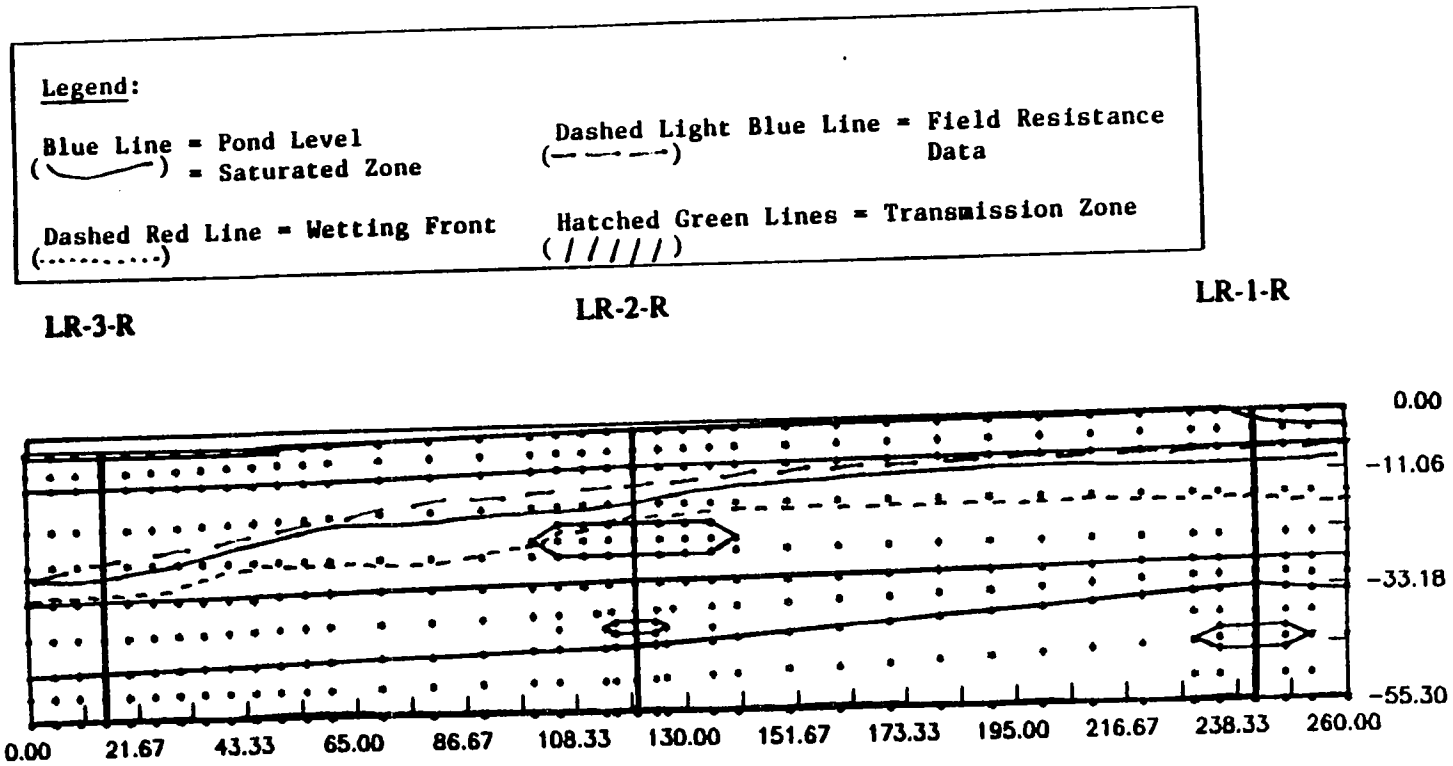

Figure 20. Saturated zone and wetting front after 3 days of simulation, corresponding to February 14, 1986. Pond level at LR-3-R is 3.19 feet (97.28 cm). Dashed light blue line indicates position of wetting front determine by field soil resistance data, used to calibrate the model. The ponded water has nearly reached LR-3-R.

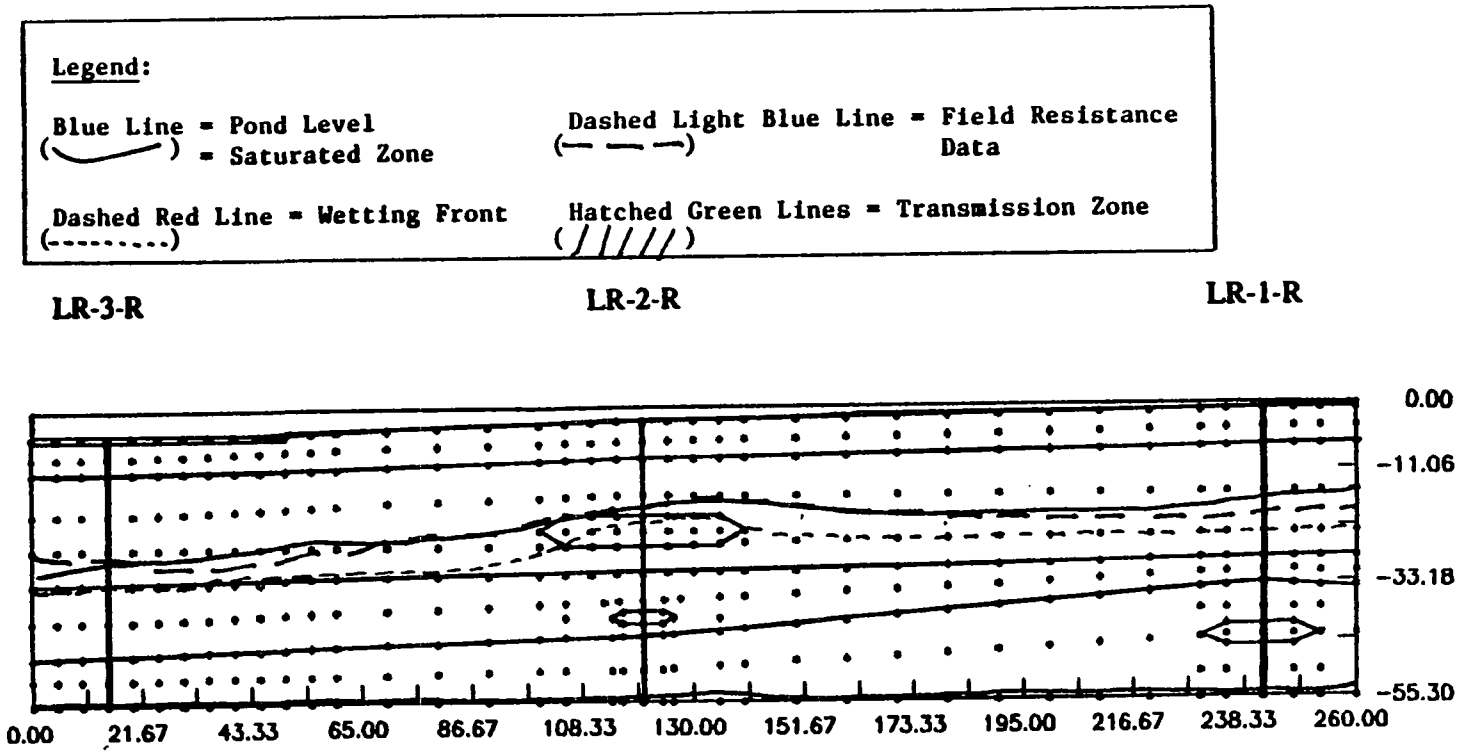

Figure 21. Saturated zone and wetting front after 4 days of simulation. Dashed light blue line indicates position of wetting front determined by field soil resistance data, used to calibrate the mode. The pond level at LR-3-R is 3.25 feet (99.21 cm). All three resistance cell strings have become submerged by this time step.

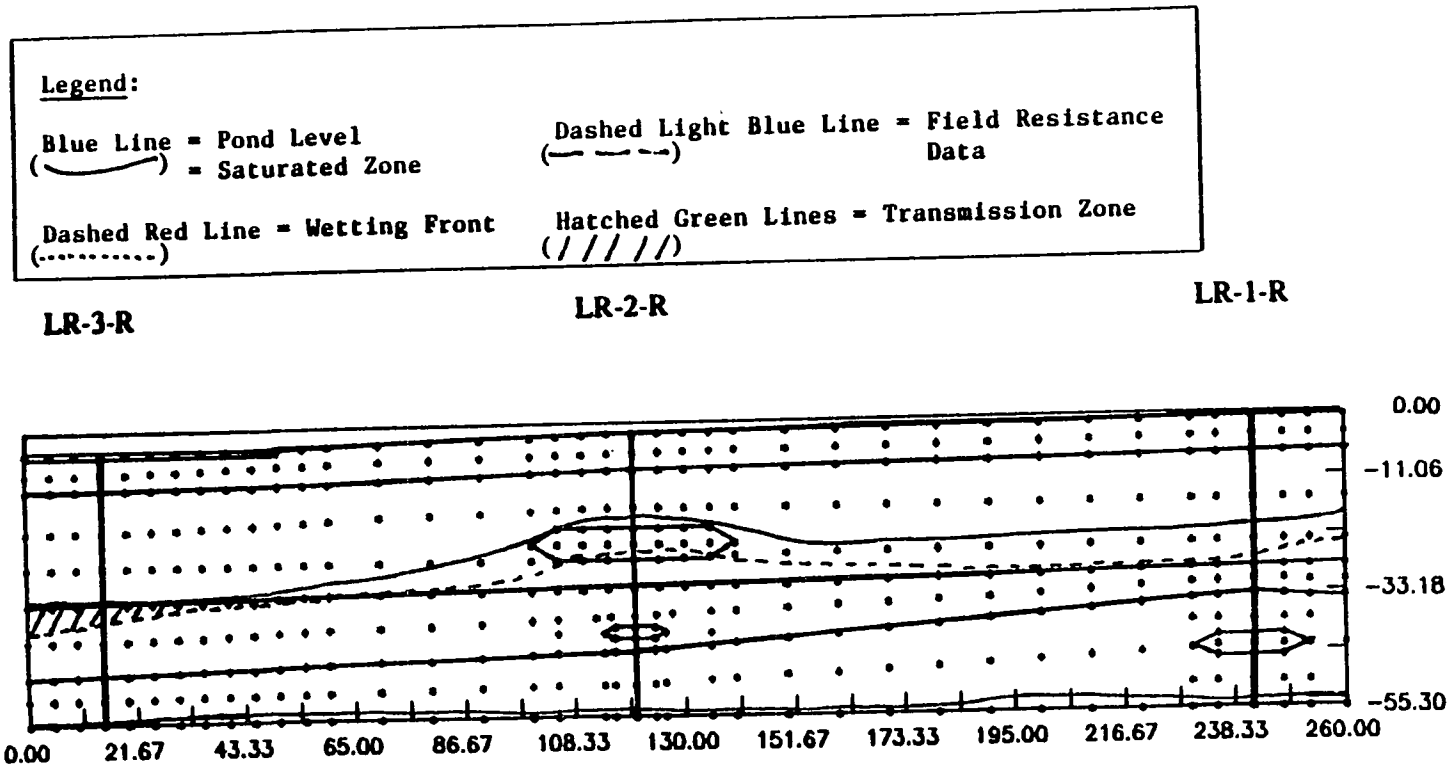

Figure 22. Saturated zone, wetting front, and transmission zone after 5 days of simulation of the February 1986 storm. Note the development of the moisture transmission zone (hatched pattern) at LR-3-R. Pond level at LR-3-R is 3.32 feet (101.14 cm).

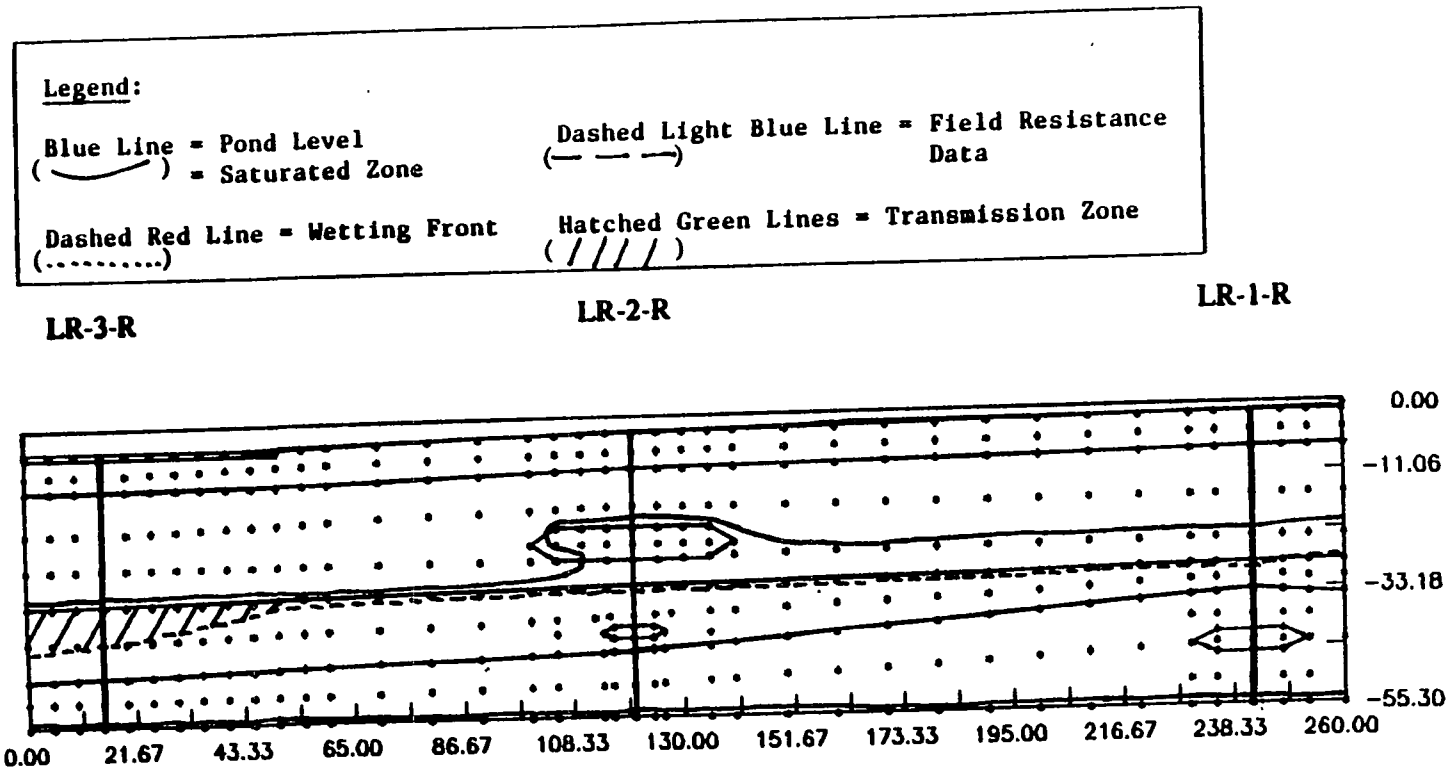

Figure 23. Wetting front, saturated zone, and transmission zone migration by the sixth day of simulation. Note the moisture penetration of the upper sand lens from the left (NW) side and the continued SE development of the transmission zone in the lower sand layer. Pond level at LR-3-R is 3.9 feet (119.02 cm).

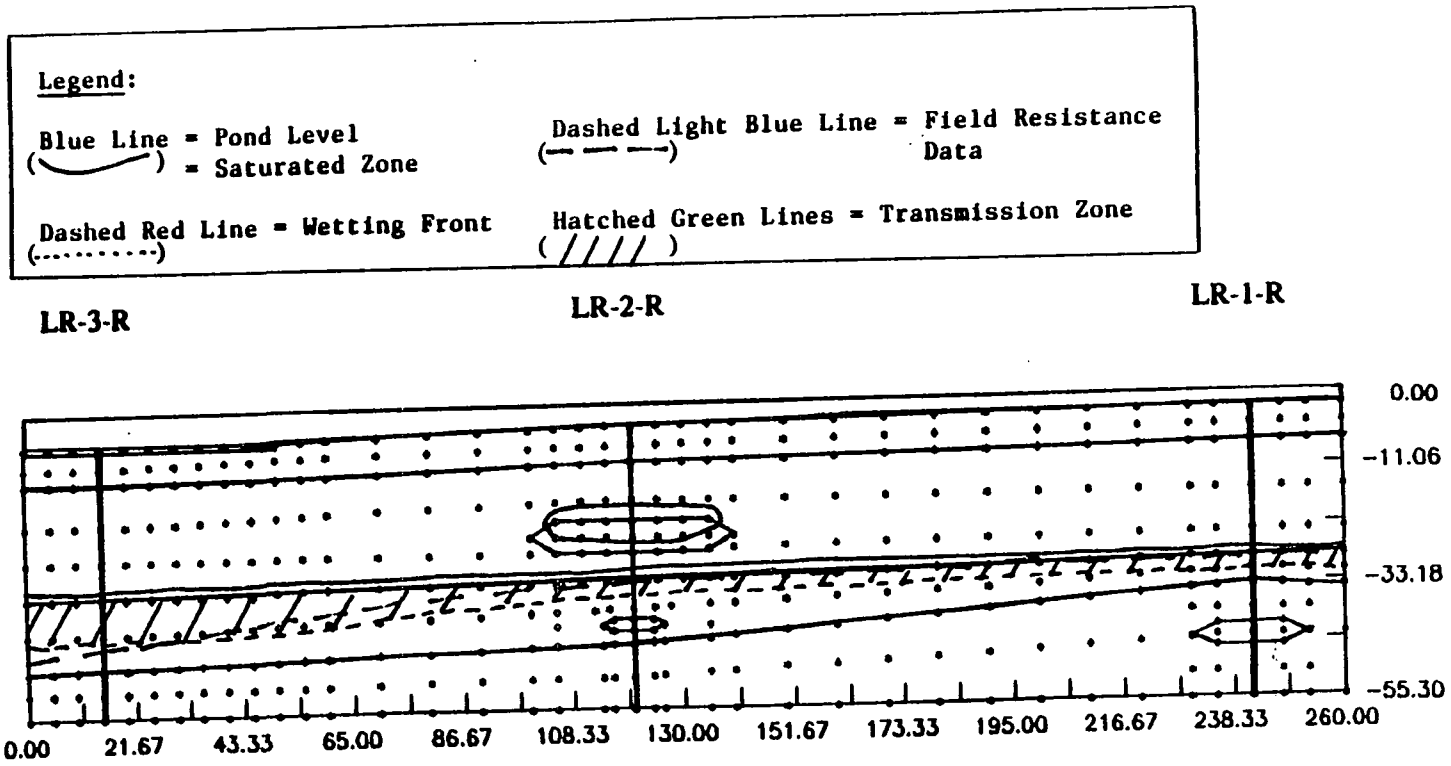

Figure 24. Wetting front, saturated zone and transmission zone movement after 7 days of storm simulation. By this time step, the saturated zone had reached the upper silt/lower sand interface and the transmission zone had fully developed along the interface. Dashed light blue line indicates position of wetting front determined by field soil resistance data, used to calibrate the model. Pond level at LR-3-R is 5.02 feet (152.86 cm).

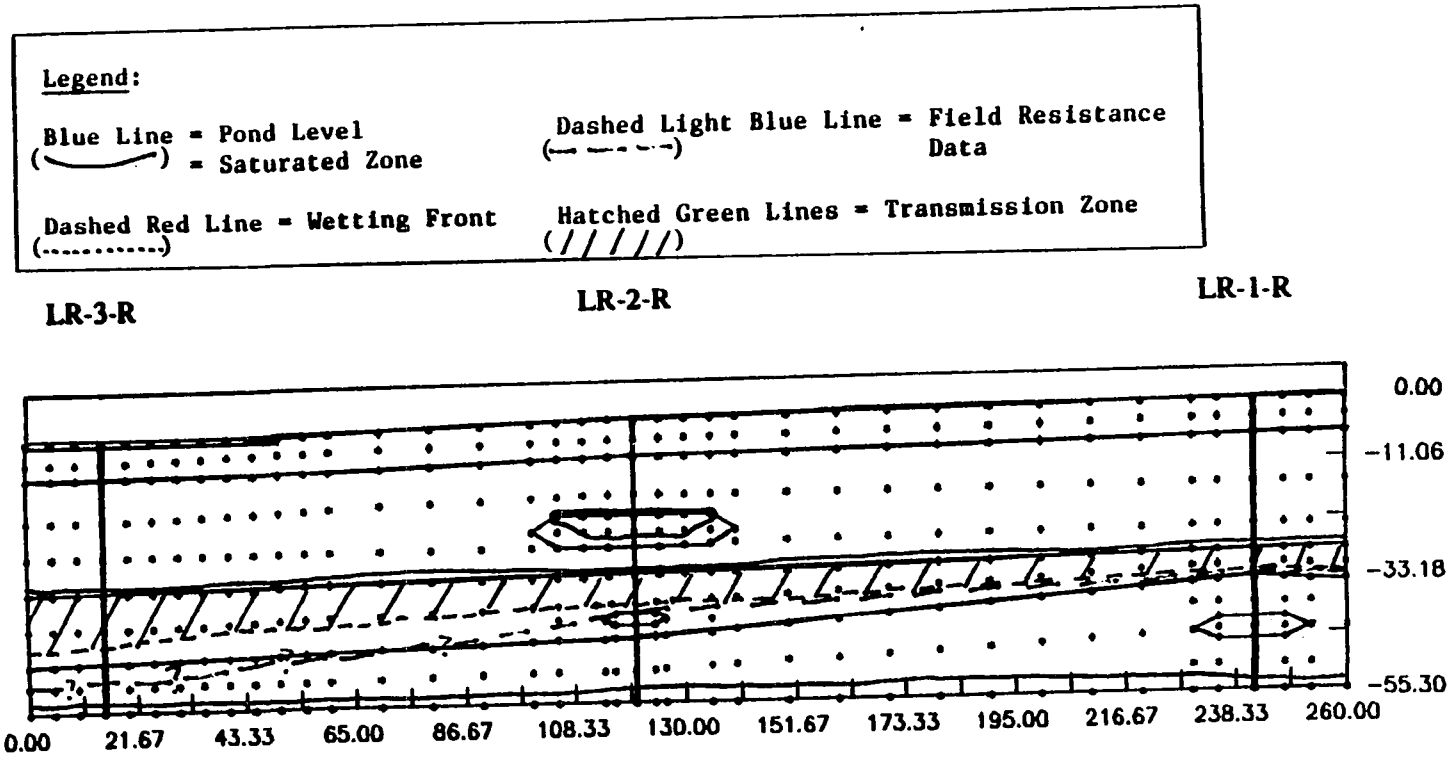

Figure 25. Saturated zone, wetting front, and transmission zone after 8 days of simulation. Dashed light blue line indicates position of wetting front determined by field soil resistance data, used to calibrate the model. Ground water table still has not risen significantly. Field data indicates an 11 foot (335 cm) rise in water table by this time step. Pond level at LR-3-R has risen to 7.79 feet (237.29 cm).

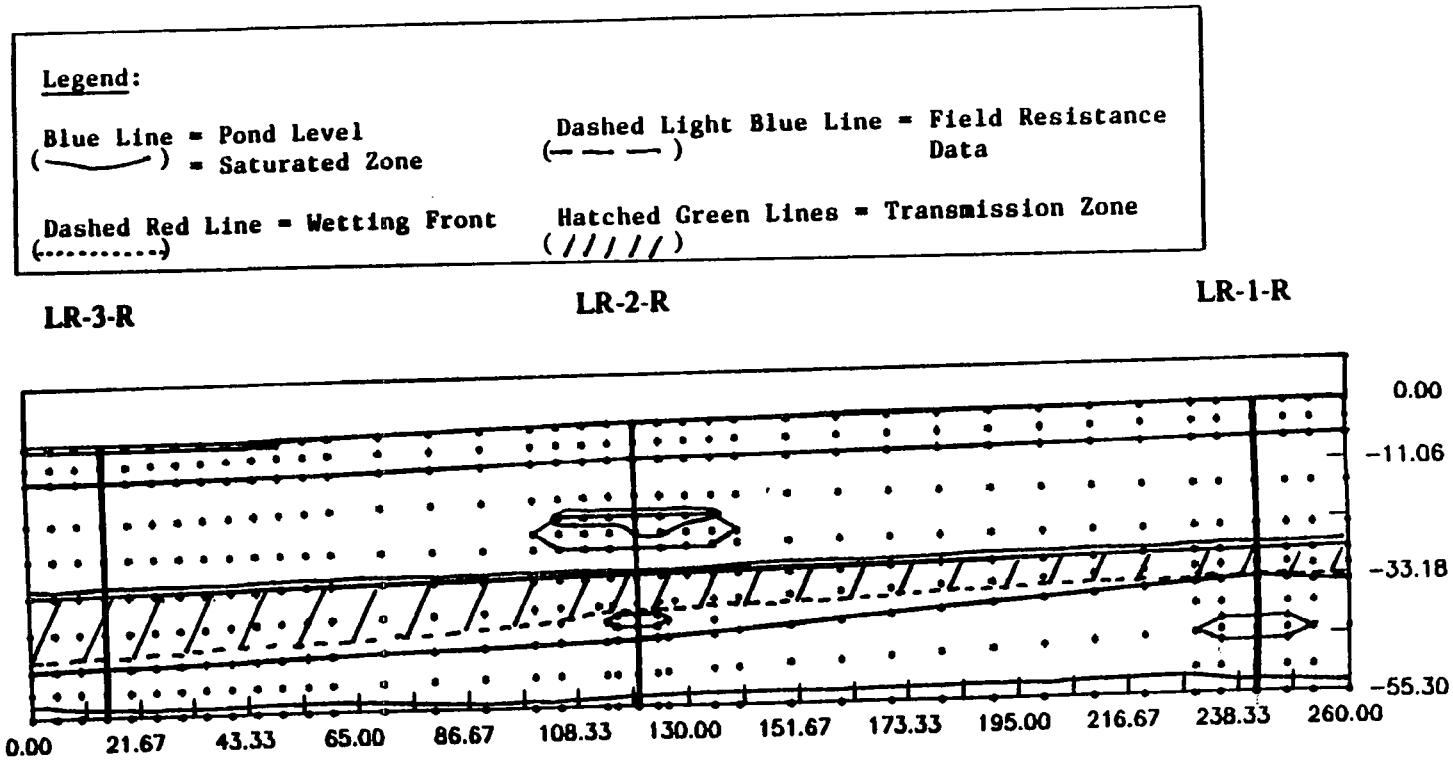

Figure 26. Saturated zone, wetting front, and transmission zone after 9 days of simulation. Note fairly stable ground water table. Pond level at LR-3-R has reached its maximum of 10 feet (304 cm).

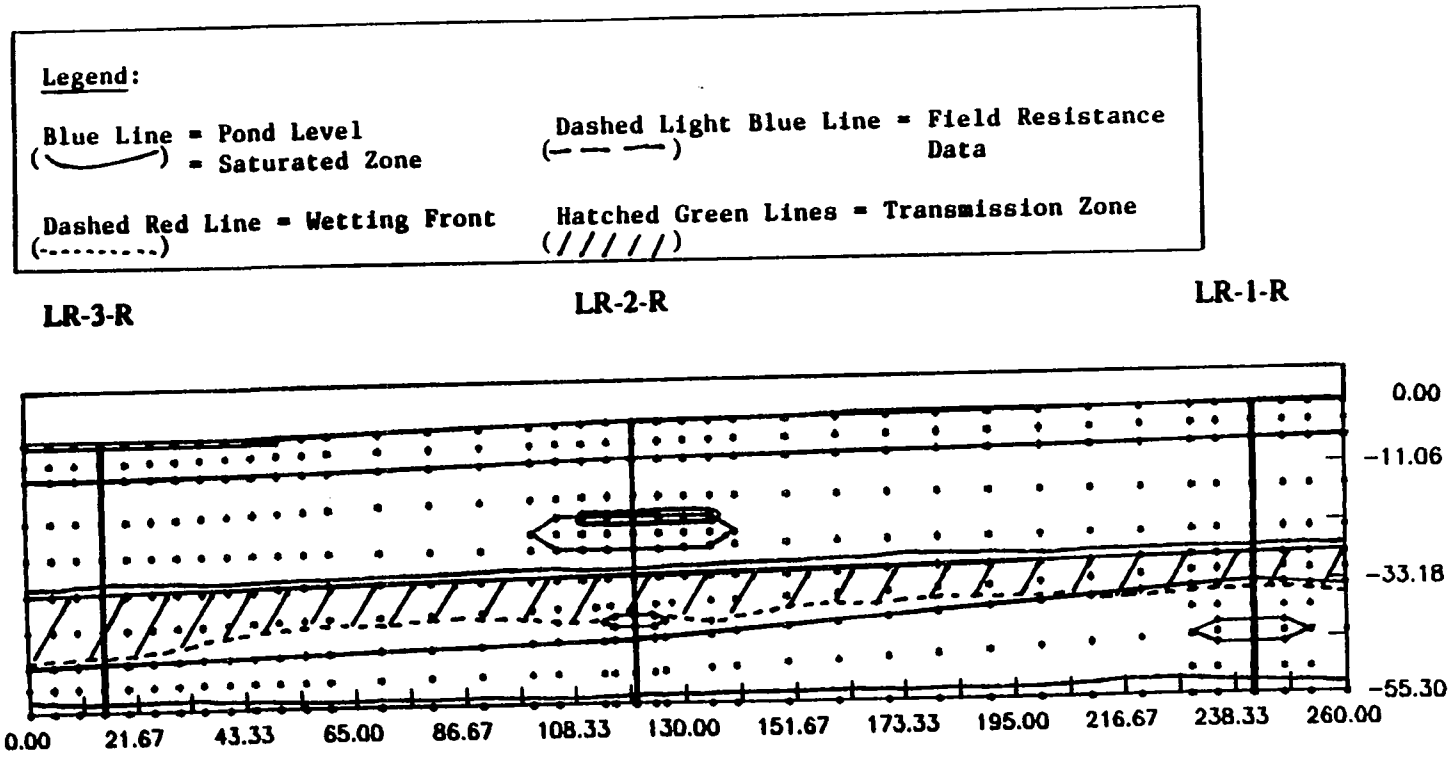

Figure 27. Saturated zone, wetting front, and transmission zone after 10 days of simulation. Note the distortion of the wetting front around the clay lens at LR-2-R. Pond level at LR-3-R has dropped to 8.36 feet (254.66 cm).

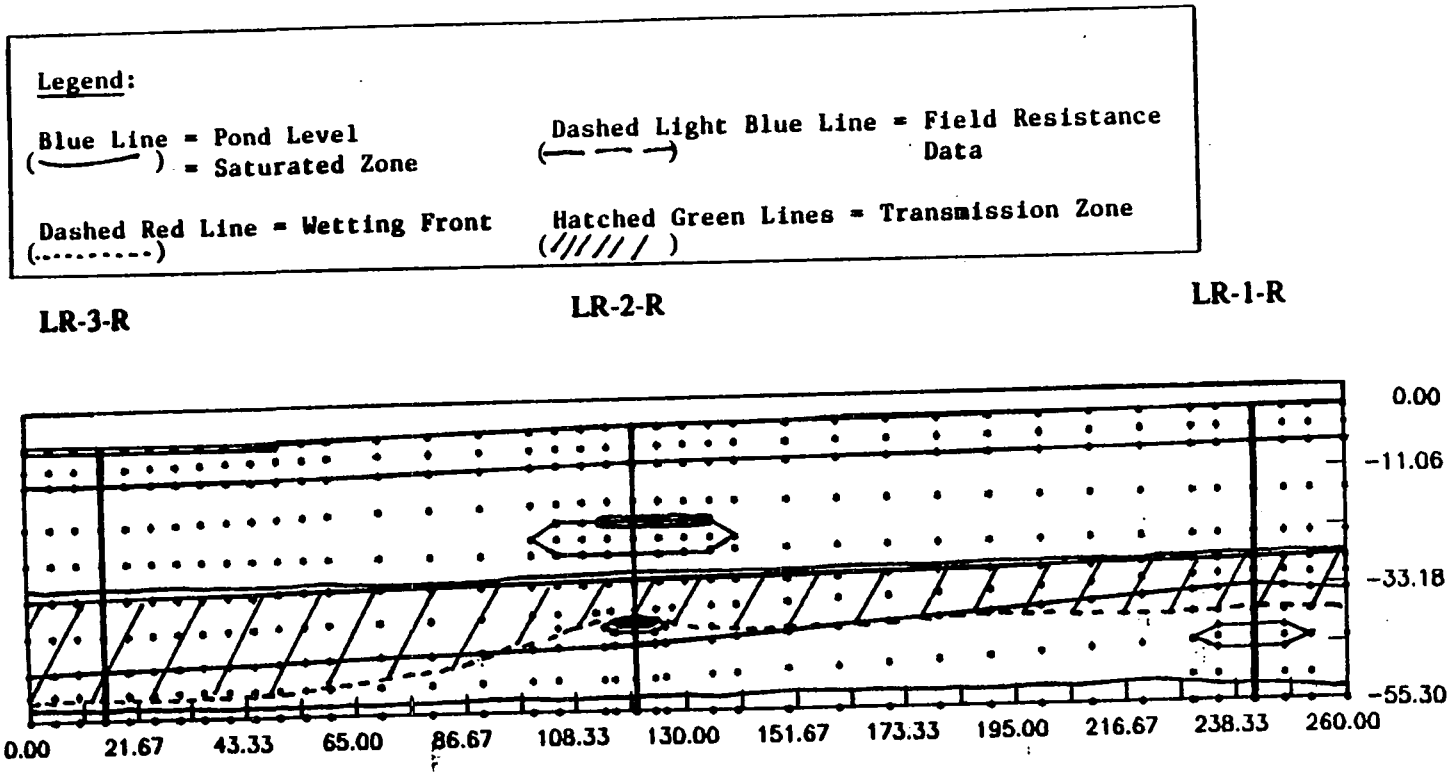

Figure 28. Wetting front, saturated zone, and transmission zone after 11 days of simulation. The wetting front has reached the water table by this time step. Note small perched moisture zone at the clay lens at LR-2-R. Pond level at LR-3-R has dropped to 6.69 feet (204.06 cm).

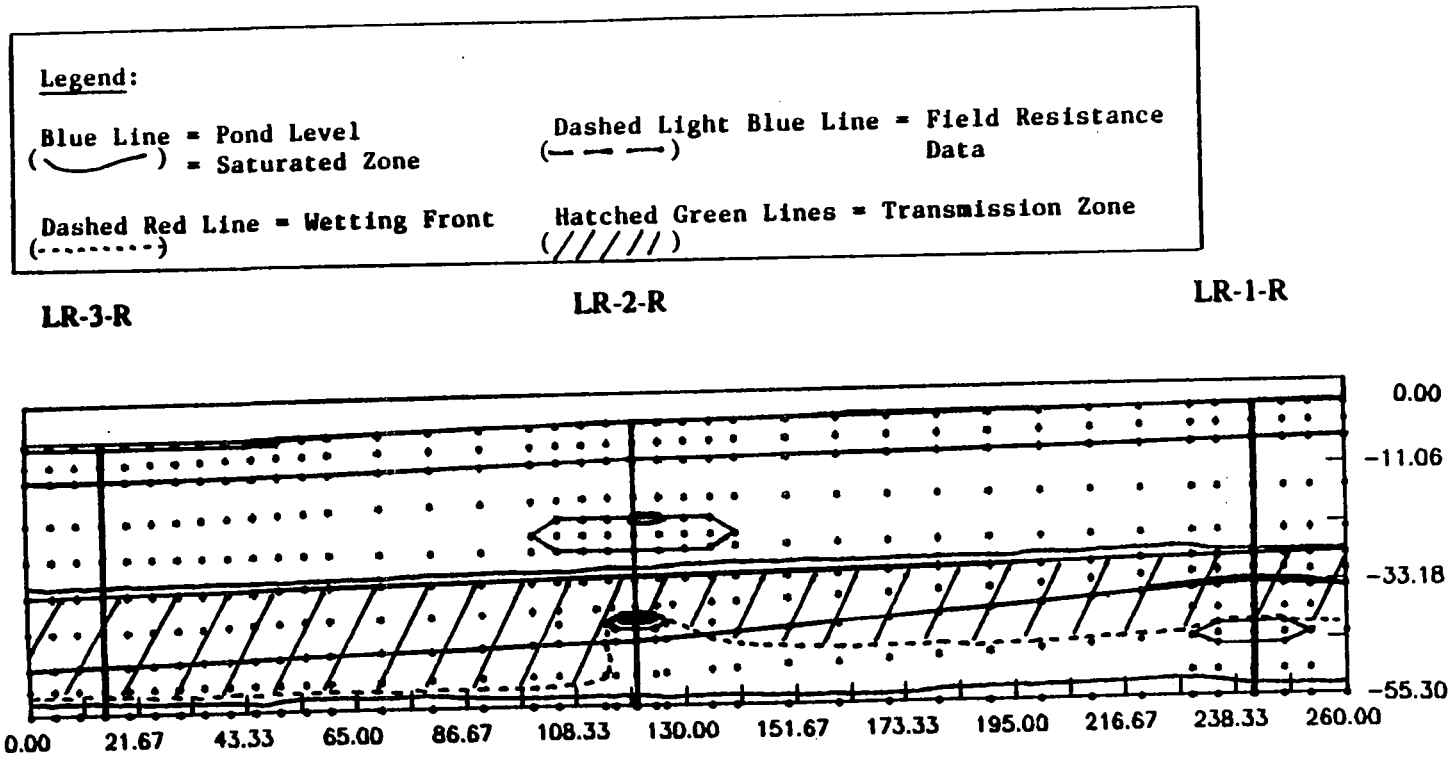

Figure 29. Saturated zone, wetting front, and transmission zone after 12 days of simulation. Note severe distoration of wetting front around the clay lens at LR-2-R and the development of a second perched moisture zone at LR-1-R. Pond Level at LR-3-R is 6.67 feet (203.15 cm).

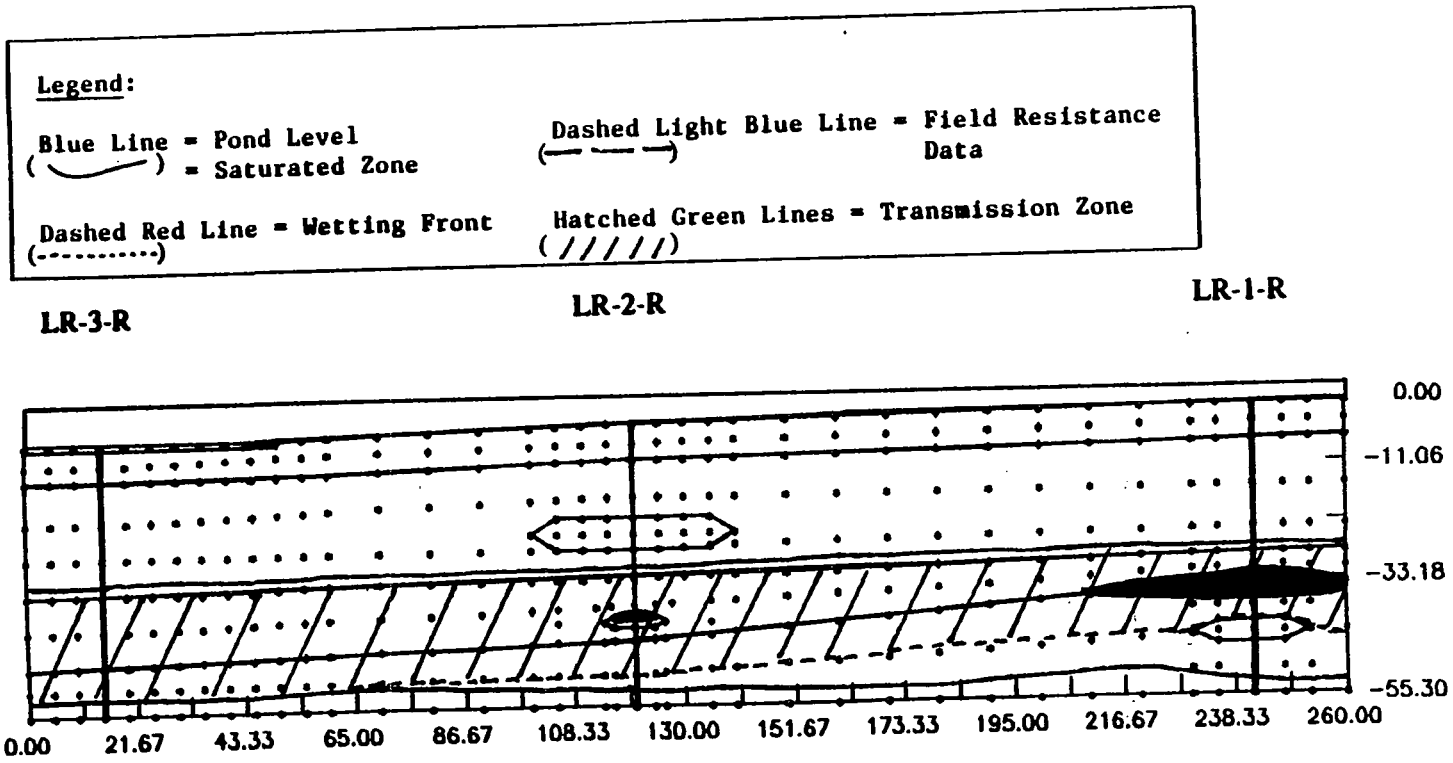

Figure 30. Saturated zone, wetting front, and transmission zone after 13 days. Note the continued development of both perched moisture zones. Pond level at LR-3-R is 5.96 feet (181.81 cm).

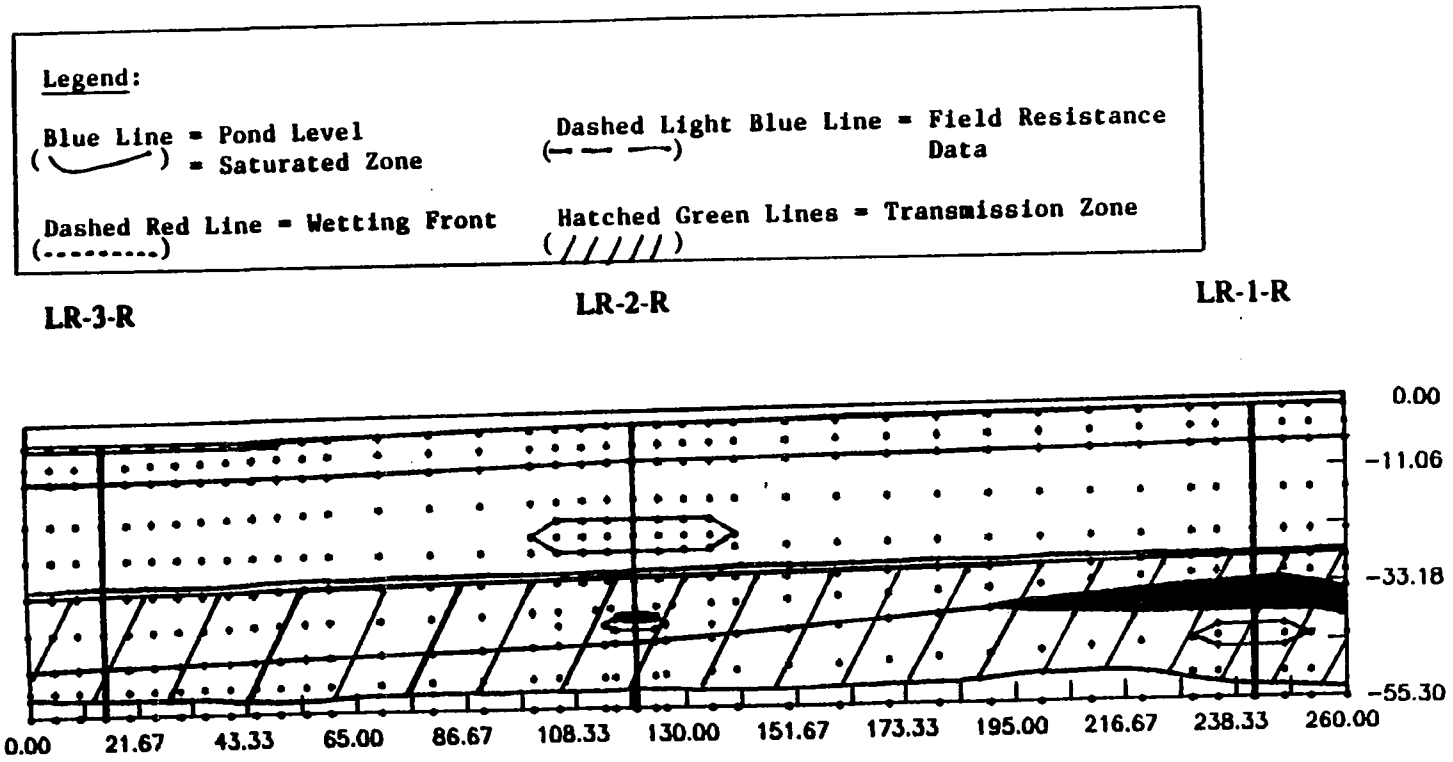

Figure 31. Saturated zone, wetting front, and transmission zone after 14 days. Note that the lower half of the basin vadose zone has been engulfed by the transmission zone and both perched moisture zones continue to grow substantially. Pond level at LR-3-R has dropped to 4.6 feet (140.1 cm). The average magnitude of the water table rise was 3.5 feet (1.1 m).

conditions, which were slightly adjusted to properly simulate the initial soil conditions preceding the February 1986 storm. This technique prevented the input of erroneously moist conditions which would have lead to premature drainage during the wetting front simulation and lead to a significant false rise in the ground water table.

Initially, the surface nodes were set equal to the depth of the ponded water, on February 11, 1986, at the specific node location (for example 1.75 ft (52.58 cm) at LR-3-R). Surface nodes between LR-2-R and LR-1-R were set at ψ=0 cm to simulate saturated surface conditions due to precipitation on February 11, 1986. The bottom nodes (no-flow boundary) were initially set at ψ=-10 cm, to simulate the capillary fringe at the top of the water table and to enable the model to simulate the ground water recharge contribution of this specific cross-section of the drainage retention basin. At each half day time step, the surface node pressure heads were reset to either the extrapolated or field measured pond level corresponding to the time step.

After one day of simulation, the wetting front (defined by a 5% increase in moisture content) had moved through the silty gravel and into the upper silt unit. The saturated zone (defined by a zero pressure head contour) had spread out in the silty gravel unit, as the result of the simulated precipitation. The saturated zone seemed to propagate as a slug, or body, of water through the upper silty gravel unit (soil material 2) between LR-2-R and LR-1-R. This pattern is consistent with the resistance data and is probably the result of the initial precipitation conditions. As expected, the pressure head and moisture content values in the upper silty gravel significantly increased, resulting in a pressure head and moisture build up above the silty gravel/upper silt layer contact. This was caused by the contrast in hydraulic conductivities between the upper silty gravel and the upper silt layer, and the location of the wetting front. The low conductivity of the silt impeded the downward propagating moisture, and created a pressure head build up in the silty gravel unit. A very

small water table response (approximately 0.1 feet, 3 cm) is seen after the first day of simulation. This is due to minor drainage from the lower silt layer, which produced saturated conditions at some of the bottom nodes at the bottom no-flow boundary.

By the second day of simulation, the wetting front had moved only a few feet downward in the upper silt unit. The silty gravel unit had become more saturated as the result of increased surface ponding of storm runoff water. Pressure heads in the upper silty gravel (material 2) had begun to augment as a result of the increased surface pressure heads (i.e., increasing pond level). The minor rise in the water table continued as a result of the slight subsurface draining and the effects of the bottom no-flow boundary. On the third day of simulation, the NW side of the wetting front (closest to LR-3-R) continued to propagate deeper into the vadose zone, more so than the SE portion (closest to LR-1-R). The differential wetting front penetration was most likely created as a result of the higher initial moisture content in the NW portion of the basin from the initial ponding, and due to the higher surface pressure head values at the NW pond surface.

A notable effect created by the contrasting, unsaturated hydrogeologic properties of the upper sand lens and the upper silt layer on the wetting front and saturated zone is predicted by the fourth day of simulation. The pressure head difference between the silt (saturated portion) and the sand lens (unsaturated) created a hydraulic conductivity contrast between the two materials, which caused the sand lens to act as a moisture barrier. The higher conductivity of the saturated portion of the silt layer and higher suction values lower in the silt layer caused the wetting front to become impeded at the top of the sand lens and to flow around it. The fine grained texture of the silt allowed the moisture to flow laterally and vertically around the coarse grained sand lens. This phenomenon is known as the "wick effect." The phenomenon of impeding moisture migration by contrasting soil material properties and causing the moisture to flow around the coarse grained "barrier"

(i.e., "wick effect") has been only recently understood and is now being used in the design of hazardous waste burial trenches (Mercer et al., 1983, and Yeh et al., 1985).

On the fifth day, pressure heads along the upper silt/lower sand unit interface began to build up in the NW portion of the cross-section. The moisture build up created a "moisture transmission zone" or moisture flux zone in the lower sand unit as the percolating water broke through the upper silt unit/lower sand unit interface. The moisture transmission zone developed as a result of the upper silt unit/lower sand unit contrast in hydrogeologic properties. The lower sand unit drains moisture at a faster rate (sand: high hydraulic conductivity) from the interface than the moisture arrives (silt: low hydraulic conductivity), resulting in the development of a zone which transmits moisture, but never really becomes saturated itself, unless the water table rises and submerges the zone. The transmission zone is a moisture flux zone defined by the saturated zone (above) and the wetting front (below). Pressure heads in the upper portion of the upper sand lens started to decrease, indicating that a critical interfacial pressure (h_c) had been reached, allowing the wetting front to pass through the upper silt/sand lens boundary. The water table had nearly stabilized by this time step (at approximately 1.5 feet, 45 cm), due to the fact that most of the nodes in the lower silt unit have finally reached more stable moisture contents/pressure heads.

By the sixth day of simulation, the wetting front had moved into the NW side of the upper sand lens and soil suction values at the base of the sand lens had decreased significantly (i.e., increased moisture content). The infiltrating water had penetrated the side of the lens and had progressed around the lens. The transmission zone continued to grow in a southeasterly direction, between LR-3-R and LR-2-R, as a result of the continued downward propagation of the wetting front. At this time step, moisture contents and pressure heads at and above the wetting front have increased significantly, while

suction in the lower sand unit remains relatively high. The continued moisture buildup in the silt layer will lead to continued moisture breakthrough into the lower sand unit and lateral growth of the transmission zone. This phenomenon is fairly characteristic of a silt texture above a sand or gravel texture.

Moisture breakthrough occurs when the fine grained material (silt) above the fine grained/coarse grained (i.e., silt/sand) interface undergoes a significant moisture and pressure head buildup. At some critical interfacial pressure (h_c), moisture breaks through the fine grained/coarse grained interface and rapidly flows into the lower coarse grained material (lower sand unit). This phenomenon occurs between the fifth and seventh days of simulation, where the moisture contents in the silt at the interface built up to approximately 95% of saturation.

By the seventh day, the transmission zone was fully developed and moisture penetrated the lower sand layer along the entire silt/sand interface. Also, the saturated zone had passed around the upper sand lens, leaving some of the lens still unsaturated, and became impeded at the upper silt unit/lower sand unit interface. This is the result of the contrasting hydrogeologic properties of the silt and sand, as mentioned above.

The author has found that the moisture breakthrough is highly influenced by the hydrogeologic properties of the fine-grained material (i.e., silt) and, therefore, the shape of the material's characteristic curves. By interchanging various shaped characteristic curves for soil material 3 (silt) during the sensitivity analysis, it was found that a larger pressure head (i.e., moisture) buildup is required for fine textured soils with high negative air entry pressure heads in order to achieve breakthrough into the underlying coarse textured material. The high negative air entry pressure heads are created as a result of the fine textured material becoming effectively saturated at a relatively high suction value, to which the corresponding hydraulic conductivity value is quite low (say, 0.5 x KSAT). The low

hydraulic conductivity impedes downward flow, and as a result, moisture is built up above the wetting front and may even flow laterally away from beneath the source.

At the eighth day, the model and the contoured resistance data, again, matched fairly well. Both indicate the the wetting front had advanced through much of the lower sand unit. However, field data indicated that the ground water level beneath the basin should have risen nearly 11 feet (335 cm) by this time step. The model only simulated a 2-3 foot (61-91 cm) rise in ground water level at this time step, some of which was due to the desaturation of some initially moist nodes. By comparing the recharge contribution of the simulated cross-section and ground water field data, the author has concluded that the fairly thick (approximately 20-30 feet, 6-9 m) permeable sandy gravel zone in the southeast portion of the basin (not modeled) is a major source of ground water recharge at the drainage retention basin. As previously mentioned, this thick permeable zone was originally suggested by the geologic log of the D-3 (Appendix A) boring in the floor of the drainage retention basin (see figure 6 for location).

Originally, the existence of the thick permeable sandy gravel in the SE basin was disputed because of extremely poor geologic correlation between D-3 and other borings in and around the basin. However, the discrepancy between the field ground water data and the recharge contribution from the simulated cross-section is cited as further evidence supporting the existence of a thick permeable zone in the southeastern portion of the basin. Finally, the reason why the recharge contribution from the SE basin could not be noted prior to the eighth day of simulation is that a minimum pond level of 4 - 4.5 feet (1.2-1.4 m), as measured at LR-3-R, is required for the SE portion of the basin to become covered with ponded water and for measurable amounts of recharge to begin to occur.

From the eighth to the tenth days of simulation, the transmission zone and wetting front slowly progressed downward through the lower sand unit. The upper sand lens

became increasingly saturated as moisture continued to fill the remaining unsaturated sand pores. The saturated zone remained stagnant at the upper silt unit/lower sand unit interface, for reasons discussed above.

By the eleventh day of simulation, the transmission zone began to penetrate the lower silt unit in the NW basin, near LR-3-R, and finally reach the water table. Moisture began to become perched on the clay lens (soil material 5) within the lower sand unit as the wetting front/transmission zone became slightly distorted around the clay lens. This is the result of the contrasting hydrogeologic properties between the more permeable sand and the less permeable clay lens, which acted as a barrier and impeded the downward propagating moisture under these relatively moist conditions.

During the twelfth day of the storm, moisture was rapidly pulled into the lower silt unit, causing the wetting front to become more distorted around the low conductivity clay lens. The author believes this was the result of the silt's "wick effect" and higher affinity for moisture. At this time step, moisture had also become perched at the lower sand unit/lower silt unit interface, near LR-1-R. This may be the effect of the no-flow boundary along the right (southeast) side of the finite element grid, and/or the simplified soil/material contact along that portion of the sand/silt interface, required for modeling purposes. At LR-1-R, the contact between the lower sand and lower silt may actually be more gradational and not as sharp as modeled. A more gradational contact at this location may allow moisture to pass more readily through the interface without becoming perched along the "contact." Unfortunately, limited geologic knowledge of the heterogeneous subsurface and model simplifications make gradational contacts difficult to model. Also, the lack of any quantitative field moisture content data makes it impossible to verify the existence of the perched moisture zone at this contact. However, perched moisture zones have been encountered in the vadose zone during the drilling of a few of the ground water monitoring

wells at the LLNL site (Dresen, personal communication, 1988). This evidence indicates that the perching of moisture in the vadose zone beneath the LLNL site is a realistic phenomenon, and, therefore, may not be a result created by the model's boundary conditions or soil contact assumptions (i.e., abrupt change in grain size across the contact).

Between the thirteenth and fourteenth days of the February 1986 storm simulation, the perched moisture zone at LR-1-R continued to grow laterally, nearly 65 feet (20 m), and to slightly thicken. By the fourteenth, and last, day of simulation, the transmission zone had expanded from the lower sand unit/upper silt unit interface down to the water table, making the entire lower portion of the vadose zone a moisture transmission zone. The water table had risen a total of 3.5 feet (107 cm) by the fourteenth day of simulation. Nearly 2 feet (61 cm) of the total water table rise may be attributed to the recharge effects of the transmission zone and 1.5 feet (45 cm) may be attributed to the earlier draining of the lower nodes, indicating that the modeled cross-section contributes only a minor amount to local ground water recharge.

Lateral Flow Simulation

To use the calibrated model as a predictive tool, a hypothetical lateral flow simulation was designed to evaluate any lateral flow components in the basin vadose zone that might be created by soil material interfaces or soil material hydrogeologic properties. To simulate the lateral flow components, the author continuously simulated 10 feet (304.8 cm) of ponded water over the northwest portion of the basin, between LR-3-R and LR-2-R, and allowed the model to run for 12 simulated days. Figures 32 through 38 display the contoured results from the lateral flow simulation. In keeping with realistic initial subsurface moisture conditions, initial subsurface moisture/pressure head conditions were assumed to be the same as the initial conditions of the February 1986 storm.

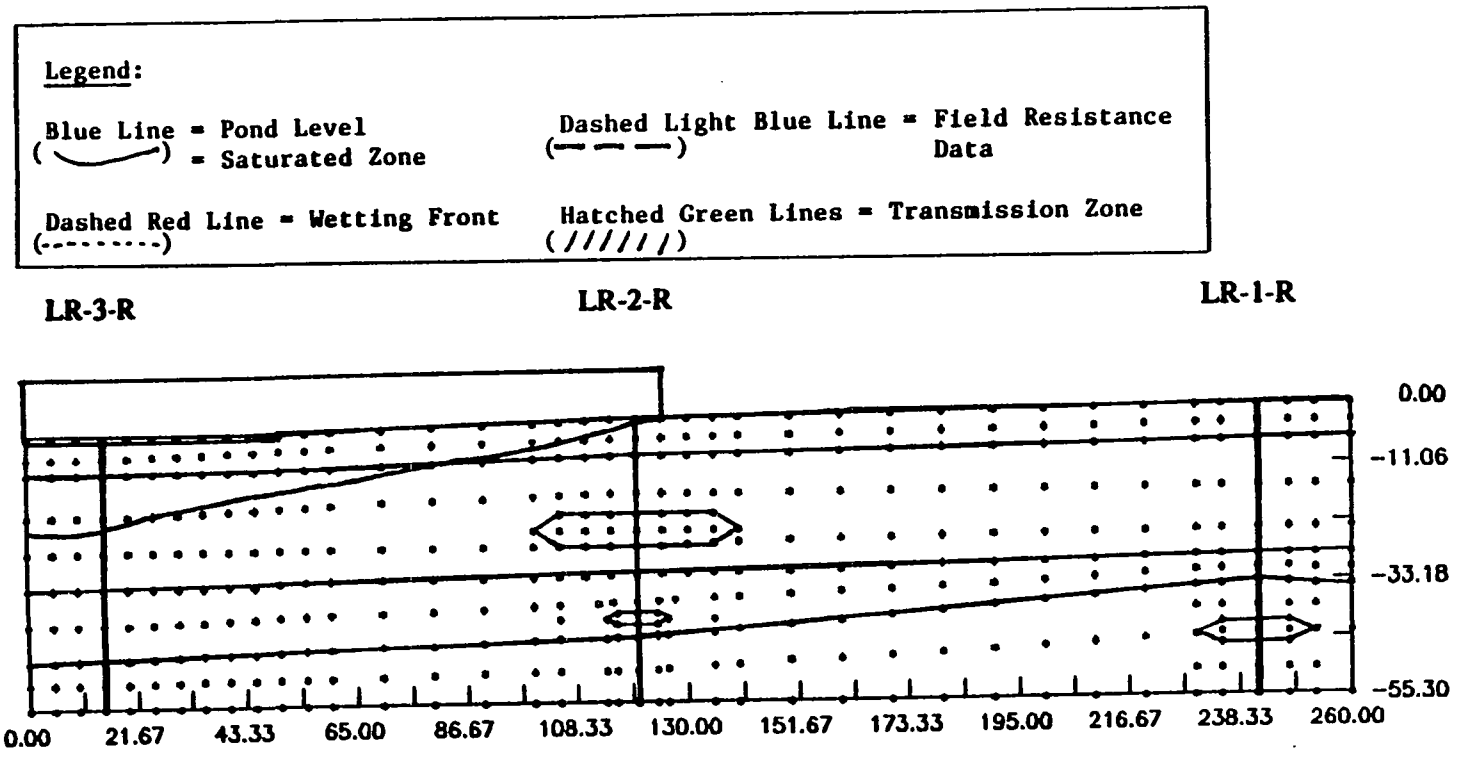

Figure 32. Initial conditions for the lateral flow simulation. Ten feet (304.8 cm) of water was continuously ponded at LR-3-R out to 125.7 feet (3,830.46 cm) along the X axis. X and Y axes are in feet.

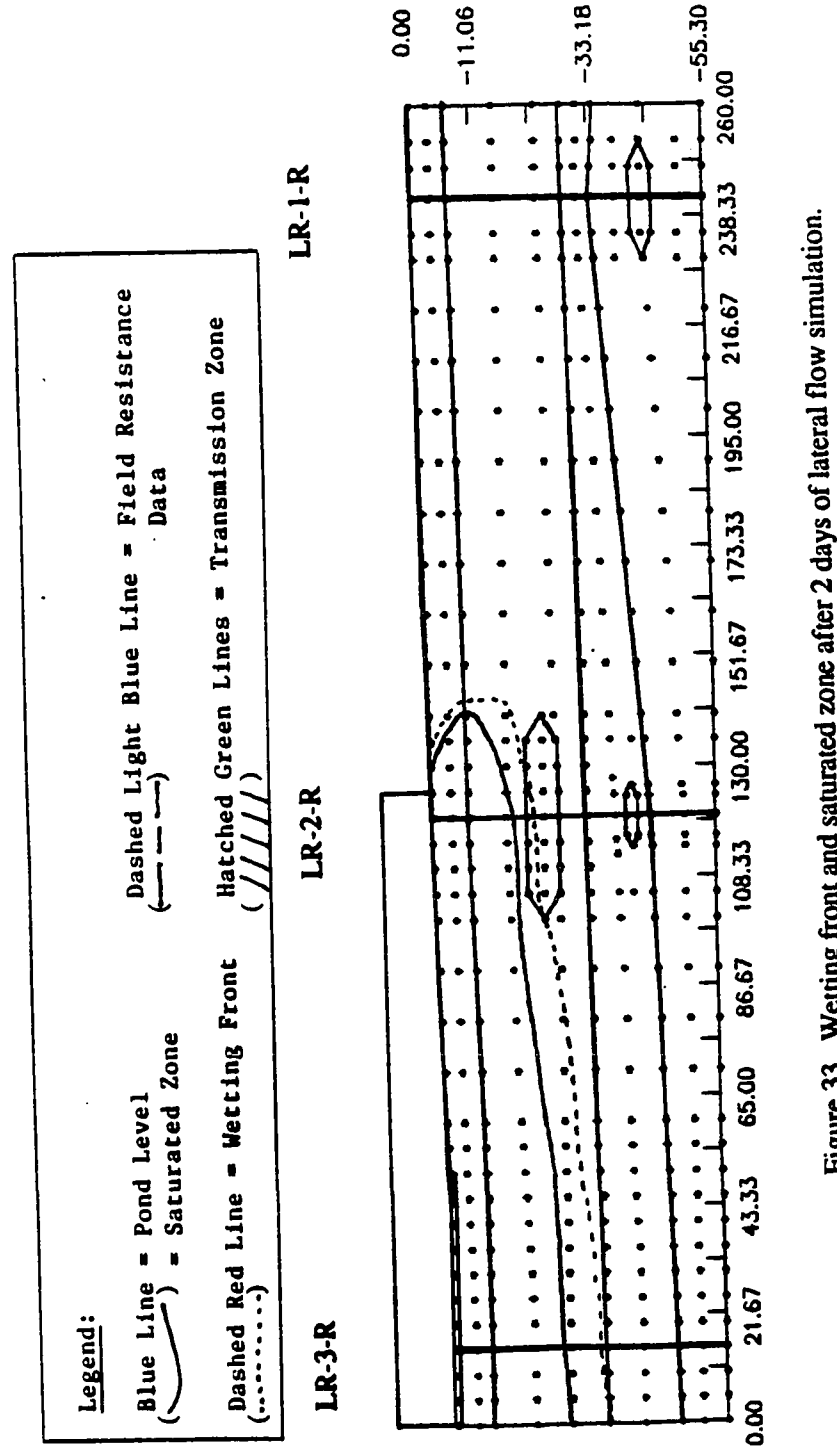

Figure 33. Wetting front and saturated zone after 2 days of lateral flow simulation.

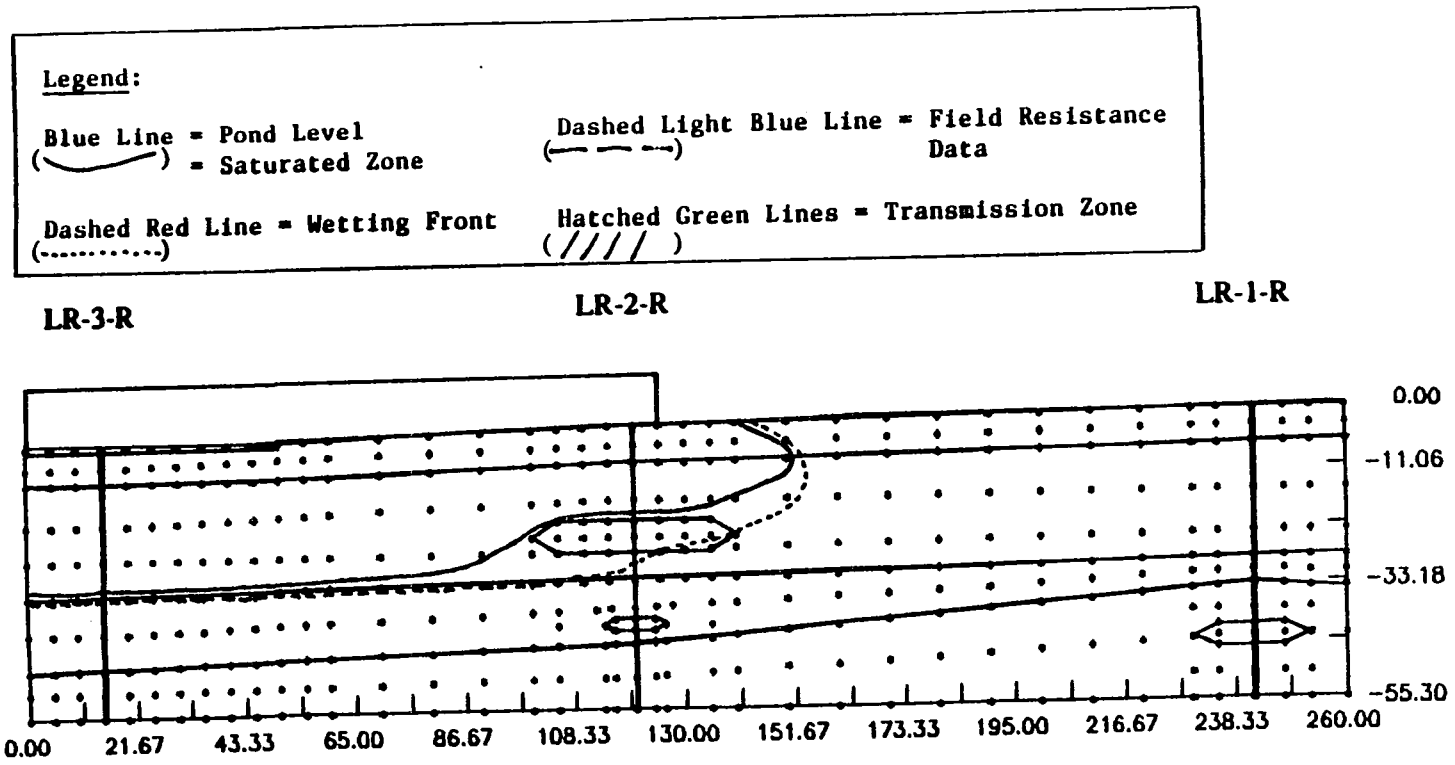

Figure 34. Wetting front and saturated zone after 4 days of lateral flow simulation. Note how the saturated zone has become distorted around the upper sand lens and how the wetting front is being "pulled" laterally in the upper silt unit.

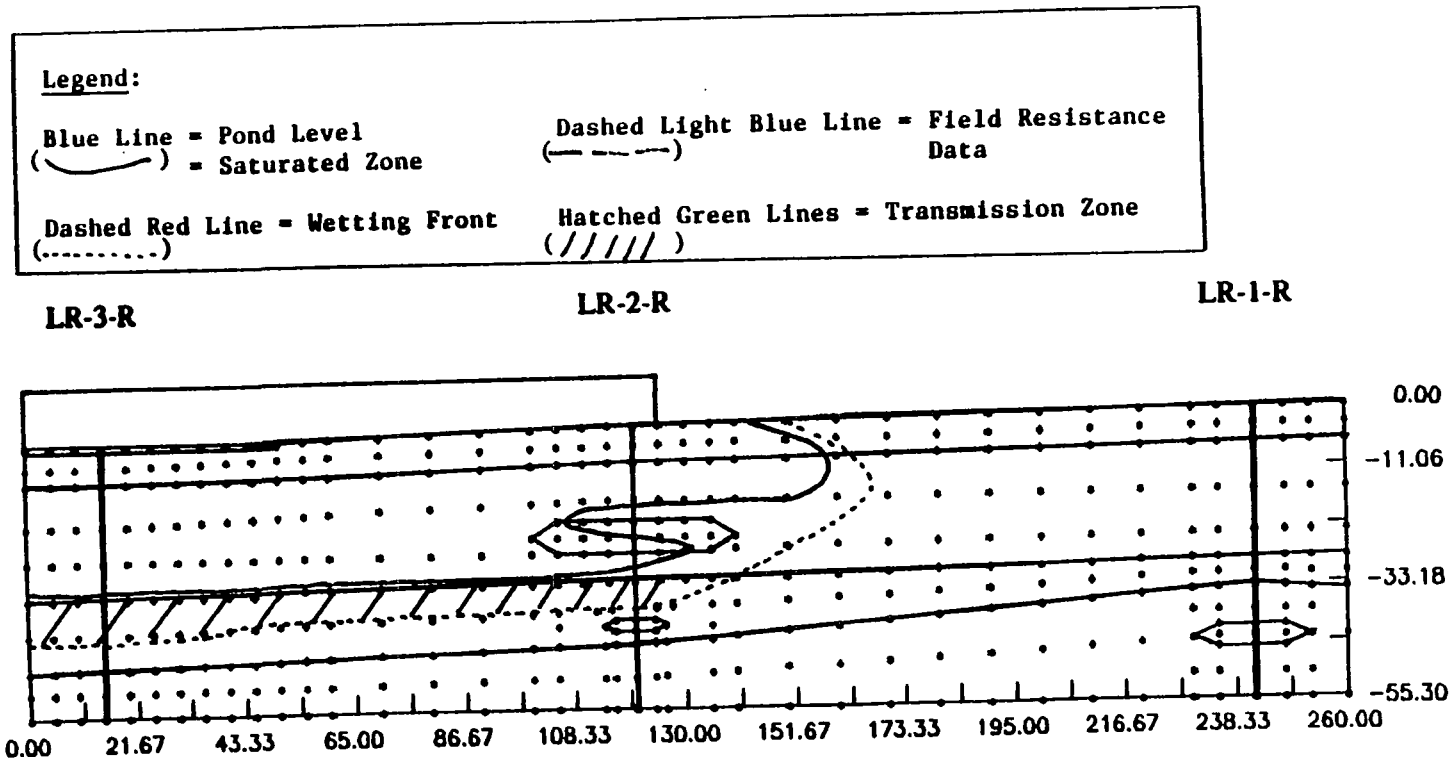

Figure 35. Wetting front, saturated zone and transmission zone after 6 days of lateral flow simulation. Note the large lateral flow components developing in the upper silt unit, as seen by the advancement of the wetting front.

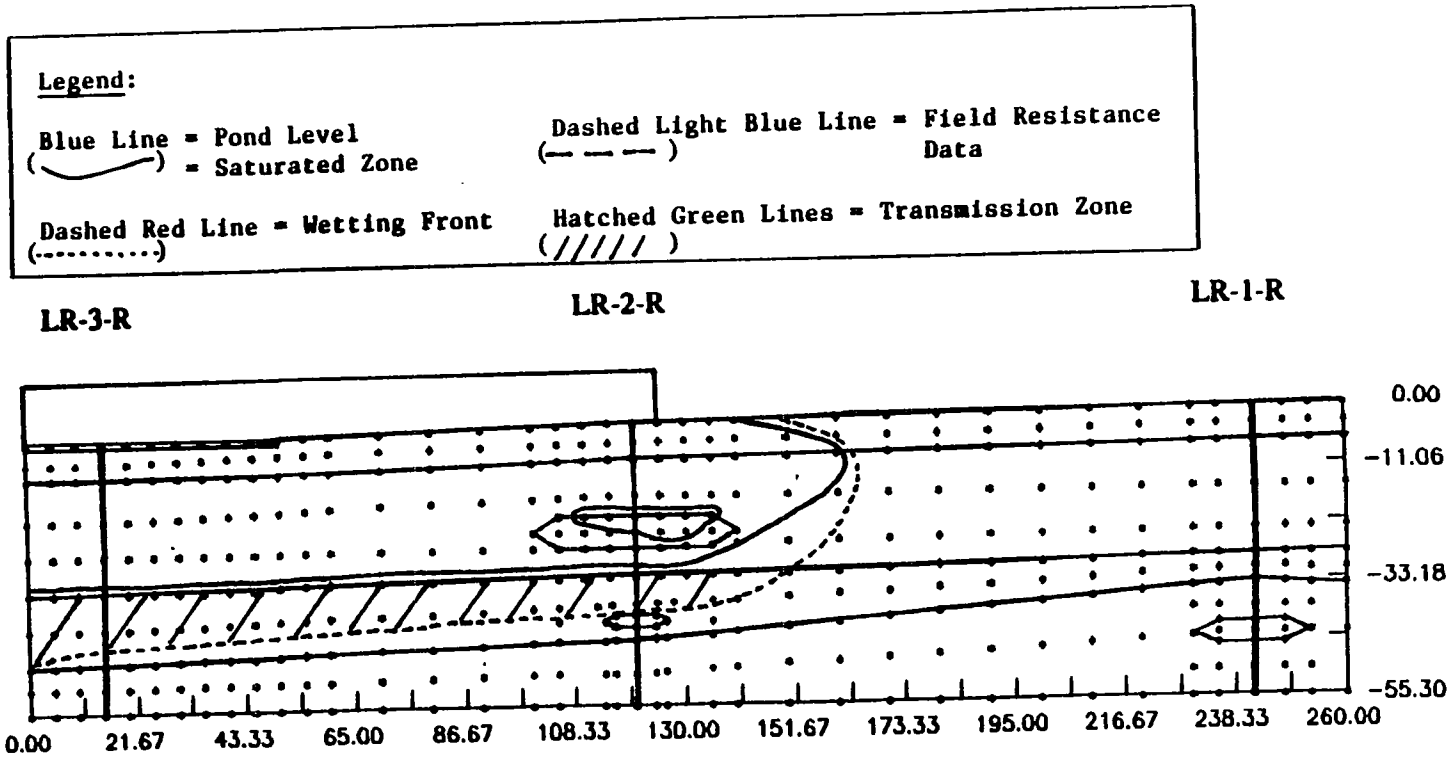

Figure 36. Wetting front, saturated zone and transmission zone after 8 days of lateral flow simulation. Note thickening of saturated zone in the upper silt unit.

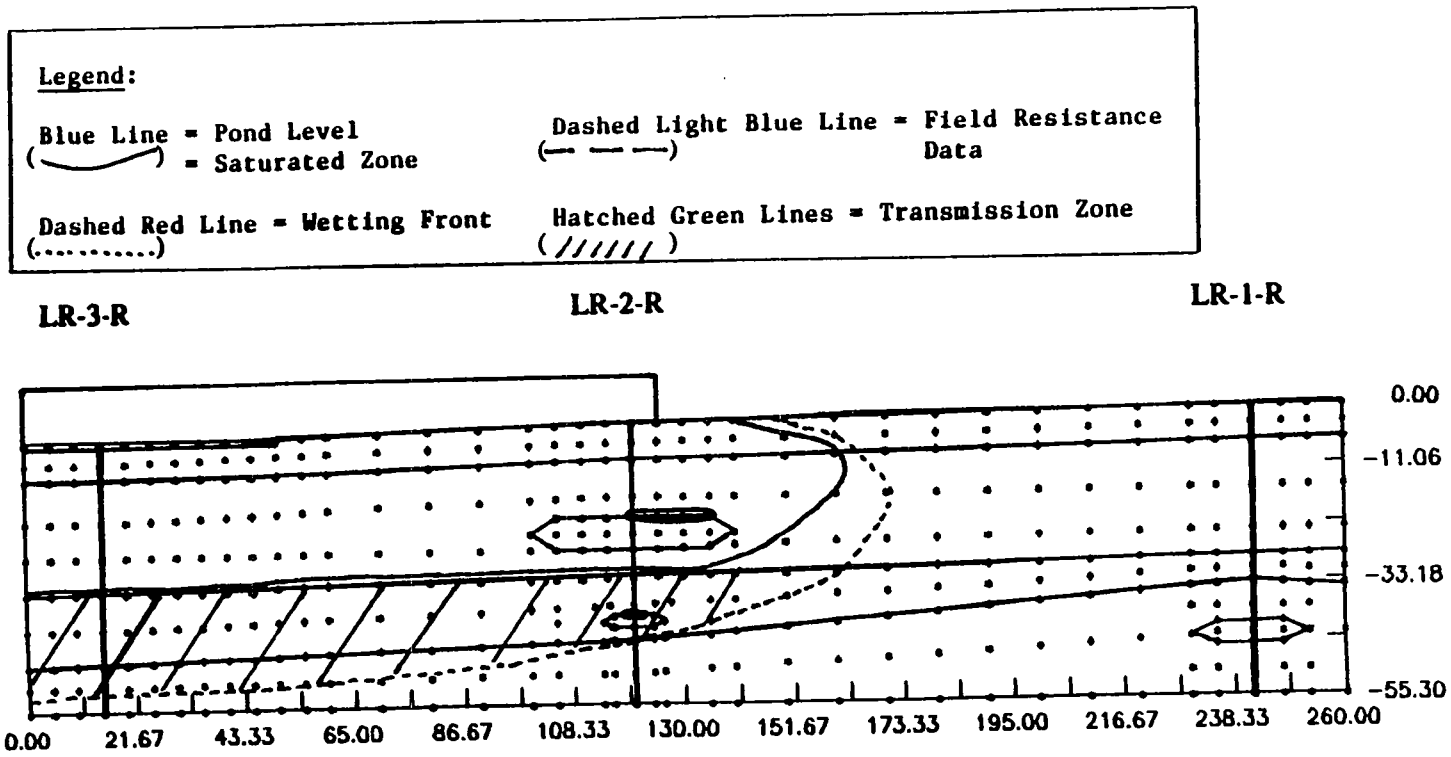

Figure 37. Wetting front, saturated zone, and transmission zone after 10 days of lateral flow simulation.

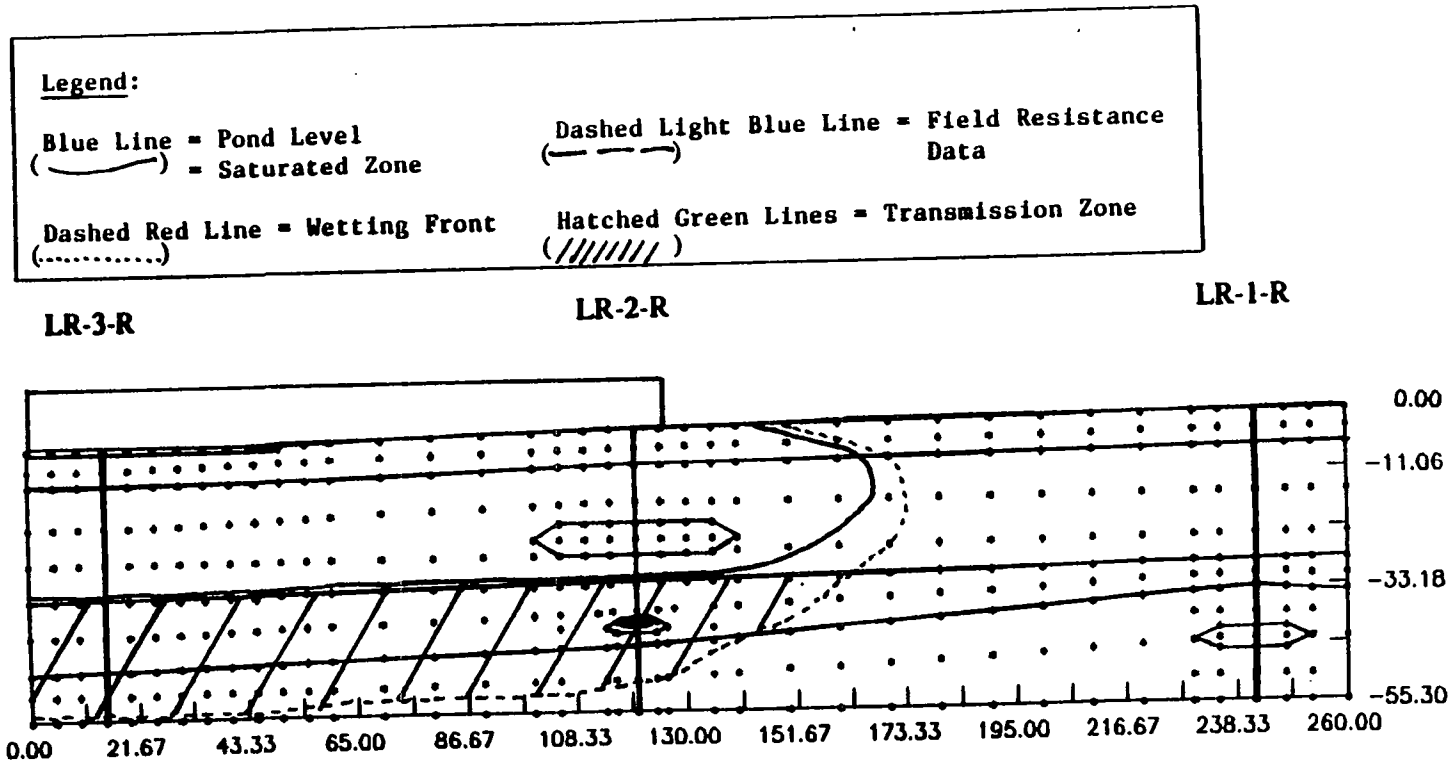

Figure 38. Wetting front, saturated zone, and transmission zone after 12 days of lateral flow simulation. Lateral and vertical components of wetting front movement are both nearly 51 feet (1554.5 cm) after 12 days of simulation.

After two days of simulation, the wetting front and saturated zone had moved a maximum of nearly 18 feet (5.5 m) laterally in the silty gravel and upper silt units. As expected, the wetting front and saturated zone moved further downward, a maximum of approximately 20 feet (6.1 m), due to the initially saturated zone at LR-3-R.

By the fourth day of simulation, the wetting front had begun to move out (laterally) a few feet ahead of the saturated zone in the upper silt unit, while they remained fairly close together in the silty gravel. Overall, the wetting front had progressed about 28 feet (8.5 m) laterally by this time step. As predicted in the February 1986 storm, the wetting front and saturated zone have become distorted by the upper sand lens and have become slightly impeded at the upper silt unit/lower sand unit interface.

The lateral flow components of the silt become evident by the sixth day of simulation. By this time step, the lateral component of the wetting front had grown to nearly 43 feet (13 m) in the upper silt unit, while the lateral flow component of the silty gravel, above, remained a bit smaller. The author believes that the "wick effect" of the fine grained texture of the silt is actually pulling the moisture laterally in the upper silt unit. Since the silty gravel (material 2) has a much coarser grained texture, the ability of the gravel to "pull" the moisture laterally is much smaller and therefore its lateral component is smaller. In addition, the author concludes that most of the lateral flow component predicted in the gravel is most likely created as a result of the hydraulic conductivity contrast between the silty gravel and the upper silt unit.

The wetting front still remained a few feet ahead of the saturated zone in the upper silt unit by the eighth day of lateral flow simulation. The saturated zone and the wetting zone (defined by the wetting front) began to thicken by this time step. In addition, it appears that the lateral flow component in the silt began to slow down, as indicated by the minimal advancement of the wetting front at this time step.

By the tenth day, the wetting front had advanced a total of 46 feet (14 m), approximately 15 feet (4.6 m) laterally ahead of the saturated zone. The wetting front and saturated zone still remain quite close together in the silty gravel unit, a consequence of the coarse grained texture of the silty gravel unit. Again, the lateral flow component in the upper silt unit may be attributed to the "wick effect," created by the fine grained silt.

At the twelfth and final day of lateral flow simulation, the wetting front appeared to have grown, both laterally and vertically, about 51 feet (16 m). This simulation indicates that a fairly significant lateral flow component exists in the silt unit, more so than in any other simulated material. As previously mentioned, the author believes that the lateral flow is created by the fine grained texture of the silt and the affinity of the silt sized particles for moisture, both responsible for the "wick effect," which causes moisture to move further in the silt than in other materials. In the event of a severe storm, causing the basin to fill for a number of days, the author believes that a significant amount of lateral flow (saturated and unsaturated) away from the basin (radially) would also occur in addition to large vertical flow components.

Both the lateral and vertical flow components of the wetting front moved a maximum of 4 feet/day (1.2 m/day). However, the individual components moved at varying rates during the simulation. The vertical flow component was primarily controlled by lithology, since the surface pressure head was constant. The lateral flow component was controlled by lithology and lateral distance away from the source, however. As the wetting front progressed laterally outward, the rate of movement decreased. The fastest lateral flow occurred at the first time step (9 feet/day, 2.7 m/day) and progressively decreased to 2.1 feet/day (0.6 m/day), due to dominate effects of the vertical flow component laterally away from the source.

After a thorough analysis of the lateral flow simulation results, it was found that the lateral flow components beneath the ponded water vary with respect to time. Initially, the extent to which lateral flow affects moisture movement directly beneath the ponded water was 9.5 feet (2.9 m), due to the initially dry subsurface conditions. By the twelfth day of simulation, subsurface moisture conditions beneath the ponded water were less transient. As a result, the extent to which lateral flow affects moisture movement beneath the ponded water decreased to 5 feet (1.5 m). It can be concluded from this analysis that the right and left no-flow boundaries do not adversely affect the moisture gradients along the right and left boundaries and are correct boundary conditions for the model. This is due to the fact that the lateral flow components have a very small effect beneath the ponded water simulated.

Deep Ponding Simulation

In another predictive, hypothetical simulation, the author simulated the flooding of the basin with 10 feet (304.8 cm) of ponded water for 20 days to predict the effects of the wetting front migration in the vadose zone. Initial subsurface moisture/pressure head conditions were assumed to be the same as for the February 1986 storm. Figures 39 through 49 display the initial conditions and the simulated results for the deep ponding simulation. Initial surface pressure heads were set at 10 feet (304.8 cm) in the deepest (northwest) portion of the basin, near LR-3-R, and decreased to 6.8 feet (207.26 cm) in the shallowest (southeast) portion of the basin, near LR-1-R, due to the slope in the basin floor. These surface pressure heads were set as a constant pressure head boundary (i.e., constant pond level) throughout the entire deep ponding simulation.

After two days of simulation, the wetting front and saturated zone had propagated downward, about halfway into the upper silt unit, much faster than the February 1986

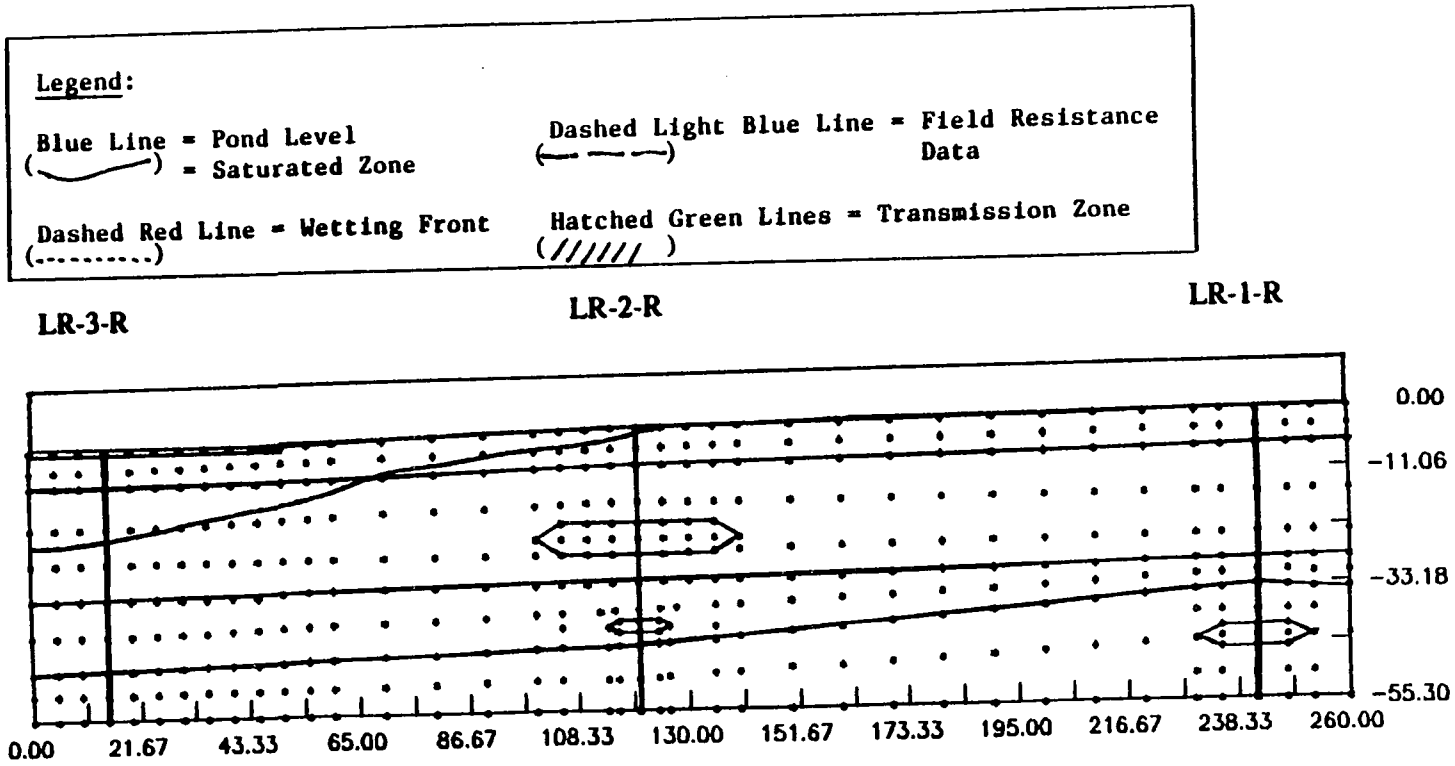

Figure 39. Initial conditions used for the deep ponding simulation. Pond level was held constant (10 feet (304.8 cm) at LR-3-R) over the entire pond surface.

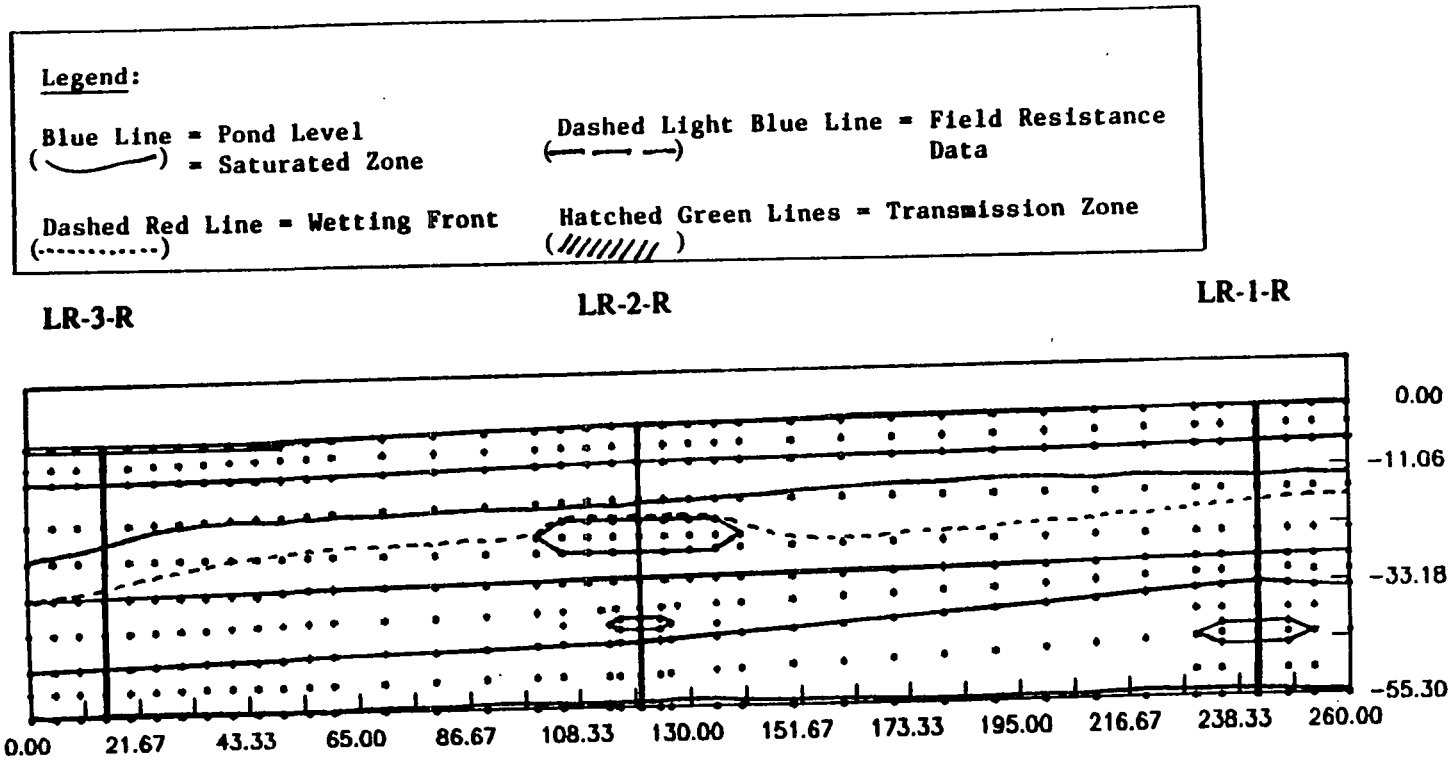

Figure 40. Wetting front and saturated zone after 2 days of deep ponding simulation. The wetting front has propagated about halfway into the upper silt unit.

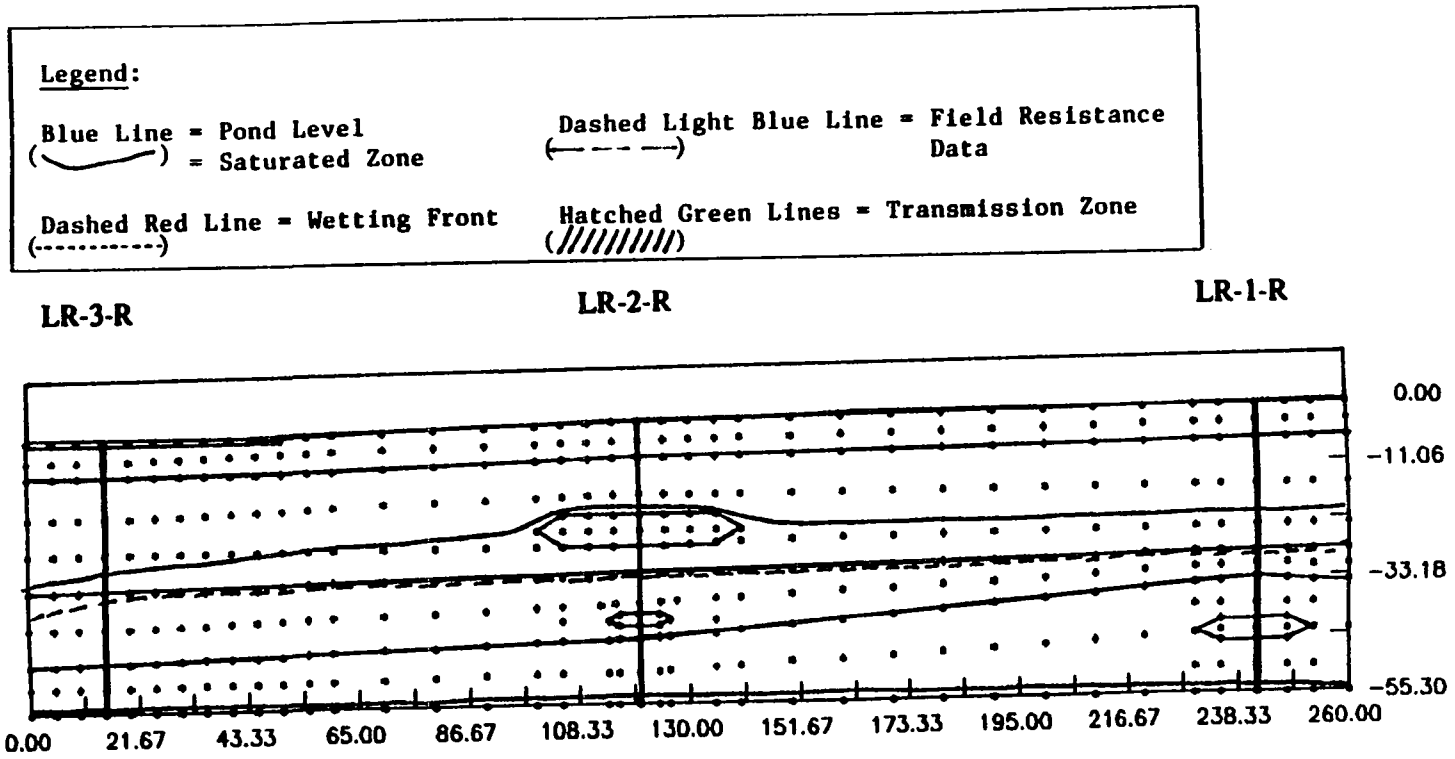

Figure 41. Wetting front, saturated zone and transmission zone after 4 days of deep ponding simulation.

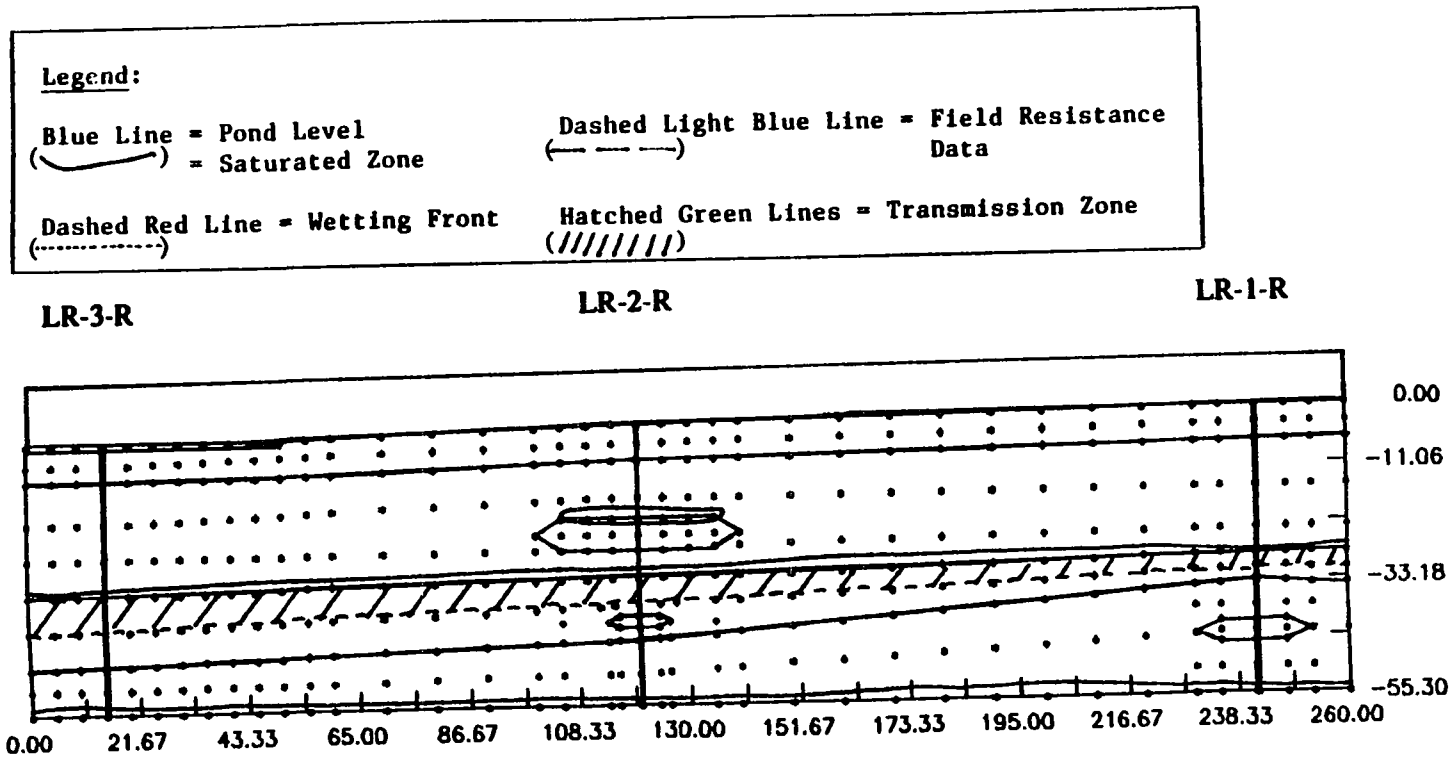

Figure 42. Wetting front, saturated zone and transmission zone after 6 days of deep ponding simulation. Note how saturated zone (blue line) has reached the upper silt unit/sand unit interface.

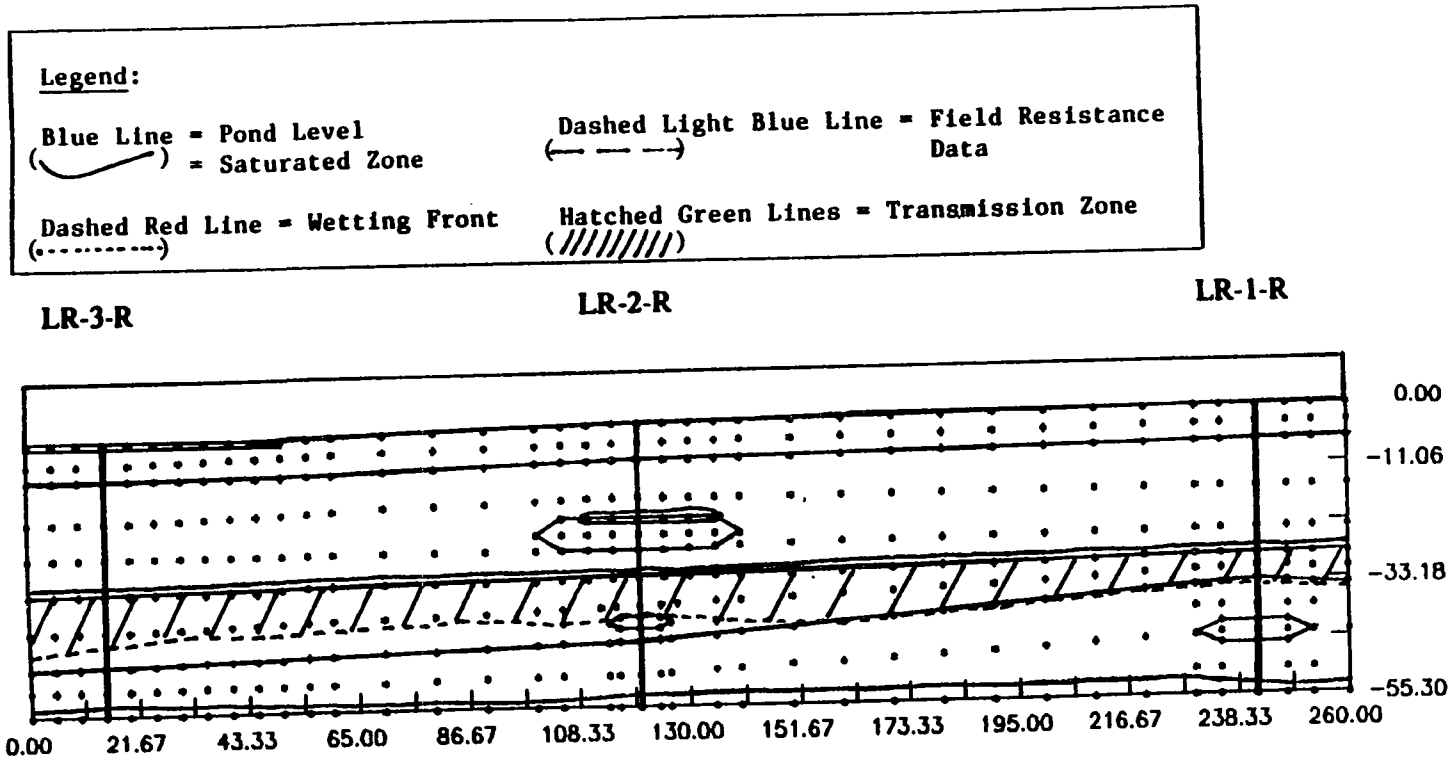

Figure 43. Wetting front, saturated zone and transmission zone after 8 days of simulation.

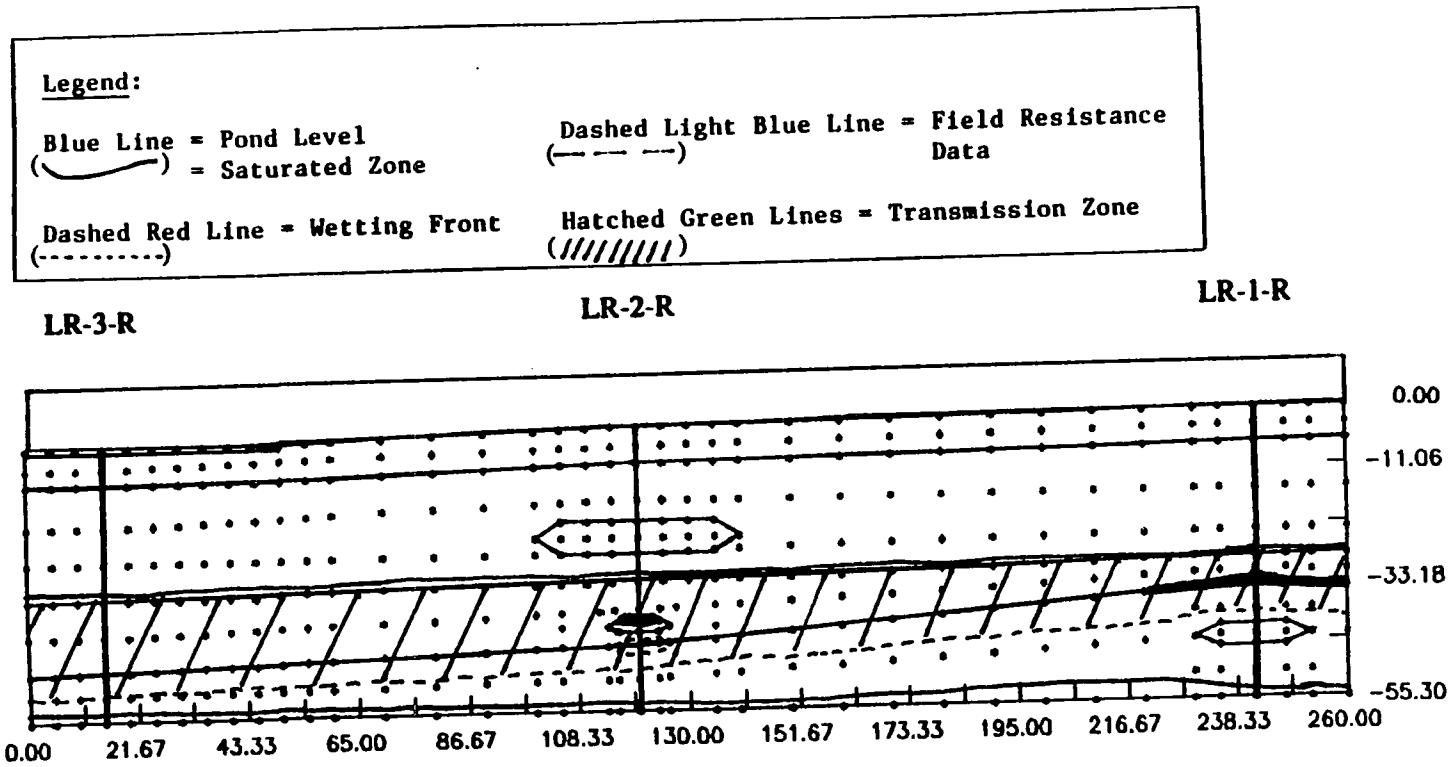

Figure 44. Wetting front, saturated zone and transmission zone after 10 days of simulation. Note the perched moisture zones at the clay lens (LR-2-R) and the lower sand unit/lower silt unit interface (LR-1-R).

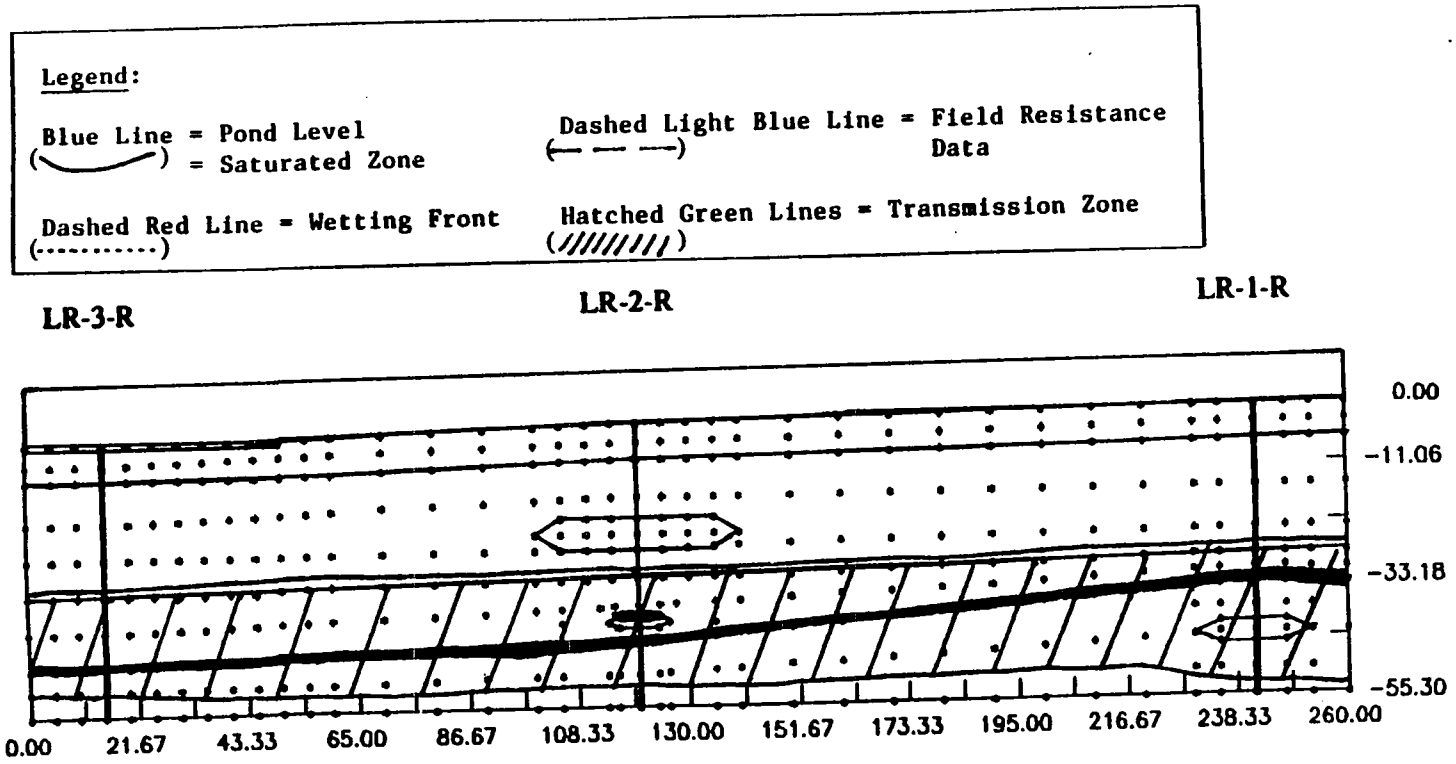

Figure 45. Saturated zone and transmission zone after 12 days of simulation. The lower half of the vadose zone has become a moisture transmission zone. The perched moisture zone at the sand/silt interface has grown the entire length of the cross-section.

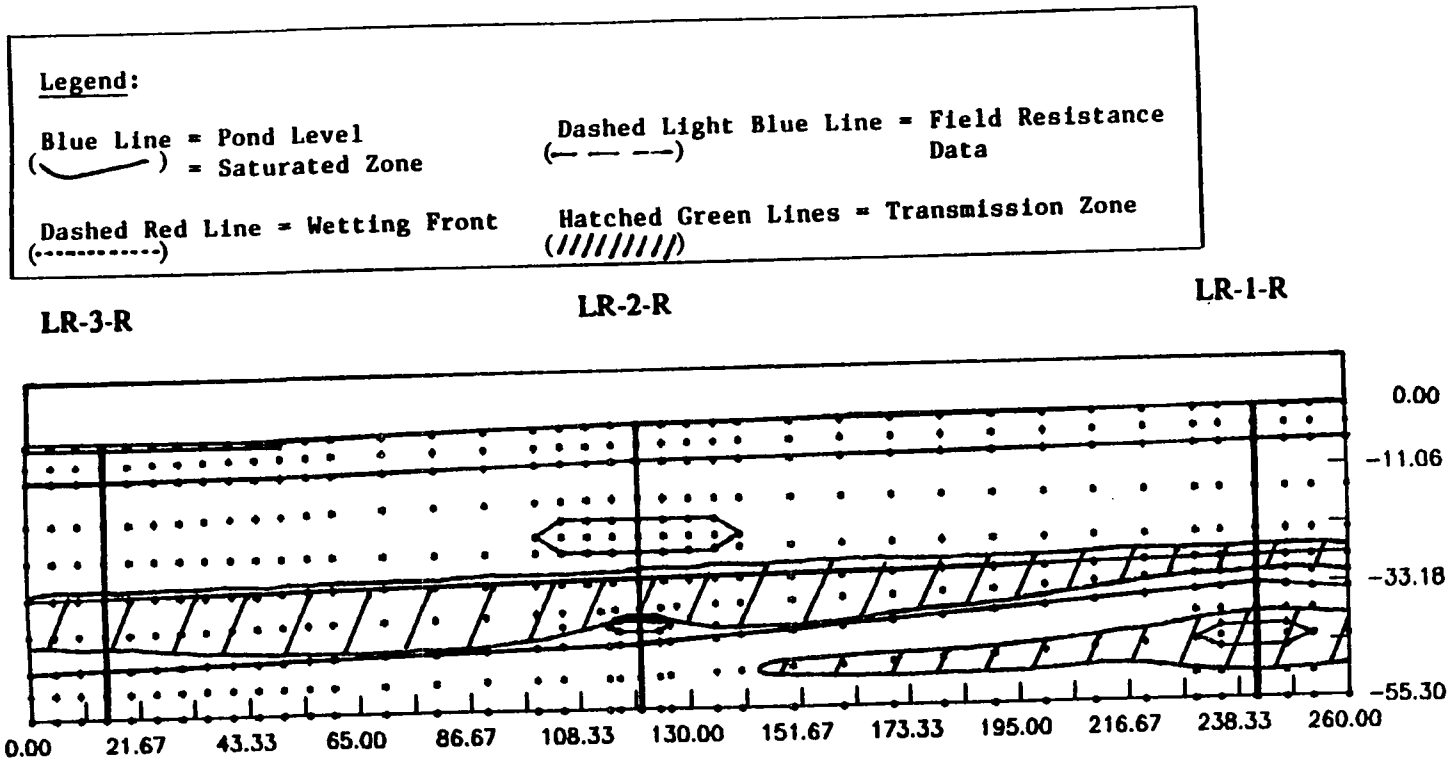

Figure 46. Saturated zone and transmission zone after 14 days of deep ponding simulation. Note the unsaturated "pocket" at -44 feet (13.4 m) at LR-1-R. This may be an artifact of the no-flow boundary conditions.

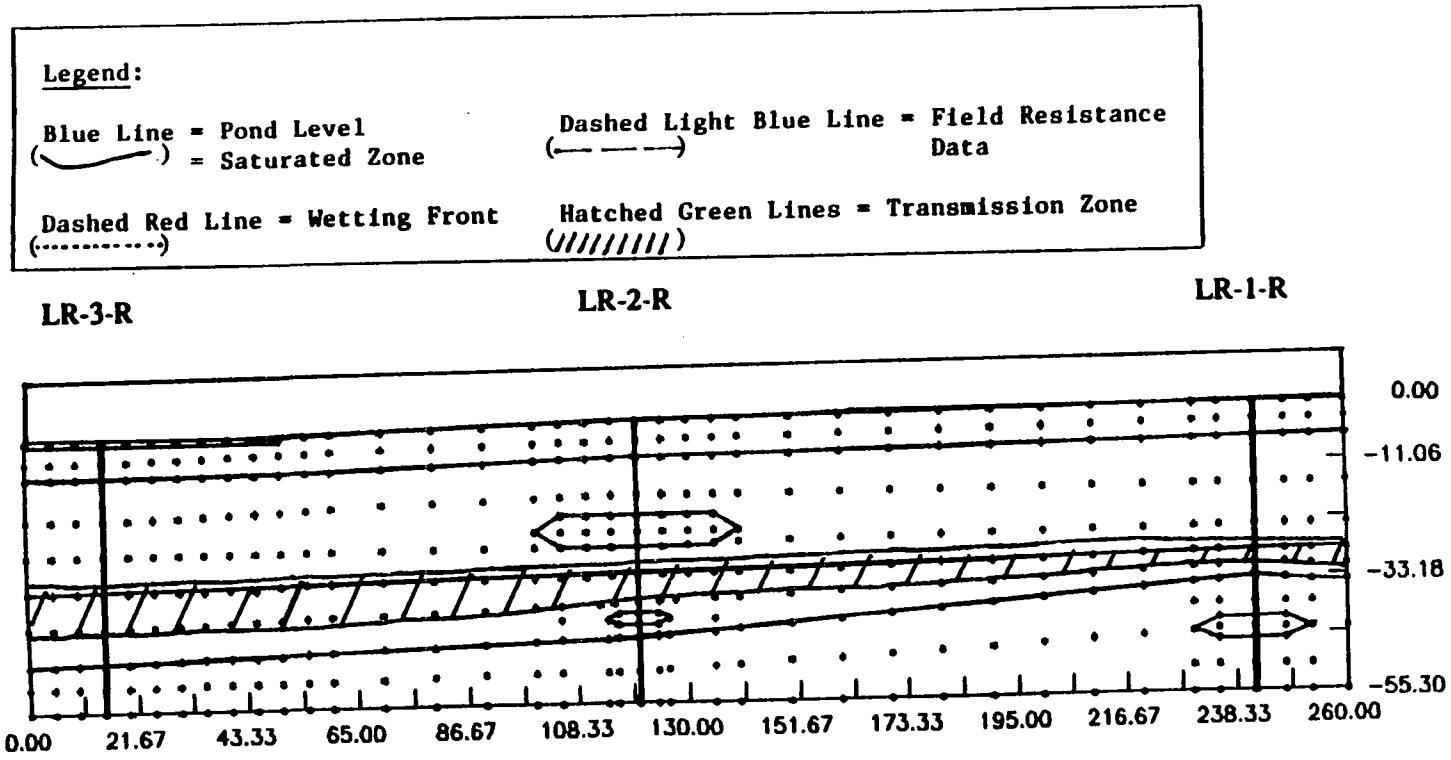

Figure 47. Saturated zone and transmission zone after 16 days of deep ponding simulation. By this time step, the water table had risen nearly 22 feet (670 cm), leaving only a small unsaturated transmission zone along the silt/sand interface.

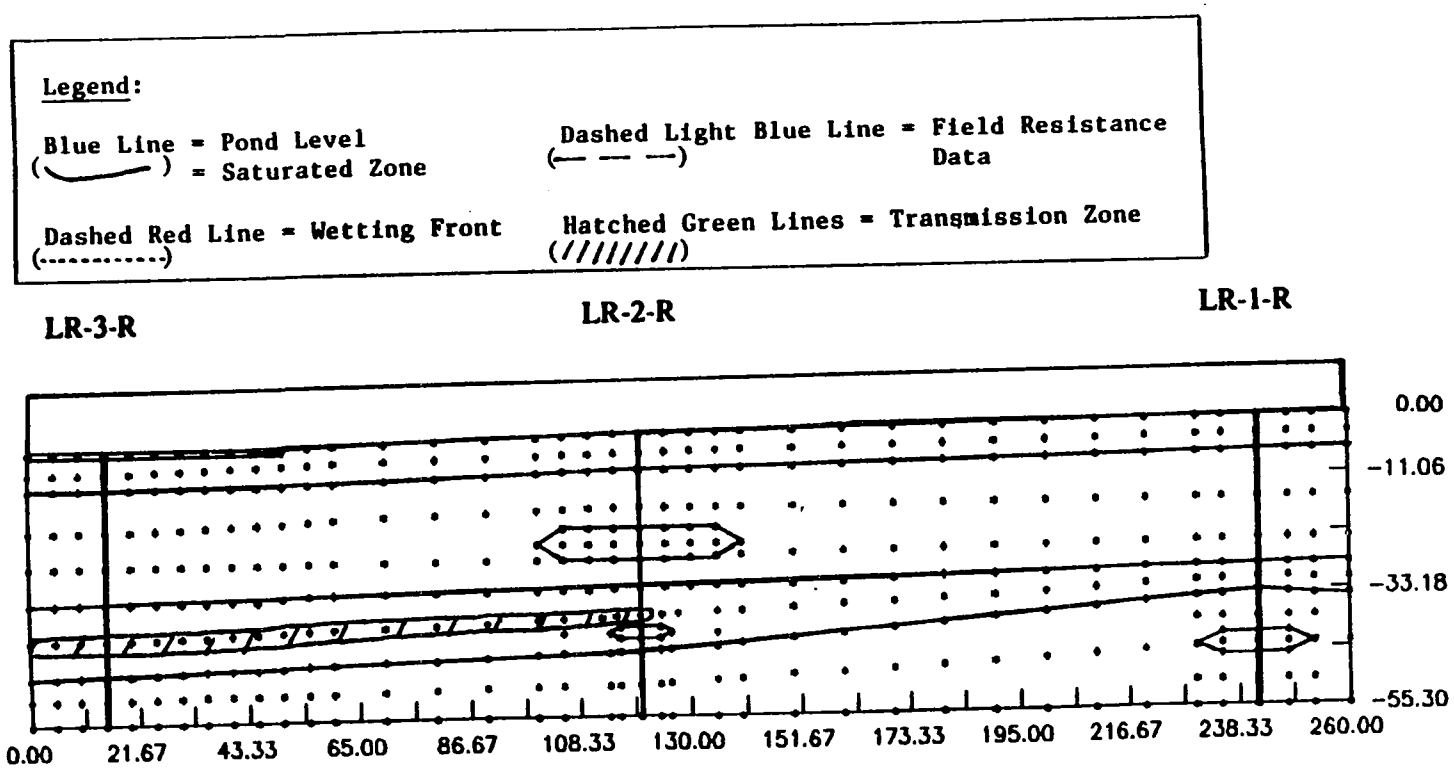

Figure 48. Saturated zone and transmission zone after 18 days of deep ponding.
By this time step, it is easy to note how the no-flow boundaries control the model's output.

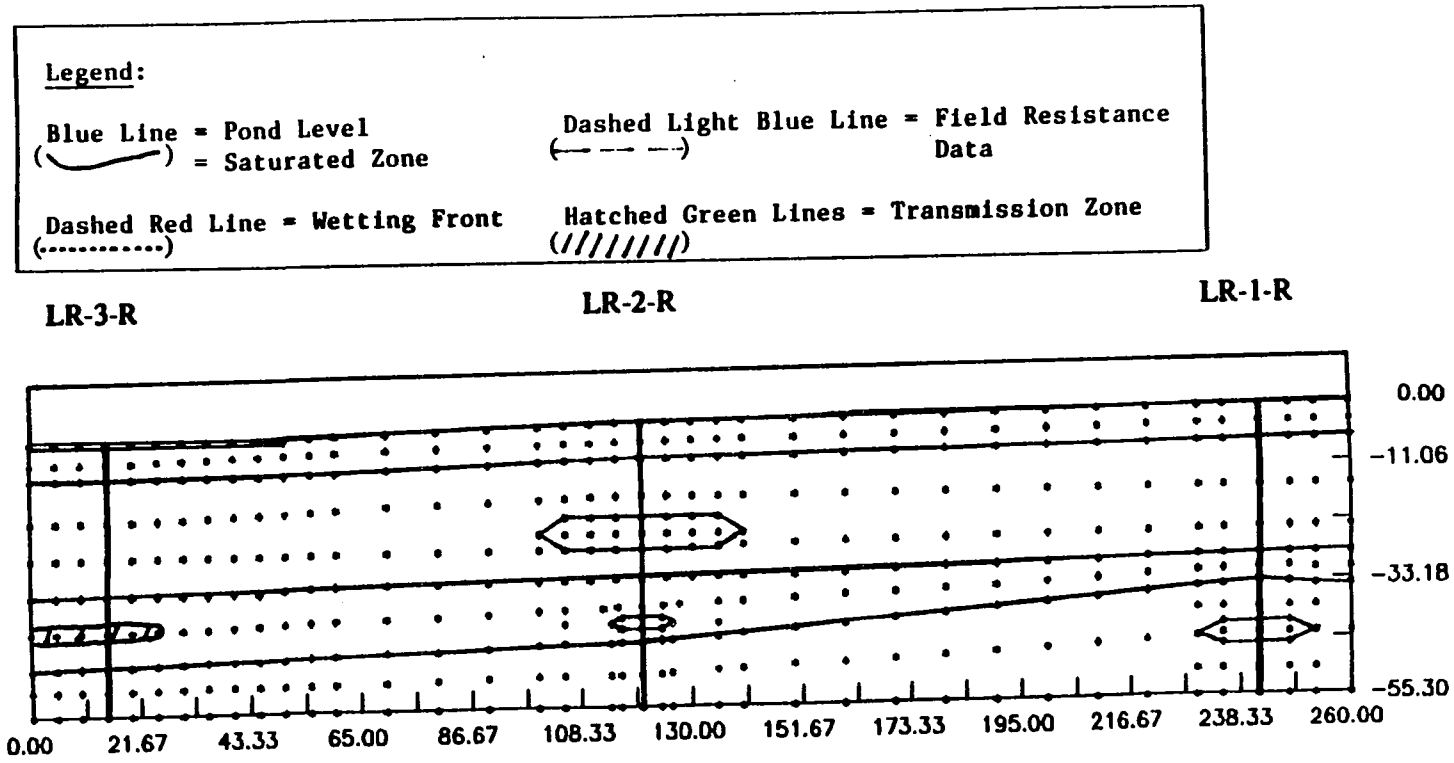

Figure 49. Saturated zone and transmission zone after 20 days of simulation. Model has become effectively "filled" with percolating moisture by this time step. Again, an artifact of the boundary conditions.

storm simulation. This is the result of the initial and constant deep pond level, covering the entire pond surface.

The wetting front had reached the upper silt unit/lower sand unit interface by the fourth day, nearly 7.5 feet (2.3 m) ahead of the saturated zone. As predicted by the February 1986 storm simulation, the saturated zone became impeded at the upper sand lens and began to flow around it.

By the sixth day, the model predicted that the saturated zone would become impeded at the upper silt unit/lower sand unit interface, and the transmission zone would fully develop across the lower sand unit. Only a small portion of the upper sand lens is left unsaturated by the sixth day of simulation. It is interesting to note how much faster the wetting front has moved as compared with the February 1986 storm. This is an obvious artifact resulting from the high surface pressure heads (i.e., deep surface ponding). Nearly the entire lower sand unit has been engulfed by the transmission zone by the eighth day. Moisture has become perched on the clay lens in the lower sand unit, an effect of the hydraulic conductivity contrasts between the sand (soil material 4) and the clay (soil material 5).

On the tenth day of deep ponding, the wetting front penetrated the lower silt unit and the upper sand lens became fully saturated, an effect not seen in the February 1986 storm simulation until the thirteenth day. In addition, a minor perched moisture zone began to develop in the southeastern portion of the cross-section at the lower sand/lower silt unit interface. Again, this may be a product of the sand/silt interface and right no-flow boundary.

By the twelfth day, the entire lower portion of the modeled vadose zone had become engulfed by the transmission zone and direct ground water recharge began to take place. The entire lower sand unit/lower silt unit interface had become a perched moisture

zone by this time step. Again, this is the result of the hydraulic conductivity contrast between the higher conductivity sand and the lower conductivity silt. The ground water recharge contribution by this time step is almost 5 feet (1.5 m), significantly more than the 2 feet (0.6 m) contribution by the twelfth day of the February 1986 storm simulation. This leads the author to conclude that the depth of ponded water has a significant influence upon the rate and, obviously, the amount by which the ground water table is recharged.

At the fourteenth day of simulation, the ground water table has risen significantly more and the perched moisture zone at the sand/silt interface has thickened quite a bit and reached the ground water table between the left no-flow boundary and LR-2-R. A long, thin zone in the lower silt unit remains unsaturated in the southeast portion of the cross-section. This unsaturated "pocket" is caused by the increased thickness of the low conductivity lower silt and the presence of the unsaturated sand lens, which acts as a moisture barrier until its moisture content increases. It is apparent by this time step that the boundary conditions (i.e, right, left, and bottom no-flow boundaries) are affecting the modeled results. The purpose of the no-flow boundaries is to isolate the cross-section to simulate the contribution to ground water recharge from the cross-section. However, the no-flow boundaries also tend to create a "glass box" effect by not allowing moisture to naturally flow outward and away from the basin. As a result of the boundary conditions, downward percolating moisture is trapped in the "glass box" and the cross-section (or box) begins to fill up during a severe ponding event, such as during this simulation.

By the sixteenth day, the simulated ground water table has risen 22 feet (6.7 m) from its initial conditions, saturating the lower portion of the basin vadose zone. The transmission zone had significantly decreased in thickness as a result of the rising ground water table. Only a very small section of the lower sand unit, 33 feet (10 m) below the surface, remains unsaturated.

Nearly the entire vadose zone became fully saturated by the twentieth day of deep ponding. As mentioned above, the simulated results after 12 days are highly influenced by the bottom, left and right no-flow boundary conditions, which create a "glass box" effect on the deep ponding simulation. It is difficult to simulate such a large scale event with a small, localized model, such as this drainage retention basin model. Proper simulation of the effects of deep ponding would require linking this simulated cross-section to a regional ground water model.

In a field situation, the author believes that a definite ground water mound would develop beneath the flooded recharge basin. However, lateral flow components in the vadose zone and regional ground water flow gradients would attenuate the mounding effect, decreasing its size and preventing the mound from "filling up" (i.e., saturating) the entire 55 foot (16.8 m) thick vadose zone.

January 1988 Storm Simulation

During the summer months of 1987, a drainage outlet was added to the northeastern portion of the drainage retention basin. This outlet now limits the basin capacity to 3.5 feet (106.7 cm) maximum depth. As a result, the volume of water available for percolation has been significantly reduced from the 28 acre-feet (3.4×10^4 cubic meters) available in 1986 when the pond was filled to its 10 foot (3 m) capacity. The purpose for modeling the January 1988 storm pond data was to predict the effects of the new drainage outlet on the movement of the wetting front in the basin vadose zone. The simulation was run for a total of 8 days. Field observations indicated that evapotranspiration had a dominant influence on the pond level after the eighth day. As a result, field pond level data after the eighth day was not indicative of the infiltration taking place. Unfortunately, the resistance data for the January 1988 storm is fairly inconclusive in that no wetting front movement could be

could be tracked. As a result, no qualitative field wetting front data may be used to verify the model's output for this simulation.

Prior to the onset of the storm, the basin had approximately 1.5 feet (45.7 cm) of water ponded in its deepest (northwestern) portion, near LR-3-R, as it typically does throughout the winter months. Again, to simulate initial subsurface moisture conditions, the initial February 1986 storm subsurface moisture conditions were assumed to hold true for this simulation. A heavy weekend storm (January 15, 16, and 17, 1988) filled the basin with 3.2 feet (97.54 cm) of runoff water. The author used the 3.2 feet (97.54 cm) of ponded water as the initial (January 19, 1988) surface pressure head conditions. At each half day time step, an extrapolated value or field pressure head value was used to simulate the falling pond level. Figures 50 through 54 display the contoured computer model output for the January 1988 storm simulation.

As the pond level fell, the model predicted that the wetting front would move into the upper silt unit by the second day of simulation. The saturated zone had filled most of the silty gravel unit and penetrated the upper silt unit in the northwestern portion of the basin, near LR-3-R.

After four days of simulated percolation, the saturated zone had moved laterally, saturating the silty gravel/upper silt unit interface along the entire length of the cross-section. As a result of the falling pond level exposing the southeastern basin surface and significantly reducing the surface recharge at this location, the author concludes that both the drainage of earlier infiltrated water and the upper silt unit's "wick effect" resulted in the lateral movement of moisture in the vadose zone, causing the entire silty gravel/upper silt interface to become saturated. The model, again, predicts the moisture impeding effects of the upper sand lens on the saturated zone and the wetting front by the fourth day.

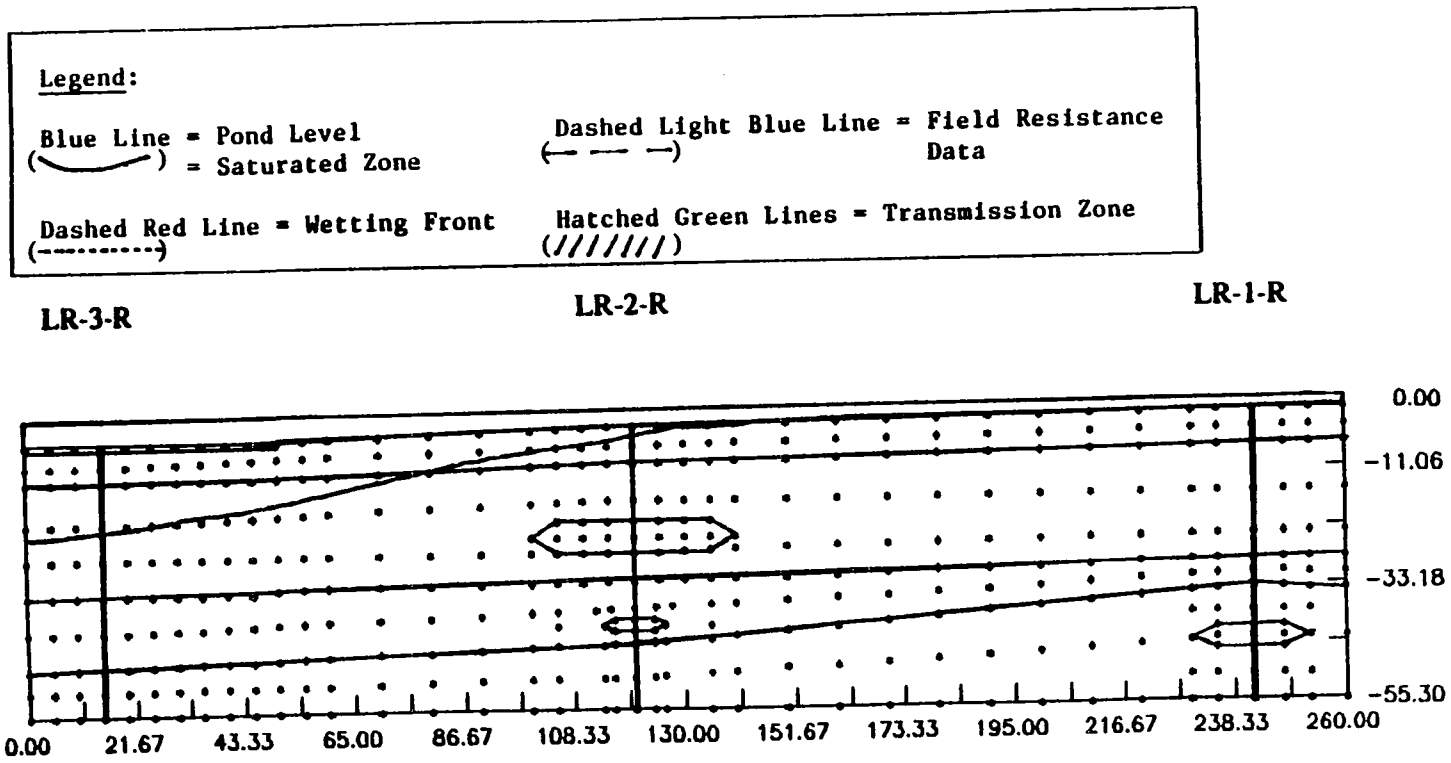

Figure 50. Initial conditions of the January 1988 storm. Pond level at LR-3-R was initially 3.2 feet (97.54 cm).

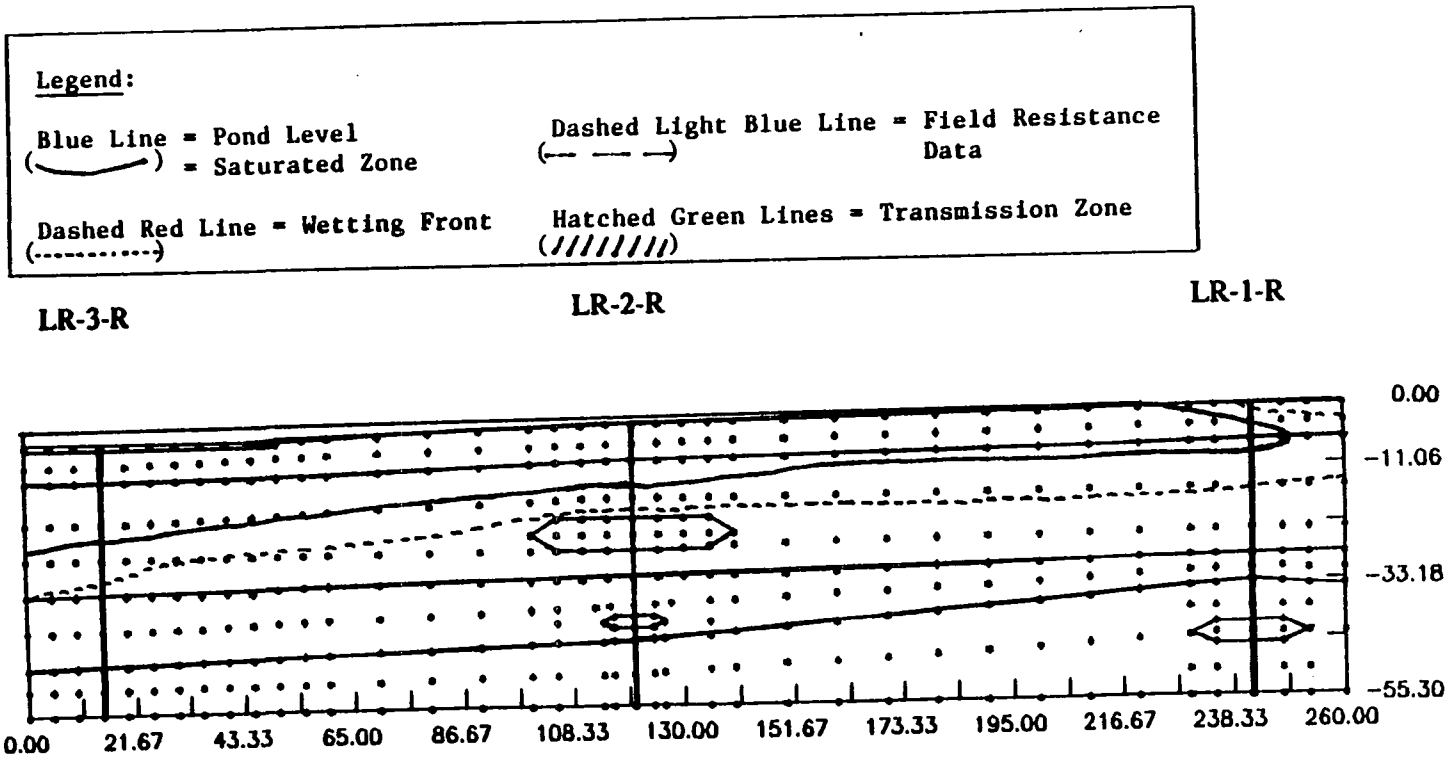

Figure 51. Wetting front and saturated zone after 2 days of simulation of the January 1988 storm. Pond level at LR-3-R was 2.99 feet (91.14 cm) after 2 days.

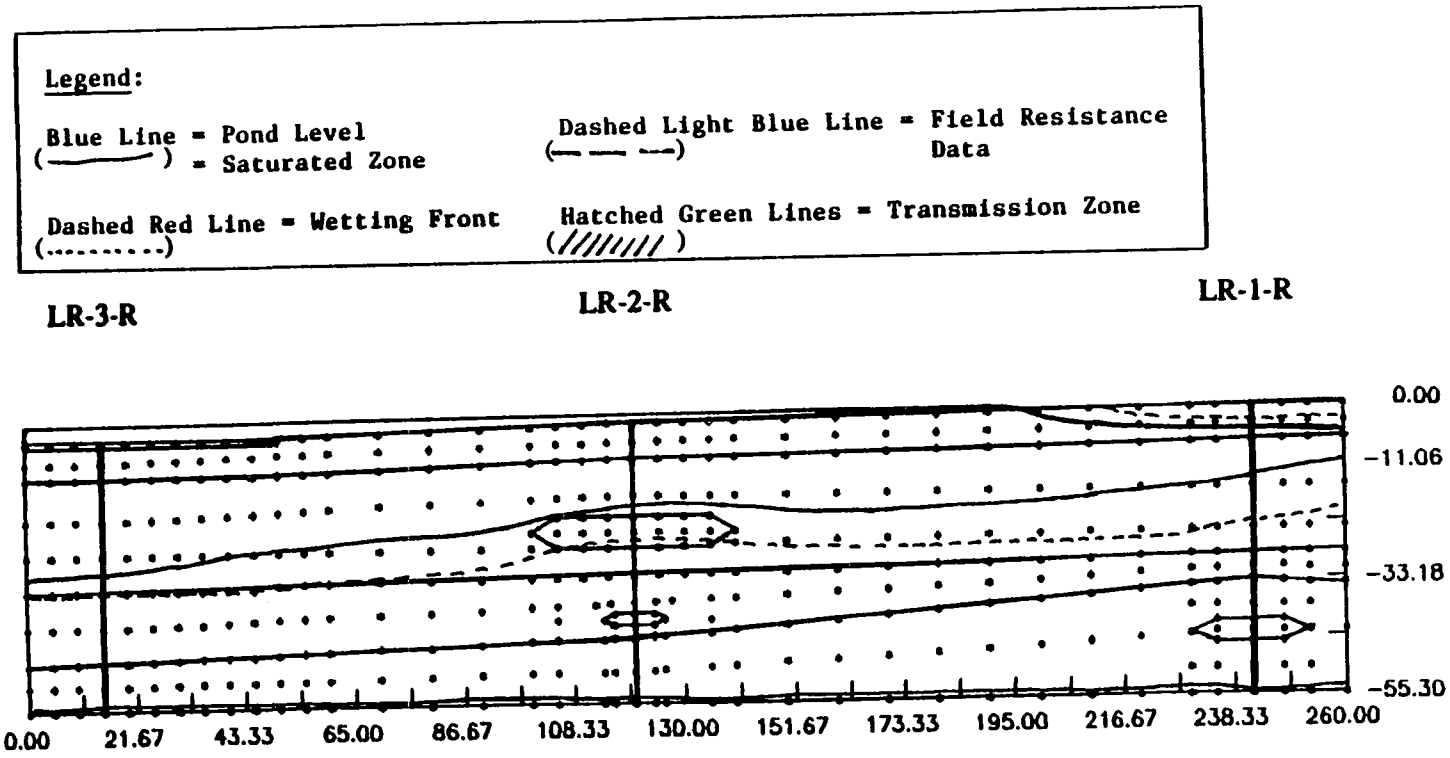

Figure 52. Wetting front and saturated zone after 4 days of simulation of the January 1988 storm. Pond level at LR-3-R was 2.68 feet (81.79 cm).

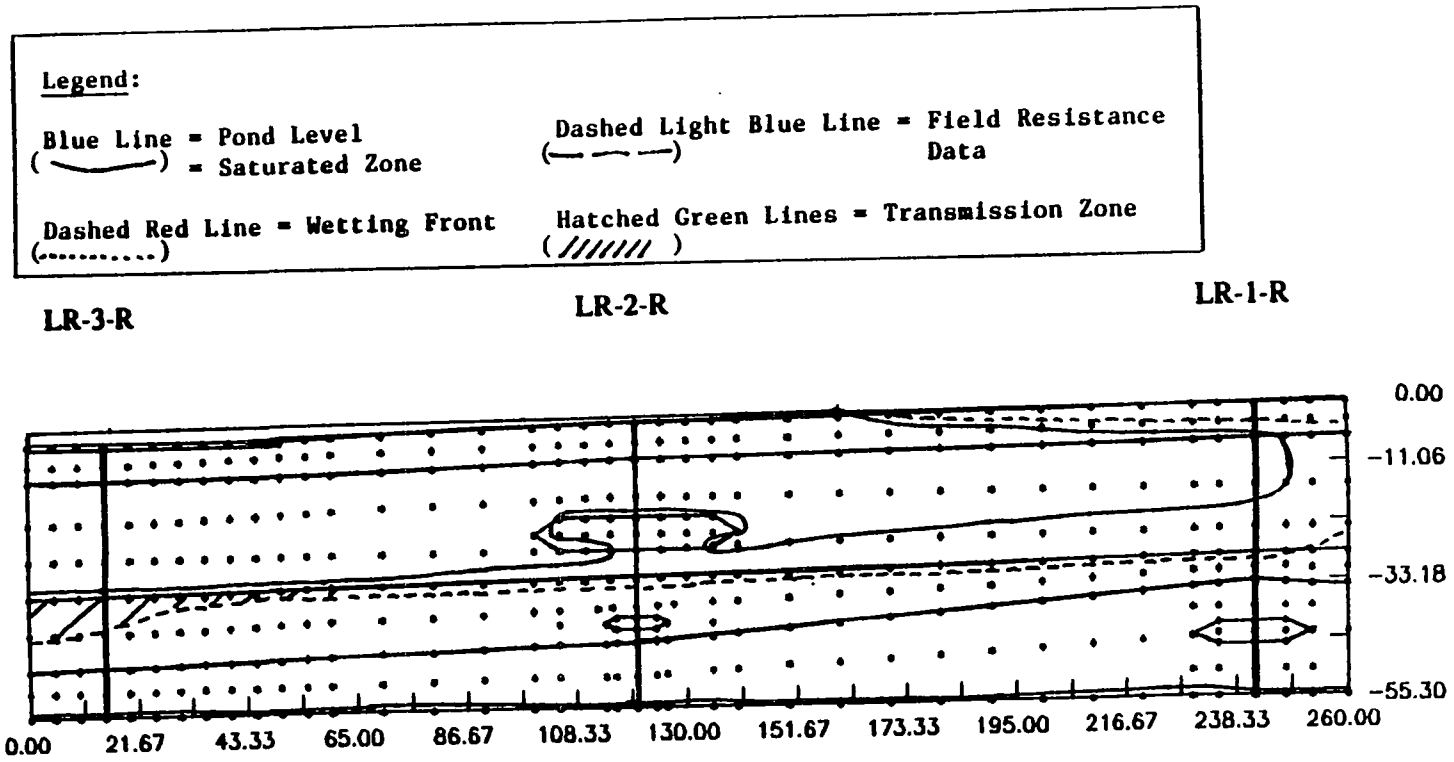

Figure 53. Wetting front, saturated zone and transmission zone after 6 days of the January 1988 storm simulation. Note the slug like movement of the saturated zone, due to the decreased surface infiltration. Pond level at LR-3-R was 2.32 feet (72.17 cm).

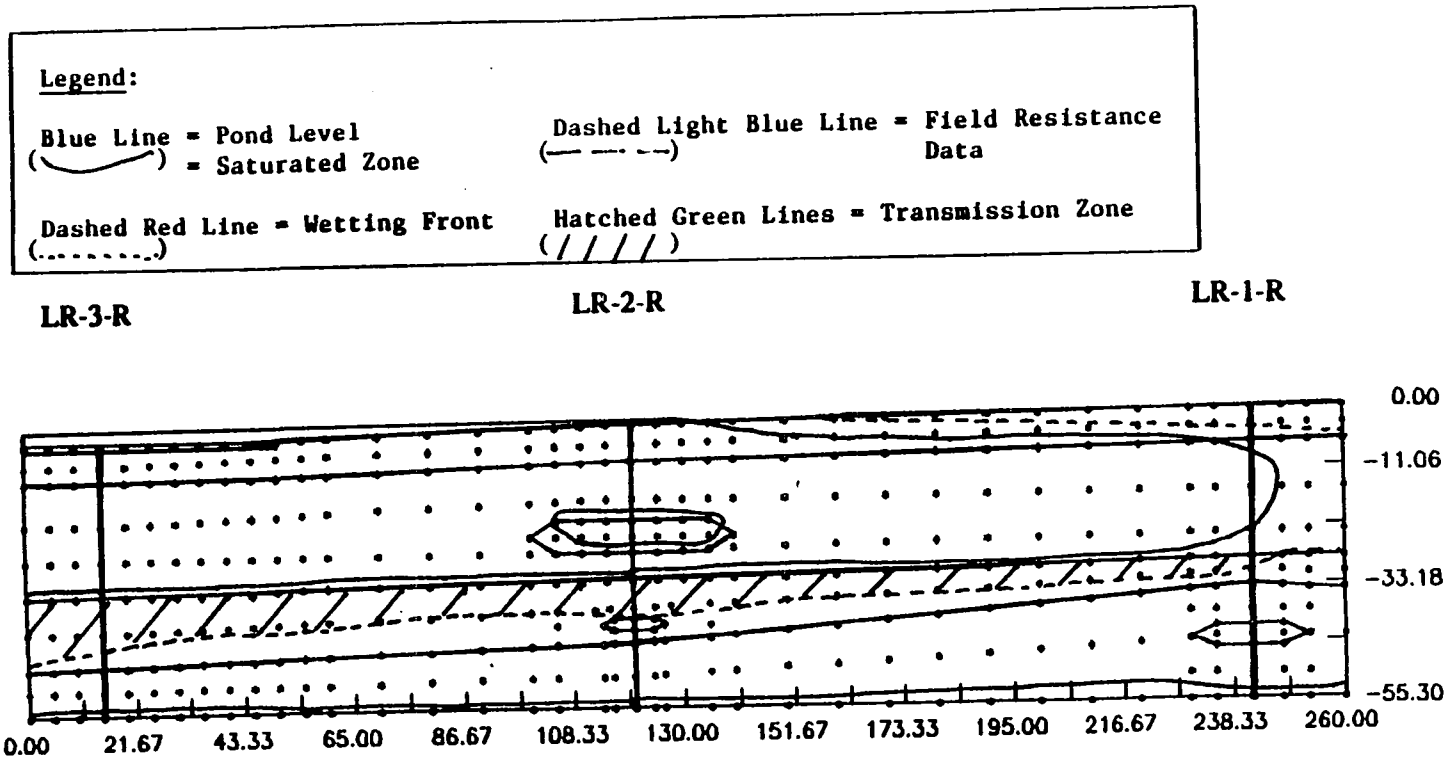

Figure 54. Wetting front, saturated zone, and transmission zone after 8 days of the January 1988 storm simulation. Pond level at LR-3-R fell to 2.07 feet (62.94 cm) after 8 days of simulation.

On the sixth day of simulation, the model predicted a "slug" type movement of the saturated zone in the vadose zone. At this time step, the saturated zone basically moved downward, under the force of gravity, and since infiltration in the southeastern portion of the basin has significantly diminished, the saturated zone moved downward, like a body or slug of water. As a result of the low surface pressure heads, the saturated zone slowly began to surround the upper sand lens and saturated it from its sides and bottoms. The wetting front had penetrated the northwest section of the lower sand unit, resulting in the development of a transmission zone in that region.

By the eighth and final day of predictive simulation, the saturated zone moved downward and thickened to engulf the upper silt unit. The southeastern upper portion of the saturated zone moved downward, out of the silty gravel. Again, the result of the decreased pond level and surface coverage near LR-1-R. By this time step, the transmission zone had progressed southeasterly along the upper silt unit/lower sand unit interface. However, the transmission zone failed to develop along the entire length of the cross-section. As mentioned above, this is the result of the decreased pond level, decreased surface coverage, and decreased volume of water available for percolation. Also, the "slug" of water (i.e., saturated zone) beneath the portion of the basin no longer ponded continued to travel downward and to broaden with time and distance traveled.

It is interesting to note that in spite of the decreasing pond level of the January 1988 storm, the pattern and timing of the progression of the wetting front between LR-3-R and LR-2-R is very similar to that produced by the February 1986 storm, through the eighth day of simulation. This is most likely due to the fact that over the first 6 days of both simulations, the average pond level was nearly the same (approximately 2.8 feet, 86 cm). As a result of the similar average pond levels, similar wetting front patterns between LR-3-R and LR-2-R developed for the first 8 days of simulation of both storms.

However, a comparison of the field ground water data for the first eight days of the February 1986 storm and the January 1988 storm indicated that the water table rose 11 feet (3.4 m) and 1.2 feet (0.4 m), respectively. The author believes that the difference in recharge between the two storms is due to the limited surface coverage, reduced pond volume, and lower pressure heads created by the NE drain outlet.

Discussion on Adjusted Hydrogeologic Parameters

Appendix F contains a comparison between the computer model saturated hydraulic conductivity for each soil material and field values, laboratory values and expected ranges for the various conductivity values. The adjusted model parameters for soil materials 1-4 all lie within the expected ranges, as catalogued by Freeze and Cherry (1979). The saturated hydraulic conductivity for soil material 5 (clay) had to be set two orders of magnitude higher to prevent model convergence problems. Minor differences (silty gravel) and major differences (silt) exist between the laboratory (permeameter) hydraulic conductivity values and the model values required to develop strong correlations with actual field behavior. However, instrument problems developed with the laboratory permeameter during core sample testing, and therefore values determined by that technique should be given less importance (Toney, personal communication, 1987). In addition, Trautwein et al. (1983) found that laboratory saturated hydraulic conductivity measurements tend to be less than those measured in the field and typically a wide range of values are obtained. This is because "laboratory tests fail to account for microscopic effects such as cracks and root holes that naturally occur in the field." Trautwein et al. also found that laboratory saturated hydraulic conductivity measurements of a clay unit at their test site ranged over five orders of magnitude! With this in mind, the calibrated computer model hydraulic

conductivity values were primarily determined by the overall model's correlation with true field behavior (soil resistance/wetting front behavior) and less so by laboratory and field conductivity values.

Trautwein et al. (1983) also firmly state that "the importance of calibrating a model cannot be over emphasized." The author has found this also to be true in his computer modeling experiences. If only laboratory values were to be used, the model would have inaccurately predicted the movement of the wetting front, because the saturated hydraulic conductivity values for the silty gravel and especially for the silt would have been much too low. It is important to keep in mind that the primary objective of this type of model is to simulate and predict the overall field effects of percolating moisture into the vadose zone. Therefore, model calibration and parameter adjustment are an extremely important process in the development of an accurate predictive model.

CONCLUSIONS

After a time consuming iterative calibration process, the model's calibrated output from the February 1986 storm developed a strong correlation with the field resistance data. By calibrating the model spatially and temporally with well-known field wetting front data, the author was able to develop a reliable predictive tool not only capable of simulating a known event, the February 1986 storm, but also useful in predicting the effects of other field type situations.

The author found that the wetting front migration was dependent upon site geology, depth of ponded water, and simulated surface conditions. The site geology had a dominant effect on the movement of the wetting front. Contrasting material/geologic properties tended to control the wetting front, for example, by causing it to distort around the upper sand lens or develop into a transmission zone at the upper silt unit/lower sand unit contact. After comparing the results of the February 1986 storm with those of the January 1988 storm, it is easy to observe the effects of depth of ponded water on migration of the wetting front. Shallow pond depths translate into smaller surface pressure heads, smaller surface coverage and a reduced volume of water available for percolation, which reduce the horizontal and vertical movement of the wetting front and reduce the effective recharge capabilities of the drainage retention basin. Last, simulated surface conditions had an important effect on the movement of the wetting front. Simulating the effects of precipitation, during the initial conditions of the February 1986 storm, on the basin surface not covered by pond water allowed the wetting front and saturation zone to develop in the southeastern section of the basin. Had the effects of precipitation not been modeled, the

model would not have properly simulated the growth of the wetting front and saturated zone by the first day of simulation.

The model predicted the development of the moisture transmission zone at the upper silt unit/lower sand unit interface. The soil resistance data were useful in determining the wetting front location, but could not be used to delineate the development of the transmission zone. The model also predicted that the saturated zone would become perched (or impeded) at the upper silt unit/lower sand unit interface. Again, the use of the resistance data was limited in that it could not be used to evaluate the occurrence of this phenomenon.

The calibrated model helped confirm the hydraulic behavior of the thick permeable sandy gravel zone in the southeast portion of the basin (not modeled). By comparing the model's output for the February 1986 storm with the contoured field resistance data and field measured ground water levels, it was concluded that the cross-section modeled was not a major source of ground water recharge. This information, field observations (high infiltration rates) and the noted lack of correlation between the D-3 boring were cited as evidence to conclude that the southeast portion of the drainage retention basin is a major site of ground water recharge.

Thorough analysis of the lateral flow simulation indicates that a significant lateral flow component exists in the upper silt unit. After 12 days of simulated percolation, the lateral movement of the wetting front in the upper silt unit nearly equaled that of the vertical component through the entire vadose zone (51 feet, 15.5 m). The author believes that the fine grained texture of the silt creates a strong affinity for moisture, hence the "wick effect," resulting in significant amounts of moisture being "pulled" (or sucked) laterally in the silt, away from the source. In addition, it was found that the lateral flow effects directly

beneath the ponded water were small and that the right and left no-flow boundaries would not adversely affect flow gradients along the finite element grid boundaries.

Upon modeling the January 1988 storm, it was concluded that the new drainage outlet in the northeast portion of the basin has a significant impact on the movement of the wetting front through the vadose zone. The drain was found to limit the depth of ponded water to 3.5 feet (1.1 m), as compared with the 10 foot (3.0 m) maximum limit in 1986. The drain also limited the pond surface coverage and the volume of ponded water available for percolation. As a result of the new drainage outlet, the model predicted that the saturated zone would move like a slug of water, in the vadose zone below the area no longer ponded, as the pond level and surface infiltration decreased, and that the saturated zone would be limited in both its vertical and horizontal extent. In addition, the development of the transmission zone was significantly reduced by the limited percolating moisture. As a result, the transmission zone failed to reach the full length of the cross-section. A comparison of the field ground water data for the first 8 days of the February 1986 storm and the January 1988 storm indicated that the water table rose 11 feet (3.4 m) and 1.2 feet (0.4 m), respectively. This recharge difference is primarily the result of the limited pond surface coverage, the decrease in volume of available water and lower pressure heads associated with shallow ponding created by the NE drain outlet.

Last, it was determined that the boundary conditions had a profound impact upon the wetting front movement and ground water table rise during the deep ponding simulation. The right, left, and bottom no-flow boundaries basically create a "glass box" (or sealed box) effect, and as a consequence, moisture may not leave the system. After nearly 12 days of deep ponding simulation, the model began to predict strange patterns of vadose zone saturation. By the twentieth day, nearly the entire cross-section was saturated, due to the "glass box" effect. To more accurately simulate a deep ponding, or extreme

flooding, this localized vadose zone model should be linked to a regional ground water model. As the present model is configured, it is not possible to accurately simulate the migration of the wetting front during deep ponding after 12 days.

REFERENCES CITED

Baver, L.D., Gardner, W. H., and Gardner, W.R., 1972, Soil Physics, Fourth Edition: John Wiley and Sons, Inc., New York, N.Y., 498 p.

Bear, J., 1979, Hydraulics of Groundwater, McGraw-Hill Series in Water Resources and Environmental Engineering: McGraw-Hill, Israel, 567 p.

Bhuiyan, S. I., Hiler, E.A., Van Bavel, C.H.M., and Aston, A.R., 1971, Dynamic Simulation of Vertical Infiltration into Unsaturated Soils: Water Resources Research, v. 7, No. 6, p. 1597-1606.

Bond, F.W., Cole, C.R., and Gutknecht, P.J., 1982, Unsaturated Groundwater Flow Model (UNSAT1D) Computer Code Manual, Report CS-2434-CCM: Prepared by Battelle Northwest Laboratories for the Electric Power Research Institute, Palo Alto, California, 194 p.

Carpenter, D.W., 1984, Assessment of Contamination in Soils and Groundwater at Lawrence Livermore National Laboratory, Sandia National Laboratory, and Adjacent Properties, Lawrence Livermore National Laboratory, Livermore, CA, UCAR-10181, 206 p.

Carpenter, D.W., Sweeny, J.J., Kasameyer, P.W., Burkhard, N.R., Knauss, K.G., and Shlemon, R.J., 1984, Geology of the Lawrence Livermore National Laboratory Site and Adjacent Areas: National Technical Information Service, U.S. Department of Commerce, Springfield, VA, 150 p.

Childs, E.C., 1969, An Introduction to the Physical Basis of Soil Water Phenomena: John Wiley and Sons, Inc., Interscience Division, New York, N.Y., 379 p.

Davis, L.A., and Neuman, S.P., 1983, Documentation and User's Guide, UNSAT2 - Variably Saturated Flow Model: Division of Waste Management, Office of Nuclear Material Safety and Safeguards, U.S. Nuclear Regulatory Commission, Washington, D.C., 203 p.

Everett, L.G., Wilson, L.G., and Hoylman. E.W., 1983, Vadose Zone Monitoring for Hazardous Waste Sites: Environmental Monitoring Systems Laboratory, Office of Research and Development, U.S. Environmental Protection Agency, Las Vegas, Nevada, 358 p.

Freeze, Allen R., 1969, The Mechanism of Natural Ground-Water Recharge and Discharge: 1. One-Dimensional, Vertical, Unsteady, Unsaturated Flow Above a Recharging or Discharging Ground-Water Flow System: Water Resources Research, v. 5, no. 1, p. 153-171.

Freeze, Allen R., 1971, Three-Dimensional, Transient, Saturated- Unsaturated Flow in a Groundwater Basin: Water Resources Research, v. 7, no. 2, p. 347-365.

Freeze, Allen R., and Cherry, John A., 1979, Groundwater: Prentice-Hall, Inc., Englewood Cliffs, New Jersey, 604 p.

Hillel, D., 1971, Soil and Water, Physical Principles and Processes: Academic Press, San Francisco, California, 288 p.

Johnson, T.M., Cartwright, K., Herzog, B. L., and Larson, T.H., 1983, Modeling of Moisture Movement Through Layered Trench Covers, in Mercer, James W., Rao, P.S.C., and Marine, I. Wendell, eds., Role of the Unsaturated Zone in Radioactive and Hazardous Waste Disposal: Ann Arbor Science, Ann Arbor, Michigan, p. 11-26.

Kirby, J.M., 1985, A Note on the Use of a Simple Numerical Model for Vertical, Unsaturated Fluid Flow: Soil Science, v. 139, no. 5, p. 462-467.

Kirkham, Don, and Powers, W.L., 1972, Advanced Soil Physics: John Wiley and Sons, Inc., Interscience Division, New York, N.Y., 534 p.

Kunze, R.J., and Nelson, D.R., 1982, Finite-Difference Solutions of the Infiltration Equation: Soil Science, v. 134, no. 2, p. 81-88. Mantoglou, Aristotelis, and Gelhar, Lynn W., 1987a, Stochastic Modeling of Large-Scale Transient Unsaturated Flow System: Water Resources Research, vol. 23, no. 1, p. 37-46.

Mantoglou, Aristotelis, and Gelhar, Lynn W., 1987, Capillary Tension Head Variance, Mean Soil Moisture Content, and Effective Specific Soil Moisture Capacity of Transient Unsaturated Flow in Stratified Soils: Water Resources Research, vol. 23, no. 1, p. 47-56.

McMahon, Peter, B., and Dennehy, Kevin, F., 1985, Water Movement in the Vadose Zone at Two Experimental Waste-Burial Trenches in South Carolina, in Proceedings of the NWWA Conference on Characterization and Monitoring of the Vadose (Unsaturated) Zone, National Water Well Publishing Co., Dublin, Ohio, p. 34-54.

Mercer, James W., Rao, P.S.C., and Marine, I., Wendell, eds., 1983, Role of the Unsaturated Zone in Radioactive and Hazardous Waste Disposal: Ann Arbor Science, Ann Arbor, Michigan, 339 p.

Maulem, Y., 1976, A Catalogue of the Hydraulic Properties of Unsaturated Soils, Development of Methods, Tools, and Solutions for Unsaturated Flow with Application to Watershed Hydrology and Other Fields, Research Project 442: Technion - Israel Institute of Technology, Hiafa, Israel, 100 p.

Neuman, Shlomo P., and Whitherspoon, Paul A., 1971, Analysis of Nonsteady Flow with a Free Surface Using the Finite Element Method: Water Resources Research, v. 7, no. 3, p. 611-623.

Neuman, Shlomo P., 1973, Saturated-Unsaturated Seepage by Finite Elements: Proceedings from the ASCE, Journal of Hydraulics Division 99, (HY12), p. 2233-2250.

Neuman, Shlomo P., 1975, Galerkin Approach to Saturated-Unsaturated Flow in Porous Media, in Gallagher, J.T., Oden, C. Taylor, and Zienkiewicz, O.C., eds., Finite Elements in Fluids, Volume I: Viscous Flow and Hydrodynamics: John Wiley and Sons, Inc., London, p. 201-217.

Neuman, Shlomo P., Feddes, Reinder A., and Bresler, 1975, Finite Element Analysis of Two-Dimensional Flow in Soils Considering Water Update by Plant Roots: I. Theory: Soil Science, v. 39, no. 2, p. 224-230.

Oberdorfer, June A. and Toney, Kenneth, 1986, Water Transport in the Vadose Zone Beneath a Drainage Retention Basin: EOS., v. 67, no. 44, p. 944.

Pinder, G.F., and Gray, W.G., 1977, Finite Element Simulation in Surface and Subsurface Hydrology: Academic Press, New York, N.Y. 295 p.

Ragab, R., Feyen. J., and Hillel, D., 1982, Comparison of Experimental and Simulated Infiltration Profiles in Sand: Soil Science, v. 133, no. 1, p. 61-64.

Rojstaczer, S.A., 1981, Moisture Movement Through Layered Soils of Highly Contrasting Texture (Unpublished M.S. Thesis): University of Illinois, 86 p.

Stone, R., Ruggieri, M.R., Rogers, L.L., Emerson, D.O., and Buddemeier, R.W., 1982, Potential for Saturated Ground-Water System Contamination at the Lawrence Livermore National Laboratory: National Technical Information Service, U.S. Department of Commerce, Springfield, VA, 105 p.

Toney, Kenneth, and Oberdorfer, June A., 1986, Quantifying Groundwater Recharge Under a Drainage Retention Basin: EOS, v. 67, no. 44, p. 944.

Toney, Kenneth, 1988, A Hydrogeological Investigation of Groundwater Recharge Near the Drainage Retention Basin, Lawrence Livermore National Laboratory, Livermore, California (Unpublished M.S. Thesis Draft): San Jose State University.

Trautwein, Steven, J., Daniel, David E., and Cooper, Michael W., 1983, Case History Study of Water Flow Through Unsaturated Soil, in Mercer, James W., Rao, P.S.C., and Marine, I. Wendell, eds., Role of the Unsaturated Zone in Radioactive and Hazardous Waste Disposal, Ann Arbor Science, Ann Arbor, Michigan, p. 229-253.

U.S. EPA, 1986, Soiliner Model - Documentation and User's Guide (Version 1): Environmental Protection Agency, Cincinnati, Ohio, 85 p.

Vauclin, M., Khanji, D., and Vachaud, G., 1979, Experimental and Numerical Study of a Transient, Two-Dimensional Unsaturated-Saturated Water Table Recharge Problem: Water Resources Research, v. 15, no. 5, p. 1089-1101.

Wang, H.F., and Anderson, M.P., 1982, Introduction to Groundwater Modeling, Finite Difference and Finite Element Methods, W.H. Freeman and Company, San Francisco, CA, 237 p.

Winter, Thomas C., 1978, Numerical Simulation of Steady Three-Dimensional Groundwater Flow Near Lakes: Water Resources Research v. 14, no. 2, p. 245-254.

Yeh, Jim T.C., Gelhar, Lynn W., and Gutjahr, Allen L., 1985, Stochastic Analysis of Unsaturated Flow in Heterogeneous Soils: 1. Statistically Isotropic Media: Water Resources Research, v. 21, no. 4, p. 447-456.

APPENDIX A

Geologic Logs of Borings

Figure 55. Geologic log for LR-1-R.

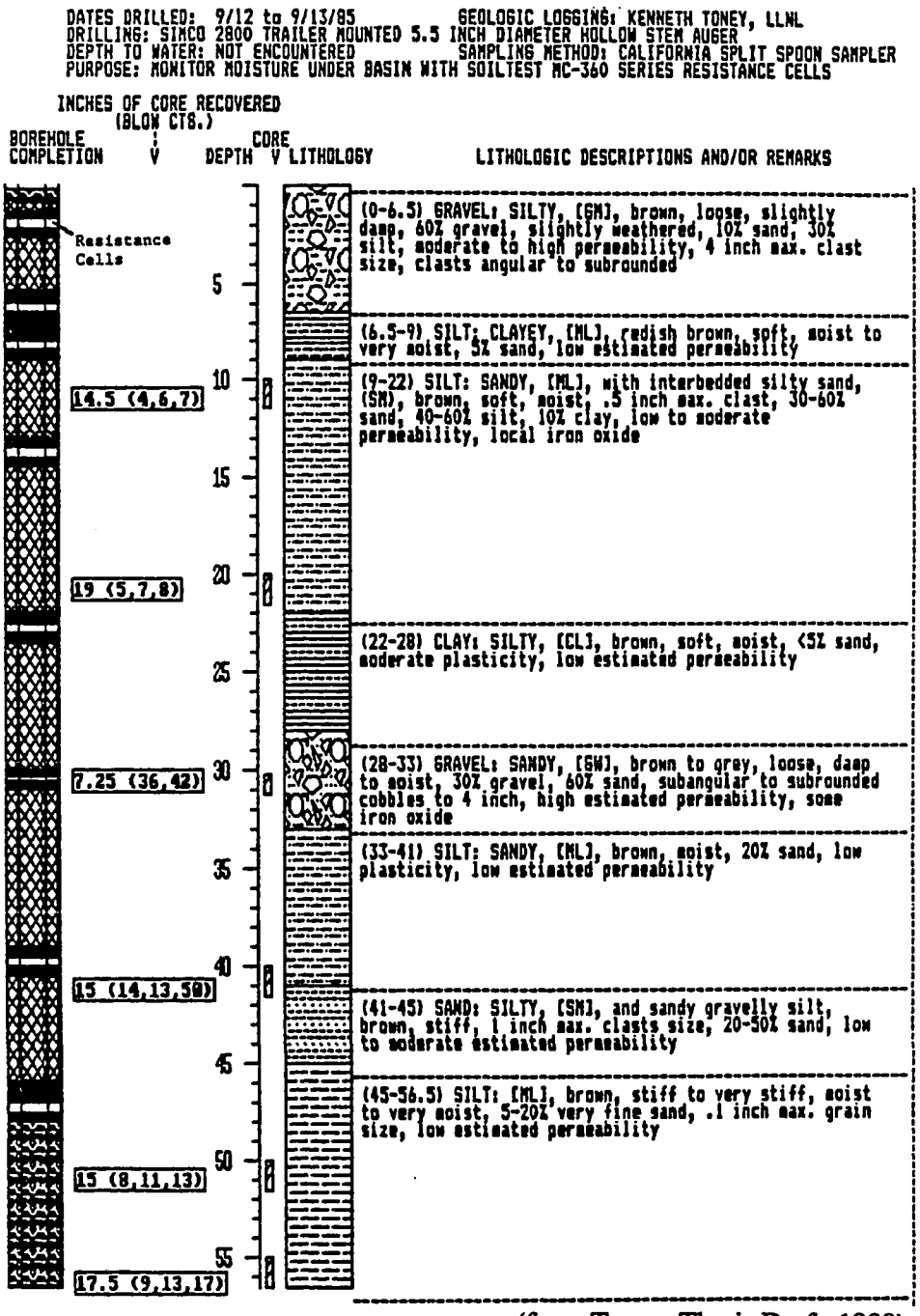

(from Toney, Thesis Draft, 1988)

Figure 56. Geologic log for LR-2-R.

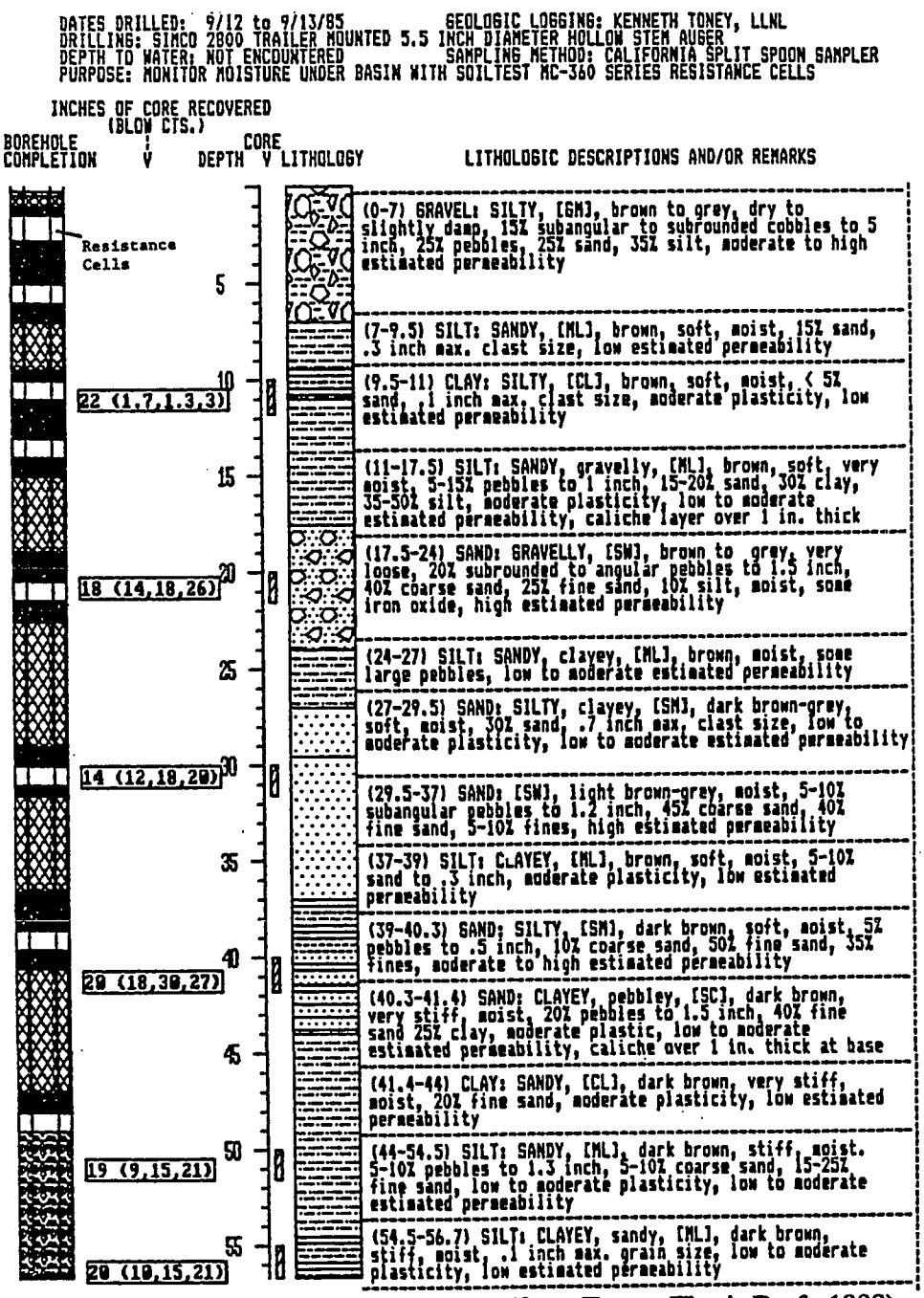

(from Toney, Thesis Draft, 1988)

Figure 57. Geologic log for LR-3-R.

DATES DRILLED: 9/12 to 9/13/85 GEOLOGIC LOGGING: KENNETH TONEY, LLNL
DRILLING: SIMCO 2800 TRAILER MOUNTED 5.5 INCH DIAMETER HOLLOW STEM AUGER
DEPTH TO WATER: NOT ENCOUNTERED SAMPLING METHOD: CALIFORNIA SPLIT SPOON SAMPLER
PURPOSE: MONITOR MOISTURE UNDER BASIN WITH SOILTEST MC-360 SERIES RESISTANCE CELLS

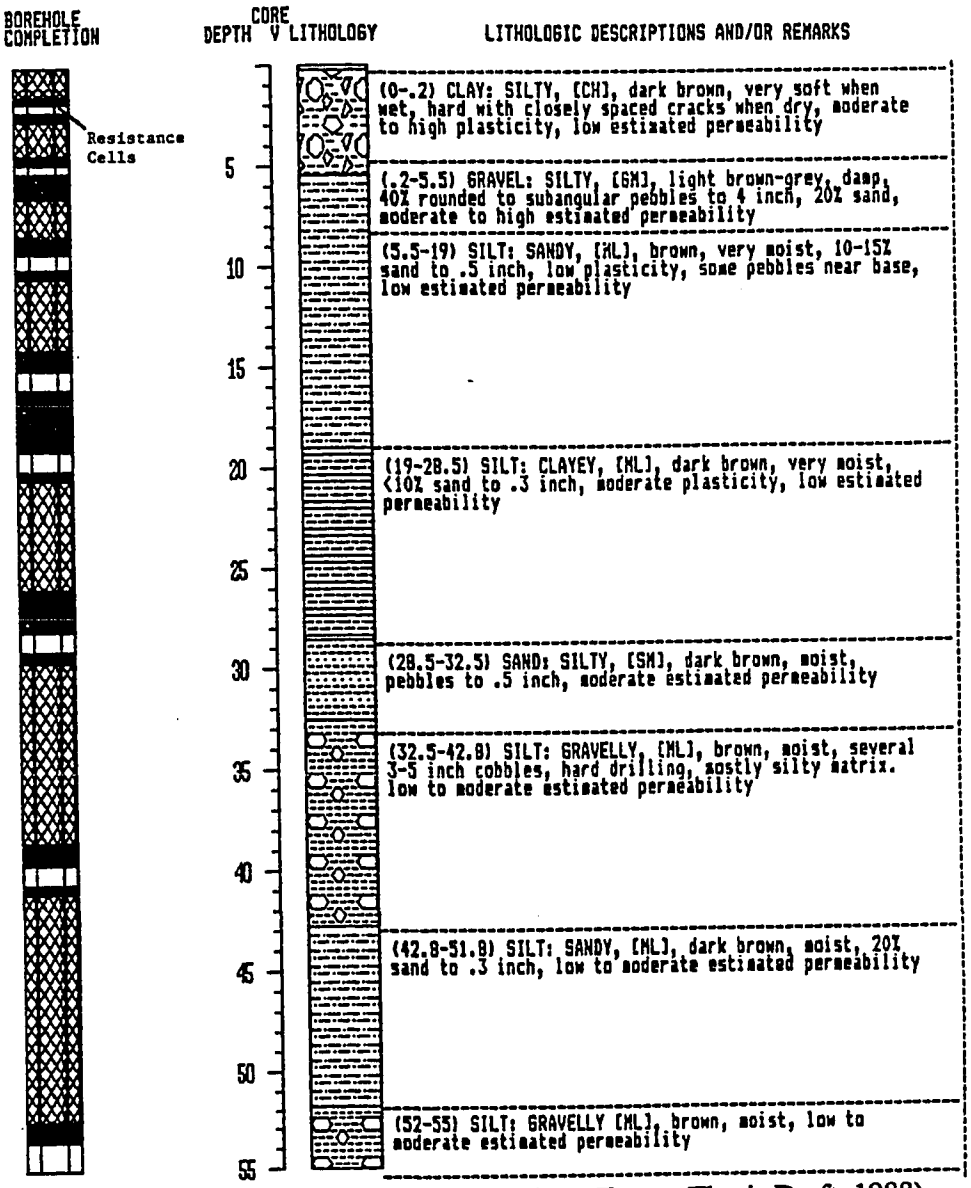

(from Toney, Thesis Draft, 1988)

Figure 58. Geologic log from LR-4-P.

PIEZOMETER LOCATION: NORTH-CENTRAL PORTION OF THE DRAINAGE RETENTION BASIN, LLNL SITE
LLNL COORDINATES: N: 11,570 E: 10,522 ELEVATION: 602.1 FEET
DATES DRILLED: 9/17 to 9/19/85 GEOLOGIC LOGGING: KENNETH TONEY, LLNL
DRILLING: SIMCO 2800 TRAILER MOUNTED 5.5 INCH DIAMETER HOLLOW STEM AUGER
DEPTH TO WATER: 53.5 FEET (STATIC) SAMPLING METHOD: CALIFORNIA SPLIT SPOON SAMPLER
PURPOSE: MONITOR WATER TABLE ELEVATION CASING: 1.5 INCH I.D. ASTM SCHEDULE 80 PVC, THREADED
SAND PACK: #3 AND #0 LONESTAR SAND WELL TESTS: UNDEVELOPED, NO GEOPHYSICAL LOGS
SCREEN: 1.5 INCH I.D. ASTM SCHEDULE 80 PVC, .01 INCH SLOTS, THREADED, CAPPED AT BOTTOM
ANNULAR SEAL: 95% CEMENT, 5% BENTONITE WITH 1 FOOT OF BENTONITE PELLETS ABOVE SAND PACK

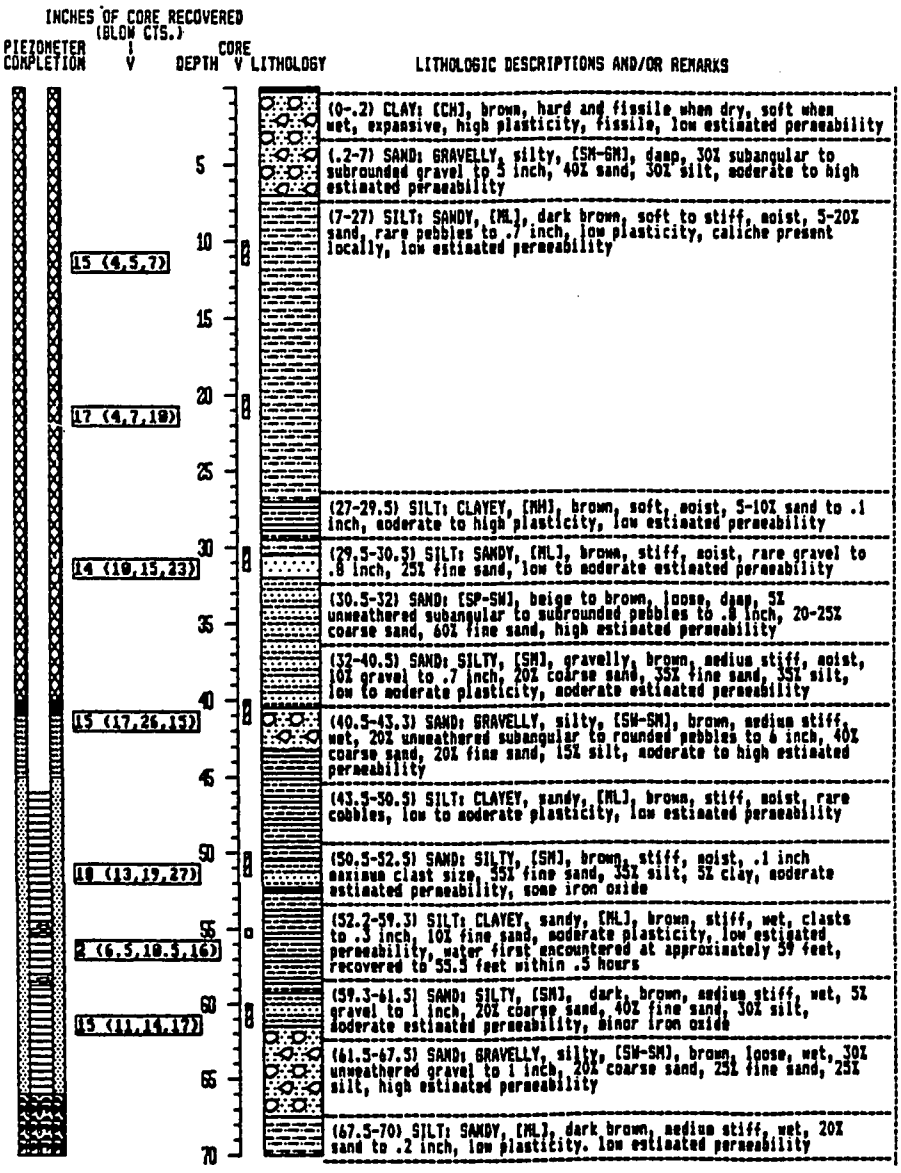

(from Toney, Thesis Draft, 1988)

Figure 59. Geologic log from D-3.

SUMMARY LOG

HOLE NO. D-3 DRILLED: 5/10/84

COORDINATES GR. ELEV.: 505.4

N: 434662.8

E: 1652219.3

LOGGED BY: G. A. Pawloski WATER: Not encountered

DEPTH FT.	DRILLING LOG	%SAMPLE REC.	SAMPLE NO. DEPTH	GEOLOGIC DESCRIPTION
0				0.0-4.0 FILL 0.0-3.0 Clayey Sand (SC): Slightly plastic, 5% suorounded gravel, well sorted, 0.5" max, 70% fine-medium sand, 25% plastic fines, minor organics, brown, moist. 3.0-4.0 Clayey Gravel (GC): Slightly plastic, 65% suorounded-subangular gravel, poorly sorted, 35% plastic fines, brown, moist.
	*	65	1A 2.2-2.7 1B 2.7-3.2	
	*	96	2A 5.9-6.4 2B 6.4-6.9	
10	*	63	3A 10.2-10.7 3B 10.7-11.2	4.0-51.6 QUATERNARY ALLUVIUM 4.0-5.6 Clayey Sand (SC): Slightly plastic, 70% fine-medium sand, 30% plastic fines, brown, moist. 5.6-10.2 Clayey Gravel (GC): Slightly plastic, 65% subrounded gravel, well graded, common red clay coatings, 35% plastic fines, red-brown to brown, moist, grades to sandy clay.
20	*	75	4A 20.5-21.0 4B 21.0-21.5	10.2-20.0 Sandy Clay (SC): Slightly plastic, 10% rounded gravel, poorly sorted, 1.75" max, 60% fine-medium sand, 30% plastic fines, minor organics, red-brown to brown, damp, grades to silty sand. 20.0-40.0 Silty Sand (SM): Non plastic, 70% fine- medium sand, 30% non plastic fines, rare organics, brown, damp, grades to sandy clay.
30	*	63	5A 30.2-30.7 5B 30.7-31.2	
40	*	75	6A 40.0-40.3 6B 40.3-40.8	40.0-50.4 Sandy Clay (CL): Moderately plastic, 5% suorounded gravel, well sorted, 0.5" max, 30% fine-medium sand, 65% plastic fines, common scattered caliched veinlets and organics, brown, damp, grades to silty sand.
50	*	83	7A 50.6-51.1 7B 51.1-51.6	50.4-51.6 Silty Sand (SM): Non plastic, 70% fine-medium sand, 30% non plastic fines, minor organics, brown, damp.
	TD 51.6'			
60				

† Augered Interval *Sampled Interval

(from Carpenter, 1984)

APPENDIX B

Soil Material Characteristic Curves

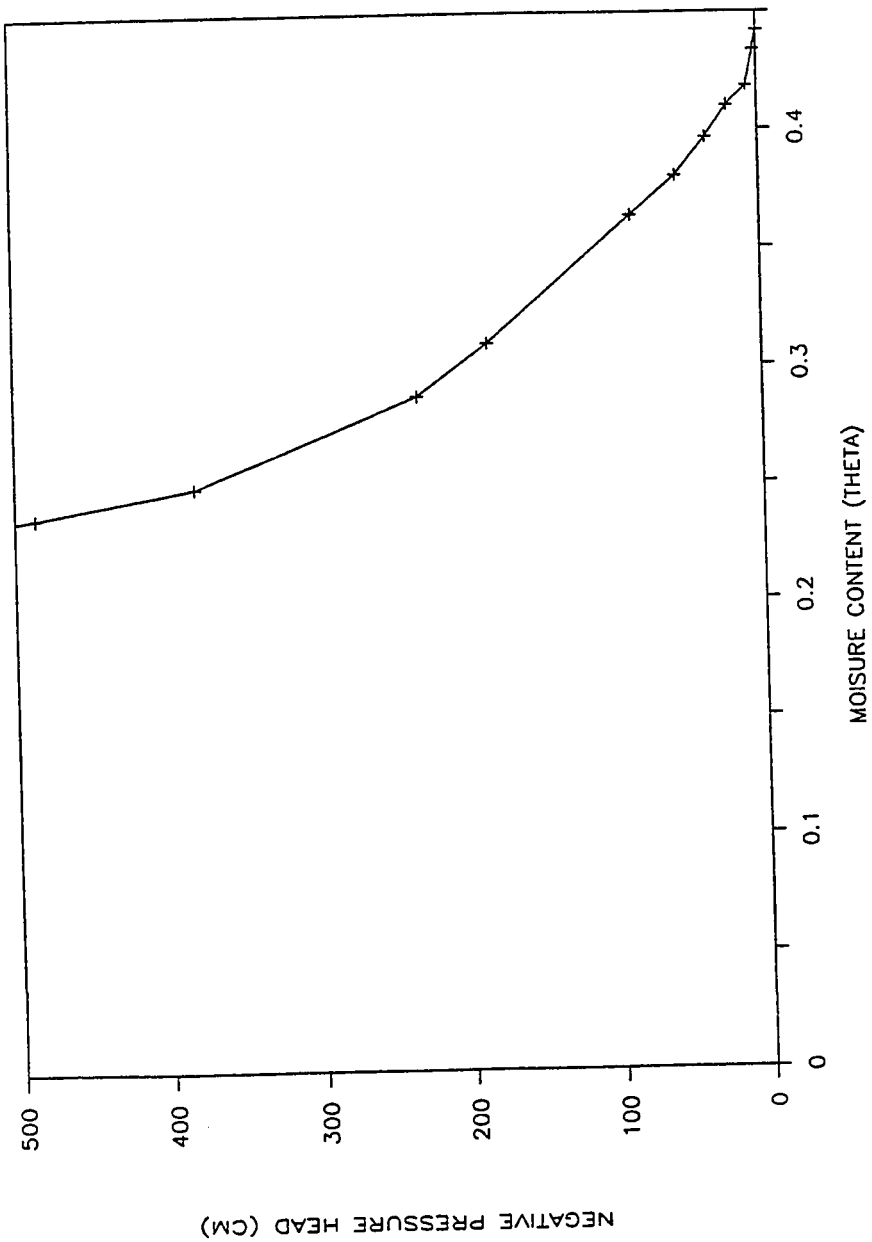

Figure 60. Soil material 1 (clayey silt) pressure head vs. moisture content characteristic curve. The saturated hydraulic conductivity is 1.85×10^{-5} cm/s. The saturated moisture content is 0.442. This curve is adapted from Mualem's (1976) Limon Silteux #2002.

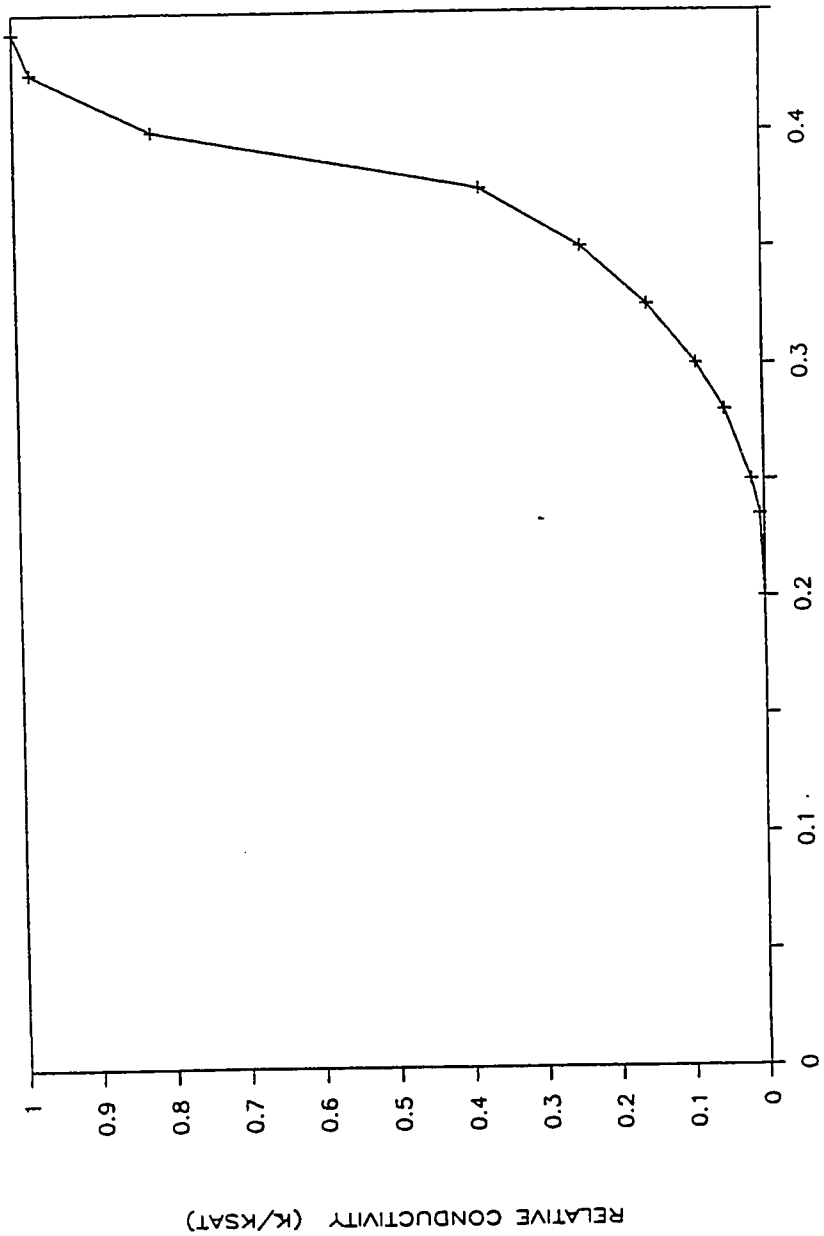

Figure 61. Soil material 1 (clayey silt) relative conductivity vs. moisture content characteristic curve. The saturated hydraulic conductivity is 1.85×10^{-5} cm/s. The saturated moisture content is 0.442. This curve is adapted from Mualem's (1976) Limon Silteux #2002.

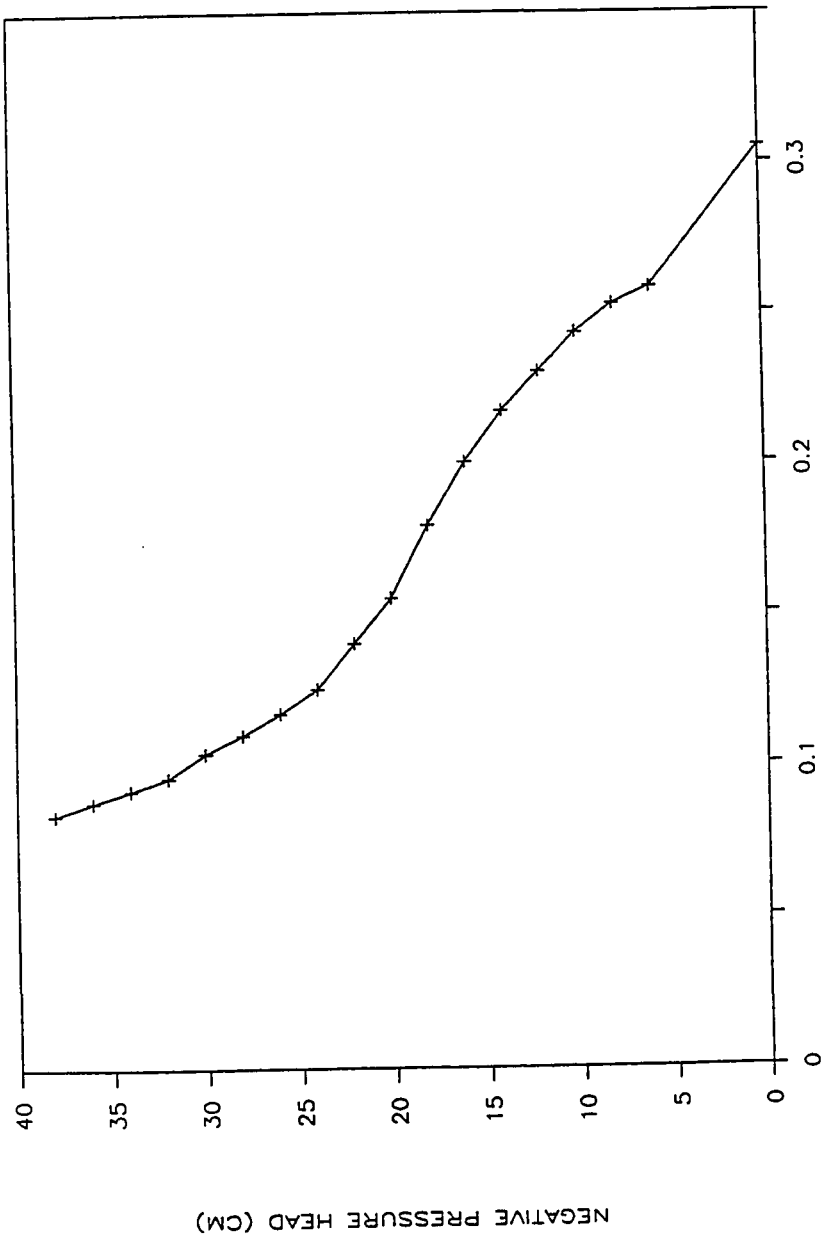

Figure 62. Soil material 2 (silty gravel) pressure head vs. moisture content characteristic curve. The saturated hydraulic conductivity is 1.39×10^{-3} cm/s. The saturated moisture content is 0.305. This curve is adapted from Mualem's (1976) Sand #4107.

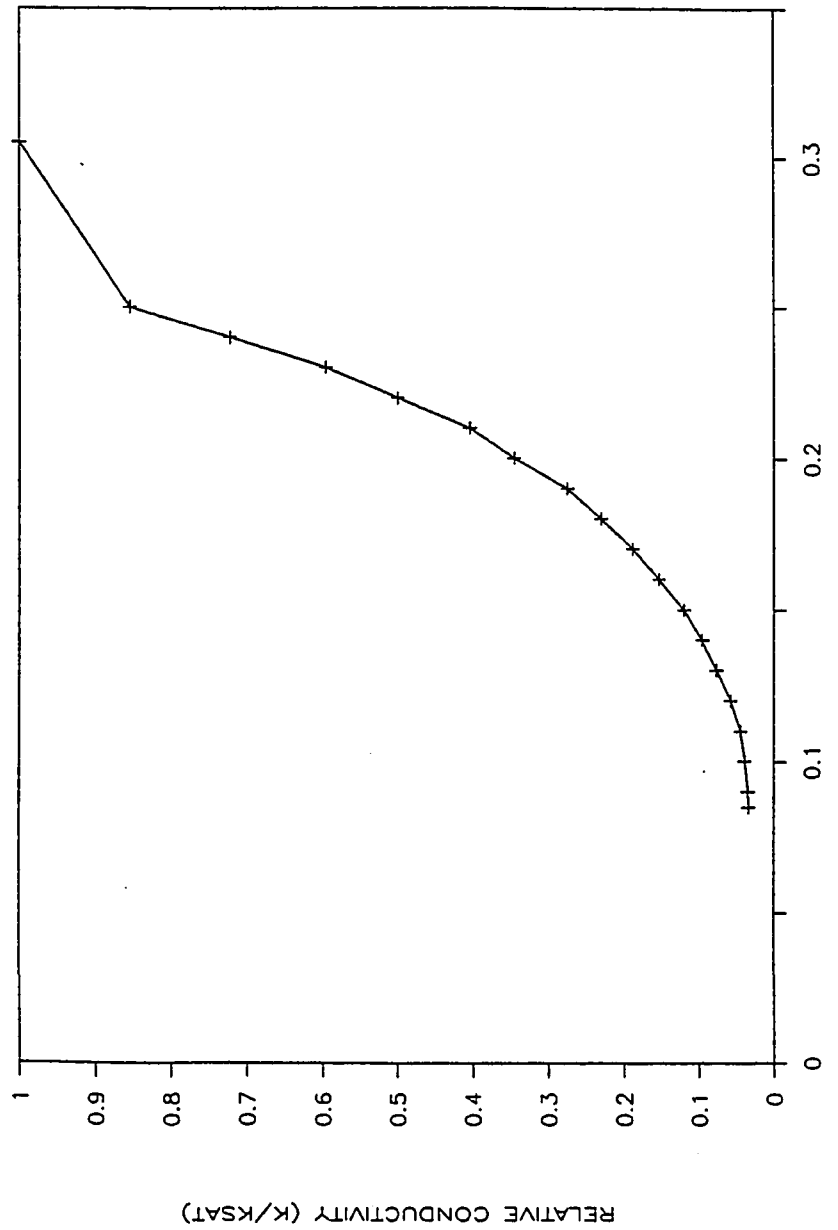

Figure 63. Soil material 2 (silty gravel) relative conductivity vs. moisture content characteristic curve. The saturated hydraulic conductivity is 1.39×10^{-3} cm/s. The saturated moisture content is 0.305. This curve is adapted from Mualem's (1976) Sand #4107.

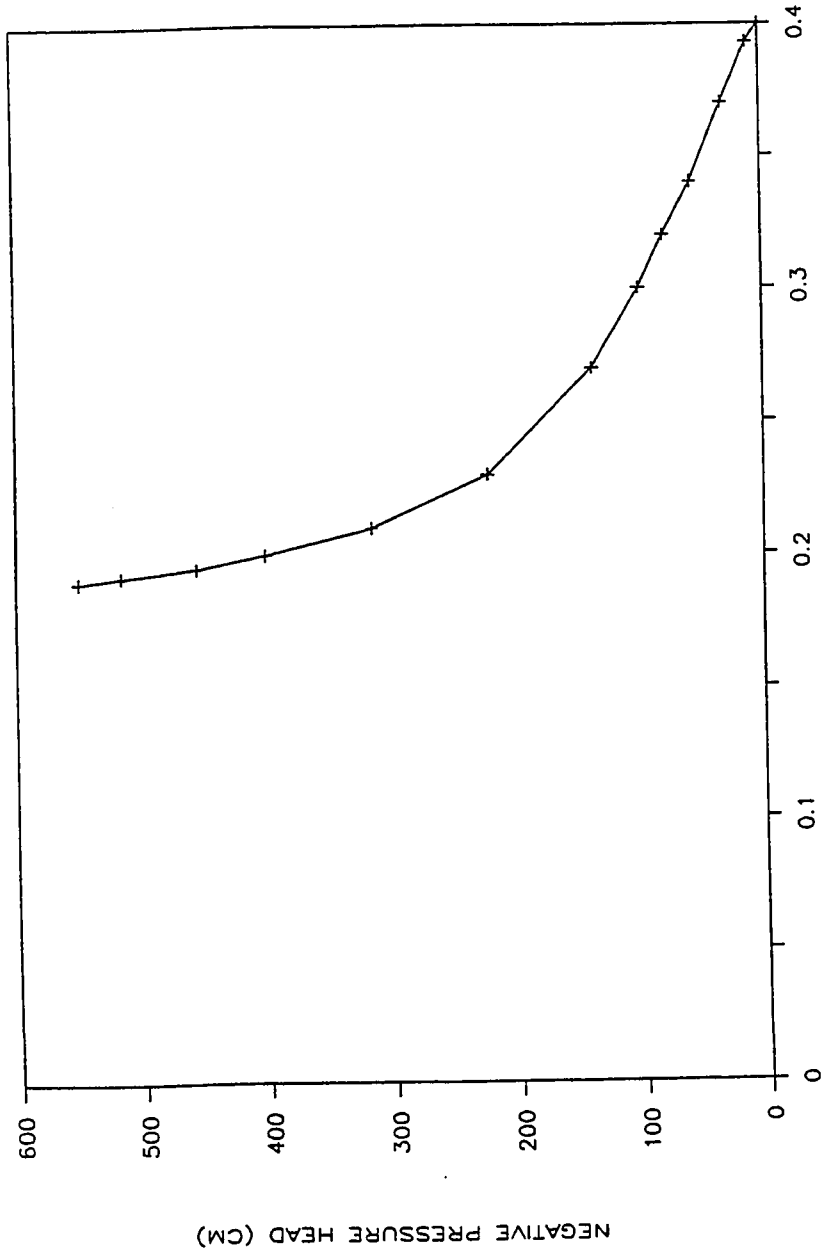

Figure 64. Soil material 3 (silt) pressure head vs. moisture content characteristic curve. The saturated hydraulic conductivity is 8.1×10^{-5} cm/s. The saturated moisture content is 0.4. This curve is adapted from Mualem's (1976) Columbia Silt #2001.

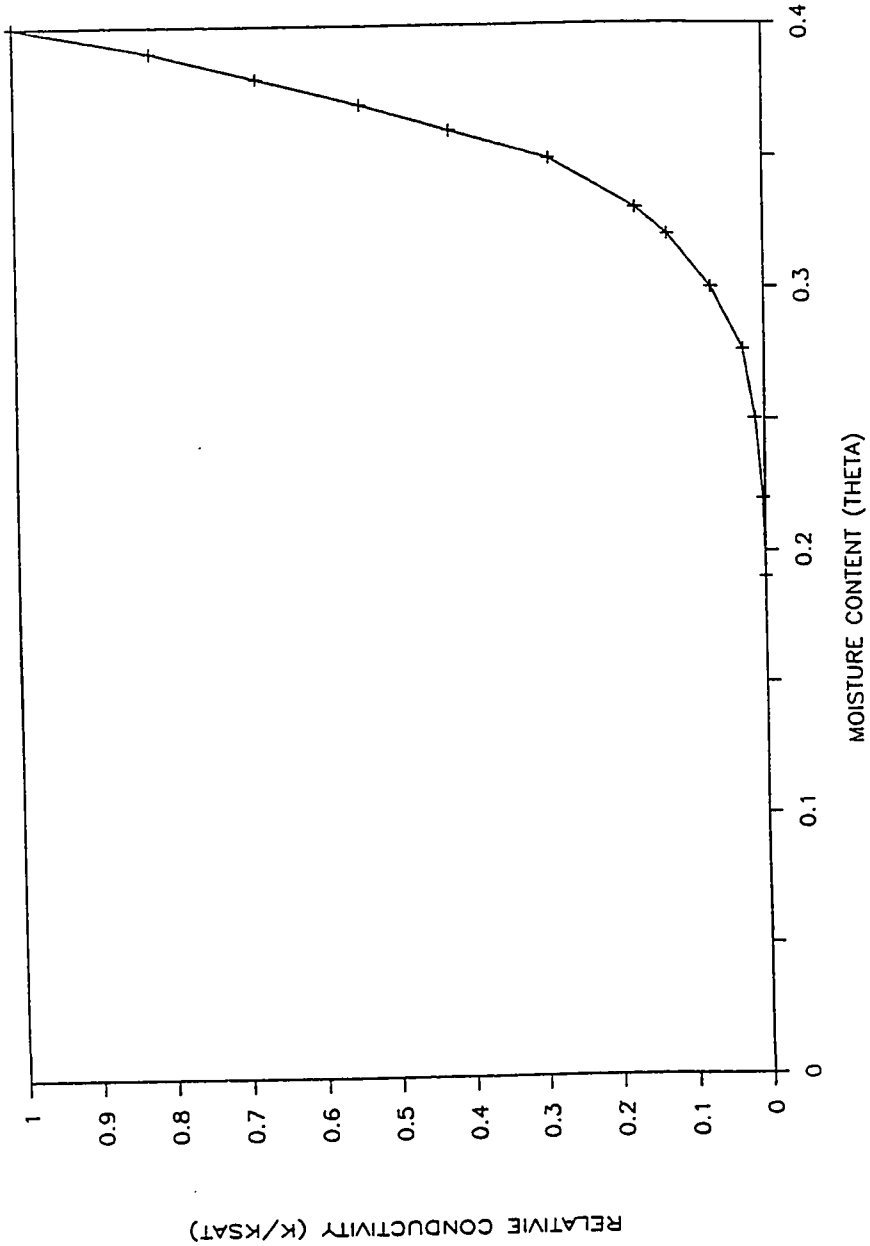

Figure 65. Soil material 3 (silt) relative conductivity vs moisture content characteristic curve. The saturated hydraulic conductivity is 8.1×10^{-5} cm/s. The saturated moisture content is 0.4. This curve is adapted from Mualem's Columbia Silt #2001.

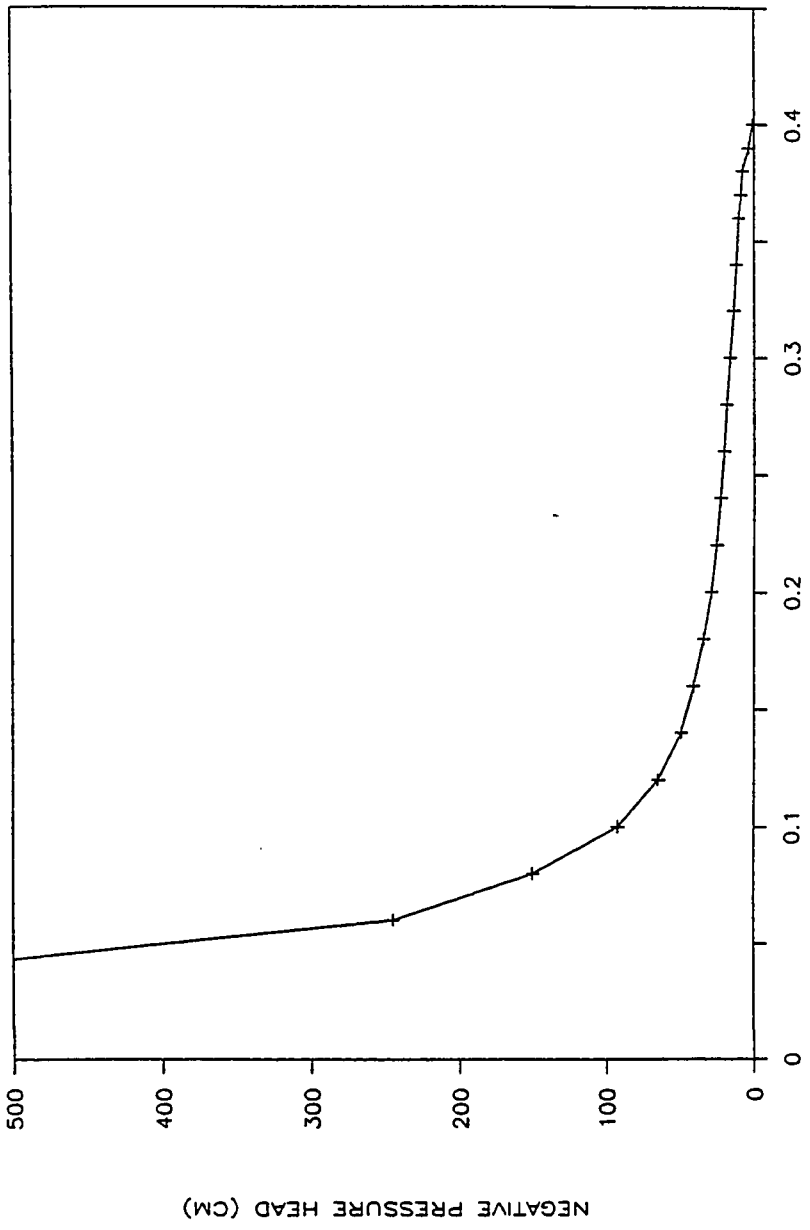

Figure 66. Soil material 4 (sand) pressure head vs moisture content characteristic curve. The saturated moisture content is 0.44. The saturated hydraulic conductivity is 7 x 10^{-4} cm/s. This curve is adapted from Mualem's (1986) Rehovot Sand #4121.

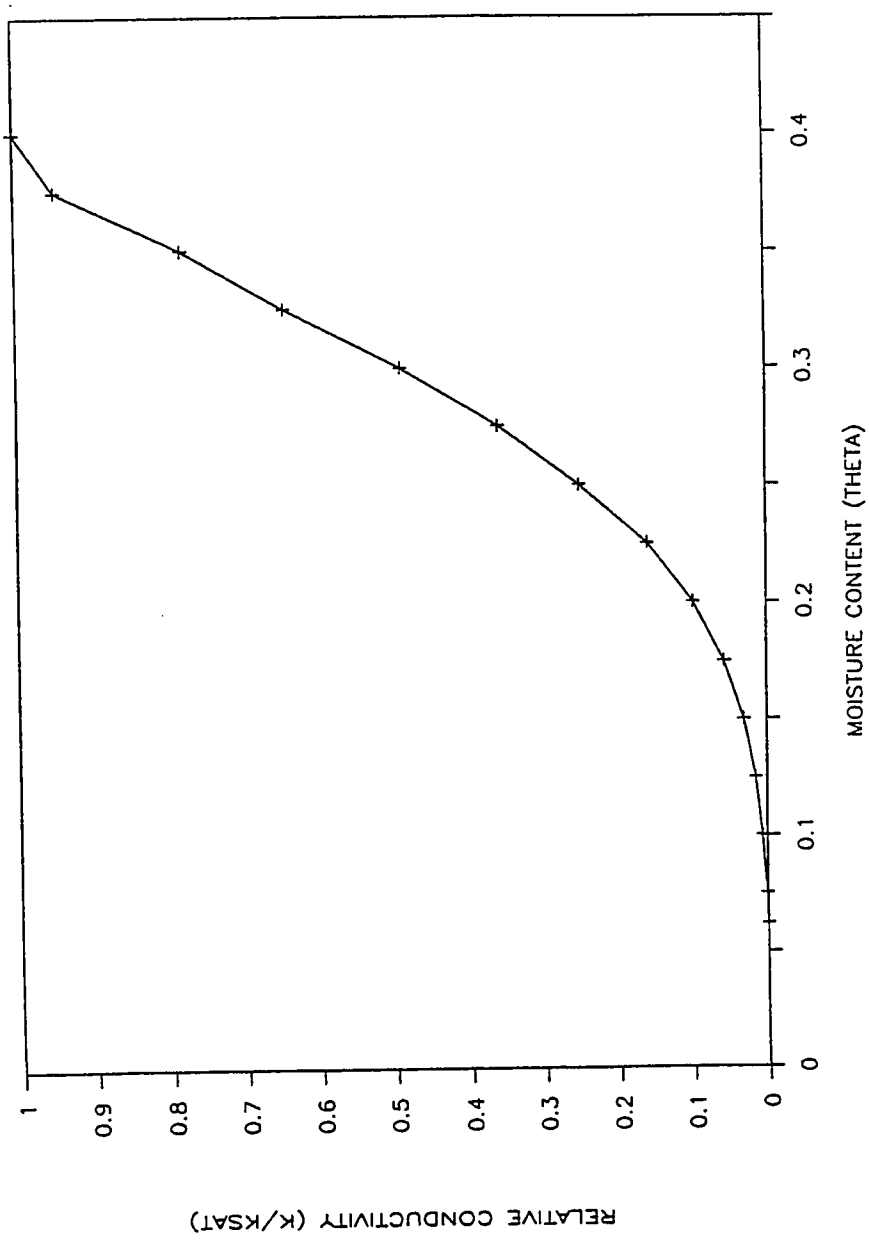

Figure 67. Soil material 4 (sand) relative conductivity vs moisture content characteristic curve. The saturated hydraulic conductivity is 7×10^{-4} cm/s. The saturated moisture content is 0.44. This curve is adapted from Mualem's (1976) Rehovot Sand #4121.

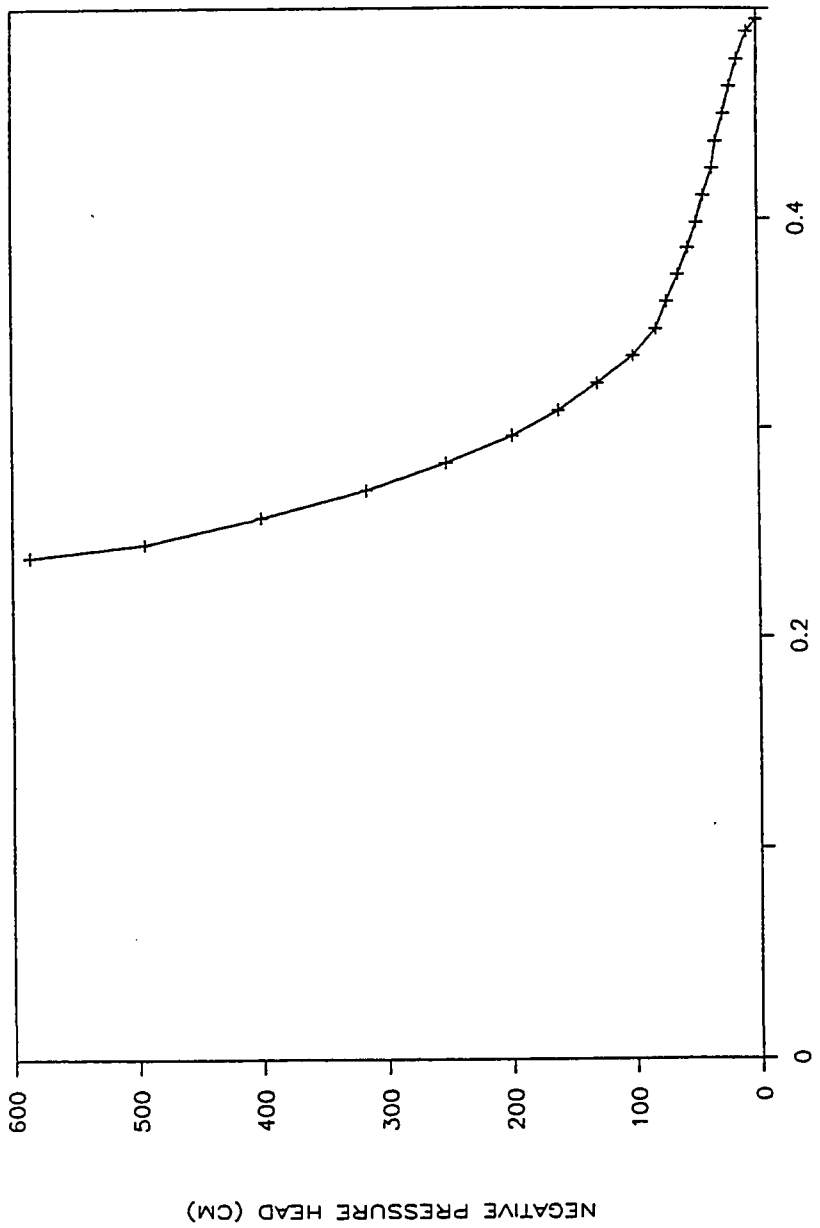

Figure 68. Soil material 5 (clay) pressure head vs. moisture content characteristic curve. The saturated moisture content is 0.495. The saturated hydraulic conductivity is 1.2×10^{-5} cm/s. This curve is adapted from Mualem's (1976) Yolo Light Clay #3102.

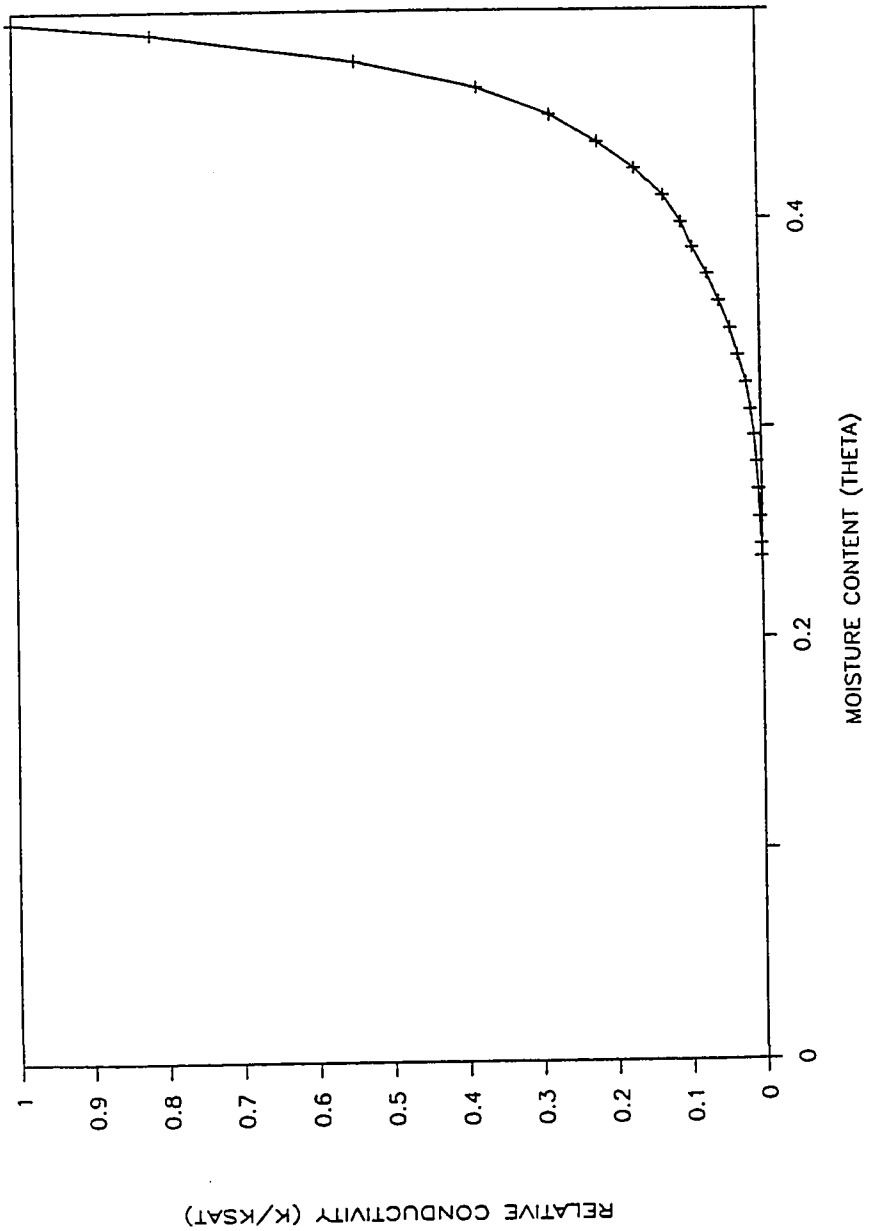

Figure 69. Soil Material 5 (clay) relative conductivity vs. moisture content characteristic curve. The saturated hydraulic conductivity is 1.2×10^{-5} cm/s. The saturated moisture content is 0.495. This curve is adapted from Mualem's (1976) Yolo Light Clay #3102.

APPENDIX C

Measured and Extrapolated Surface Node Pressure Heads

Table 2. Measured and extrapolated surface node pressure heads in centimeters, used in the February 1986 storm simulation and calibration.

SIMULATION DAY	DATE	NODE NUMBER 11	22	33	44	55
	* FEB 11	52.58	52.58	52.58	52.58	52.58
DAY 1	FEB 11.5	54.03	54.03	54.03	54.03	54.03
	* FEB 12	55.47	55.47	55.47	55.47	55.47
DAY 2	FEB 12.5	75.90	75.90	75.90	75.90	75.90
	* FEB 13	96.32	96.32	96.32	96.32	96.32
DAY 3	FEB 13.5	97.28	97.28	97.28	97.28	97.28
	FEB 14	98.25	98.25	98.25	98.25	98.25
DAY 4	FEB 14.5	99.21	99.21	99.21	99.21	99.21
	FEB 15	100.18	100.18	100.18	100.18	100.18
DAY 5	FEB15.5	101.14	101.14	101.14	101.14	101.14
	* FEB 16	102.11	102.11	102.11	102.11	102.11
DAY 6	FEB 16.5	119.02	119.02	119.02	119.02	119.02
	FEB 17	135.94	135.94	135.94	135.94	135.94
DAY 7	FEB 17.5	152.86	152.86	152.86	152.86	152.86
	* FEB 18	169.77	169.77	169.77	169.77	169.77
DAY 8	FEB 18.5	237.29	237.29	237.29	237.29	237.29
	* FEB 19	304.80	304.80	304.80	304.80	304.80
DAY 9	FEB 19.5	304.80	304.80	304.80	304.80	304.80
	* FEB 20	304.80	304.80	304.80	304.80	304.80
DAY 10	FEB 20.5	254.66	254.66	254.66	254.66	254.66
	* FEB 21	204.52	204.52	204.52	204.52	204.52
DAY 11	FEB 21.5	204.06	204.06	204.06	204.06	204.06
	FEB 22	203.61	203.61	203.61	203.61	203.61
DAY 12	FEB 22.5	203.15	203.15	203.15	203.15	203.15
	* FEB 23	202.69	202.69	202.69	202.69	202.69
DAY 13	FEB 23.5	181.81	181.81	181.81	181.81	181.81
	FEB 24	160.93	160.93	160.93	160.93	160.93
DAY 14	FEB 24.5	140.06	140.06	140.06	140.06	140.06
	* FEB 25	119.18	119.18	119.18	119.18	119.18

* MEASURED DATA POINT + VALUE DURING SIMULATION

SIMULATION DAY	DATE	NODE NUMBER 66	77	88	99	110
	* FEB 11	52.58	52.58	52.58	52.58	52.58
DAY 1	FEB 11.5	54.03	54.03	54.03	54.03	54.03
	* FEB 12	55.47	55.47	55.47	55.47	55.47
DAY 2	FEB 12.5	75.90	75.90	75.90	75.90	75.90
	* FEB 13	96.32	96.32	96.32	96.32	96.32
DAY 3	FEB 13.5	97.28	97.28	97.28	97.28	97.28
	FEB 14	98.25	98.25	98.25	98.25	98.25
DAY 4	FEB 14.5	99.21	99.21	99.21	99.21	99.21
	FEB 15	100.18	100.18	100.18	100.18	100.18
DAY 5	FEB15.5	101.14	101.14	101.14	101.14	101.14
	* FEB 16	102.11	102.11	102.11	102.11	102.11
DAY 6	FEB 16.5	119.02	119.02	119.02	119.02	119.02
	FEB 17	135.94	135.94	135.94	135.94	135.94
DAY 7	FEB 17.5	152.86	152.86	152.86	152.86	152.86
	* FEB 18	169.77	169.77	169.77	169.77	169.77
DAY 8	FEB 18.5	237.29	237.29	237.29	237.29	237.29
	* FEB 19	304.80	304.80	304.80	304.80	304.80
DAY 9	FEB 19.5	304.80	304.80	304.80	304.80	304.80
	* FEB 20	304.80	304.80	304.80	304.80	304.80
DAY 10	FEB 20.5	254.66	254.66	254.66	254.66	254.66
	* FEB 21	204.52	204.52	204.52	204.52	204.52
DAY 11	FEB 21.5	204.06	204.06	204.06	204.06	204.06
	FEB 22	203.61	203.61	203.61	203.61	203.61
DAY 12	FEB 22.5	203.15	203.15	203.15	203.15	203.15
	* FEB 23	202.69	202.69	202.69	202.69	202.69
DAY 13	FEB 23.5	181.81	181.81	181.81	181.81	181.81
	FEB 24	160.93	160.93	160.93	160.93	160.93
DAY 14	FEB 24.5	140.06	140.06	140.06	140.06	140.06
	* FEB 25	119.18	119.18	119.18	119.18	119.18

* MEASURED DATA POINT + VALUE DURING SIMULATION

SIMULATION DAY	DATE	NODE NUMBER 121	131	141	151	161
	* FEB 11	52.58	49.53	43.43	37.34	28.19
DAY 1	FEB 11.5	54.03	50.98	44.88	38.79	29.64
	* FEB 12	55.47	52.42	46.33	40.23	31.09
DAY 2	FEB 12.5	75.90	72.85	66.75	60.66	51.51
	* FEB 13	96.32	93.27	87.17	81.08	71.93
DAY 3	FEB 13.5	97.28	94.23	88.14	82.04	72.90
	FEB 14	98.25	95.20	89.10	83.01	73.86
DAY 4	FEB 14.5	99.21	96.16	90.07	83.97	74.83
	FEB 15	100.18	97.13	91.03	84.94	75.79
DAY 5	FEB15.5	101.14	98.09	92.00	85.90	76.76
	* FEB 16	102.11	99.06	92.96	86.87	77.72
DAY 6	FEB 16.5	119.02	115.97	109.88	103.78	94.64
	FEB 17	135.94	132.89	126.80	120.70	111.56
DAY 7	FEB 17.5	152.86	149.81	143.71	137.62	128.47
	* FEB 18	169.77	166.72	160.63	154.53	145.39
DAY 8	FEB 18.5	237.29	234.24	228.14	222.05	212.90
	* FEB 19	304.80	301.75	295.66	289.56	280.42
DAY 9	FEB 19.5	304.80	301.75	295.66	289.56	280.42
	* FEB 20	304.80	301.75	295.66	289.56	280.42
DAY 10	FEB 20.5	254.66	251.61	245.52	239.42	230.28
	* FEB 21	204.52	201.47	195.38	189.28	180.14
DAY 11	FEB 21.5	204.06	201.01	194.92	188.82	179.68
	FEB 22	203.61	200.56	194.46	188.37	179.22
DAY 12	FEB 22.5	203.15	200.10	194.01	187.91	178.77
	* FEB 23	202.69	199.64	193.55	187.45	178.31
DAY 13	FEB 23.5	181.81	178.76	172.67	166.57	157.43
	FEB 24	160.93	157.88	151.79	145.69	136.55
DAY 14	FEB 24.5	140.06	137.01	130.91	124.82	115.67
	* FEB 25	119.18	116.13	110.03	103.94	94.79

* MEASURED DATA POINT + VALUE DURING SIMULATION

SIMULATION DAY	DATE	NODE NUMBER 171	182	195	208	222
	* FEB 11	19.05	11.43	6.86	0.00	0.00
DAY 1	FEB 11.5	20.50	12.88	8.31	0.69	+
	* FEB 12	21.95	14.33	9.75	2.13	0.00
DAY 2	FEB 12.5	42.37	34.75	30.18	22.56	17.98
	* FEB 13	62.79	55.17	50.60	42.98	38.40
DAY 3	FEB 13.5	63.75	56.13	51.56	43.94	39.37
	FEB 14	64.72	57.10	52.53	44.91	40.34
DAY 4	FEB 14.5	65.68	58.06	53.49	45.87	41.30
	FEB 15	66.65	59.03	54.46	46.84	42.27
DAY 5	FEB15.5	67.61	59.99	55.42	47.80	43.23
	* FEB 16	68.58	60.96	56.39	48.77	44.20
DAY 6	FEB 16.5	85.50	77.88	73.30	65.68	61.11
	FEB 17	102.41	94.79	90.22	82.60	78.03
DAY 7	FEB 17.5	119.33	111.71	107.14	99.52	94.95
	* FEB 18	136.25	128.63	124.05	116.43	111.86
DAY 8	FEB 18.5	203.76	196.14	191.57	183.95	179.37
	* FEB 19	271.27	263.65	259.08	251.46	246.89
DAY 9	FEB 19.5	271.27	263.65	259.08	251.46	246.89
	* FEB 20	271.27	263.65	259.08	251.46	246.89
DAY 10	FEB 20.5	221.13	213.51	208.94	201.32	196.75
	* FEB 21	170.99	163.37	158.80	151.18	146.61
DAY 11	FEB 21.5	170.54	162.92	158.34	150.72	146.15
	FEB 22	170.08	162.46	157.89	150.27	145.69
DAY 12	FEB 22.5	169.62	162.00	157.43	149.81	145.24
	* FEB 23	169.16	161.54	156.97	149.35	144.78
DAY 13	FEB 23.5	148.29	140.67	136.09	128.47	123.90
	FEB 24	127.41	119.79	115.21	107.59	103.02
DAY 14	FEB 24.5	106.53	98.91	94.34	86.72	82.14
	* FEB 25	85.65	78.03	73.46	65.84	61.26

* MEASURED DATA POINT + VALUE DURING SIMULATION

SIMULATION DAY	DATE	NODE NUMBER 236	250	263	276	287
	* FEB 11	0.00	0.00	0.00	0.00	0.00
DAY 1	FEB 11.5	+	+	+	+	+
	* FEB 12	0.00	0.00	0.00	0.00	0.00
DAY 2	FEB 12.5	14.94	14.94	13.41	11.89	10.36
	* FEB 13	35.36	35.36	33.83	32.31	30.78
DAY 3	FEB 13.5	36.32	36.32	34.80	33.27	31.75
	FEB 14	37.29	37.29	35.76	34.24	32.72
DAY 4	FEB 14.5	38.25	38.25	36.73	35.20	33.68
	FEB 15	39.22	39.22	37.69	36.17	34.65
DAY 5	FEB15.5	40.18	40.18	38.66	37.13	35.61
	* FEB 16	41.15	41.15	39.62	38.10	36.58
DAY 6	FEB 16.5	58.06	58.06	56.54	55.02	53.49
	FEB 17	74.98	74.98	73.46	71.93	70.41
DAY 7	FEB 17.5	91.90	91.90	90.37	88.85	87.33
	* FEB 18	108.81	108.81	107.29	105.77	104.24
DAY 8	FEB 18.5	176.33	176.33	174.80	173.28	171.75
	* FEB 19	243.84	243.84	242.32	240.79	239.27
DAY 9	FEB 19.5	243.84	243.84	242.32	240.79	239.27
	* FEB 20	243.84	243.84	242.32	240.79	239.27
DAY 10	FEB 20.5	193.70	193.70	192.18	190.65	189.13
	* FEB 21	143.56	143.56	142.04	140.51	138.99
DAY 11	FEB 21.5	143.10	143.10	141.58	140.06	138.53
	FEB 22	142.65	142.65	141.12	139.60	138.07
DAY 12	FEB 22.5	142.19	142.19	140.67	139.14	137.62
	* FEB 23	141.73	141.73	140.21	138.68	137.16
DAY 13	FEB 23.5	120.85	120.85	119.33	117.81	116.28
	FEB 24	99.97	99.97	98.45	96.93	95.40
DAY 14	FEB 24.5	79.10	79.10	77.57	76.05	74.52
	* FEB 25	58.22	58.22	56.69	55.17	53.64

* MEASURED DATA POINT + VALUE DURING SIMULATION

SIMULATION DAY	DATE	NODE NUMBER 297	307	317	327	337
	* FEB 11	0.00	0.00	0.00	0.00	0.00
DAY 1	FEB 11.5	+	+	+	+	+
	* FEB 12	0.00	0.00	0.00	0.00	0.00
DAY 2	FEB 12.5	7.32	4.27	1.22	+	+
	* FEB 13	27.74	24.69	21.64	18.59	15.54
DAY 3	FEB 13.5	28.70	25.65	22.61	19.56	16.51
	FEB 14	29.67	26.62	23.57	20.52	17.48
DAY 4	FEB 14.5	30.63	27.58	24.54	21.49	18.44
	FEB 15	31.60	28.55	25.50	22.45	19.41
DAY 5	FEB15.5	32.56	29.51	26.47	23.42	20.37
	* FEB 16	33.53	30.48	27.43	24.38	21.34
DAY 6	FEB 16.5	50.44	47.40	44.35	41.30	38.25
	FEB 17	67.36	64.31	61.26	58.22	55.17
DAY 7	FEB 17.5	84.28	81.23	78.18	75.13	72.09
	* FEB 18	101.19	98.15	95.10	92.05	89.00
DAY 8	FEB 18.5	168.71	165.66	162.61	159.56	156.51
	* FEB 19	236.22	233.17	230.12	227.08	224.03
DAY 9	FEB 19.5	236.22	233.17	230.12	227.08	224.03
	* FEB 20	236.22	233.17	230.12	227.08	224.03
DAY 10	FEB 20.5	186.08	183.03	179.98	176.94	173.89
	* FEB 21	135.94	132.89	129.84	126.80	123.75
DAY 11	FEB 21.5	135.48	132.44	129.39	126.34	123.29
	FEB 22	135.03	131.98	128.93	125.88	122.83
DAY 12	FEB 22.5	134.57	131.52	128.47	125.43	122.38
	* FEB 23	134.11	131.06	128.02	124.97	121.92
DAY 13	FEB 23.5	113.23	110.19	107.14	104.09	101.04
	FEB 24	92.35	89.31	86.26	83.21	80.16
DAY 14	FEB 24.5	71.48	68.43	65.38	62.33	59.28
	* FEB 25	50.60	47.55	44.50	41.45	38.40

* MEASURED DATA POINT + VALUE DURING SIMULATION

SIMULATION DAY	DATE	NODE NUMBER 347	357	367	379	393
	* FEB 11	0.00	0.00	0.00	0.00	0.00
DAY 1	FEB 11.5	+	+	+	+	+
	* FEB 12	0.00	0.00	0.00	0.00	0.00
DAY 2	FEB 12.5	+	+	+	+	+
	* FEB 13	12.50	9.45	6.40	3.35	1.83
DAY 3	FEB 13.5	13.46	10.41	7.37	4.32	2.79
	FEB 14	14.43	11.38	8.33	5.28	3.76
DAY 4	FEB 14.5	15.39	12.34	9.30	6.25	4.72
	FEB 15	16.36	13.31	10.26	7.21	5.69
DAY 5	FEB15.5	17.32	14.27	11.23	8.18	6.65
	* FEB 16	18.29	15.24	12.19	9.14	7.62
DAY 6	FEB 16.5	35.20	32.16	29.11	26.06	24.54
	FEB 17	52.12	49.07	46.02	42.98	41.45
DAY 7	FEB 17.5	69.04	65.99	62.94	59.89	58.37
	* FEB 18	85.95	82.91	79.86	76.81	75.29
DAY 8	FEB 18.5	153.47	150.42	147.37	144.32	142.80
	* FEB 19	220.98	217.93	214.88	211.84	210.31
DAY 9	FEB 19.5	220.98	217.93	214.88	211.84	210.31
	* FEB 20	220.98	217.93	214.88	211.84	210.31
DAY 10	FEB 20.5	170.84	167.79	164.74	161.70	160.17
	* FEB 21	120.70	117.65	114.60	111.56	110.03
DAY 11	FEB 21.5	120.24	117.20	114.15	111.10	109.58
	FEB 22	119.79	116.74	113.69	110.64	109.12
DAY 12	FEB 22.5	119.33	116.28	113.23	110.19	108.66
	* FEB 23	118.87	115.82	112.78	109.73	108.20
DAY 13	FEB 23.5	97.99	94.95	91.90	88.85	87.33
	FEB 24	77.11	74.07	71.02	67.97	66.45
DAY 14	FEB 24.5	56.24	53.19	50.14	47.09	45.57
	* FEB 25	35.36	32.31	29.26	26.21	24.69

* MEASURED DATA POINT + VALUE DURING SIMULATION

SIMULATION DAY	DATE	NODE NUMBER 407	421	433	443
	* FEB 11	0.00	0.00	0.00	0.00
DAY 1	FEB 11.5	+	+	+	+
	* FEB 12	0.00	0.00	0.00	0.00
DAY 2	FEB 12.5	+	+	+	+
	* FEB 13	0.00	0.00	0.00	0.00
DAY 3	FEB 13.5	+	+	+	+
	FEB 14	0.71	0.71	0.71	0.71
DAY 4	FEB 14.5	1.68	1.68	1.68	1.68
	FEB 15	2.64	2.64	2.64	2.64
DAY 5	FEB15.5	3.61	3.61	3.61	3.61
	* FEB 16	4.57	4.57	4.57	4.57
DAY 6	FEB 16.5	21.49	21.49	21.49	21.49
	FEB 17	38.40	38.40	38.40	38.40
DAY 7	FEB 17.5	55.32	55.32	55.32	55.32
	* FEB 18	72.24	72.24	72.24	72.24
DAY 8	FEB 18.5	139.75	139.75	139.75	139.75
	* FEB 19	207.26	207.26	207.26	207.26
DAY 9	FEB 19.5	207.26	207.26	207.26	207.26
	* FEB 20	207.26	207.26	207.26	207.26
DAY 10	FEB 20.5	157.12	157.12	157.12	157.12
	* FEB 21	106.98	106.98	106.98	106.98
DAY 11	FEB 21.5	106.53	106.53	106.53	106.53
	FEB 22	106.07	106.07	106.07	106.07
DAY 12	FEB 22.5	105.61	105.61	105.61	105.61
	* FEB 23	105.16	105.16	105.16	105.16
DAY 13	FEB 23.5	84.28	84.28	84.28	84.28
	FEB 24	63.40	63.40	63.40	63.40
DAY 14	FEB 24.5	42.52	42.52	42.52	42.52
	* FEB 25	21.64	21.64	21.64	21.64

APPENDIX D

Computer Input File used for the February 1986
Storm Simulation

Table 3. Input data for the February 1986 storm simulation.

```
...FEBRUARY 1986 STORM SIMULATION INPUT FILE.....................
  443   14  414    2    5    0   30    1    3   15
    0    0    0    0    0    0    0    0    0    0
   11   18   19   17   13   13   16   23   22   22
   15   -1
    1   12   23   34   45   56   67   78   89  100  111  122  132  142  152
   15   -1
  162  172  183  196  209  223  237  251  264  277  288  298  308  318  328
    9   -1
  338  348  358  368  380  394  408  422  434
   0.5        0.5       1.0       0.5       0.1
   1.0        1.0
1.6000     1.6000       0.442     0.0
 120.0      120.0       0.305     0.0
 7.0        7.0         0.400     0.0
 65.0       65.0        0.44      0.0
1.0368     1.0368       0.495     0.0
   0.2      0.0         0.235     0.00575   0.25      0.0161    0.28      0.0517
   0.3      0.0895      0.325     0.155     0.35      0.245     0.375     0.379
   0.4      0.815       0.425     0.977     0.442     1.0
   0.03     96000.0     0.04      54000.0   0.06      24000.0   0.0904    10000.0
   0.15     3000.0      0.1912    1300.0    0.213     790.0     0.2367    486.0
   0.2488   380.0       0.2874    231.0     0.3097    184.0     0.3636    87.0
   0.3803   57.0        0.3965    36.0      0.41      21.0      0.4183    7.6
   0.4338   2.6         0.442     0.0
   0.085    0.0337      0.09      0.0346    0.1       0.0385    0.11      0.04425
   0.12     0.0576      0.13      0.077     0.14      0.09625   0.15      0.12
   0.16     0.154       0.17      0.189     0.18      0.2305    0.19      0.2755
   0.2      0.346       0.21      0.404     0.22      0.5       0.23      0.596
   0.24     0.7225      0.25      0.855     0.305     1.00
   0.084    38.0        0.088     36.0      0.092     34.0      0.096     32.0
   0.104    30.0        0.11      28.0      0.117     26.0      0.125     24.0
   0.14     22.0        0.155     20.0      0.179     18.0      0.2       16.0
   0.217    14.0        0.23      12.0      0.243     10.0      0.2525    8.0
   0.305    0.0
   0.19     0.00        0.22      0.003     0.2504    0.0129    0.2765    0.0286
   0.3      0.0715      0.32      0.129     0.33      0.171     0.349     0.286
   0.36     0.42        0.37      0.54      0.38      0.677     0.39      0.818
   0.4      1.0
   0.19     550.0       0.192     516.0     0.195     455.0     0.2       400.0
   0.21     315.0       0.23      222.0     0.27      138.0     0.3       100.0
   0.32     80.0        0.34      57.0      0.37      31.0      0.393     10.0
   0.4      0.0
   0.062    0.0002121   0.075     0.00125   0.1       0.006061  0.125     0.01515
   0.15     0.03076     0.175     0.05682   0.2       0.09848   0.225     0.1591
   0.25     0.25        0.275     0.3591    0.3       0.4879    0.325     0.6439
   0.35     0.7803      0.375     0.9469    0.4       0.98      0.44      1.00
```

0.02	2500.0	0.04	550.0	0.06	245.0	0.08	150.0
0.1	92.5	0.12	65.5	0.14	50.0	0.16	41.5
0.18	34.5	0.2	29.3	0.22	25.5	0.24	23.0
0.26	20.6	0.28	18.8	0.3	16.5	0.32	14.0
0.34	12.2	0.36	10.5	0.37	9.0	0.38	7.75
0.39	4.0	0.4	1.0	0.44	0.0		
0.238	0.0009821	0.244	0.00138	0.257	0.00252	0.27	0.00414
0.283	0.006091	0.296	0.008778	0.308	0.01348	0.321	0.01902
0.334	0.03	0.347	0.04	0.36	0.055	0.373	0.07
0.386	0.08943	0.398	0.1041	0.411	0.1276	0.424	0.1658
0.437	0.2154	0.45	0.2789	0.463	0.3764	0.476	0.5398
0.489	0.813	0.495	1.00				
0.238	586.0	0.244	494.0	0.257	400.0	0.27	316.0
0.283	252.0	0.296	199.0	0.308	161.0	0.321	129.0
0.334	100.0	0.347	82.0	0.36	73.0	0.373	64.0
0.386	56.0	0.398	49.0	0.411	43.0	0.424	36.0
0.437	33.0	0.45	27.0	0.463	22.0	0.476	16.0
0.489	8.0	0.495	0.00				

1	0	0.0	0.00	-10.00	0.0
2	0	0.0	143.25	-130.0	0.0
3	0	0.0	271.27	-120.0	0.0
4	0	0.0	487.68	-120.0	0.0
5	0	0.0	701.04	-100.0	0.0
6	0	0.0	914.40	-100.0	0.0
7	0	0.0	1127.76	0.0	0.0
8	0	0.0	1371.60	0.0	0.0
9	0	0.0	1463.04	0.0	0.0
10	0	0.0	1581.91	0.0	0.0
11	1	0.0	1588.01	52.58	0.0
12	0	152.4	0.00	-10.00	0.0
13	0	152.4	143.26	-130.0	0.0
14	0	152.4	274.32	-120.0	0.0
15	0	152.4	487.68	-120.0	0.0
16	0	152.4	701.04	-100.0	0.0
17	0	152.4	914.40	-100.0	0.0
18	0	152.4	1127.76	0.0	0.0
19	0	152.4	1371.60	0.0	0.0
20	0	152.4	1463.04	0.0	0.0
21	0	152.4	1581.91	0.0	0.0
22	1	152.4	1588.01	52.58	0.0
23	0	304.8	0.00	-10.00	0.0
24	0	304.8	143.26	-130.0	0.0
25	0	304.8	277.37	-120.0	0.0
26	0	304.8	487.68	-120.0	0.0
27	0	304.8	701.04	-100.0	0.0
28	0	304.8	914.40	-100.0	0.0
29	0	304.8	1127.76	0.0	0.0
30	0	304.8	1371.60	0.0	0.0

31	0	304.8	1463.04	0.0	0.0
32	0	304.8	1581.91	0.0	0.0
33	1	304.8	1588.01	52.58	0.0
34	0	457.2	0.00	-10.00	0.0
35	0	457.2	143.26	-130.0	0.0
36	0	457.2	265.42	-120.0	0.0
37	0	457.2	487.68	-120.0	0.0
38	0	457.2	701.04	-100.0	0.0
39	0	457.2	914.40	-100.0	0.0
40	0	457.2	1127.76	0.0	0.0
41	0	457.2	1371.60	0.0	0.0
42	0	457.2	1463.04	0.0	0.0
43	0	457.2	1581.91	0.0	0.0
44	1	457.2	1588.01	52.58	0.0
45	0	609.6	0.00	-10.00	0.0
46	0	609.6	143.26	-130.0	0.0
47	0	609.6	265.42	-120.0	0.0
48	0	609.6	487.68	-120.0	0.0
49	0	609.6	701.04	-100.0	0.0
50	0	609.6	914.40	-100.0	0.0
51	0	609.6	1127.76	0.0	0.0
52	0	609.6	1371.60	0.0	0.0
53	0	609.6	1466.09	0.0	0.0
54	0	609.6	1581.91	0.0	0.0
55	1	609.6	1588.01	52.58	0.0
56	0	762.0	0.00	-10.00	0.0
57	0	762.0	144.78	-130.0	0.0
58	0	762.0	286.51	-120.0	0.0
59	0	762.0	492.25	-120.0	0.0
60	0	762.0	701.04	-100.0	0.0
61	0	762.0	914.40	-100.0	0.0
62	0	762.0	1130.81	0.0	0.0
63	0	762.0	1371.60	0.0	0.0
64	0	762.0	1470.66	0.0	0.0
65	0	762.0	1581.91	0.0	0.0
66	1	762.0	1588.01	52.58	0.0
67	0	914.4	0.00	-10.00	0.0
68	0	914.4	149.35	-130.0	0.0
69	0	914.4	295.66	-120.0	0.0
70	0	914.4	496.82	-120.0	0.0
71	0	914.4	701.04	-100.0	0.0
72	0	914.4	914.40	-100.0	0.0
73	0	914.4	1133.86	-100.0	0.0
74	0	914.4	1371.60	0.0	0.0
75	0	914.4	1475.23	0.0	0.0
76	0	914.4	1581.91	0.0	0.0
77	1	914.4	1588.01	52.58	0.0
78	0	1066.8	0.00	-10.00	0.0

79	0	1066.8	152.40	-130.0	0.0
80	0	1066.8	304.65	-120.0	0.0
81	0	1066.8	501.40	-120.0	0.0
82	0	1066.8	701.04	-100.0	0.0
83	0	1066.8	914.40	-100.0	0.0
84	0	1066.8	1139.95	-100.0	0.0
85	0	1066.8	1371.60	0.0	0.0
86	0	1066.8	1479.80	0.0	0.0
87	0	1066.8	1581.91	0.0	0.0
88	1	1066.8	1588.01	52.58	0.0
89	0	1219.2	0.00	-10.00	0.0
90	0	1219.2	152.40	-130.0	0.0
91	0	1219.2	304.80	-120.0	0.0
92	0	1219.2	509.02	-120.0	0.0
93	0	1219.2	707.14	-100.0	0.0
94	0	1219.2	914.40	-100.0	0.0
95	0	1219.2	1146.05	-100.0	0.0
96	0	1219.2	1371.60	0.0	0.0
97	0	1219.2	1484.38	0.0	0.0
98	0	1219.2	1581.91	0.0	0.0
99	1	1219.2	1588.01	52.58	0.0
100	0	1371.6	0.00	-10.00	0.0
101	0	1371.6	152.40	-130.0	0.0
102	0	1371.6	304.80	-120.0	0.0
103	0	1371.6	515.11	-120.0	0.0
104	0	1371.6	707.14	-100.0	0.0
105	0	1371.6	914.40	-100.0	0.0
106	0	1371.6	1152.14	-100.0	0.0
107	0	1371.6	1374.65	0.0	0.0
108	0	1371.6	1488.95	0.0	0.0
109	0	1371.6	1581.91	0.0	0.0
110	1	1371.6	1588.01	52.58	0.0
111	0	1524.0	0.00	-10.00	0.0
112	0	1524.0	152.40	-130.0	0.0
113	0	1524.0	307.85	-120.0	0.0
114	0	1524.0	518.16	-120.0	0.0
115	0	1524.0	716.28	-100.0	0.0
116	0	1524.0	914.40	-100.0	0.0
117	0	1524.0	1158.24	-100.0	0.0
118	0	1524.0	1377.70	0.0	0.0
119	0	1524.0	1492.00	0.0	0.0
120	0	1524.0	1581.91	0.0	0.0
121	1	1524.0	1588.01	52.58	0.0
122	0	1676.4	0.00	-10.00	0.0
123	0	1676.4	152.40	-130.0	0.0
124	0	1676.4	320.04	-120.0	0.0
125	0	1676.4	524.26	-120.0	0.0
126	0	1676.4	725.42	-100.0	0.0

127	0	1676.4	914.40	-100.0	0.0
128	0	1676.4	1161.29	-100.0	0.0
129	0	1676.4	1380.75	0.0	0.0
130	0	1676.4	1493.52	0.0	0.0
131	1	1676.4	1591.06	49.53	0.0
132	0	1828.8	0.00	-10.00	0.0
133	0	1828.8	156.97	-132.0	0.0
134	0	1828.8	323.09	-120.0	0.0
135	0	1828.8	530.35	-120.0	0.0
136	0	1828.8	728.47	-100.0	0.0
137	0	1828.8	914.40	-100.0	0.0
138	0	1828.8	1170.43	-100.0	0.0
139	0	1828.8	1383.79	0.0	0.0
140	0	1828.8	1499.62	0.0	0.0
141	1	1828.8	1597.15	43.43	0.0
142	0	2133.6	0.00	-10.00	0.0
143	0	2133.6	161.54	-134.0	0.0
144	0	2133.6	335.28	-120.0	0.0
145	0	2133.6	536.45	-120.0	0.0
146	0	2133.6	731.52	-100.0	0.0
147	0	2133.6	914.40	-100.0	0.0
148	0	2133.6	1182.62	-100.0	0.0
149	0	2133.6	1392.94	0.0	0.0
150	0	2133.6	1505.71	0.0	0.0
151	1	2133.6	1603.25	37.34	0.0
152	0	2438.4	0.00	-10.00	0.0
153	0	2438.4	167.64	-140.0	0.0
154	0	2438.4	335.28	-120.0	0.0
155	0	2438.4	542.54	-120.0	0.0
156	0	2438.4	731.52	-100.0	0.0
157	0	2438.4	914.40	-100.0	0.0
158	0	2438.4	1188.72	-100.0	0.0
159	0	2438.4	1402.08	-95.00	0.0
160	0	2438.4	1511.81	0.0	0.0
161	1	2438.4	1612.39	28.19	0.0
162	0	2743.2	0.00	-10.00	0.0
163	0	2743.2	173.74	-146.0	0.0
164	0	2743.2	350.52	-120.0	0.0
165	0	2743.2	551.69	-120.0	0.0
166	0	2743.2	731.52	-100.0	0.0
167	0	2743.2	914.40	-100.0	0.0
168	0	2743.2	1194.82	-100.0	0.0
169	0	2743.2	1411.22	-95.00	0.0
170	0	2743.2	1517.90	0.0	0.0
171	1	2743.2	1621.54	19.05	0.0
172	0	3048.0	0.00	-10.00	0.0
173	0	3048.0	179.83	-150.0	0.0
174	0	3048.0	365.76	-120.0	0.0

175	0	3048.0	566.93	-120.0	0.0
176	0	3048.0	734.57	-100.0	0.0
177	0	3048.0	914.40	-100.0	0.0
178	0	3048.0	1005.84	-60.00	0.0
179	0	3048.0	1207.01	-150.0	0.0
180	0	3048.0	1424.94	-95.00	0.0
181	0	3048.0	1524.00	0.0	0.0
182	1	3048.0	1629.16	11.43	0.0
183	0	3200.4	0.00	-10.00	0.0
184	0	3200.4	182.88	-150.0	0.0
185	0	3200.4	371.86	-120.0	0.0
186	0	3200.4	487.68	-120.0	0.0
187	0	3200.4	573.02	-120.0	0.0
188	0	3200.4	737.62	-100.0	0.0
189	0	3200.4	914.40	-60.00	0.0
190	0	3200.4	1005.84	-60.00	0.0
191	0	3200.4	1097.28	-60.00	0.0
192	0	3200.4	1213.10	-150.0	0.0
193	0	3200.4	1429.51	-95.00	0.0
194	0	3200.4	1527.05	0.0	0.0
195	1	3200.4	1633.73	6.86	0.0
196	0	3474.7	0.00	-10.00	0.0
197	0	3474.7	182.88	-150.0	0.0
198	0	3474.7	372.77	-120.0	0.0
199	0	3474.7	487.68	-90.00	0.0
200	0	3429.0	579.12	-120.0	0.0
201	0	3352.8	740.66	-85.00	0.0
202	0	3352.8	914.40	-60.00	0.0
203	0	3352.8	1005.84	-60.00	0.0
204	0	3352.8	1097.28	-60.00	0.0
205	0	3352.8	1219.20	-150.0	0.0
206	0	3352.8	1432.56	-95.00	0.0
207	0	3352.8	1530.10	00.0	0.0
208	1	3352.8	1641.35	0.00	0.0
209	0	3535.7	0.00	-10.00	0.0
210	0	3535.7	182.88	-150.0	0.0
211	0	3535.7	377.95	-120.0	0.0
212	0	3535.7	457.20	-100.0	0.0
213	0	3535.7	518.16	-80.00	0.0
214	0	3514.3	583.69	-120.0	0.0
215	0	3505.2	743.71	-85.00	0.0
216	0	3505.2	914.40	-60.00	0.0
217	0	3505.2	1005.84	-60.00	0.0
218	0	3505.2	1097.28	-60.00	0.0
219	0	3505.2	1222.25	-150.0	0.0
220	0	3505.2	1435.61	-95.00	0.0
221	0	3505.2	1533.14	-95.00	0.0
222	1	3505.2	1645.92	00.0	0.0

223	0	3657.6	0.00	-10.00	0.0
224	0	3657.6	182.88	-150.0	0.0
225	0	3657.6	381.00	-120.0	0.0
226	0	3657.6	457.20	-100.0	0.0
227	0	3657.6	518.16	-80.00	0.0
228	0	3657.6	588.26	-120.0	0.0
229	0	3657.6	746.76	-85.00	0.0
230	0	3657.6	914.40	-60.00	0.0
231	0	3657.6	1005.84	-60.00	0.0
232	0	3657.6	1097.28	-60.00	0.0
233	0	3657.6	1225.30	-150.0	0.0
234	0	3657.6	1435.61	-95.00	0.0
235	0	3657.6	1536.19	-95.00	0.0
236	1	3657.6	1648.97	00.0	0.0
237	0	3779.5	0.00	-10.00	0.0
238	0	3779.5	188.98	-155.0	0.0
239	0	3779.5	390.14	-122.0	0.0
240	0	3779.5	457.20	-100.0	0.0
241	0	3779.5	518.16	-80.00	0.0
242	0	3788.7	594.36	-120.0	0.0
243	0	3810.0	752.86	-85.00	0.0
244	0	3810.0	914.40	-60.00	0.0
245	0	3810.0	1005.84	-60.00	0.0
246	0	3810.0	1097.28	-60.00	0.0
247	0	3810.0	1222.25	-150.0	0.0
248	0	3810.0	1437.13	-95.00	0.0
249	0	3810.0	1539.24	-95.00	0.0
250	1	3810.0	1648.97	00.0	0.0
251	0	3840.5	0.00	-10.00	0.0
252	0	3840.5	195.07	-155.0	0.0
253	0	3840.5	393.19	-122.0	0.0
254	0	3840.5	487.68	-90.00	0.0
255	0	3886.2	600.46	-120.0	0.0
256	0	3962.4	757.43	-85.00	0.0
257	0	3962.4	922.02	-60.00	0.0
258	0	3962.4	1005.84	-60.00	0.0
259	0	3962.4	1097.28	-60.00	0.0
260	0	3962.4	1219.20	-150.0	0.0
261	0	3962.4	1438.66	-95.00	0.0
262	0	3962.4	1542.29	-95.00	0.0
263	1	3962.4	1650.49	00.0	0.0
264	0	4114.8	0.00	-10.00	0.0
265	0	4114.8	213.36	-165.0	0.0
266	0	4114.8	408.43	-124.0	0.0
267	0	4114.8	487.68	-120.0	0.0
268	0	4114.8	609.60	-120.0	0.0
269	0	4114.8	760.48	-85.00	0.0
270	0	4114.8	929.64	-60.00	0.0

271	0	4114.8	1005.84	-60.00	0.0
272	0	4114.8	1097.28	-60.00	0.0
273	0	4114.8	1219.20	-150.0	0.0
274	0	4114.8	1440.18	-95.00	0.0
275	0	4114.8	1545.34	-95.00	0.0
276	1	4114.8	1652.02	00.0	0.0
277	0	4267.2	0.00	-10.00	0.0
278	0	4267.2	219.46	-165.0	0.0
279	0	4267.2	426.72	-124.0	0.0
280	0	4267.2	612.65	-120.0	0.0
281	0	4267.2	762.00	-85.00	0.0
282	0	4267.2	937.26	-90.00	0.0
283	0	4267.2	1005.84	-60.00	0.0
284	0	4267.2	1219.20	-150.0	0.0
285	0	4267.2	1441.70	-95.00	0.0
286	0	4267.2	1548.38	-95.00	0.0
287	1	4267.2	1653.54	00.0	0.0
288	0	4572.0	0.00	-10.00	0.0
289	0	4572.0	237.74	-165.0	0.0
290	0	4572.0	451.10	-126.0	0.0
291	0	4572.0	624.84	-120.0	0.0
292	0	4572.0	762.00	-100.0	0.0
293	0	4572.0	944.88	-100.0	0.0
294	0	4572.0	1219.20	-100.0	0.0
295	0	4572.0	1446.28	-95.00	0.0
296	0	4572.0	1551.43	-95.00	0.0
297	1	4572.0	1656.59	00.0	0.0
298	0	4876.8	0.00	-10.00	0.0
299	0	4876.8	243.84	-180.0	0.0
300	0	4876.8	472.44	-126.0	0.0
301	0	4876.8	640.08	-120.0	0.0
302	0	4876.8	768.10	-100.0	0.0
303	0	4876.8	947.93	-100.0	0.0
304	0	4876.8	1219.20	-100.0	0.0
305	0	4876.8	1450.85	-95.00	0.0
306	0	4876.8	1554.48	-95.00	0.0
307	1	4876.8	1659.64	00.0	0.0
308	0	5181.6	0.00	-10.00	0.0
309	0	5181.6	259.08	-180.0	0.0
310	0	5181.6	499.87	-126.0	0.0
311	0	5181.6	649.22	-120.0	0.0
312	0	5181.6	780.29	-100.0	0.0
313	0	5181.6	950.98	-100.0	0.0
314	0	5181.6	1219.20	-100.0	0.0
315	0	5181.6	1456.94	-95.00	0.0
316	0	5181.6	1557.53	-95.00	0.0
317	1	5181.6	1662.68	00.0	0.0
318	0	5486.4	0.00	-10.00	0.0

319	0	5486.4	274.32	-180.0	0.0
320	0	5486.4	518.16	-126.0	0.0
321	0	5486.4	659.89	-120.0	0.0
322	0	5486.4	792.48	-100.0	0.0
323	0	5486.4	954.02	-100.0	0.0
324	0	5486.4	1219.20	-100.0	0.0
325	0	5486.4	1463.04	-95.00	0.0
326	0	5486.4	1560.58	-95.00	0.0
327	1	5486.4	1665.73	00.0	0.0
328	0	5791.2	0.00	-10.00	0.0
329	0	5791.2	289.56	-180.0	0.0
330	0	5791.2	548.64	-126.0	0.0
331	0	5791.2	670.56	-120.0	0.0
332	0	5791.2	792.48	-100.0	0.0
333	0	5791.2	957.07	-100.0	0.0
334	0	5791.2	1219.20	-100.0	0.0
335	0	5791.2	1466.09	-95.00	0.0
336	0	5791.2	1563.62	-95.00	0.0
337	1	5791.2	1668.78	00.0	0.0
338	0	6096.0	0.00	-10.00	0.0
339	0	6096.0	304.80	-180.0	0.0
340	0	6096.0	569.98	-126.0	0.0
341	0	6096.0	685.80	-120.0	0.0
342	0	6096.0	795.53	-100.0	0.0
343	0	6096.0	960.12	-100.0	0.0
344	0	6096.0	1219.20	-100.0	0.0
345	0	6096.0	1469.14	-95.00	0.0
346	0	6096.0	1568.20	-95.00	0.0
347	1	6096.0	1671.83	00.0	0.0
348	0	6400.8	0.00	-10.00	0.0
349	0	6400.8	320.04	-180.0	0.0
350	0	6400.8	591.31	-126.0	0.0
351	0	6400.8	701.04	-120.0	0.0
352	0	6400.8	804.67	-100.0	0.0
353	0	6400.8	963.17	-100.0	0.0
354	0	6400.8	1219.20	-100.0	0.0
355	0	6400.8	1472.18	-95.00	0.0
356	0	6400.8	1572.77	-95.00	0.0
357	1	6400.8	1674.88	00.0	0.0
358	0	6705.6	0.00	-10.00	0.0
359	0	6705.6	335.28	-180.0	0.0
360	0	6705.6	615.70	-126.0	0.0
361	0	6705.6	716.28	-120.0	0.0
362	0	6705.6	816.86	-100.0	0.0
363	0	6705.6	966.22	-100.0	0.0
364	0	6705.6	1219.20	-100.0	0.0
365	0	6705.6	1475.23	-95.00	0.0
366	0	6705.6	1577.34	-95.00	0.0

367	1	6705.6	1677.92	00.0	0.0
368	0	7010.4	0.00	-10.00	0.0
369	0	7010.4	152.40	-121.0	0.0
370	0	7010.4	353.57	-70.00	0.0
371	0	7010.4	518.16	-120.0	0.0
372	0	7010.4	680.08	-126.0	0.0
373	0	7010.4	731.52	-120.0	0.0
374	0	7010.4	822.96	-100.0	0.0
375	0	7010.4	969.26	-100.0	0.0
376	0	7010.4	1219.20	-100.0	0.0
377	0	7010.4	1478.28	-95.00	0.0
378	0	7010.4	1580.39	-95.00	0.0
379	1	7010.4	1680.97	00.0	0.0
380	0	7162.8	0.00	-10.00	0.0
381	0	7162.8	152.40	-121.0	0.0
382	0	7162.8	304.80	-70.00	0.0
383	0	7162.8	365.76	-70.00	0.0
384	0	7162.8	426.72	-70.00	0.0
385	0	7162.8	518.16	-120.0	0.0
386	0	7162.8	649.22	-126.0	0.0
387	0	7162.8	736.09	-120.0	0.0
388	0	7162.8	822.96	-100.0	0.0
389	0	7162.8	972.31	-100.0	0.0
390	0	7162.8	1219.20	-100.0	0.0
391	0	7162.8	1481.33	-95.00	0.0
392	0	7162.8	1581.91	-95.00	0.0
393	1	7162.8	1682.50	00.0	0.0
394	0	7376.2	0.00	-10.00	0.0
395	0	7376.2	152.40	-121.0	0.0
396	0	7376.2	304.80	-70.00	0.0
397	0	7376.2	365.76	-70.00	0.0
398	0	7376.2	426.72	-70.00	0.0
399	0	7376.2	518.16	-120.0	0.0
400	0	7376.2	670.56	-126.0	0.0
401	0	7376.2	746.76	-120.0	0.0
402	0	7376.2	822.96	-100.0	0.0
403	0	7376.2	975.36	-100.0	0.0
404	0	7376.2	1219.20	-100.0	0.0
405	0	7376.2	1487.42	-95.00	0.0
406	0	7376.2	1584.96	-95.00	0.0
407	1	7376.2	1685.54	00.0	0.0
408	0	7559.0	0.00	-10.00	0.0
409	0	7559.0	152.40	-121.0	0.0
410	0	7559.0	304.80	-70.00	0.0
411	0	7559.0	365.76	-70.00	0.0
412	0	7559.0	426.72	-70.00	0.0
413	0	7559.0	518.16	-120.0	0.0
414	0	7559.0	655.32	-126.0	0.0

415	0 7559.0	746.76	-120.0	0.0
416	0 7559.0	822.96	-100.0	0.0
417	0 7559.0	975.36	-100.0	0.0
418	0 7559.0	1219.20	-100.0	0.0
419	0 7559.0	1487.42	-95.00	0.0
420	0 7559.0	1584.96	-95.00	0.0
421	1 7559.0	1685.54	00.0	0.0
422	0 7711.4	0.00	-10.00	0.0
423	0 7711.4	152.40	-121.0	0.0
424	0 7711.4	365.76	-70.00	0.0
425	0 7711.4	518.16	-120.0	0.0
426	0 7711.4	680.08	-126.0	0.0
427	0 7711.4	731.52	-120.0	0.0
428	0 7711.4	822.96	-100.0	0.0
429	0 7711.4	975.36	-100.0	0.0
430	0 7711.4	1219.20	-100.0	0.0
431	0 7711.4	1487.42	-95.00	0.0
432	0 7711.4	1584.96	-95.00	0.0
433	1 7711.4	1685.54	00.0	0.0
434	0 7924.8	0.00	-10.00	0.0
435	0 7924.8	365.76	-180.0	0.0
436	0 7924.8	680.08	-126.0	0.0
437	0 7924.8	731.52	-120.0	0.0
438	0 7924.8	822.96	-100.0	0.0
439	0 7924.8	975.36	-100.0	0.0
440	0 7924.8	1219.20	-100.0	0.0
441	0 7924.8	1487.42	-95.00	0.0
442	0 7924.8	1584.96	-95.00	0.0
443	1 7924.8	1685.54	00.0	0.0

1	1	12	13	2	3
2	2	13	14	3	3
3	3	14	15	4	4
4	4	15	16	5	4
5	5	16	17	6	3
6	6	17	18	7	3
7	7	18	19	8	3
8	8	19	20	9	2
9	9	20	21	10	2
10	10	21	22	11	1
11	12	23	24	13	3
12	13	24	25	14	3
13	14	25	26	15	4
14	15	26	27	16	4
15	16	27	28	17	3
16	17	28	29	18	3
17	18	29	30	19	3
18	19	30	31	20	2
19	20	31	32	21	2

20	21	32	33	22	1
21	23	34	35	24	3
22	24	35	36	25	3
23	25	36	37	26	4
24	26	37	38	27	4
25	27	38	39	28	3
26	28	39	40	29	3
27	29	40	41	30	3
28	30	41	42	31	2
29	31	42	43	32	2
30	32	43	44	33	1
31	34	45	46	35	3
32	35	46	47	36	3
33	36	47	48	37	4
34	37	48	49	38	4
35	38	49	50	39	3
36	39	50	51	40	3
37	40	51	52	41	3
38	41	52	53	42	2
39	42	53	54	43	2
40	43	54	55	44	1
41	45	56	57	46	3
42	46	57	58	47	3
43	47	58	59	48	4
44	48	59	60	49	4
45	49	60	61	50	3
46	50	61	62	51	3
47	51	62	63	52	3
48	52	63	64	53	2
49	53	64	65	54	2
50	54	65	66	55	1
51	56	67	68	57	3
52	57	68	69	58	3
53	58	69	70	59	4
54	59	70	71	60	4
55	60	71	72	61	3
56	61	72	73	62	3
57	62	73	74	63	3
58	63	74	75	64	2
59	64	75	76	65	2
60	65	76	77	66	1
61	67	78	79	68	3
62	68	79	80	69	3
63	69	80	81	70	4
64	70	81	82	71	4
65	71	82	83	72	3
66	72	83	84	73	3
67	73	84	85	74	3

68	74	85	86	75	2
69	75	86	87	76	2
70	76	87	88	77	1
71	78	89	90	79	3
72	79	90	91	80	3
73	80	91	92	81	4
74	81	92	93	82	4
75	82	93	94	83	3
76	83	94	95	84	3
77	84	95	96	85	3
78	85	96	97	86	2
79	86	97	98	87	2
80	87	98	99	88	1
81	89	100	101	90	3
82	90	101	102	91	3
83	91	102	103	92	4
84	92	103	104	93	4
85	93	104	105	94	3
86	94	105	106	95	3
87	95	106	107	96	3
88	96	107	108	97	2
89	97	108	109	98	2
90	98	109	110	99	1
91	100	111	112	101	3
92	101	112	113	102	3
93	102	113	114	103	4
94	103	114	115	104	4
95	104	115	116	105	3
96	105	116	117	106	3
97	106	117	118	107	3
98	107	118	119	108	2
99	108	119	120	109	2
100	109	120	121	110	1
101	111	122	123	112	3
102	112	123	124	113	3
103	113	124	125	114	4
104	114	125	126	115	4
105	115	126	127	116	3
106	116	127	128	117	3
107	117	128	129	118	3
108	118	129	130	119	2
109	119	130	120	120	2
110	120	130	131	131	2
111	120	131	121	121	2
112	122	132	133	123	3
113	123	133	134	124	3
114	124	134	135	125	4
115	125	135	136	126	4

116	126	136	137	127	3
117	127	137	138	128	3
118	128	138	139	129	3
119	129	139	140	130	2
120	130	140	141	131	2
121	132	142	143	133	3
122	133	143	144	134	3
123	134	144	145	135	4
124	135	145	146	136	4
125	136	146	147	137	3
126	137	147	148	138	3
127	138	148	149	139	3
128	139	149	150	140	2
129	140	150	151	141	2
130	142	152	153	143	3
131	143	153	154	144	3
132	144	154	155	145	4
133	145	155	156	146	4
134	146	156	157	147	3
135	147	157	158	148	3
136	148	158	159	149	3
137	149	159	160	150	2
138	150	160	161	151	2
139	152	162	163	153	3
140	153	163	164	154	3
141	154	164	165	155	4
142	155	165	166	156	4
143	156	166	167	157	3
144	157	167	168	158	3
145	158	168	169	159	3
146	159	169	170	160	2
147	160	170	171	161	2
148	162	172	173	163	3
149	163	173	174	164	3
150	164	174	175	165	4
151	165	175	176	166	4
152	166	176	177	167	3
153	167	177	178	178	3
154	167	178	168	168	3
155	168	178	179	179	3
156	168	179	180	169	3
157	169	180	181	170	2
158	170	181	182	171	2
159	172	183	184	173	3
160	173	184	185	174	3
161	174	185	186	186	4
162	174	186	175	175	4
163	175	186	187	187	4

164	175	187	188	176	4
165	176	188	189	177	3
166	177	189	178	178	3
167	178	189	190	190	4
168	178	190	191	191	4
169	178	191	192	179	3
170	179	192	193	180	3
171	180	193	194	181	2
172	181	194	195	182	2
173	183	196	197	184	3
174	184	197	198	185	3
175	185	198	199	186	4
176	186	199	200	187	4
177	187	200	201	188	4
178	188	201	202	189	3
179	189	202	203	190	4
180	190	203	204	191	4
181	191	204	205	192	3
182	192	205	206	193	3
183	193	206	207	194	2
184	194	207	208	195	2
185	196	209	210	197	3
186	197	210	211	198	3
187	198	211	212	199	4
188	199	212	213	213	5
189	199	213	214	200	4
190	200	214	215	201	4
191	201	215	216	202	3
192	202	216	217	203	4
193	203	217	218	204	4
194	204	218	219	205	3
195	205	219	220	206	3
196	206	220	221	207	2
197	207	221	222	208	2
198	209	223	224	210	3
199	210	224	225	211	3
200	211	225	226	212	4
201	212	226	227	213	5
202	213	227	228	214	4
203	214	228	229	215	4
204	215	229	230	216	3
205	216	230	231	217	4
206	217	231	232	218	4
207	218	232	233	219	3
208	219	233	234	220	3
209	220	234	235	221	2
210	221	235	236	222	2
211	223	237	238	224	3

212	224	238	239	225	3
213	225	239	240	226	4
214	226	240	241	227	5
215	227	241	242	228	4
216	228	242	243	229	4
217	229	243	244	230	3
218	230	244	245	231	4
219	231	245	246	232	4
220	232	246	247	233	3
221	233	247	248	234	3
222	234	248	249	235	2
223	235	249	250	236	2
224	237	251	252	238	3
225	238	252	253	239	3
226	239	253	254	240	4
227	240	254	241	241	5
228	241	254	255	242	4
229	242	255	256	243	4
230	243	256	257	244	3
231	244	257	258	245	4
232	245	258	259	246	4
233	246	259	260	247	3
234	247	260	261	248	3
235	248	261	262	249	2
236	249	262	263	250	2
237	251	264	265	252	3
238	252	265	266	253	3
239	253	266	267	254	4
240	254	267	268	255	4
241	255	268	269	256	4
242	256	269	270	257	3
243	257	270	271	258	4
244	258	271	272	259	4
245	259	272	273	260	3
246	260	273	274	261	3
247	261	274	275	262	2
248	262	275	276	263	2
249	264	277	278	265	3
250	265	278	279	266	3
251	266	279	267	267	4
252	267	279	280	280	4
253	267	280	268	268	4
254	268	280	281	269	4
255	269	281	282	270	3
256	270	282	283	283	3
257	270	283	271	271	4
258	271	283	272	272	4
259	272	283	284	273	3

260	273	284	285	274	3
261	274	285	286	275	2
262	275	286	287	276	2
263	277	288	289	278	3
264	278	289	290	279	3
265	279	290	291	280	4
266	280	291	292	281	4
267	281	292	293	282	3
268	282	293	283	283	3
269	283	293	294	294	3
270	283	294	284	284	3
271	284	294	295	285	3
272	285	295	296	286	2
273	286	296	297	287	2
274	288	298	299	289	3
275	289	299	300	290	3
276	290	300	301	291	4
277	291	301	302	292	4
278	292	302	303	293	3
279	293	303	304	294	3
280	294	304	305	295	3
281	295	305	306	296	2
282	296	306	307	297	2
283	298	308	309	299	3
284	299	309	310	300	3
285	300	310	311	301	4
286	301	311	312	302	4
287	302	312	313	303	3
288	303	313	314	304	3
289	304	314	315	305	3
290	305	315	316	306	2
291	306	316	317	307	2
292	308	318	319	309	3
293	309	319	320	310	3
294	310	320	321	311	4
295	311	321	322	312	4
296	312	322	323	313	3
297	313	323	324	314	3
298	314	324	325	315	3
299	315	325	326	316	2
300	316	326	327	317	2
301	318	328	329	319	3
302	319	329	330	320	3
303	320	330	331	321	4
304	321	331	332	322	4
305	322	332	333	323	3
306	323	333	334	324	3
307	324	334	335	325	3

308	325	335	336	326	2
309	326	336	337	327	2
310	328	338	339	329	3
311	329	339	340	330	3
312	330	340	341	331	4
313	331	341	342	332	4
314	332	342	343	333	3
315	333	343	344	334	3
316	334	344	345	335	3
317	335	345	346	336	2
318	336	346	347	337	2
319	338	348	349	339	3
320	339	349	350	340	3
321	340	350	351	341	4
322	341	351	352	342	4
323	342	352	353	343	3
324	343	353	354	344	3
325	344	354	355	345	3
326	345	355	356	346	2
327	346	356	357	347	2
328	348	358	359	349	3
329	349	359	360	350	3
330	350	360	361	351	4
331	351	361	362	352	4
332	352	362	363	353	3
333	353	363	364	354	3
334	354	364	365	355	3
335	355	365	366	356	2
336	356	366	367	357	2
337	358	368	369	369	3
338	358	369	359	359	3
339	359	369	370	370	3
340	359	370	371	371	3
341	359	371	360	360	3
342	360	371	372	372	3
343	360	372	373	361	4
344	361	373	374	362	4
345	362	374	375	363	3
346	363	375	376	364	3
347	364	376	377	365	3
348	365	377	378	366	2
349	366	378	379	367	2
350	368	380	381	369	3
351	369	381	382	370	3
352	370	382	383	383	4
353	370	383	384	384	4
354	370	384	385	371	3
355	371	385	386	372	3

356	372	386	387	373	4
357	373	387	388	374	4
358	374	388	389	375	3
359	375	389	390	376	3
360	376	390	391	377	3
361	377	391	392	378	2
362	378	392	393	379	2
363	380	394	395	381	3
364	381	395	396	382	3
365	382	396	397	383	4
366	383	397	398	384	4
367	384	398	399	385	3
368	385	399	400	386	3
369	386	400	401	387	4
370	387	401	402	388	4
371	388	402	403	389	3
372	389	403	404	390	3
373	390	404	405	391	3
374	391	405	406	392	2
375	392	406	407	393	2
376	394	408	409	395	3
377	395	409	410	396	3
378	396	410	411	397	4
379	397	411	412	398	4
380	398	412	413	399	3
381	399	413	414	400	3
382	400	414	415	401	4
383	401	415	416	402	4
384	402	416	417	403	3
385	403	417	418	404	3
386	404	418	419	405	3
387	405	419	420	406	2
388	406	420	421	407	2
389	408	422	423	409	3
390	409	423	424	410	3
391	410	424	411	411	4
392	411	424	412	412	4
393	412	424	425	413	3
394	413	425	426	414	3
395	414	426	427	415	4
396	415	427	428	416	4
397	416	428	429	417	3
398	417	429	430	418	3
399	418	430	431	419	3
400	419	431	432	420	2
401	420	432	433	421	2
402	422	434	423	423	3
403	423	434	435	435	3

```
 404  423  435  424  424    3
 405  424  435  425  425    3
 406  425  435  436  436    3
 407  425  436  426  426    3
 408  426  436  437  427    4
 409  427  437  438  428    4
 410  428  438  439  429    3
 411  429  439  440  430    3
 412  430  440  441  431    3
 413  431  441  442  432    2
 414  432  442  443  433    2
restart.......RESTART  # 1  ........................................
   2    0
  30        0.5        0.5        1.0        1.0       0.10
  11    1    54.03
  22    1    54.03
  33    1    54.03
  44    1    54.03
  55    1    54.03
  66    1    54.03
  77    1    54.03
  88    1    54.03
  99    1    54.03
 110    1    54.03
 121    1    54.03
 131    1    50.98
 141    1    44.88
 151    1    38.79
 161    1    29.64
 171    1    20.50
 182    1    12.88
 195    1    8.31
 208    1    0.69
 222    0    0.0
 236    0    0.0
 250    0    0.0
 263    0    0.0
 276    0    0.0
 287    0    0.0
 297    0    0.0
 307    0    0.0
 317    0    0.0
 327    0    0.0
 337    0    0.0
 347    0    0.0
 357    0    0.0
 367    0    0.0
 379    0    0.0
```

```
 393    0    0.0
 407    0    0.0
 421    0    0.0
 433    0    0.0
 443    0    0.0

restart.....RESTART # 2.....................................
   2   0
  30        0.5        0.5        1.0        1.5        0.10
  11    1    55.47
  22    1    55.47
  33    1    55.47
  44    1    55.47
  55    1    55.47
  66    1    55.47
  77    1    55.47
  88    1    55.47
  99    1    55.47
 110    1    55.47
 121    1    55.47
 131    1    52.42
 141    1    46.33
 151    1    40.23
 161    1    31.09
 171    1    21.95
 182    1    14.33
 195    1    9.75
 208    1    2.13
 222    1    0.00
 236    1    0.00
 250    1    0.00
 263    1    0.00
 276    1    0.00
 287    1    0.00
 297    1    0.00
 307    1    0.00
 317    1    0.00
 327    1    0.00
 337    1    0.00
 347    1    0.00
 357    1    0.00
 367    1    0.00
 379    1    0.00
 393    1    0.00
 407    1    0.00
 421    1    0.00
 433    1    0.00
 443    1    0.00
```

```
restart.......RESTART #3.....................................
   2    0
  30       0.5       0.5       1.0       2.0       0.10
  11    1    75.90
  22    1    75.90
  33    1    75.90
  44    1    75.90
  55    1    75.90
  66    1    75.90
  77    1    75.90
  88    1    75.90
  99    1    75.90
 110    1    75.90
 121    1    75.90
 131    1    72.85
 141    1    66.75
 151    1    60.66
 161    1    51.51
 171    1    42.37
 182    1    34.75
 195    1    30.18
 208    1    22.56
 222    1    17.98
 236    1    14.94
 250    1    14.94
 263    1    13.41
 276    1    11.89
 287    1    10.36
 297    1    7.32
 307    1    4.27
 317    1    1.22
 327    0    0.0
 337    0    0.0
 347    0    0.0
 357    0    0.0
 367    0    0.0
 379    0    0.0
 393    0    0.0
 407    0    0.0
 421    0    0.0
 433    0    0.0
 443    0    0.0

restart.......RESTART  #4.....................................
   2    0
  30       0.5       0.5       1.0       2.5       0.10
  11    1    96.32
```

```
 22    1    96.32
 33    1    96.32
 44    1    96.32
 55    1    96.32
 66    1    96.32
 77    1    96.32
 88    1    96.32
 99    1    96.32
110    1    96.32
121    1    96.32
131    1    93.27
141    1    87.17
151    1    81.08
161    1    71.93
171    1    62.79
182    1    55.17
195    1    50.60
208    1    42.98
222    1    38.40
236    1    35.36
250    1    35.36
263    1    33.83
276    1    32.31
287    1    30.78
297    1    27.74
307    1    24.69
317    1    21.64
327    1    18.59
337    1    15.54
347    1    12.50
357    1    9.45
367    1    6.40
379    1    3.35
393    1    1.83
407    1    0.0
421    1    0.0
433    1    0.0
443    1    0.0

restart.....RESTART #5.....................................
  2    0
 30        0.5       0.5       1.0       3.0       0.10
 11    1    97.28
 22    1    97.28
 33    1    97.28
 44    1    97.28
 55    1    97.28
 66    1    97.28
```

```
 77    1    97.28
 88    1    97.28
 99    1    97.28
110    1    97.28
121    1    97.28
131    1    94.23
141    1    88.14
151    1    82.04
161    1    72.90
171    1    63.75
182    1    56.13
195    1    51.56
208    1    43.94
222    1    39.37
236    1    36.32
250    1    36.32
263    1    34.80
276    1    33.27
287    1    31.75
297    1    28.70
307    1    25.65
317    1    22.61
327    1    19.56
337    1    16.51
347    1    13.46
357    1    10.41
367    1    7.37
379    1    4.32
393    1    2.79
407    0    0.0
421    0    0.0
433    0    0.0
443    0    0.0

restart.............RESTART  #6.....FEBRUARY     1986.............
  2    0
 30       0.5       0.5       1.0       3.5       0.10
 11    1    98.25
 22    1    98.25
 33    1    98.25
 44    1    98.25
 55    1    98.25
 66    1    98.25
 77    1    98.25
 88    1    98.25
 99    1    98.25
110    1    98.25
121    1    98.25
```

```
131    1    95.20
141    1    89.10
151    1    83.01
161    1    73.86
171    1    64.72
182    1    57.10
195    1    52.53
208    1    44.91
222    1    40.34
236    1    37.29
250    1    37.29
263    1    35.76
276    1    34.24
287    1    32.72
297    1    29.67
307    1    26.62
317    1    23.57
327    1    20.52
337    1    17.48
347    1    14.43
357    1    11.38
367    1    8.33
379    1    5.28
393    1    3.76
407    1    0.71
421    1    0.71
433    1    0.71
443    1    0.71

restart.....RESTART  #7.....................................................
  2    0
 30       0.5       0.5       1.0       4.0       0.10
 11    1    99.21
 22    1    99.21
 33    1    99.21
 44    1    99.21
 55    1    99.21
 66    1    99.21
 77    1    99.21
 88    1    99.21
 99    1    99.21
110    1    99.21
121    1    99.21
131    1    96.16
141    1    90.07
151    1    83.97
161    1    74.83
171    1    65.68
```

```
 182    1    58.06
 195    1    53.49
 208    1    45.87
 222    1    41.30
 236    1    38.25
 250    1    38.25
 263    1    36.73
 276    1    35.20
 287    1    33.68
 297    1    30.63
 307    1    27.58
 317    1    24.54
 327    1    21.49
 337    1    18.44
 347    1    15.39
 357    1    12.34
 367    1    9.30
 379    1    6.25
 393    1    4.72
 407    1    1.68
 421    1    1.68
 433    1    1.68
 443    1    1.68

restart.....RESTART     #8.....................................
   2    0
  30       0.5       0.5       1.0       4.5       0.10
  11    1    100.18
  22    1    100.18
  33    1    100.18
  44    1    100.18
  55    1    100.18
  66    1    100.18
  77    1    100.18
  88    1    100.18
  99    1    100.18
 110    1    100.18
 121    1    100.18
 131    1    97.13
 141    1    91.03
 151    1    84.94
 161    1    75.79
 171    1    66.65
 182    1    59.03
 195    1    54.49
 208    1    46.84
 222    1    42.27
 236    1    39.22
```

```
 250    1    39.22
 263    1    37.69
 276    1    36.17
 287    1    34.65
 297    1    31.60
 307    1    28.55
 317    1    25.50
 327    1    22.45
 337    1    19.41
 347    1    16.36
 357    1    13.31
 367    1    10.26
 379    1    7.21
 393    1    5.69
 407    1    2.64
 421    1    2.64
 433    1    2.64
 443    1    2.64

restart.....RESTART  #9.....
   2    0
  30       0.5       0.5       1.0       5.0       0.10
  11    1    101.14
  22    1    101.14
  33    1    101.14
  44    1    101.14
  55    1    101.14
  66    1    101.14
  77    1    101.14
  88    1    101.14
  99    1    101.14
 110    1    101.14
 121    1    101.14
 131    1    98.09
 141    1    92.00
 151    1    85.90
 161    1    76.76
 171    1    67.61
 182    1    59.99
 195    1    55.42
 208    1    47.80
 222    1    43.23
 236    1    40.18
 250    1    40.18
 263    1    38.66
 276    1    37.13
 287    1    35.61
 297    1    32.56
```

```
307    1    29.51
317    1    26.47
327    1    23.42
337    1    20.37
347    1    17.32
357    1    14.27
367    1    11.23
379    1    8.18
393    1    6.65
407    1    3.61
421    1    3.61
433    1    3.61
443    1    3.61

restart.....................RESTART  # 10.............................
  2    0
 30       0.5       0.5       1.0       5.5       0.10
 11    1    102.11
 22    1    102.11
 33    1    102.11
 44    1    102.11
 55    1    102.11
 66    1    102.11
 77    1    102.11
 88    1    102.11
 99    1    102.11
110    1    102.11
121    1    102.11
131    1    99.06
141    1    92.96
151    1    86.87
161    1    77.72
171    1    68.58
182    1    60.96
195    1    56.39
208    1    44.20
222    1    44.20
236    1    41.15
250    1    41.15
263    1    39.62
276    1    38.10
297    1    33.53
307    1    30.48
317    1    27.43
327    1    24.38
337    1    21.34
347    1    18.29
357    1    15.24
```

```
  367    1    12.19
  379    1    9.14
  393    1    7.62
  407    1    4.57
  421    1    4.57
  433    1    4.57
  443    1    4.57

restart.................RESTART  #11.....................................
    2    0
   30        0.5       0.5       1.0       6.0       0.10
   11    1    119.02
   22    1    119.02
   33    1    119.02
   44    1    119.02
   55    1    119.02
   66    1    119.02
   77    1    119.02
   88    1    119.02
   99    1    119.02
  110    1    119.02
  121    1    119.02
  131    1    115.97
  141    1    109.88
  151    1    103.78
  161    1    94.64
  171    1    85.50
  182    1    77.88
  195    1    73.30
  208    1    65.68
  222    1    61.11
  236    1    58.06
  250    1    58.06
  263    1    56.54
  276    1    55.02
  287    1    53.49
  297    1    50.44
  307    1    47.40
  317    1    44.35
  327    1    41.30
  337    1    38.25
  347    1    35.20
  357    1    32.16
  367    1    29.11
  379    1    26.06
  393    1    24.54
  407    1    21.49
  421    1    21.49
```

```
  433    1    21.49
  443    1    21.49

restart.............RESTART  #12.................................
    2    0
   30        0.5        0.5        1.0        6.5  .    0.10
   11    1    135.94
   22    1    135.94
   33    1    135.94
   44    1    135.94
   55    1    135.94
   66    1    135.94
   77    1    135.94
   88    1    135.94
   99    1    135.94
  110    1    135.94
  121    1    135.94
  131    1    132.89
  141    1    126.80
  151    1    120.70
  161    1    111.56
  171    1    102.41
  182    1    94.79
  195    1    90.22
  208    1    82.60
  222    1    78.03
  236    1    74.98
  250    1    74.98
  263    1    73.46
  276    1    71.93
  287    1    70.41
  297    1    67.36
  307    1    64.31
  317    1    61.26
  327    1    58.22
  337    1    55.17
  347    1    52.12
  357    1    49.07
  367    1    46.02
  379    1    42.98
  393    1    41.45
  407    1    38.40
  421    1    38.40
  433    1    38.40
  443    1    38.40

 restart.............RESTART  #13.....................................
    2    0
```

```
 30       0.5       0.5       1.0       7.0       0.10
 11    1    152.86
 22    1    152.86
 33    1    152.86
 44    1    152.86
 55    1    152.86
 66    1    152.86
 77    1    152.86
 88    1    152.86
 99    1    152.86
110    1    152.86
121    1    152.86
131    1    149.81
141    1    143.71
151    1    137.62
161    1    128.47
171    1    119.33
182    1    111.71
195    1    107.14
208    1    99.52
222    1    94.95
236    1    91.90
250    1    91.90
263    1    90.37
276    1    88.85
287    1    87.33
297    1    84.28
307    1    81.23
317    1    78.18
327    1    75.13
337    1    72.09
347    1    69.04
357    1    65.99
367    1    62.94
379    1    59.89
393    1    58.37
407    1    55.32
421    1    55.32
433    1    55.32
443    1    55.32

restart.....................RESTART  #14.........................
   2    0
  30       0.5       0.5       1.0       7.5       0.10
  11    1    169.77
  22    1    169.77
  33    1    169.77
  44    1    169.77
```

```
 55    1    169.77
 66    1    169.77
 77    1    169.77
 88    1    169.77
 99    1    169.77
110    1    169.77
121    1    169.77
131    1    166.72
141    1    160.63
151    1    154.53
161    1    145.39
171    1    136.25
182    1    128.63
195    1    124.05
208    1    116.43
222    1    111.86
236    1    108.81
250    1    108.81
263    1    107.29
276    1    105.77
287    1    104.24
297    1    101.19
307    1    98.15
317    1    95.10
327    1    92.05
337    1    89.00
347    1    85.95
357    1    82.91
367    1    79.86
379    1    76.81
393    1    75.29
407    1    72.24
421    1    72.24
433    1    72.24
443    1    72.24

restart.............RESTART  #15.................................
  2    0
 30      0.5       0.5       1.0       8.0       0.10
 11    1    237.29
 22    1    237.29
 33    1    237.29
 44    1    237.29
 55    1    237.29
 66    1    237.29
 77    1    237.29
 88    1    237.29
 99    1    237.29
```

```
110    1    237.29
121    1    237.29
131    1    234.24
141    1    228.14
151    1    222.05
161    1    212.90
171    1    203.76
182    1    196.14
195    1    191.57
208    1    183.95
222    1    179.37
236    1    176.33
250    1    176.33
263    1    174.80
276    1    173.28
287    1    171.75
297    1    168.71
307    1    165.66
317    1    162.61
327    1    159.56
337    1    156.51
347    1    153.47
357    1    150.42
367    1    147.37
379    1    144.32
393    1    142.80
407    1    139.75
421    1    139.75
433    1    139.75
443    1    139.75

restart.............RESTART  #16.................................
  2    0
 30       0.5       0.5       1.0       8.5       0.10
 11    1    304.80
 22    1    304.80
 33    1    304.80
 44    1    304.80
 55    1    304.80
 66    1    304.80
 77    1    304.80
 88    1    304.80
 99    1    304.80
110    1    304.80
121    1    304.80
131    1    301.75
141    1    295.66
151    1    289.56
```

```
161    1    280.42
171    1    271.27
182    1    263.65
195    1    259.08
208    1    251.46
222    1    246.89
236    1    243.84
250    1    243.84
263    1    242.32
276    1    240.79
287    1    239.27
297    1    236.22
307    1    233.17
317    1    230.12
327    1    227.08
337    1    224.03
347    1    220.98
357    1    217.93
367    1    214.88
379    1    211.84
393    1    210.31
407    1    207.26
421    1    207.26
433    1    207.26
443    1    207.26

restart.....RESTART  #17.....................................
  2    0
 30      0.5       0.5       1.0       9.0       0.10
 11    1    304.80
 22    1    304.80
 33    1    304.80
 44    1    304.80
 55    1    304.80
 66    1    304.80
 77    1    304.80
 88    1    304.80
 99    1    304.80
110    1    304.80
121    1    304.80
131    1    301.75
141    1    295.66
151    1    289.56
161    1    280.42
171    1    271.27
182    1    263.65
195    1    259.08
208    1    251.46
```

```
222    1    246.89
236    1    243.84
250    1    243.84
263    1    242.32
276    1    240.79
287    1    239.27
297    1    236.22
307    1    233.17
317    1    230.12
327    1    227.08
337    1    224.03
347    1    220.98
357    1    217.93
367    1    214.88
379    1    211.84
393    1    210.31
407    1    207.26
421    1    207.26
433    1    207.26
443    1    207.26

restart.............RESTART  #18.............................
  2    0
 30       0.5       0.5       1.0       9.5       0.10
 11    1    304.80
 22    1    304.80
 33    1    304.80
 44    1    304.80
 55    1    304.80
 66    1    304.80
 77    1    304.80
 88    1    304.80
 99    1    304.80
110    1    304.80
121    1    304.80
131    1    301.75
141    1    295.66
151    1    289.56
161    1    280.42
171    1    271.27
182    1    263.65
195    1    259.08
208    1    251.45
222    1    246.89
236    1    243.84
250    1    243.84
263    1    242.32
276    1    240.79
```

```
287    1    239.27
297    1    236.22
307    1    233.17
317    1    230.12
327    1    227.08
337    1    224.03
347    1    220.98
357    1    217.93
367    1    214.88
379    1    211.84
393    1    210.31
407    1    207.26
421    1    207.26
433    1    207.26
443    1    207.26

restart.............RESTART  #19.............................
  2    0
 30       0.5       0.5       1.0       10.0       0.10
 11    1    254.66
 22    1    254.66
 33    1    254.66
 44    1    254.66
 55    1    254.66
 66    1    254.66
 77    1    254.66
 88    1    254.66
 99    1    254.66
110    1    254.66
121    1    254.66
131    1    251.61
141    1    245.52
151    1    239.42
161    1    230.28
171    1    221.13
182    1    213.51
195    1    208.94
208    1    201.32
222    1    196.75
236    1    193.70
250    1    193.70
263    1    192.18
276    1    190.65
287    1    189.13
297    1    186.08
307    1    183.03
317    1    179.98
327    1    176.94
```

```
337    1    173.89
347    1    170.84
357    1    167.79
367    1    164.74
379    1    161.70
393    1    160.17
407    1    157.12
421    1    157.12
433    1    157.12
443    1    157.12

restart.............RESTART  #20.................................
  2    0
 30       0.5       0.5       1.0       10.5      0.10
 11    1    204.52
 22    1    204.52
 33    1    204.52
 44    1    204.52
 55    1    204.52
 66    1    204.52
 77    1    204.52
 88    1    204.52
 99    1    204.52
110    1    204.52
121    1    204.52
131    1    201.47
141    1    195.38
151    1    189.28
161    1    180.14
171    1    170.99
182    1    163.37
195    1    158.80
208    1    151.18
222    1    146.61
236    1    143.56
250    1    143.56
263    1    142.04
276    1    140.51
287    1    138.99
297    1    135.94
307    1    132.89
317    1    129.39
327    1    126.80
337    1    123.75
347    1    120.70
357    1    117.65
367    1    114.60
379    1    111.10
```

```
 393    1    110.03
 407    1    106.98
 421    1    106.98
 433    1    106.98
 443    1    106.98

restart.....................RESTART  #21.................................
   2    0
  30       0.5       0.5       1.0       11.0       0.10
  11    1    204.06
  22    1    204.06
  33    1    204.06
  44    1    204.06
  55    1    204.06
  66    1    204.06
  77    1    204.06
  88    1    204.06
  99    1    204.06
 110    1    204.06
 121    1    204.06
 131    1    201.01
 141    1    194.92
 151    1    188.82
 161    1    179.68
 171    1    170.54
 182    1    162.92
 195    1    158.34
 208    1    150.72
 222    1    146.15
 236    1    143.10
 250    1    143.10
 263    1    141.58
 276    1    140.06
 287    1    138.53
 297    1    135.48
 307    1    132.44
 317    1    129.39
 327    1    126.34
 337    1    123.29
 347    1    120.24
 357    1    117.20
 367    1    114.15
 379    1    111.10
 393    1    109.58
 407    1    106.53
 421    1    106.53
 433    1    106.53
 443    1    106.53
```

```
restart.....RESTART #22 .....
   2    0
  30       0.5       0.5       1.0       11.5       0.10
  11    1    203.61
  22    1    203.61
  33    1    203.61
  44    1    203.61
  55    1    203.61
  66    1    203.61
  77    1    203.61
  88    1    203.61
  99    1    203.61
 110    1    203.61
 121    1    203.61
 131    1    200.56
 141    1    194.46
 151    1    188.37
 161    1    179.22
 171    1    170.08
 182    1    162.46
 195    1    157.89
 208    1    150.27
 222    1    145.69
 236    1    142.65
 250    1    142.65
 263    1    141.12
 276    1    139.60
 287    1    138.07
 297    1    135.03
 307    1    131.98
 317    1    128.93
 327    1    125.88
 337    1    122.83
 347    1    119.79
 357    1    116.74
 367    1    113.69
 379    1    110.64
 393    1    109.12
 407    1    106.07
 421    1    106.07
 433    1    106.07
 443    1    106.07

restart.....RESTART  #23.....
   2    0
  30       0.5       0.5       1.0       12.0       0.10
  11    1    203.15
```

```
 22    1    203.15
 33    1    203.15
 44    1    203.15
 55    1    203.15
 66    1    203.15
 77    1    203.15
 88    1    203.15
 99    1    203.15
110    1    203.15
121    1    203.15
131    1    200.10
141    1    194.01
151    1    187.91
161    1    178.77
171    1    169.62
182    1    162.00
195    1    157.43
208    1    149.81
222    1    145.24
236    1    142.19
250    1    142.19
263    1    140.67
276    1    139.14
287    1    137.62
297    1    134.57
307    1    131.52
317    1    128.47
327    1    125.43
337    1    122.38
347    1    119.33
357    1    116.28
367    1    113.23
379    1    110.19
393    1    108.66
407    1    105.61
421    1    105.61
433    1    105.61
443    1    105.61

restart.....................RESTART  #24.................................
  2    0
 30       0.5       0.5       1.0       12.5       0.10
 11    1    202.69
 22    1    202.69
 33    1    202.69
 44    1    202.69
 55    1    202.69
 66    1    202.69
```

```
 77    1    202.69
 88    1    202.69
 99    1    202.69
110    1    202.69
121    1    202.69
131    1    199.64
141    1    193.55
151    1    187.45
161    1    178.31
171    1    169.16
182    1    161.54
195    1    156.97
208    1    149.35
222    1    144.78
236    1    141.73
250    1    141.73
263    1    140.21
276    1    138.68
287    1    137.16
297    1    134.11
307    1    131.06
317    1    128.02
327    1    124.97
337    1    121.92
347    1    118.87
357    1    115.52
367    1    112.78
379    1    109.73
393    1    108.20
407    1    105.16
421    1    105.16
433    1    105.16
443    1    105.16

restart.............RESTART #25.....................................
  2    0
 30        0.5       0.5       1.0       13.0       0.10
 11    1    181.81
 22    1    181.81
 33    1    181.81
 44    1    181.81
 55    1    181.81
 66    1    181.81
 77    1    181.81
 88    1    181.81
 99    1    181.81
110    1    181.81
121    1    181.81
```

```
131    1    178.76
141    1    172.67
151    1    166.57
161    1    157.43
171    1    148.29
182    1    140.67
195    1    136.09
208    1    128.47
222    1    123.90
236    1    120.85
250    1    120.85
263    1    119.33
276    1    117.81
287    1    116.28
297    1    113.23
307    1    110.19
317    1    107.14
327    1    104.09
337    1    101.04
347    1    97.99
357    1    94.95
367    1    91.90
379    1    88.85
393    1    87.33
407    1    84.28
421    1    84.28
433    1    84.28
443    1    84.28

restart.....................RESTART #26.........................
   2    0
  30        0.5        0.5        1.0        13.5        0.10
  11    1    160.93
  22    1    160.93
  33    1    160.93
  44    1    160.93
  55    1    160.93
  66    1    160.93
  77    1    160.93
  88    1    160.93
  99    1    160.93
 110    1    160.93
 121    1    160.93
 131    1    157.88
 141    1    151.79
 151    1    145.69
 161    1    136.55
 171    1    127.41
```

```
182    1    119.79
195    1    115.21
208    1    107.59
222    1    103.02
236    1    99.97
250    1    99.97
263    1    98.45
276    1    96.93
287    1    95.40
297    1    92.35
307    1    89.31
317    1    86.26
327    1    83.21
337    1    80.16
347    1    77.11
357    1    74.07
367    1    71.02
379    1    67.97
393    1    66.45
407    1    63.40
421    1    63.40
433    1    63.40
443    1    63.40

restart.....RESTART #27.....................................
  2    0
 30       0.5       0.5       1.0       14.0       0.10
 11    1    140.06
 22    1    140.06
 33    1    140.06
 44    1    140.06
 55    1    140.06
 66    1    140.06
 77    1    140.06
 88    1    140.06
 99    1    140.06
110    1    140.06
121    1    140.06
131    1    137.01
141    1    130.91
151    1    124.82
161    1    115.67
171    1    106.53
182    1    98.91
195    1    94.34
208    1    86.72
222    1    82.14
236    1    79.10
```

```
250     1     79.10
263     1     77.57
276     1     76.05
287     1     74.52
297     1     71.48
307     1     68.43
317     1     65.38
327     1     62.33
337     1     59.28
347     1     56.24
357     1     53.19
367     1     50.14
379     1     47.09
393     1     45.57
407     1     42.52
421     1     42.52
433     1     42.52
443     1     42.52

end
```

APPENDIX E

Relative Moisture Content Plots

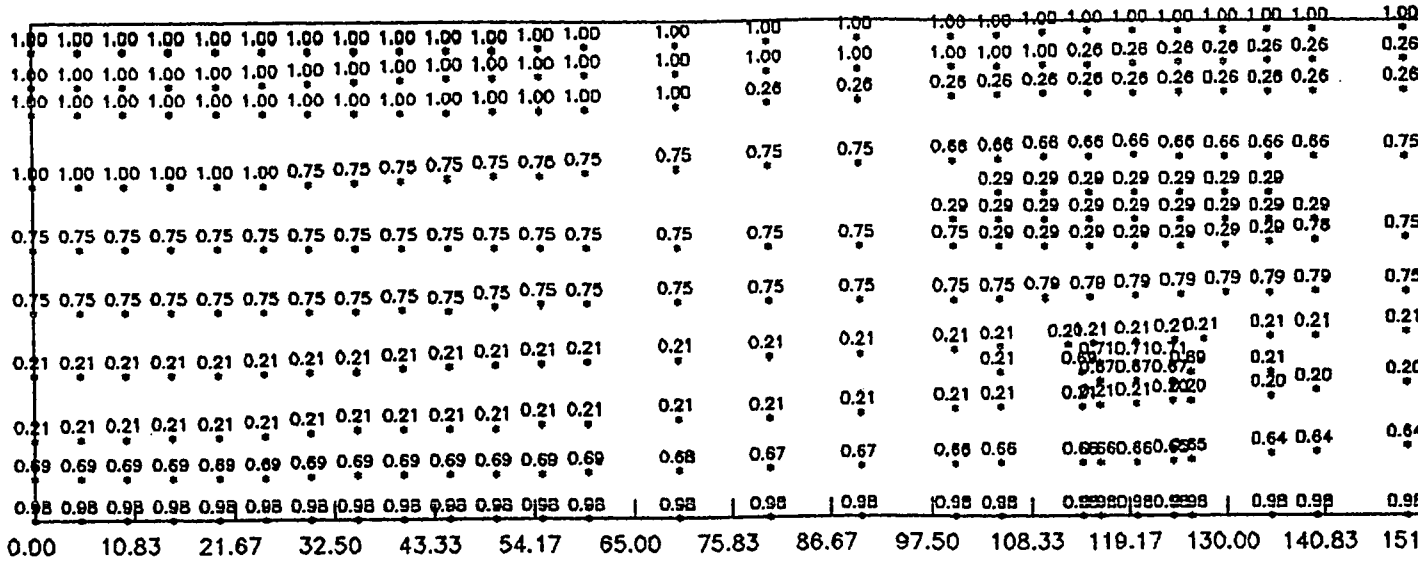

Figure 70. Initial relative moisture content plot of the February 1986 storm. X and Y coordinates are in feet.

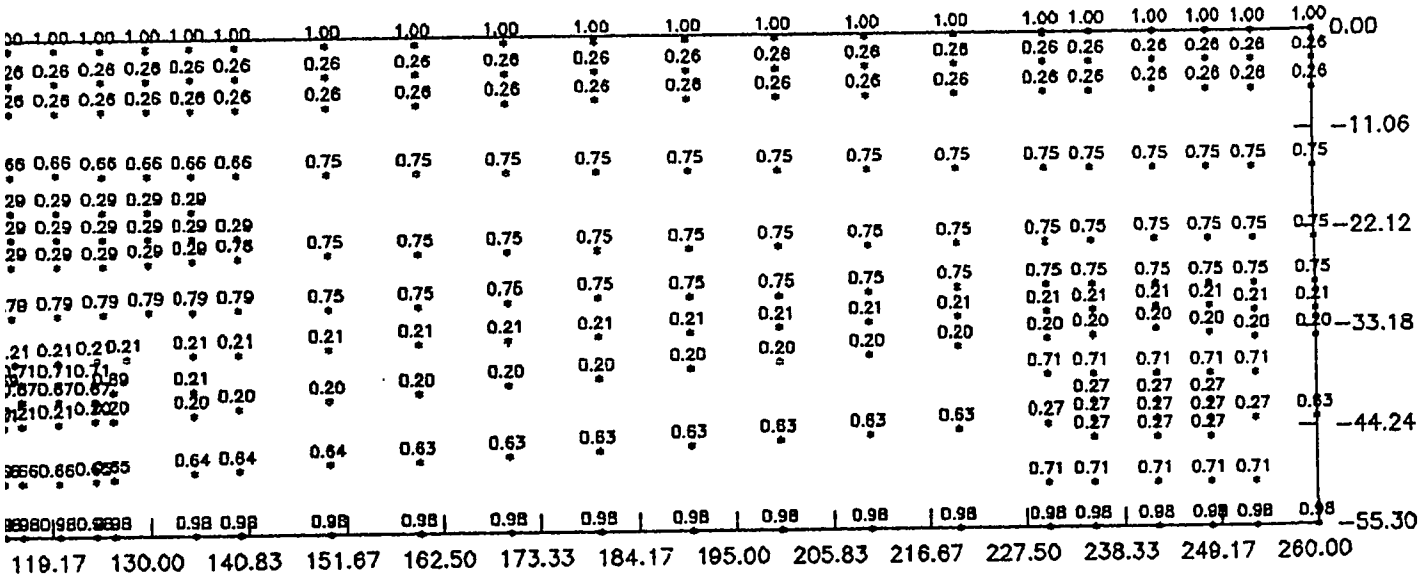
0.00
-11.06
-22.12
-33.18
-44.24
-55.30
119.17
130.00
140.83
151.67
162.50
173.33
184.17
195.00
205.83
216.67
227.50
238.33
249.17
260.00

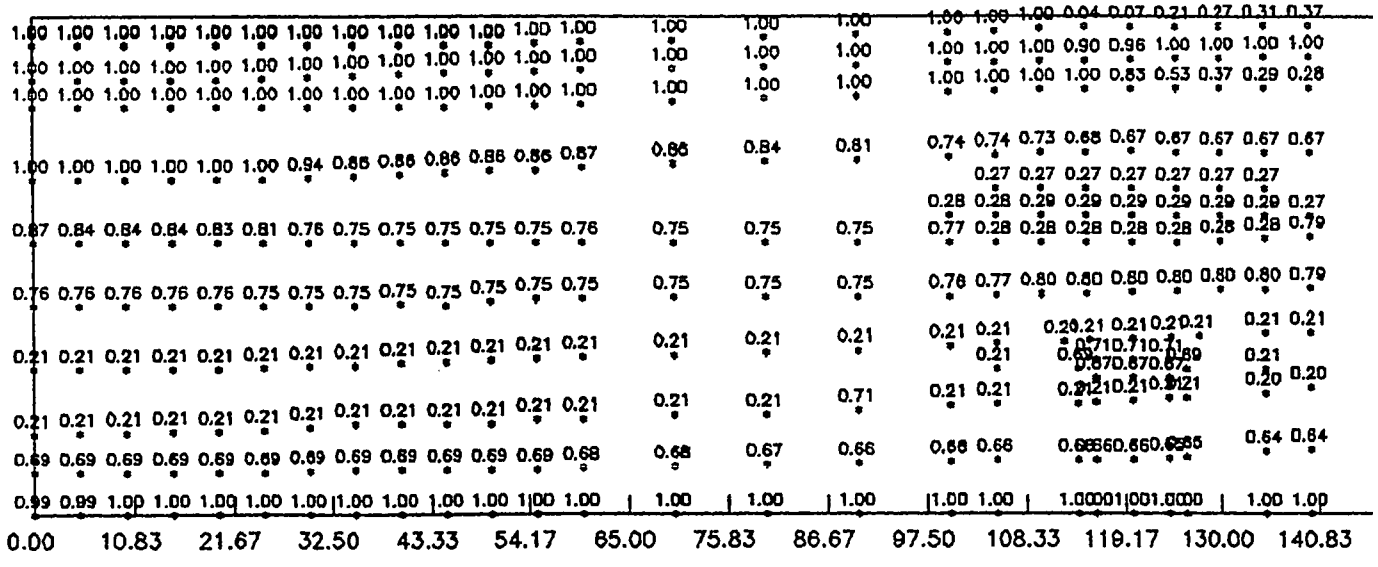

Figure 71. Relative moisture content plot of the February 1986 storm after 1 day of simulation. X and Y coordinates are in feet.

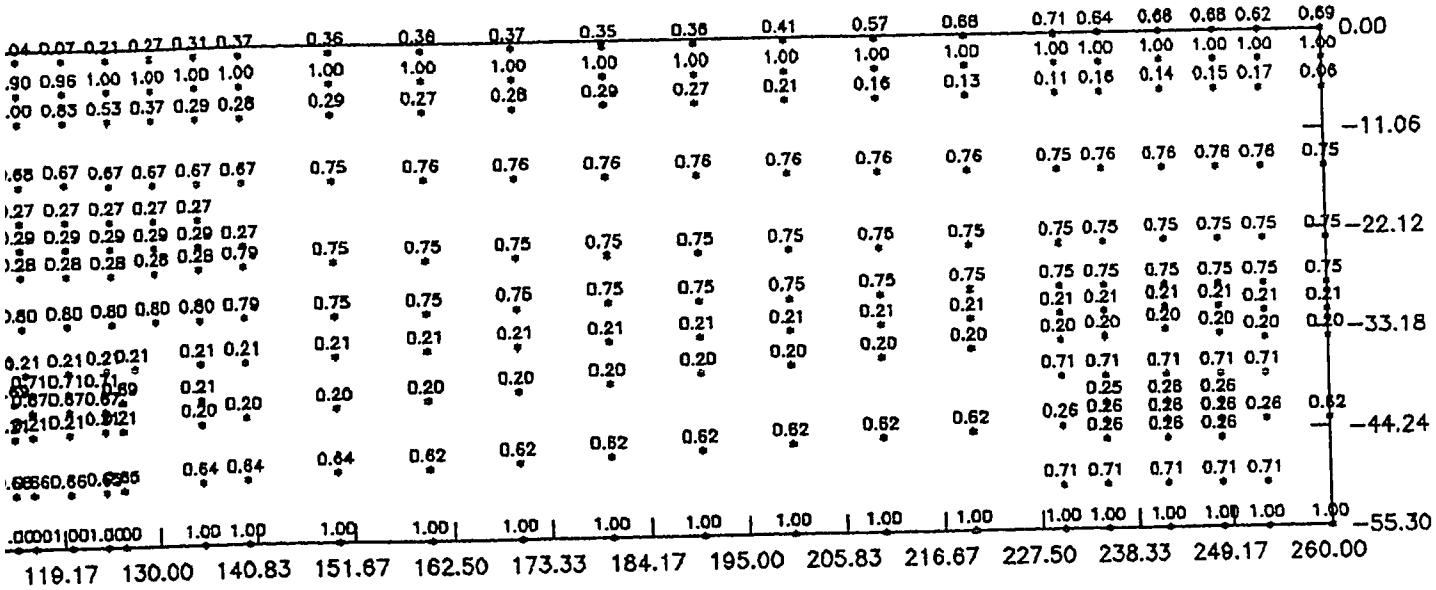
0.00
−11.06
−22.12
−33.18
−44.24
−55.30
119.17
130.00
140.83
151.67
162.50
173.33
184.17
195.00
205.83
216.67
227.50
238.33
249.17
260.00

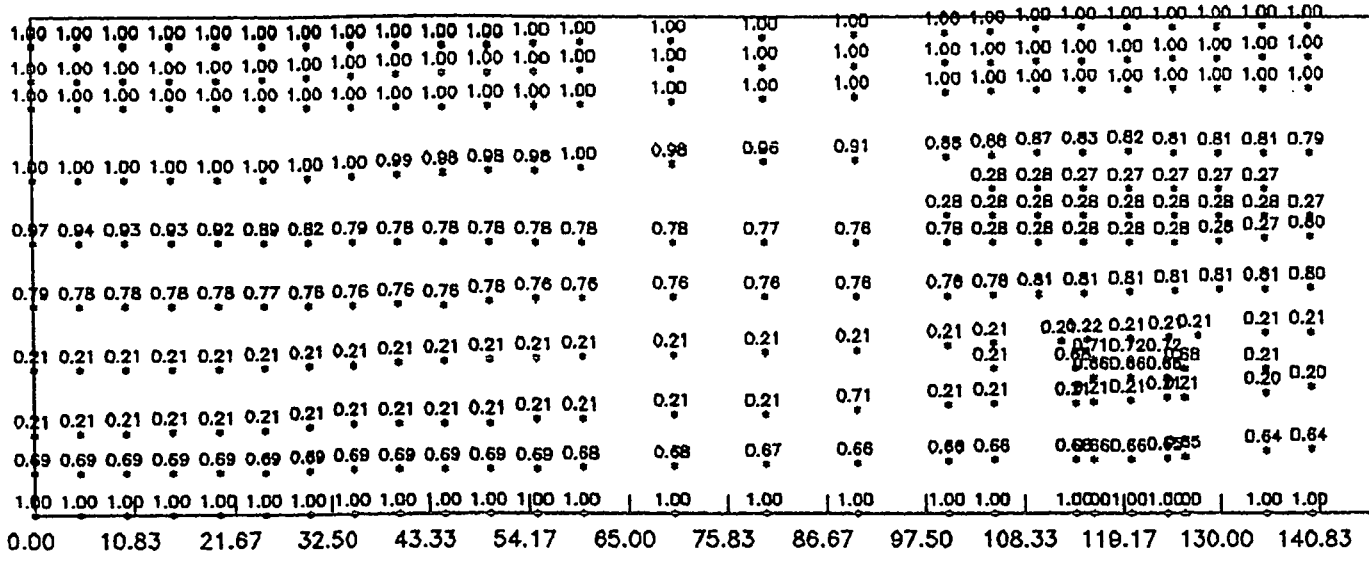

Figure 72. Relative moisture content plot of the February 1986 storm after 2 days of simulation. X and Y coordinates are in feet.

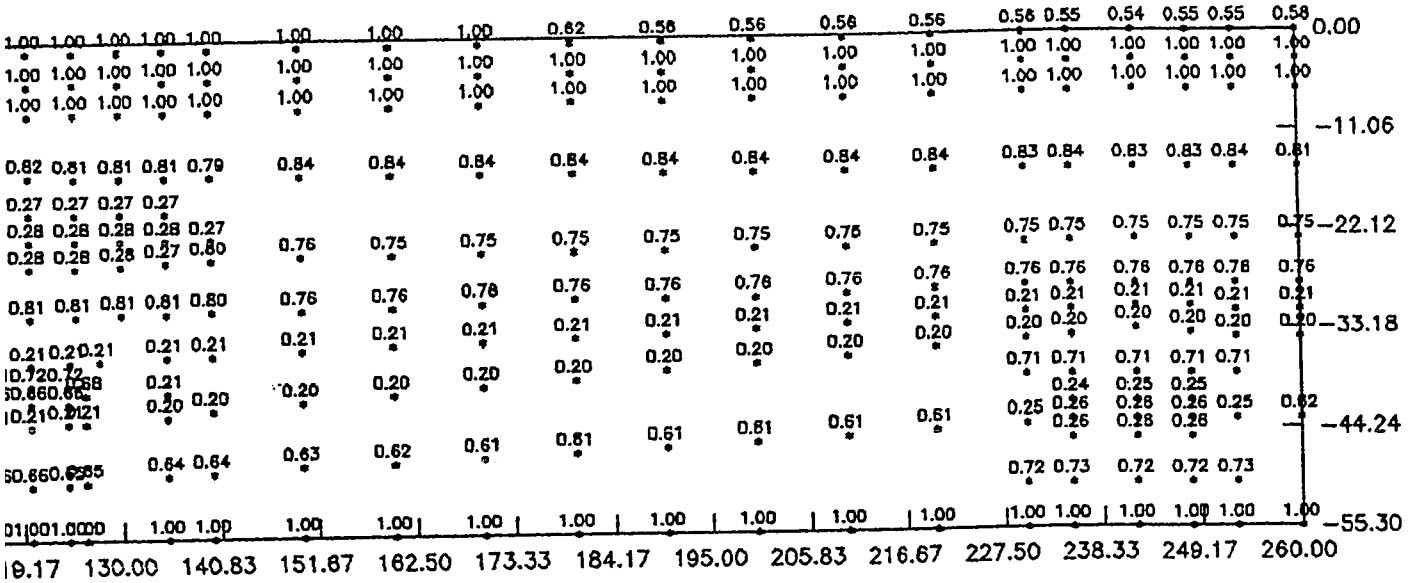
0.00
-11.06
-22.12
-33.18
-44.24
-55.30
130.00
140.83
151.67
162.50
173.33
184.17
195.00
205.83
216.67
227.50
238.33
249.17
260.00

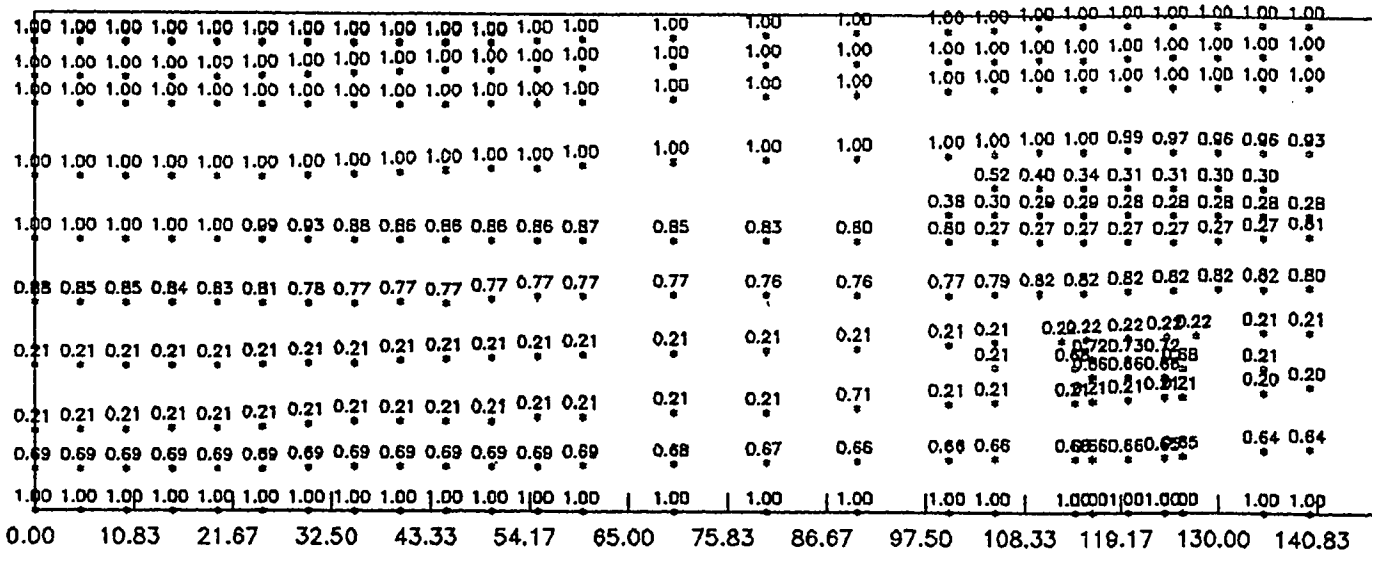

Figure 73. Relative moisture content plot of the February 1986 storm after 3 days of simulation. X and Y coordinates are in feet.

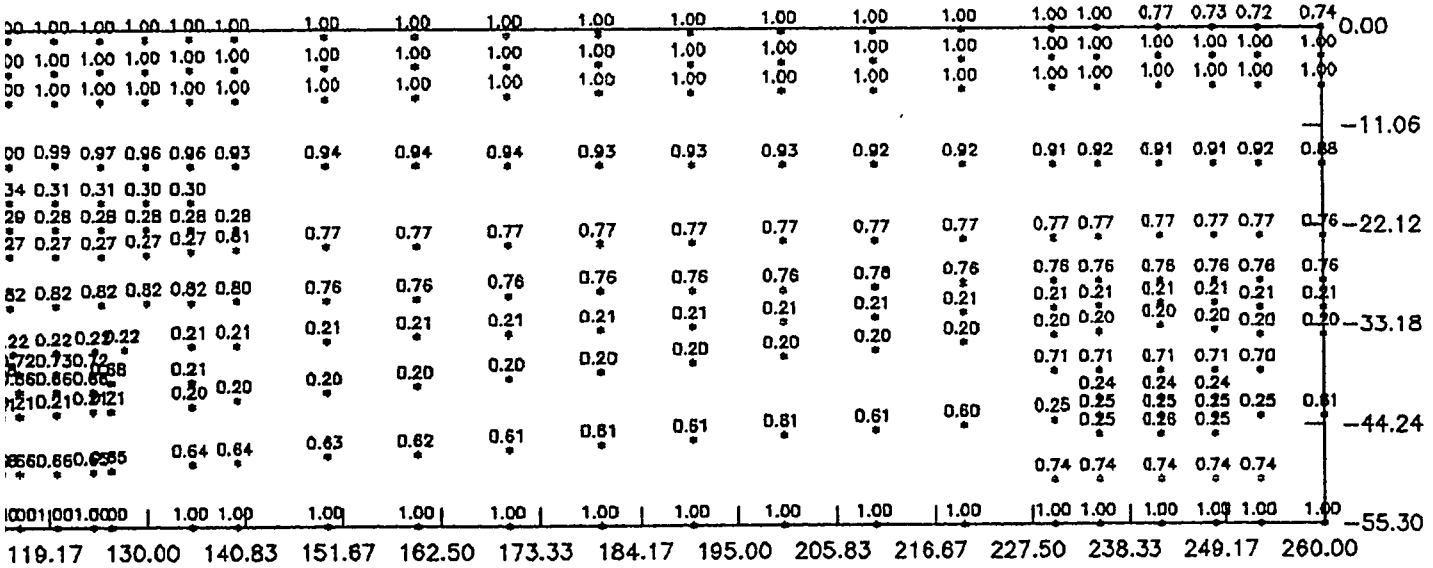
0.00
-11.06
-22.12
-33.18
-44.24
-55.30
119.17
130.00
140.83
151.67
162.50
173.33
184.17
195.00
205.83
216.67
227.50
238.33
249.17
260.00

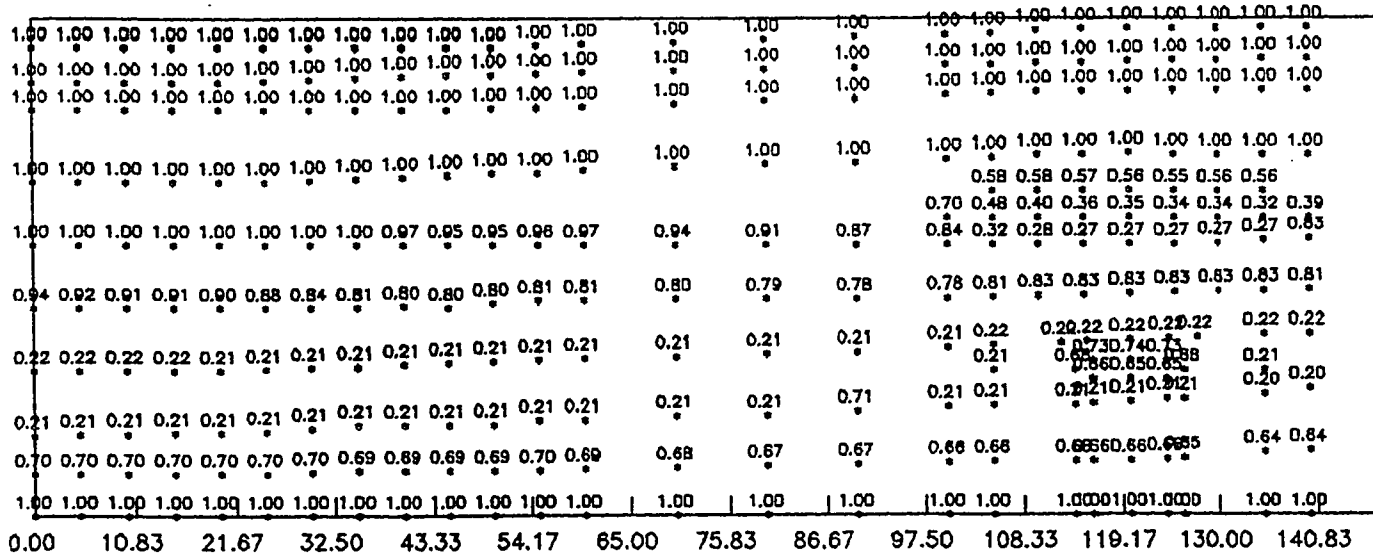

Figure 74. Relative moisture content plot of the February 1986 storm after 4 days of simulation. X and Y coordinates are in feet.

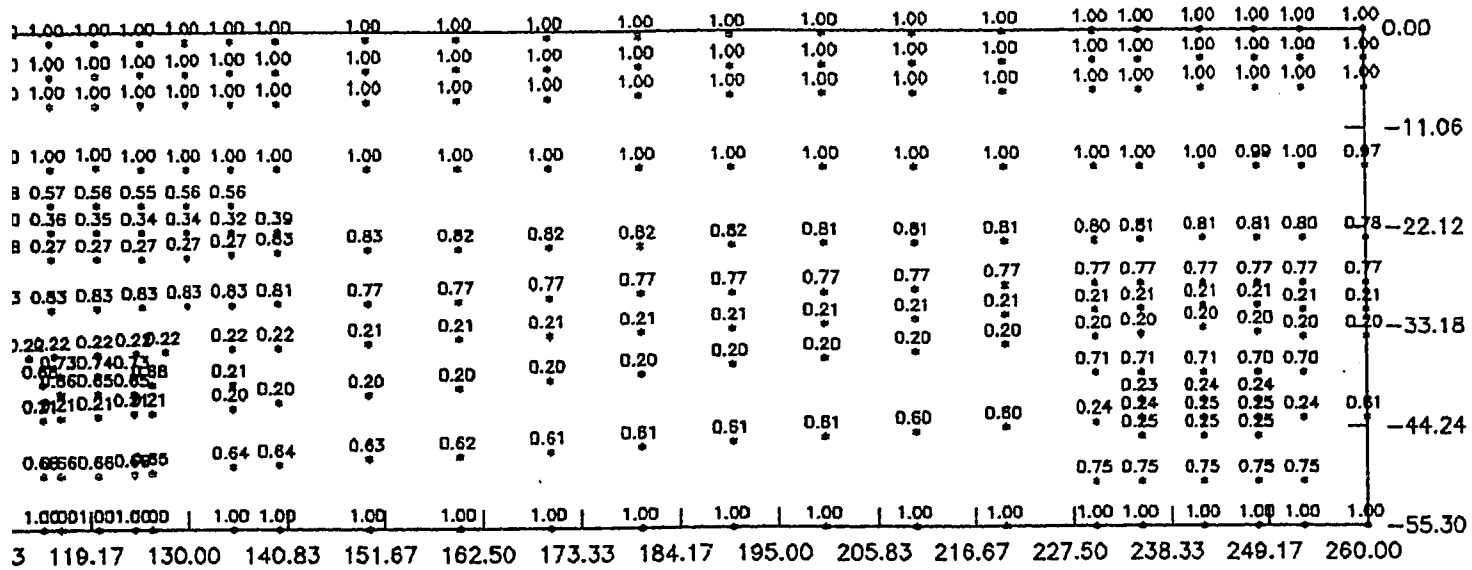
0.00
-11.06
-22.12
-33.18
-44.24
-55.30
119.17
130.00
140.83
151.67
162.50
173.33
184.17
195.00
205.83
216.67
227.50
238.33
249.17
260.00

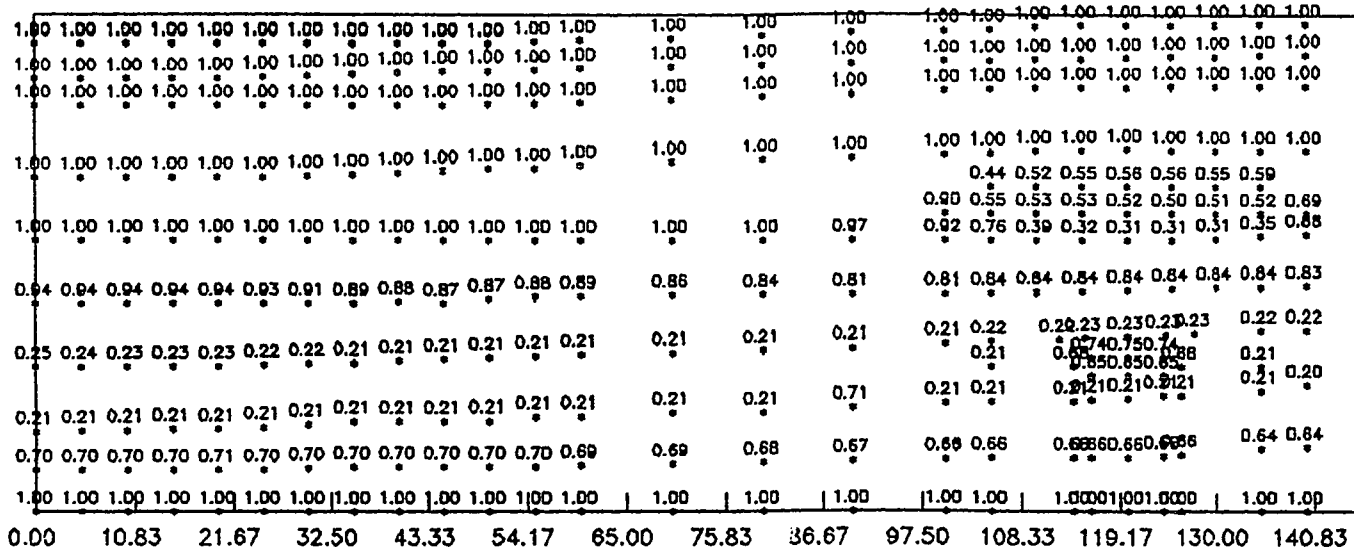

Figure 75. Relative moisture content plot of the February 1986 storm after 5 days of simulation. X and Y coordinates are in feet.

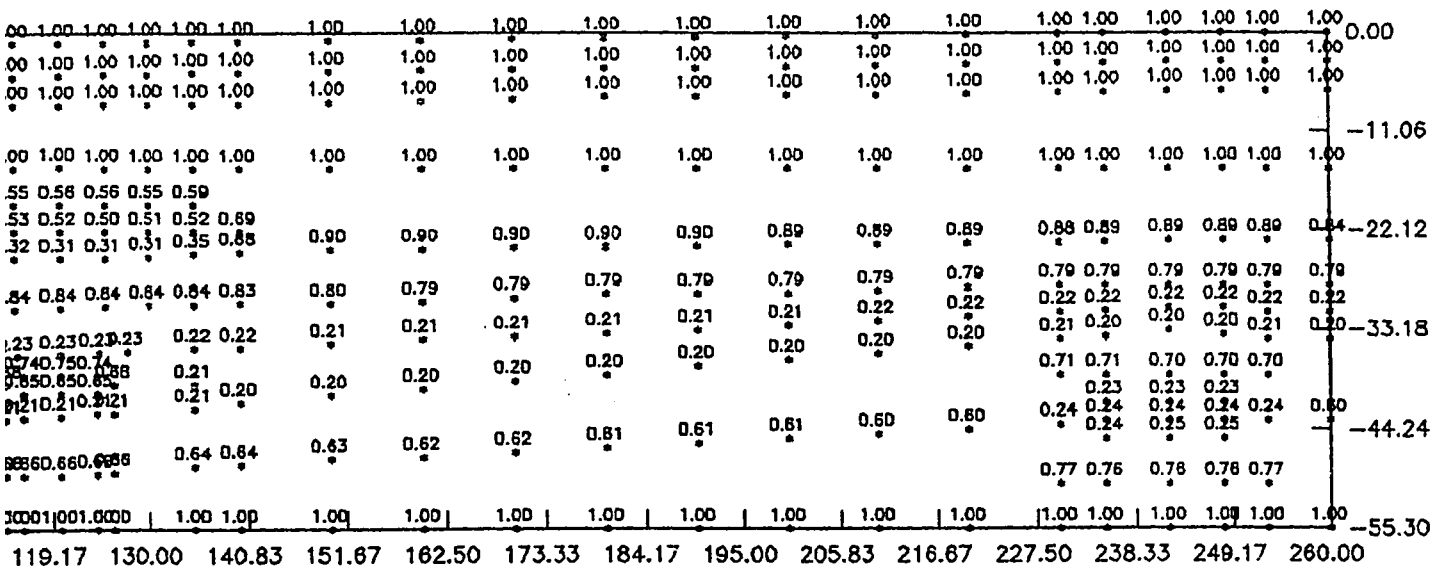
0.00
-11.06
-22.12
-33.18
-44.24
-55.30
119.17
130.00
140.83
151.67
162.50
173.33
184.17
195.00
205.83
216.67
227.50
238.33
249.17
260.00

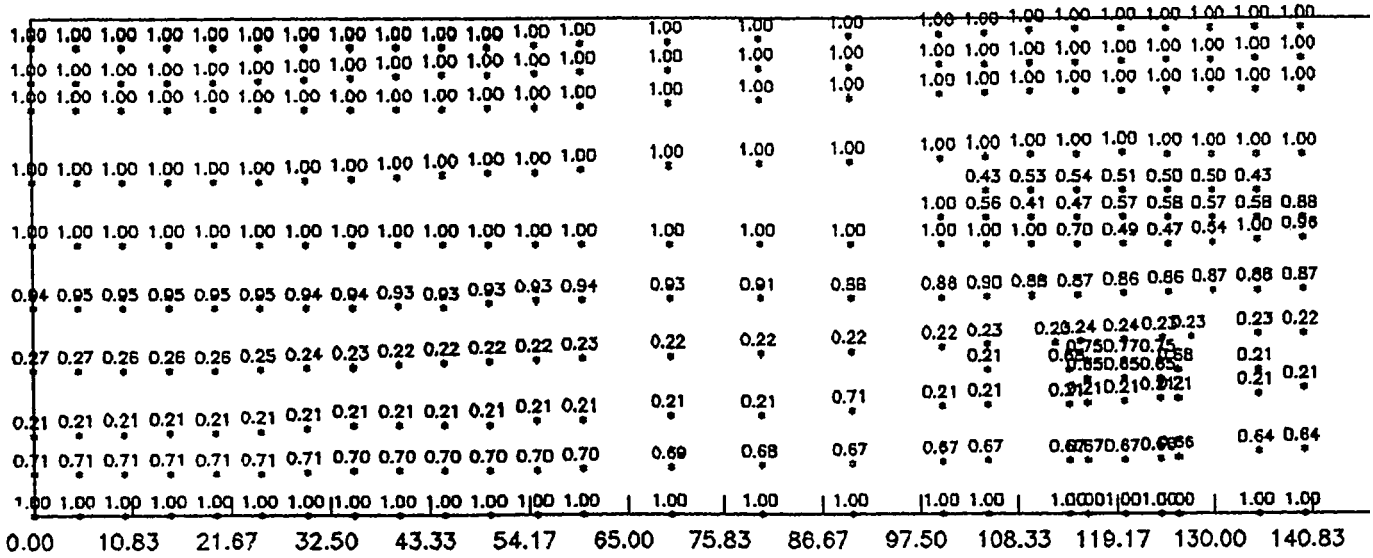

Figure 76. Relative moisture content plot of the February 1986 storm after 6 days of simulation. X and Y coordinates are in feet.

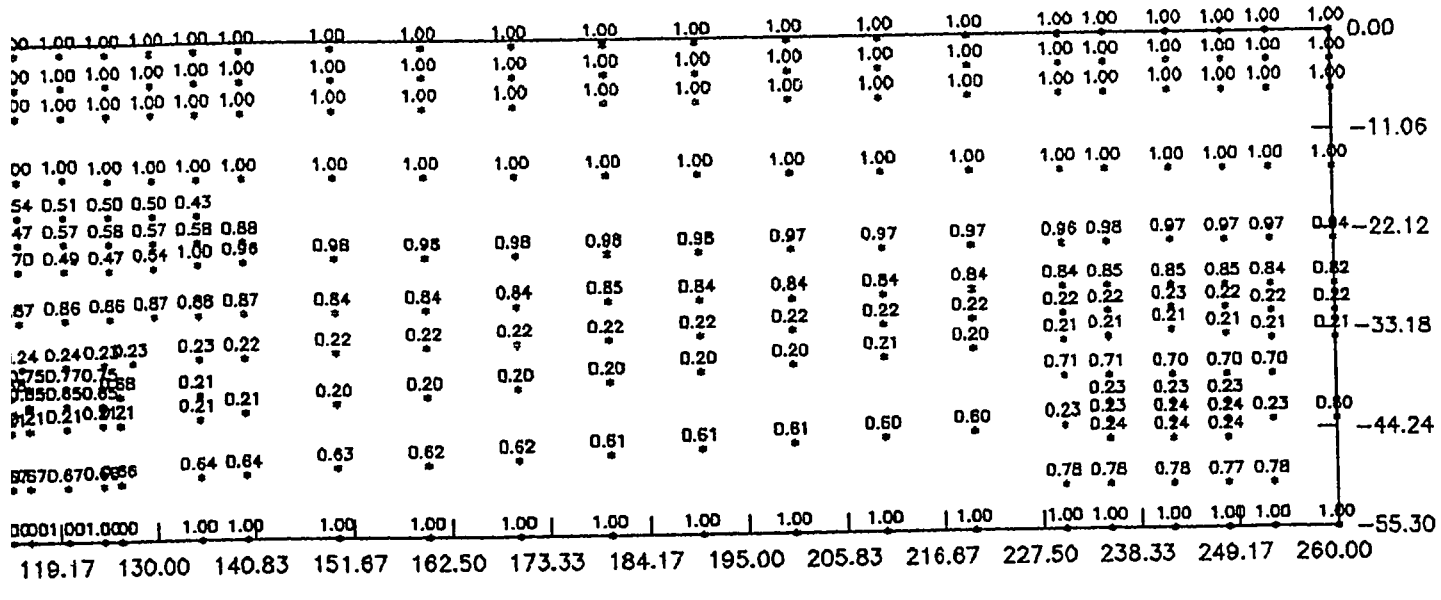
0.00
-11.06
-22.12
-33.18
-44.24
-55.30
119.17
130.00
140.83
151.67
162.50
173.33
184.17
195.00
205.83
216.67
227.50
238.33
249.17
260.00

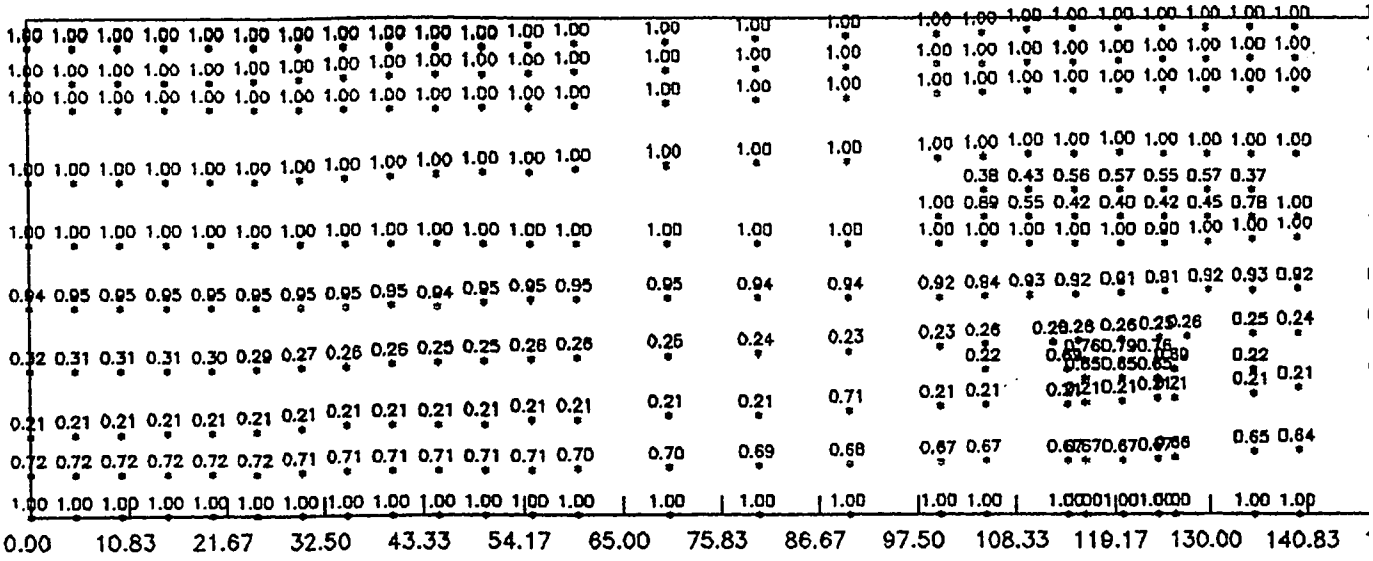

Figure 77. Relative moisture content plot of the February 1986 storm after 7 days of simulation. X and Y coordinates are in feet.

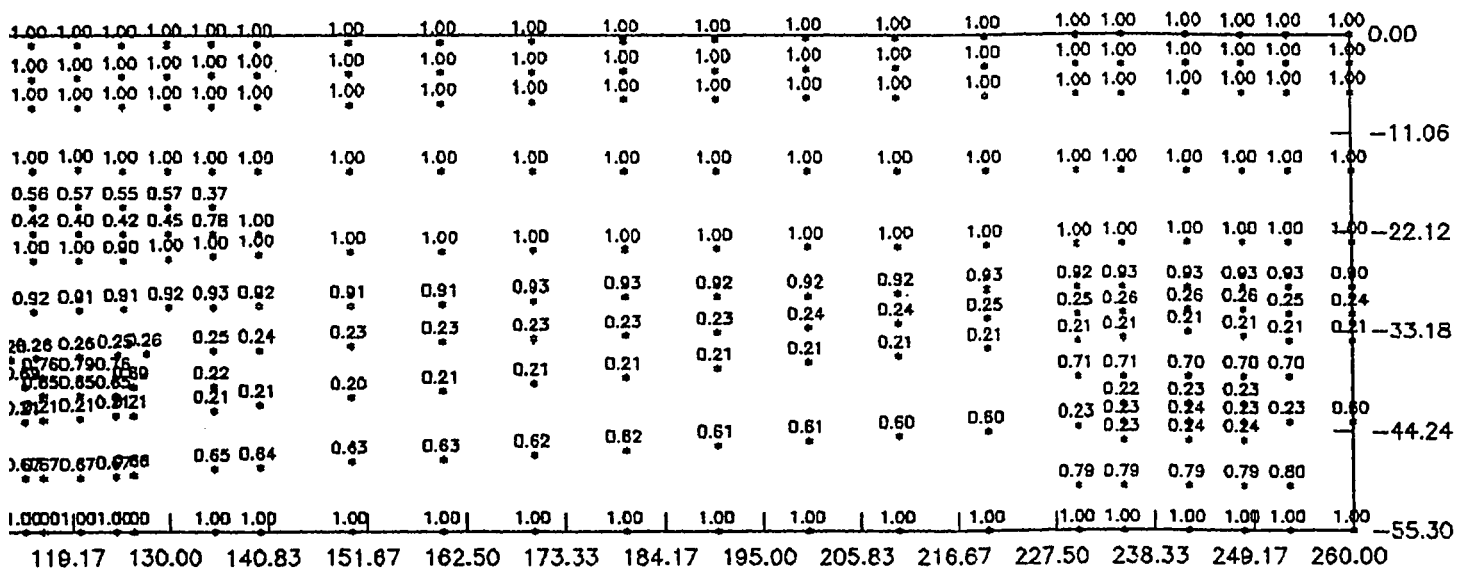
0.00
-11.06
-22.12
-33.18
-44.24
-55.30
119.17
130.00
140.83
151.67
162.50
173.33
184.17
195.00
205.83
216.67
227.50
238.33
249.17
260.00

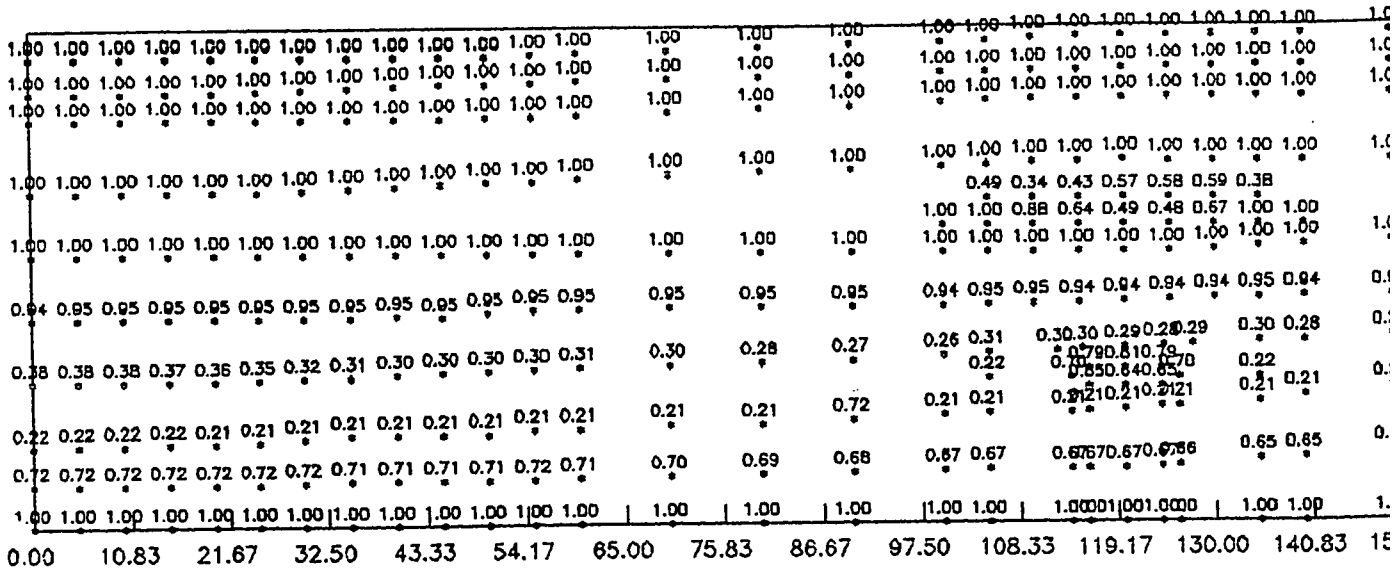

Figure 78. Relative moisture content plot of the February 1986 storm after 8 days of simulation. X and Y coordinates are in feet.

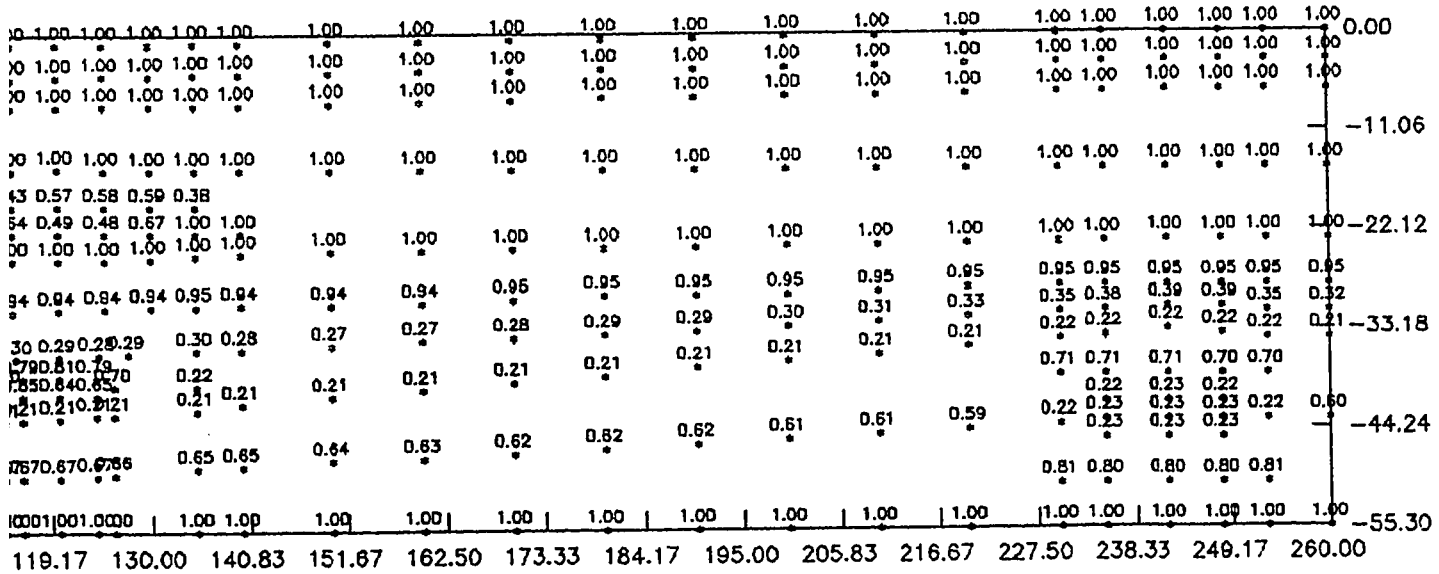
0.00
-11.06
-22.12
-33.18
-44.24
-55.30
119.17
130.00
140.83
151.67
162.50
173.33
184.17
195.00
205.83
216.67
227.50
238.33
249.17
260.00

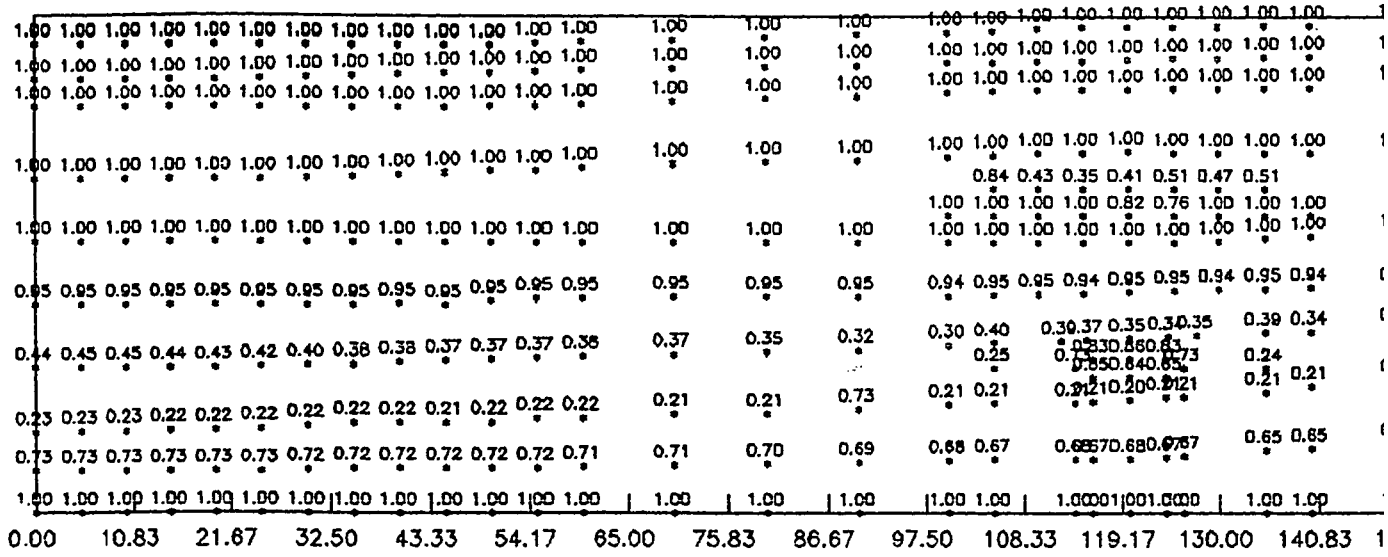

Figure 79. Relative moisture content plot of the February 1986 storm after 9 days of simulation. X and Y coordinates are in feet.

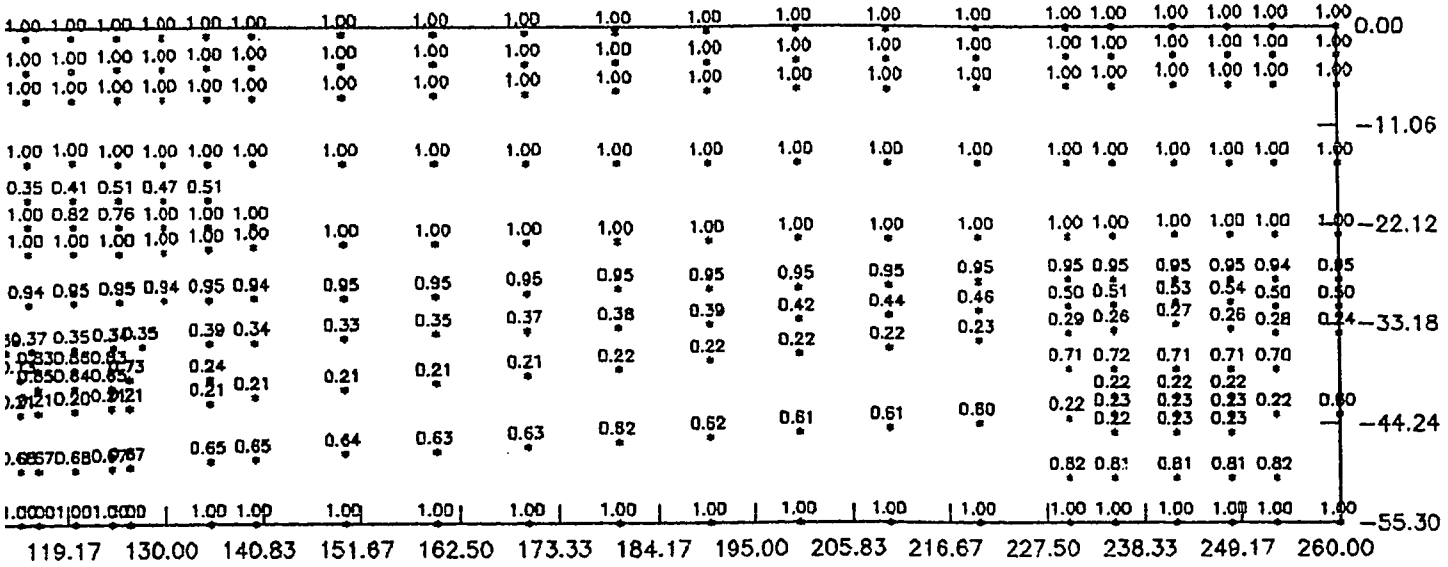
0.00
-11.06
-22.12
-33.18
-44.24
-55.30
119.17
130.00
140.83
151.67
162.50
173.33
184.17
195.00
205.83
216.67
227.50
238.33
249.17
260.00

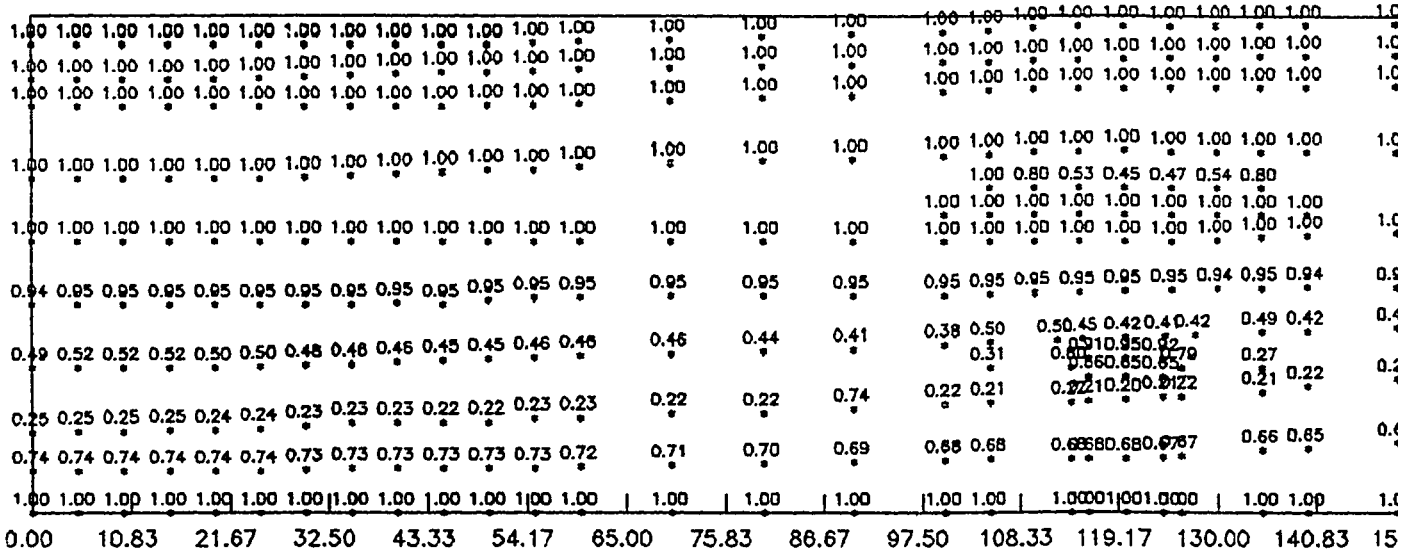

Figure 80. Relative moisture content plot of the February 1986 storm after 10 days of simulation. X and Y coordinates are in feet.

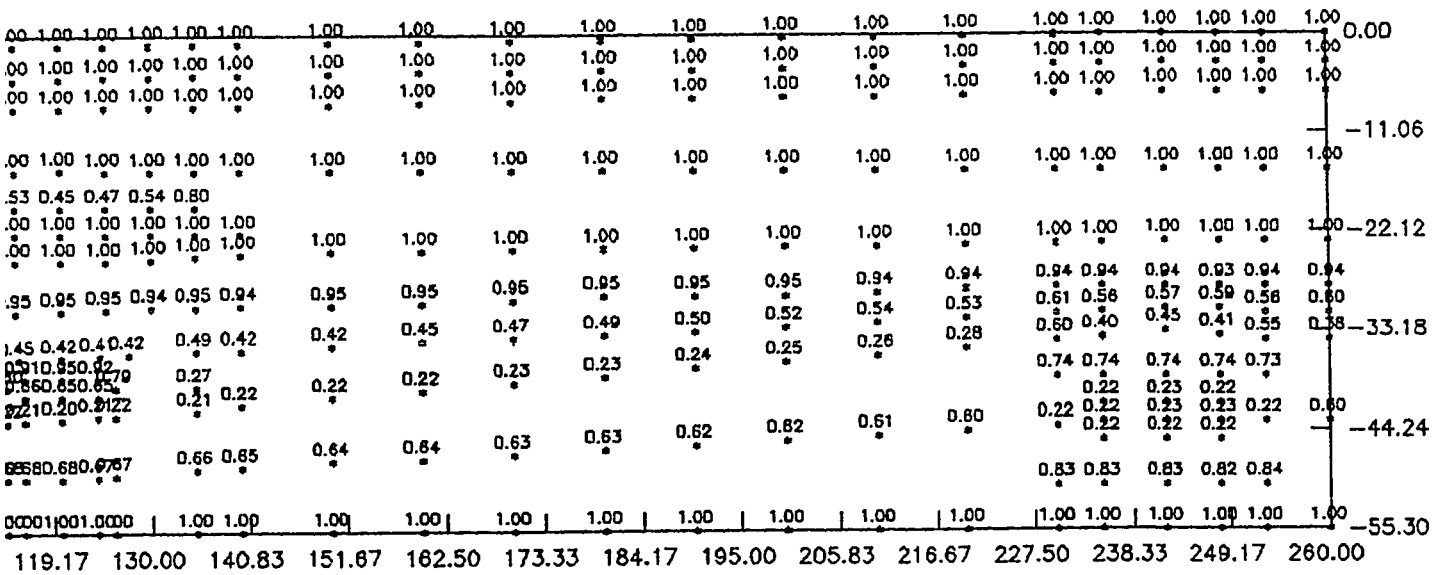
0.00
-11.06
-22.12
-33.18
-44.24
-55.30
119.17
130.00
140.83
151.67
162.50
173.33
184.17
195.00
205.83
216.67
227.50
238.33
249.17
260.00

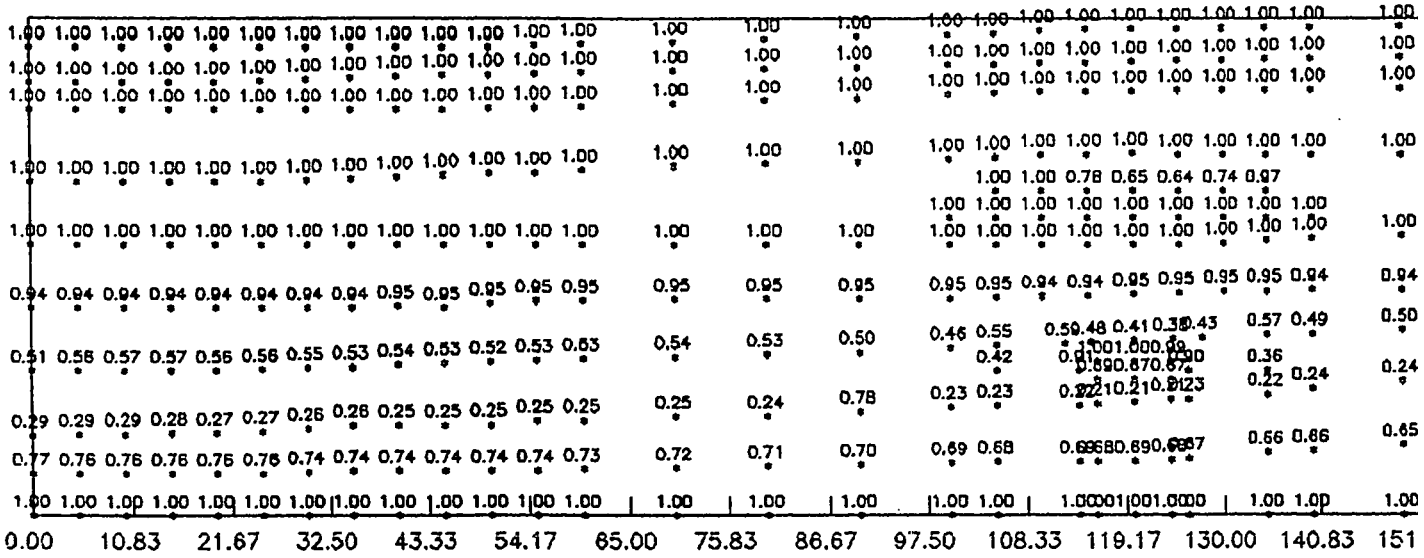

Figure 81. Relative moisture content plot of the February 1986 storm after 11 days of simulation. X and Y coordinates are in feet.

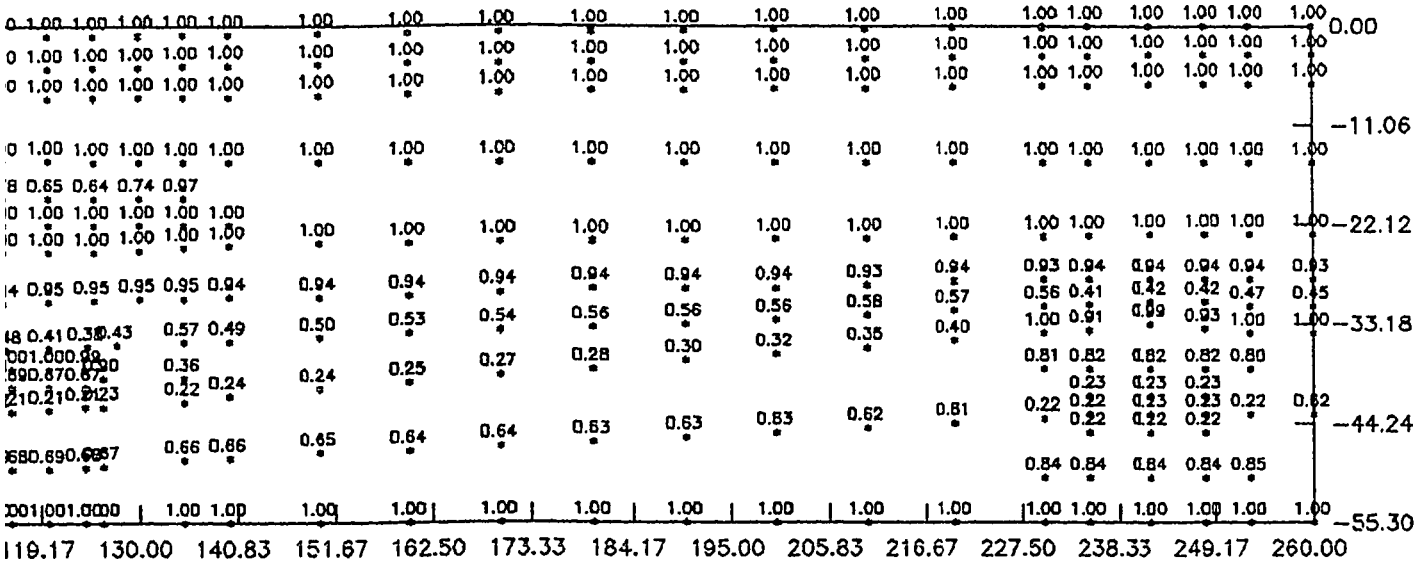
0.00
-11.06
-22.12
-33.18
-44.24
-55.30
119.17
130.00
140.83
151.67
162.50
173.33
184.17
195.00
205.83
216.67
227.50
238.33
249.17
260.00

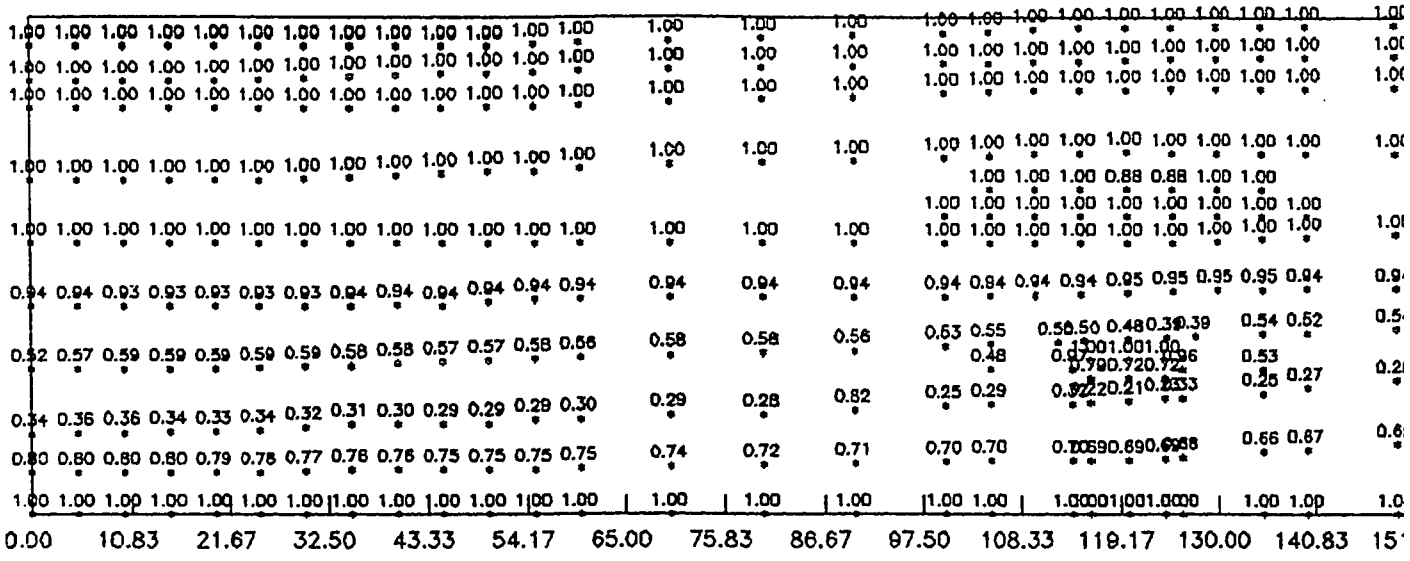

Figure 82. Relative moisture content plot of the February 1986 storm after 12 days of simulation. X and Y coordinates are in feet.

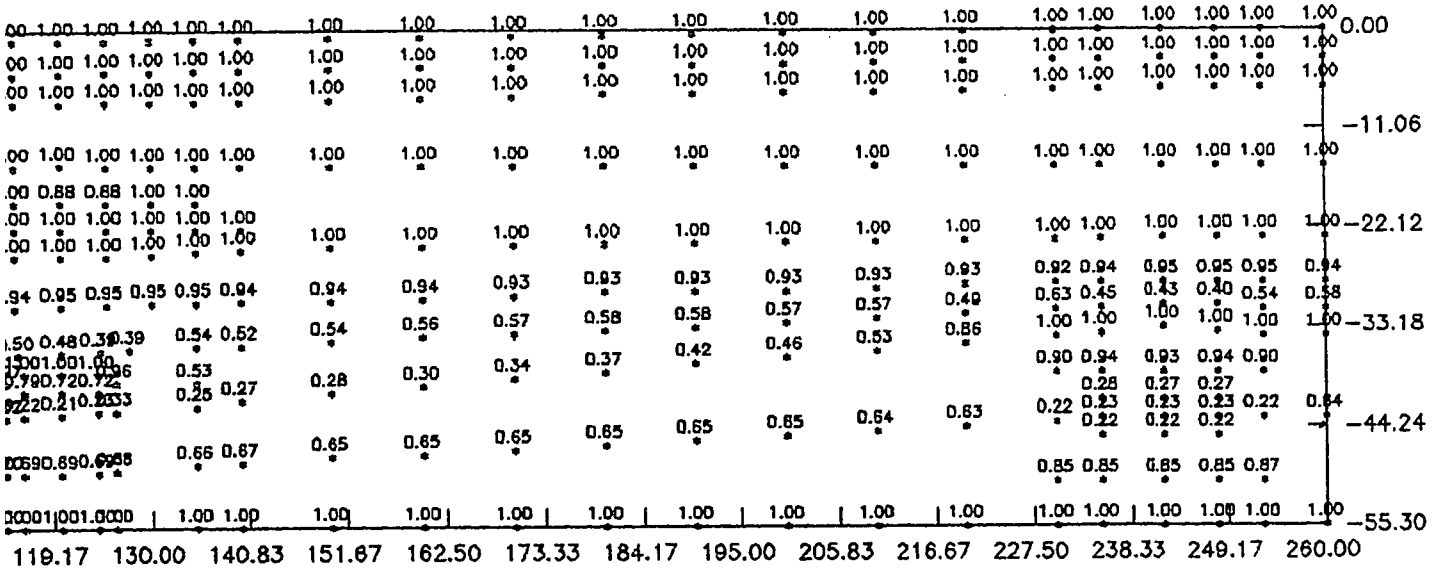
0.00
-11.06
-22.12
-33.18
-44.24
-55.30
119.17
130.00
140.83
151.67
162.50
173.33
184.17
195.00
205.83
216.67
227.50
238.33
249.17
260.00

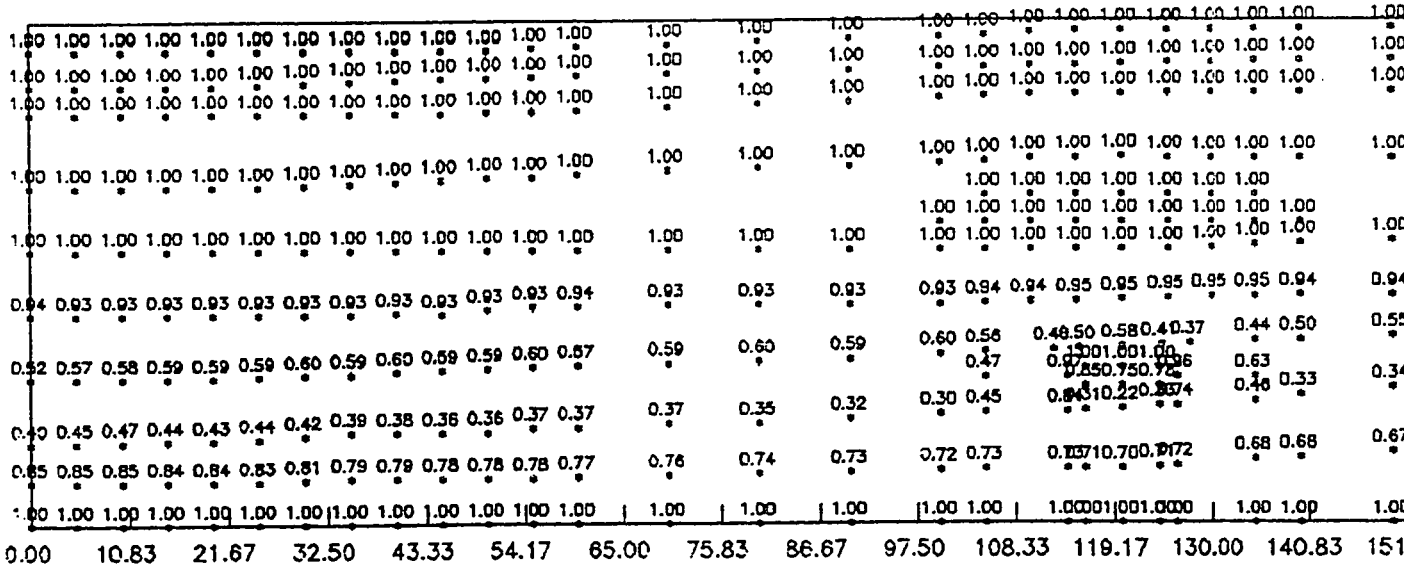

Figure 83. Relative moisture content plot of the February 1986 storm after 13 days of simulation. X and Y coordinates are in feet.

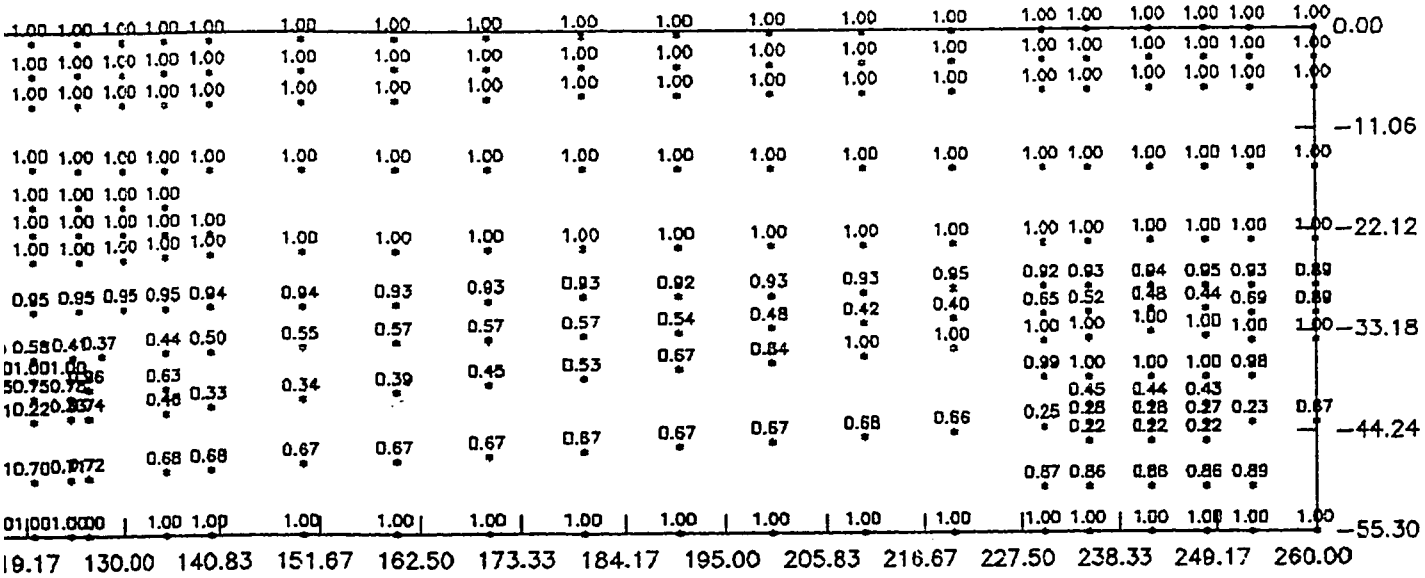
0.00
-11.06
-22.12
-33.18
-44.24
-55.30
9.17
130.00
140.83
151.67
162.50
173.33
184.17
195.00
205.83
216.67
227.50
238.33
249.17
260.00

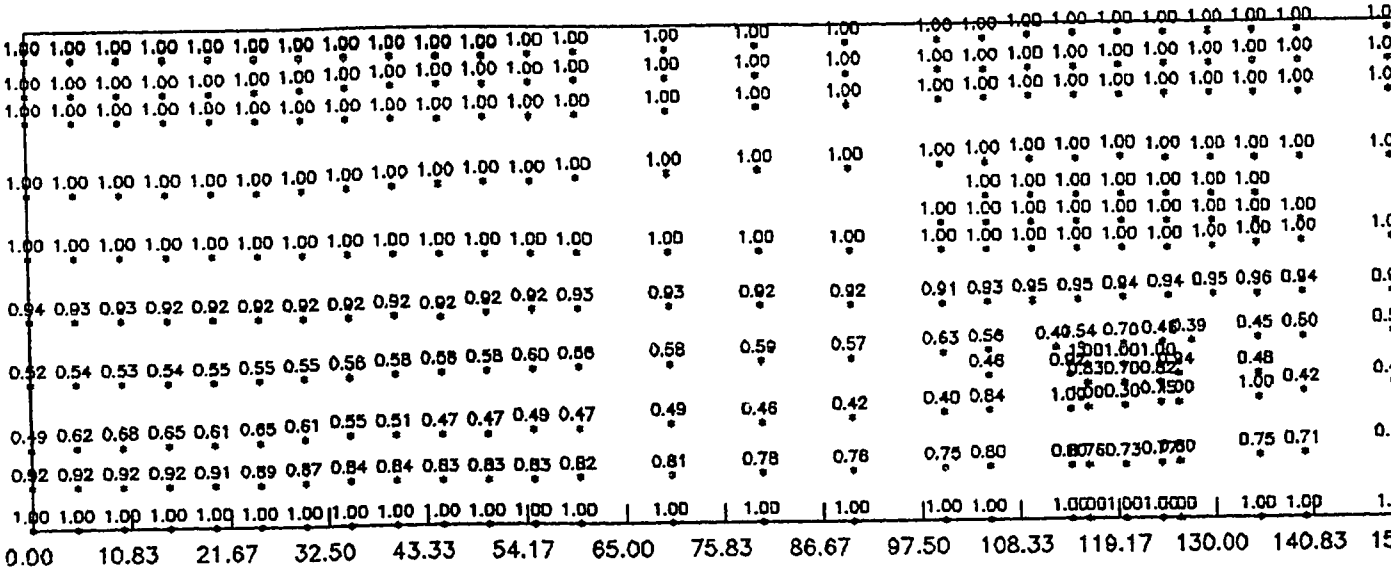

Figure 84. Relative moisture content plot of the February 1986 storm after 14 days of simulation. X and Y coordinates are in feet.

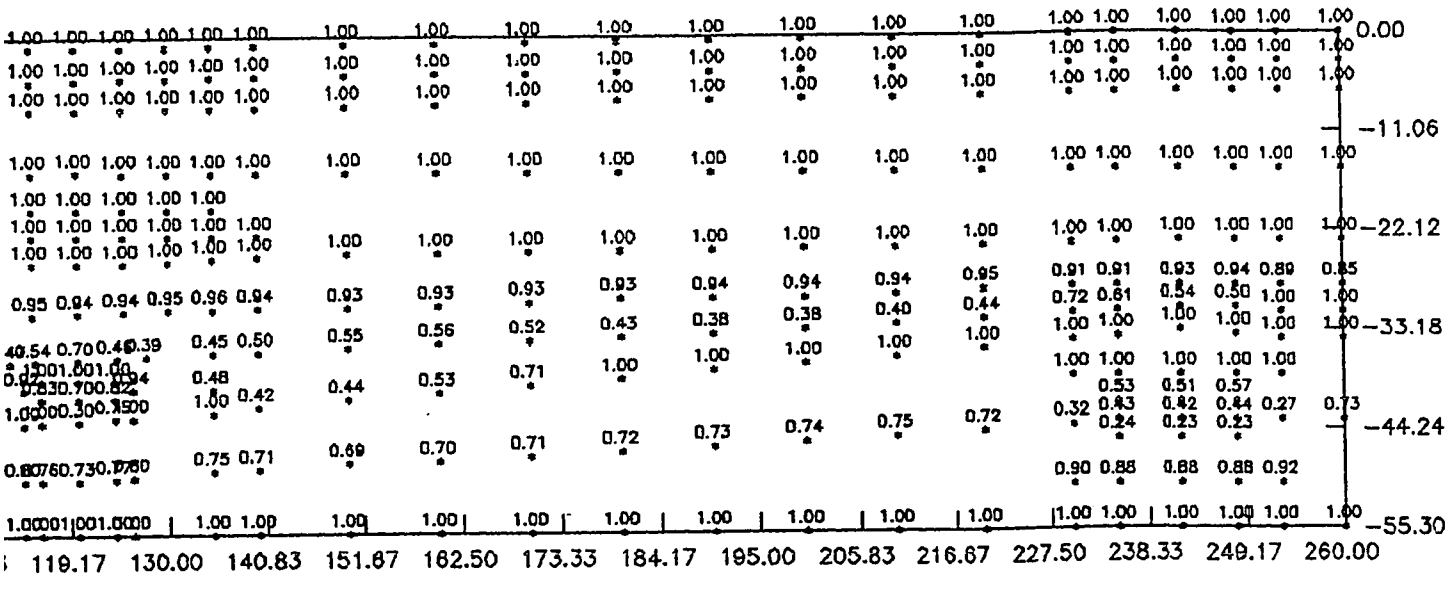
0.00
-11.06
-22.12
-33.18
-44.24
-55.30
119.17
130.00
140.83
151.67
162.50
173.33
184.17
195.00
205.83
216.67
227.50
238.33
249.17
260.00

APPENDIX F

Table Comparing Saturated Hydraulic Conductivities

Table 4. Table comparing the saturated hydraulic conductivities used in the model with those generated from field data and acceptable ranges of expected hydraulic conductivity values for each material.

Comparison of Saturated Hydraulic Conductivity Values of Soils Used in the Computer Model.

Material	Description	A	B	C	D
1	Clayey silt	N/A	<3	0.001–1	1.6
2	Silty gravel	N/A	60	100–10000	120
3	Silt	N/A	N/A	0.001–10	7
4	Sand	680	N/A	1–10000	65
5	Clay	N/A	N/A	0.000001–0.01	1.04

A = Hydraulic Conductivity from Permeameter Test (cm/day)

B = Hydraulic Conductivity from Infiltrometer Test (cm/day)

C = Range of Hydraulic Conductivity Values from Freeze and Cherry (1979) (cm/day)

D = Model Saturated Hydraulic Conductivity Input (cm/day)